UNIVERSIDAD COMPLUTENSE DE MADRID

FACULTAD DE CIENCIAS FÍSICAS

Departamento de Física Aplicada I

TESIS DOCTORAL

Design, preparation and characterization of hollow fiber membranes for desalinisation by membrane distillation

Diseño, preparación y caracterización de membranas de fibra hueca para la desalación por destilación en membrana

MEMORIA PARA OPTAR AL GRADO DE DOCTOR

PRESENTADA POR

Loreto García Fernández

Director

Mohamed Khayet Souhaimi
María del Carmen García Payo

Madrid, 2017

UNIVERSIDAD
COMPLUTENSE
MADRID

Design, preparation and characterization of hollow fiber membranes for desalination by membrane distillation

Diseño, preparación y caracterización de membranas de fibra hueca para la desalación por destilación en membrana

Doctoral Thesis

LORETO GARCÍA FERNÁNDEZ

Supervisors

Mohamed Khayet Souhaimi and María del Carmen García Payo

DEPARTAMENTO DE FÍSICA APLICADA I

FACULTAD DE CIENCIAS FÍSICAS

Madrid, 2017

UNIVERSIDAD
COMPLUTENSE
MADRID

Design, preparation and characterization of hollow fiber membranes for desalination by membrane distillation

Diseño, preparación y caracterización de membranas de fibra hueca para la desalación por destilación en membrana

Doctoral thesis submitted by Loreto García Fernández in fulfillment of the requirements for the degree of Doctor of Physics with European mention at Universidad Complutense de Madrid

Madrid, 2017

"*Soy de las que piensan que la ciencia tiene una gran belleza. Un científico en su laboratorio no es sólo un técnico: es también un niño colocado ante fenómenos naturales que le impresionan como un cuento de hadas*" – Marie Curie.

"*Science knows no country, because knowledge belongs to humanity, and is the torch which illuminates the world*" – Louis Pasteur.

A mi familia, en especial a mis abuelos

Agradecimientos

Esta tesis doctoral ha marcado una etapa de mi vida que me ha desarrollado tanto personal como profesionalmente. Me he formado como investigadora enfrentándome siempre con entusiasmo a los retos que se han planteado. En esta labor, han tenido mucho que ver mis directores de tesis, Mohamed y Carmen, a los cuales les estoy enormemente agradecida. Gracias por brindarme la oportunidad de pertenecer a este grupo de investigación y por compartir conmigo todos vuestros conocimientos sobre la Ciencia y Tecnología de Membranas. Mohamed, gracias por tu dedicación, por transmitirme tu profesionalidad y perseverancia en el trabajo, y por mostrarme las nuevas oportunidades que me ofrece el mundo científico. A ti Carmen, darte las gracias por transmitirme tu pasión por la investigación y por enseñarme el buen proceder en el laboratorio. Siempre recordaré nuestras largas charlas sobre resultados difíciles de interpretar. Pero principalmente quería agradecerte tu tiempo, ayuda y cariño incondicional.

Como buenos experimentales, es mucho el tiempo compartido en el laboratorio con mis compañeros del grupo de investigación y con los estudiantes que han pasado por él. Todos me habéis acompañado durante el desarrollo de mi tesis, y por ello quiero agradeceros los buenos momentos que me habéis hecho pasar, vuestro gran compañerismo y vuestra ayuda en todo momento. Essalhi, ya estabas allí cuando me embarqué en mi camino de la investigación. Gracias por enseñarme las destrezas del laboratorio y por ayudarme siempre que lo he necesitado. Gracias también a mis magníficos compañeros, Alia, Catalina, y Julio, siempre me he sentido como en familia con vosotros. Y como no, a mi gran amiga Paula. Desde antes de empezar la universidad emprendimos juntas este viaje, siempre has sido un grandísimo apoyo para mí, tanto en lo profesional como en lo personal, siempre me has animado y me has dado fuerzas. Ha sido toda una suerte poder compartir esta etapa de mi vida contigo.

Durante todo este tiempo también he recibido la estimable ayuda y consejos de los integrantes del Departamento de Física Aplicada I. A muchos de vosotros os conozco desde que entré la carrera y a muchos otros os he ido conociendo a lo largo de estos años. Todos me habéis mostrado siempre una gran disposición, amabilidad e interés. Ha sido todo un placer.

Durante mi investigación son muchas las personas que me han ayudado a solventar problemas prácticos que me han ido surgiendo y que han hecho que las cosas fueran más fáciles. Quería destacar la gran ayuda ofrecida por los técnicos de la Facultad de Física y del Centro de Microscopía. En especial, a Antonio Paz por tus consejos sobre montajes eléctricos y por tus arreglos; y a Esther Garrido, por ayudarme en las medidas realizadas con el

microscopio óptico y por dar luz a las ideas que intentaba llevar a cabo con él, siempre con mucho interés y motivación.

También agradecer a muchos otros compañeros y amigos de otros departamentos con los que también he compartido muchos cafés, celebraciones de cumpleaños y unas buenas risas. A los electrónicos, a Edgar, a Oscar, a Cris y a muchos otros. Un gracias especial a ti Cris, por tu sonrisa, tu gran amistad y por todas las experiencias que hemos compartido tanto dentro como fuera de la facultad. Creo que la tesis nos ha unido un poco más.

También me gustaría dedicar unas palabras a los miembros del grupo de investigación del Imperial College London, donde realicé mi estancia predoctoral de investigación. *It was a fruitful and pleasant experience. Prof. Kang Li, thank you very much for giving me the opportunity to do my research stay in your group. Dr. Bo Wang, I am really grateful to you for sharing your knowledge about ceramic membranes with me, I learnt so much from you, and thank you also for facilitating everything that I needed during and after my time at Imperial. Special thanks to my friends there, I felt very welcome from the moment I arrived, you always made me feel like a member of your group.*

Muchas más personas han estado junto a mí durante todo este tiempo, ya sea desde un ámbito más académico o personal. Empezaré por mis primeras andanzas en el mundo de la Física. Carmenchu, gracias por generar esa curiosidad en mí acerca del porqué de las cosas, cualidad que posee todo físico, y por la cual comprendí que la física era mi vocación. A lo largo de la carrera y del máster he tenido muy buenas experiencias tanto con magníficos profesores de la Facultad de Física, los cuales han mantenido mi motivación por la física, como con mis compañeros. Mención especial al grupo piloto y a muy buenas amistades que me han acompañado de manera especial en este viaje como son mis amigas, Gema y Ana.

Gracias también a mis amigas de baile, me habéis ayudado a desconectar cada viernes; a Marina y familia, por vuestros ánimos, confianza y visión de futuro; a mi profesora de inglés ahora amiga, Amanda, por tus consejos especialmente en traducciones de términos técnicos y no tan técnicos; a mis amigos; a Nieves; a Verónica y a la familia Flández Santos por preocuparse por mí y mostrar siempre su interés por mis cosas.

Y en especial, a Rodrigo por estar siempre a mi lado apoyándome, animándome y sobre todo reconfortándome cuando más lo he necesitado. Por compartir conmigo tantas cosas y por sacarme siempre una sonrisa.

Finalmente, a mi familia por su comprensión, y apoyo incondicional durante todo este tiempo. Pero, sobre todo, gracias por todos los valores que me habéis transmitido y que me han hecho ser quien soy hoy y me han permitido alcanzar mis metas. Por todo ello siempre os estaré tremendamente agradecida.

A todos, ¡GRACIAS!

Esta tesis doctoral ha sido realizada con una ayuda predoctoral para la Formación de Profesorado Universitario (FPU12/02817) otorgada por el Ministerio de Educación, Cultura y Deporte (MECD), una ayuda para la realización de la estancia predoctoral del MECD, y mediante la financiación de varios proyectos de investigación que enumero a continuación. Proyecto I+D+I MAT2010-19249 concedido por el Ministerio de Ciencia e Innovación, Proyecto CTM2015-65348-C2-2-R concedido por el Ministerio de Economía y Competitividad, Proyecto A/032278/10 concedido por la Agencia Española de Cooperación Internacional, y varios proyectos concedidos por la Universidad Complutense de Madrid al grupo de investigación Membranas y Energías Renovables.

Contents

Abstract

Water scarcity is nowadays a worldwide problem that requires new water resources and more efficient separation treatment techniques. Membrane distillation (MD) is a non-isothermal process whose driving force is the transmembrane vapor pressure. In this process, non-volatile solutes can be removed from a wide variety of feed aqueous solutions due to the transport of vapor molecules through microporous and hydrophobic membranes. Owing to its various advantages, water desalination by MD is an environmentally-friendly alternative, which can tackle the water shortage issue.

The main challenge of MD is the design and preparation of improved membranes with suitable characteristics for this process. Hollow fiber is currently the most attractive membrane geometry for MD industrial implementation. Consequently, membrane engineers are endeavoring to develop novel hollow fiber membranes that meet the demanding MD requirements. In this PhD Thesis, advanced hollow fiber membranes have been prepared by the dry/wet or wet/wet spinning technique for desalination by MD. A comprehensive analysis of different spinning parameters effects on the membrane formation mechanism, characteristics and MD performance has been carried out.

The highly hydrophobic copolymer, poly(vinylidene fluoride-co-hexafluoropropylene) (PVDF-HFP), has been chosen for the preparation of the organic hollow fiber membranes. Prior membrane preparation, the type of solvent and the mixed solvent used to prepare the PVDF-HFP dope solution have been studied taking into account the characteristics of the dope solution, which dictates the coagulation kinetic and the thermodynamic precipitation of the membrane formation. The adequate mixed solvent was found when the dope solution became thermodynamically more stable and the coagulation rate of the membrane phase inversion was slower due to the increase of the viscosity of the dope solution. The hollow fiber membrane prepared under these conditions exhibited macro-void free and thick sponge-like structure, resulting in suitable characteristics for MD and high direct contact membrane distillation (DCMD) permeate flux.

Besides the improvement of the membrane cross-section morphology, it is necessary to prepare hollow fibers with more porous surfaces and without dense skin-layers. This objective has been achieved by using weak nonsolvents (i.e. solvent/water mixtures) as internal and external coagulants that have reduced the coagulation rate of the membrane phase inversion. The Hansen solubility parameter (HSP) distance has been a key factor to understand the coagulation power effect on the membrane formation mechanism. The limit of the nonsolvent composition has been determined in terms of membrane preparation viability. The highest

concentrations of solvent in both the internal and external coagulant mixtures have been found to be the most promising conditions for MD hollow fiber membrane preparation. The DCMD performance has been improved further when using weak nonsolvent mixtures as simultaneous internal and external coagulants.

The morphological structure of the prepared membranes has been predicted by the spinning solution characterization techniques and the HSP interactions of the copolymer-solvent-nonsolvent system. This demonstrates the usefulness and validity of the followed analysis to design promising MD membranes with a minimum number of experimental tests.

In order to overcome the temperature polarization phenomenon of MD, PVDF-HFP hollow fiber membranes with corrugated outer surfaces have been successfully prepared for the first time for MD application. A micro-engineered (star-shaped) triple-orifice spinneret, a novel fiber outer layer wetting mode (spray micro-jets), different gap distances and external coagulant flow rates have been employed. The degree of corrugation of the outer surface has been evaluated. It was found that the corrugations not only enhanced the effective surface area for condensation, but also acted as micro-turbulence promoters, reducing the temperature polarization and increasing the DCMD permeate flux as consequence. The hollow fiber membrane prepared by spraying the external coagulant with micro-jet nozzles along gap distance exhibited highly but irregularly corrugated outer surface, resulting in higher DCMD performance than the PVDF-HFP hollow fiber membranes proposed so far for MD.

Trying to benefit from the advantages of the excellent mechanical, thermal and chemical properties associated to ceramic membranes, alumina hollow fiber membranes with different morphological designs have been prepared by changing simultaneously various spinning parameters and inorganic suspensions. After sintering, the membranes have been successfully modified to be hydrophobic. The effects of the alumina hollow fiber membrane morphology on the MD membrane characteristics and on the air gap membrane distillation (AGMD) desalination performance have been studied. It was observed that the hollow fibers with long and numerous micro-channels along their cross-section were better than those with tight sponge-like structure, because the detected improvement of the AGMD transport. It is worth noting that the prepared alumina hollow fibers in this PhD Thesis exhibited excellent salt rejection factors and the highest obtained AGMD performance was better than other grafted alumina hollow fiber membranes used so far in desalination by AGMD and DCMD.

In conclusion, this PhD Thesis provides a comprehensive guideline for the design and preparation of advanced hollow fiber membranes for MD applications.

Resumen

La escasez de agua es un problema mundial que requiere encontrar nuevos recursos hídricos y técnicas de separación más eficientes. La destilación en membrana (DM) es un proceso no isotermo cuya fuerza motriz es la diferencia de presiones de vapor a través de la membrana. En este proceso los solutos no volátiles pueden ser extraídos de una gran variedad de disoluciones acuosas ya que solo los compuestos volátiles pueden atravesar la membrana microporosa e hidrófoba. Debido a las ventajas de esta tecnología, la desalación de aguas mediante DM es una alternativa respetuosa con el medio ambiente que puede hacer frente al problema de la demanda de agua que sufrimos en la actualidad.

El principal desafío de la DM es el diseño y la preparación de membranas con características adecuadas para este proceso. La membrana de fibra hueca es actualmente la geometría más atractiva para la implementación industrial de la DM. Por consiguiente, los expertos en membranas están esforzándose para desarrollar membranas novedosas de fibra hueca que cumplan los exigentes requisitos de este proceso. En esta tesis, se han preparado membranas avanzadas de fibra hueca mediante el método de hilatura de inversión de fase seco/mojado o mojado/mojado para la desalación por DM. Se ha llevado a cabo un análisis exhaustivo de los efectos de los diferentes parámetros de fabricación sobre el mecanismo de formación, las características de las membranas y su eficiencia en DM.

Se ha seleccionado un copolímero altamente hidrófobo, fluoruro de polivinilideno-co-hexafluoropropileno (PVDF-HFP), para la preparación de membranas de fibra hueca orgánicas. Previo a la fabricación, se ha estudiado el tipo de disolvente utilizado en la disolución copolimérica considerando las características de dicha disolución, las cuales dictaminan la cinética de la coagulación y la termodinámica de la precipitación durante la formación de la membrana. Se encontró el disolvente mixto adecuado que conseguía que la disolución copolimérica fuese termodinámicamente más estable y el ritmo de coagulación más lento debido a un incremento de la viscosidad de la misma. La membrana de fibra hueca preparada bajo estas condiciones exhibió una estructura libre de huecos, con zonas esponjosas anchas, obteniéndose un flujo de permeado alto en DM con contacto directo (DMCD).

Además de mejorar la morfología de la sección transversal de la membrana, también es necesario que las fibras huecas posean superficies más porosas. Este objetivo se ha logrado utilizando coagulantes débiles (mezclas de disolvente/agua) tanto internos como externos, los cuales redujeron el ritmo de la inversión de fase de la membrana. El parámetro de solubilidad de Hansen (PSH) ha sido un factor clave en la interpretación del efecto de la coagulación sobre el mecanismo de formación de la membrana. Se determinó la composición límite del

coagulante en función de la viabilidad en la fabricación de la membrana. Se concluyó que las concentraciones más altas de disolvente tanto en el coagulante interno como en el externo resultaron ser las más prometedoras para la preparación de membranas de fibra hueca para DM. La eficiencia en el proceso de DMCD mejoró aún más cuando se emplearon mezclas disolvente/agua como coagulante interno y externo de manera simultánea.

La estructura morfológica de las membranas preparadas fue predicha por las técnicas de caracterización de la disolución copolimérica y por las interacciones descritas por el PSH para el sistema copolímero-disolvente-coagulante. Esto demuestra la validez y la utilidad del procedimiento descrito para el diseño de membranas adecuadas para DM, minimizando el número de experimentos.

Con el fin de abordar el fenómeno de la polarización de temperaturas característico de la DM, se prepararon por primera vez membranas de fibra hueca de PVDF-HFP con superficies externas corrugadas. Se emplearon un hilador microestructurado de tres orificios (forma estrellada), un método novedoso de mojado para la parte externa de la fibra (micro-chorros de pulverización), diferentes distancias entre el hilador y el baño de coagulación, y distintos flujos de coagulante externo. El grado de corrugación de la superficie externa fue evaluado y se determinó que las corrugaciones no sólo mejoraron el área superficial efectiva de condensación sino que también actuaron como generadores de micro-turbulencias, reduciendo la polarización de temperaturas y aumentando el flujo de permeado en DMCD. La superficie de la membrana preparada mediante la pulverización del coagulante sobre la cara externa de la fibra resultó ser altamente corrugada e irregular, lo que proporcionó una eficiencia en DMCD superior a la de otras fibras de PVDF-HFP utilizadas hasta el momento.

Teniendo en cuenta las excelentes propiedades mecánicas, térmicas y químicas de las membranas cerámicas, se prepararon fibras huecas de alúmina con diferentes diseños morfológicos cambiando varios parámetros de fabricación incluida la suspensión inorgánica. Tras el proceso de sinterización, las membranas fueron modificadas con éxito convirtiéndolas en hidrófobas. Se estudiaron los efectos de la morfología de las membranas de alúmina sobre sus características estructurales y sobre su eficiencia en la desalación por DM con cámara de aire (DMCA). Se observó que las membranas que presentaron largos y numerosos microcanales en su sección transversal dieron mejores prestaciones en DMCA que las que poseían estructuras esponjosas compactas. Es importante destacar que las membranas de alúmina de fibra hueca preparadas en esta tesis exhibieron excelentes factores de separación y que la eficiencia más alta obtenida fue mejor que la hallada hasta el momento por otras membranas del mismo tipo empleadas en la desalación por DMCA y DMCD.

En conclusión, esta tesis doctoral proporciona una guía completa para el diseño y la preparación de membranas avanzadas de fibra hueca para aplicaciones en DM.

Publications, Research stay and Conferences

Publications derived from the PhD Thesis

1. Loreto García-Fernández, Carmen García-Payo, Mohamed Khayet, Hollow fiber membranes with different external corrugated surfaces for desalination by membrane distillation, Applied Surface Science 416 (2017) 932-946.

2. L. García-Fernández, Bo Wang, M.C. García-Payo, K. Li, M. Khayet, Morphological design of alumina hollow fiber membranes for desalination by air gap membrane distillation, Desalination (2017) Submitted, in revision.

3. L. García-Fernández, M.C. García-Payo, M. Khayet, Mechanism of formation of hollow fiber membranes for membrane distillation: 1. Inner coagulation power effect on morphological characteristics, Journal of Membrane Science (2017) In Press, Corrected Proof (http://dx.doi.org/10.1016/j.memsci.2017.03.036).

4. L. García-Fernández, M.C. García-Payo, M. Khayet, Mechanism of formation of hollow fiber membranes for membrane distillation: 2. Outer coagulation power effect on morphological characteristics, Journal of Membrane Science (2017) In Press, Corrected Proof (http://dx.doi.org/10.1016/j.memsci.2017.03.038).

5. L. García-Fernández, M.C. García-Payo, M. Khayet, Effects of mixed solvents on the structural morphology and membrane distillation performance of PVDF-HFP hollow fiber membranes, Journal of Membrane Science 468 (2014) 324-338.

Chapter book

6. L. García-Fernández, M. Khayet, M.C. García-Payo, Membranes used in membrane distillation: preparation and characterization, chapter 11 in book "Pervaporation, vapour permeation and membrane distillation: principles and applications", A. Basile, A. Figoli and M. Khayet, Elsevier (Imprint: Woodhead Publishing) (2015) 317-359, ISBN: 9781782422464.

Journal details: Impact factor (JCR 2015) / Quartile (category)

Applied Surface Science: 3.150 / Q1 (Materials Science, Coatings); Desalination: 4.412 / Q1 (Engineering, Chemical); Journal of Membrane Science: 5.557 / Q1 (Engineering, Chemical).

Other publications

7. M. Khayet, C. Cojocaru, M. Essalhi, M.C. García-Payo, P. Arribas, L. García-Fernández, Hollow fiber spinning experimental design and analysis of defects for fabrication of optimized membranes for membrane distillation, Desalination 287 (2012) 146-158.

8. M. Essalhi, L. Fernández, P. Arribas, M.C. García-Payo, M. Khayet, Spinning an optimized hollow fiber membrane for desalination by membrane distillation using experimental statistical designs, Procedia Engineeiring 44 (2012) 1786-1787.

9. M.C. García-Payo, M. Essalhi, M. Khayet, L. García-Fernández, K. Charfi y H. Arafat, Water desalination by membrane distillation using PVDF-HFP hollow fiber membranes, Membrane Water Treatment 1 (2010) 215-230.

Research stay

Host Institution: Imperial College London, Faculty of Engineering, Department of Chemical Engineering

Supervisor: Professor Kang Li

Temporary stay: from 15/01/16 to 15/04/16

Project: "Fabrication of hydrophobic ceramic hollow fiber membranes for membrane distillation"

Most of the hollow fiber membranes used in membrane distillation (MD) are prepared with polymeric materials. However, very few research studies have been performed so far, using ceramic materials although these exhibit excellent chemical, thermal and structural characteristics. Therefore, the main objective of this research project is to develop ceramic hollow fiber membranes with good MD performance. In order to use ceramic membranes in MD process, these should be hydrophobic and porous.

Conferences

1. L.García-Fernández, M. Khayet, M.C. García-Payo, Design of hollow fiber membranes for membrane distillation applications, Poster, Leading edge technologies for the removal of emerging pollutants, November 2016, Madrid, Spain.

2. Loreto García-Fernández, Paula Arribas, Carmen García-Payo and Mohamed Khayet, Thermodynamic and kinetic effects on the fabrication of hydrophobic porous membranes for membrane distillation, Poster, 12th International Meeting on Thermodiffusion, May - June 2016, Madrid (Spain). Poster award.

3. L. García-Fernández, M.C. García-Payo, M. Khayet, Thermodynamic and kinetic study of copolymeric dope solutions and their effects on the structure and morphology of hollow fiber membranes (in Spanish), Oral communication, Biennial Meeting of the Royal Spanish Society of Physics, July 2015, Gijón (Spain).

4. L. García-Fernández, M.C. García-Payo, M. Khayet, Modification of the morphological characteristics of membrane distillation hollow fibers via internal and external mixed coagulants, Poster, Euromembrane 2015, September 2015, Aachen (Germany). European Membrane Society travel grant award.

5. L. García-Fernández, M. Essalhi, M.C. García-Payo, M. Khayet, Energy efficiency study of air gap membrane distillation using polymeric hollow fiber membranes (in Spanish), Oral communication, XXXIV Biennial Meeting of the Royal Spanish Society of Physics, July 2013, Valencia (Spain).

6. L. García-Fernández, M.C. García-Payo, M. Khayet, Influence of solvent and internal coagulant on the structural characteristics and desalination performance of hollow fiber membranes prepared for membrane distillation, Oral communication, 1st International Conference on Desalination using Membrane Technology, April 2013, Sitges (Spain).

7. M. Essalhi, L. García-Fernández, P. Arribas, M.C. García-Payo, M. Khayet, Spinning an optimized hollow fiber membrane for desalination by membrane distillation using experimental statistical designs, Poster, Euromembrane 2012, September 2012, London (UK).

8. L. García-Fernández, P. Arribas, M.C. García-Payo, M. Khayet, Effects of solvent type on the structural morphology and membrane distillation performance of PVDF-HFP hollow fiber membranes, Poster, International Workshop on Membrane Distillation and Related Technologies, October 2011, Ravello (Italy).

9. L. García-Fernández, M.C. García-Payo, M. Khayet, Solvent and internal coagulant effect in hollow fibers for membrane distillation (in Spanish), Oral communication, XXXIII Biennial Meeting of the Royal Spanish Society of Physics, September 2011, Santander (Spain).

1

Introduction

1.1 Membrane distillation: general description, fundamentals and membrane requirements

1.2 Membranes used in membrane distillation: preparation and characterization

1.3 Development of hollow fiber membranes: motivation and objectives

1.1 Membrane distillation: general description, fundamentals and membrane requirements

1.1.1 General description

Membrane distillation (MD) is a non-isothermal separation process whose driven force is the transmembrane vapor pressure (ΔP_v). This technology is useful to remove non-volatile solutes from a broader variety of feed liquids to be treated, commonly salt aqueous solutions. In this process, vapor is transported through a microporous omniphobic membrane [1]. The omniphobicity prevents both water (i.e. hydrohobicity) and liquids with different surface tension to penetrate into the membrane pores [2, 3], while the porosity is required for vapor permeation. Both heat and mass are simultaneously transferred through the membrane, which stands the liquid/vapor interface at the pore entrance (see Fig. 1.1.1) [4].

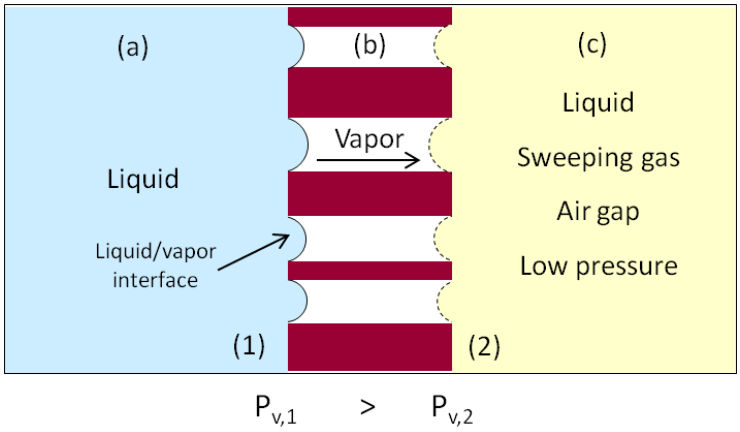

Fig.1.1.1. Liquid/vapor interface and MD transport.

The mass transport can be described as follows (see Fig. 1.1.1): First, the volatile component of the feed solution to be treated is evaporated at the feed side of the membrane (a), subsequently the vapor molecules are transported through the membrane pores due to the pressure vapor difference (i.e. the transmembrane driving force) (b), and finally it is condensed at the other side of the membrane (c). The feed solution is maintained always in direct contact with the selective side of the membrane (1), which is kept at a higher vapor pressure ($P_{v,1}$), while in the permeate side of the membrane (2), the lower vapor pressure ($P_{v,2}$) can be applied

by means of different methods [1, 5-7]. According to the selected technology, there are different MD configurations (see Fig. 1.1.2) [1, 5, 8, 9]:

- Direct Contact Membrane Distillation (DCMD) (see Fig. 1.1.2 (a)): A hot solution is brought in direct contact with the feed side of the membrane while a colder liquid solution is maintained in its permeate side. Both the feed and permeate aqueous solutions are circulated tangentially to the membrane surfaces. In this configuration the vapor pressure difference is induced by the transmembrane temperature difference. The feed volatile molecules evaporate at the hot liquid/vapor interface cross the membrane pores in vapor phase and then condense in the cold liquid/vapor interface inside the membrane module. The main disadvantage of this configuration is the heat loss by conduction through the membrane.

- Sweeping Gas Membrane Distillation (SGMD) (see Fig. 1.1.2 (b)): A cold inert gas is used to sweep the vapor at the permeate side of the membrane carrying it outside the membrane module for condensation. In this configuration, owing to the heat transferred through the membrane (i.e. from feed towards the permeate side), the sweeping gas temperature increases considerably along the membrane module length. Therefore, the gas temperature should be reduced in order to increase the efficiency of the process by placing a cold wall in the permeate side (see Fig. 1.1.2 (c)). This SGMD variant is called thermostatic sweeping gas membrane distillation (TSGMD). In general, the SGMD configuration exhibits a high temperature polarization effect, which is reduced by its alternative variant TSGMD.

- Air Gap Membrane Distillation (AGMD): A stagnant air gap is introduced between the membrane and the condensation surface, as can be seen in Fig. 1.1.2 (d). The evaporated molecules cross both the membrane pores and the air gap to finally condense on the cold surface inside the membrane module. This configuration reduces both the membrane wetting risk and heat loss by conduction through the membrane. However, the air gap represents an additional resistance to mass transfer. If the space between the membrane and the cold surface is filled with liquid, the process is termed liquid gap membrane distillation (LGMD) (see Fig. 1.1.2 (e)). Compared to AGMD, this variant involves higher heat loss by conduction through the membrane.

- Vacuum Membrane Distillation (VMD): In this configuration (see Fig. 1.1.2 (f)), vacuum is applied in the permeate side of the membrane module. The vacuum pressure must be lower than the saturation pressure of the volatile molecules of the feed solution. In this case, condensation of the evaporated molecules at the liquid/vapor interface is carried out outside of the membrane module. The main drawback of this configuration is the high risk of membrane pore wetting. On the contrary, the heat lost by conduction is insignificant.

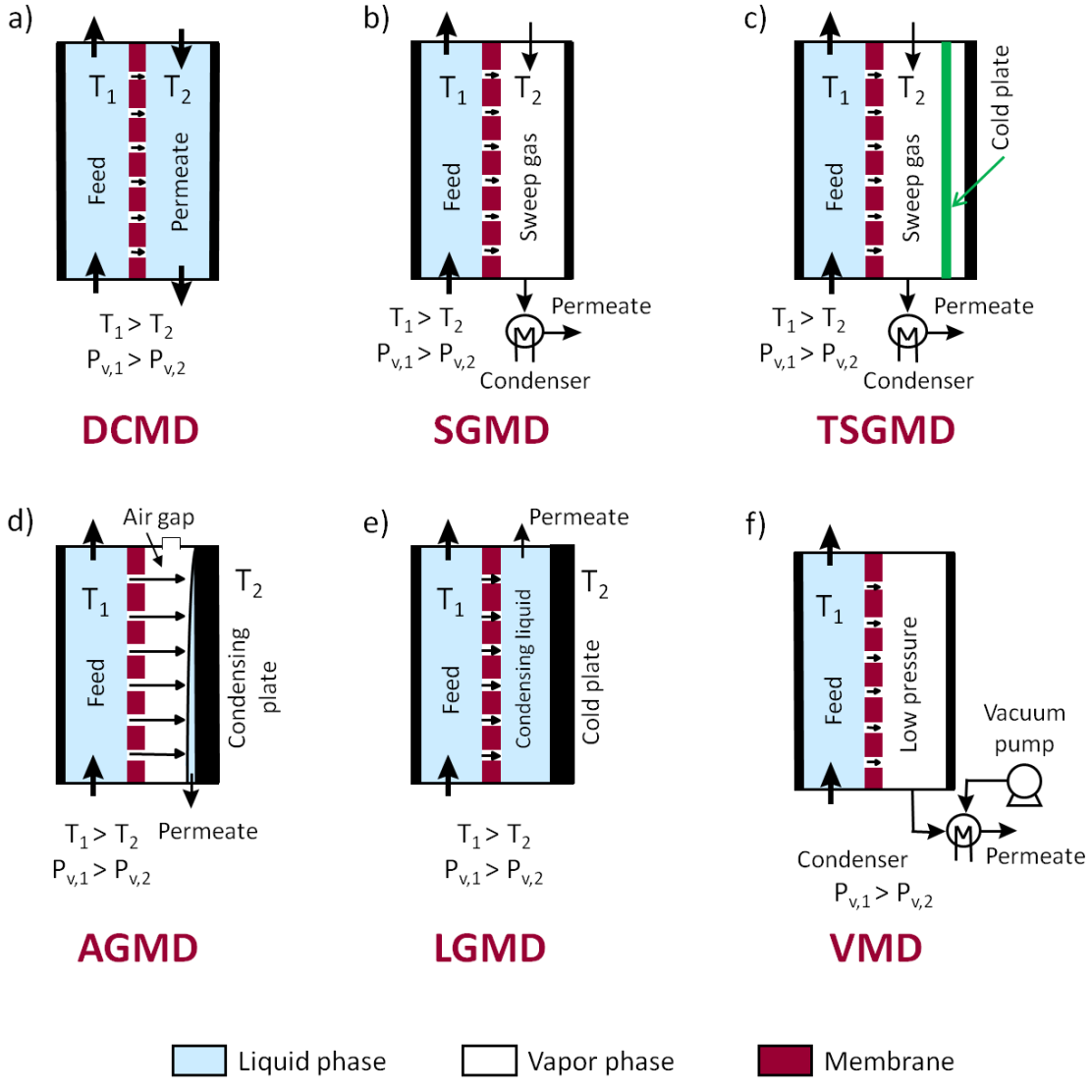

Fig. 1.1.2. MD configurations.

It must be pointed out that the MD separation technique has received increasing attention in the recent years owing to the following advantages [1, 5, 9, 10]:

- A high retention of non-volatile solutes, close to 100%.
- Operating temperatures lower than conventional distillation technologies.
- Operating hydrostatic pressures lower than the pressure-driven membrane process, and consequently less demanded membrane mechanical properties.
- Possibility to treat brine or high concentrated saline solutions near saturation concentration, for which other conventional separation techniques are seriously limited, permitting therefore to avoid brine discharge to the environment.
- Possibility to use waste heat or alternative energy sources, such us solar and geothermal energy.
- Possibility to be combined with other separation techniques (i.e. hybrid systems) to improve either the water quality or efficiency of the whole hybrid system.

In accordance with this characteristics, water desalination by MD is an environmentally-friendly alternative capable to tackle the global water shortage in combination with other water treatment techniques and by using renewable/waste energy sources [9-13]. In addition to desalination, other emerging MD applications have been reported in the literature [14].

Coupling solar energy systems (i.e. solar thermal collectors and photovoltaic panels) to MD process is totally feasible taking into consideration the MD requirements (i.e. low temperature and electric power). The resultant technology is named solar-powered membrane distillation (SPMD) and its applicability interest in desalination is growing worldwide. Not only the SPMD systems are eco-friendly and reduce the MD energy consumption, but also small scale and portable SPMD units can sort out the freshwater necessity in remote arid areas [10, 12].

Pressure driven separation process such as reverse osmosis (RO), forward osmosis (FO) and micro/ultra/nanofiltration (MF, UF, NF), as well as, conventional separation technology (i.e. distillation, precipitation, crystallization, photocatalysis, multi-effect distillation (MED)) may be combined with MD process. The formed hybrid MD systems can enhance both mass and energy efficiency as well as the economical performance of the global separation process, maintaining the high water productivity and quality, improving the water total recovery and reducing the environmental emissions [1, 9]. Combining desalination processes in a hybrid system (i.e. RO-MD, FO-MD, NF-MD, MED-MD) tends to pursue two aims mainly: purifying even more the permeate or concentrating even more the retentate. It is worth quoting that MD is considered the most preferred technology for hybrid system implementation [9, 13]. In fact, compared to other membrane separation processes, MD is less

affected by the salt concentration of the feed solution because it can be operated concentrating saline solutions up to saturation [15]. This makes the recovering of valuable solutes dissolved in aqueous solutions viable by means of a crystallizer (i.e. MD-crystallizer integrated system, MDC) and avoids brine discharge to the environment [16, 17].

Notwithstanding the great potential of MD process, its commercialization is still under consideration limited mainly by the lack of commercial membranes specifically designed for this process [1, 5]. Currently, the available commercial membranes are designed for other processes such as the hydrophobic microfiltration membranes. These meet the basic requirements of an MD membrane (i.e. hydrophobic and microporous). Nevertheless, advanced membranes with improved characteristics are needed in order to enhance the MD performance making this technology more competitive [4, 6].

1.1.2 Fundamentals and membrane requirements

Suitable MD membranes should satisfy certain demanding features according to the mechanisms of mass and heat transport through the membrane [6, 7, 14], which can be briefly described as follows [4, 8, 18].

1.1.2.1 Mass transport

The MD permeate flux (J) can be easily calculated from the produced water mass (Δm) per unit of membrane surface area (A_m) during certain period of time (Δt) (Eq. (1.1.1)). This experimental result is associated to the transport of the vapor molecules through the membrane pores and it is related to the process driving force (ΔP_v) and to the mass transfer coefficient (C_m) (Eq. (1.1.2)).

$$J = \frac{\Delta m}{A_m \, \Delta t} \tag{1.1.1}$$

$$J = C_m \, \Delta P_v \tag{1.1.2}$$

where C_m depends on the membrane properties as shown in the following general relationship:

$$C_m \sim \frac{\varepsilon \, r_p^{\,n}}{\tau \, \delta} \tag{1.1.3}$$

where ε is the membrane porosity, τ is the tortuosity of the membrane pores, δ is the membrane thickness and r_p is the mean pore radius, with n = 0, 1 or 2 for molecular diffusion, Knudsen diffusion and viscous type of flow, respectively. The Knudsen number (Kn) determines the main mechanism of transport as it represents the ratio of the mean free path (λ) of the molecules to the pore diameter (d_p) (see Fig. 1.1.3). It is worth noting that the global

MD mechanism of transport not only is determined by the type of transport of the vapor molecules through the membrane, but it also depends on the used MD configuration [14, 18].

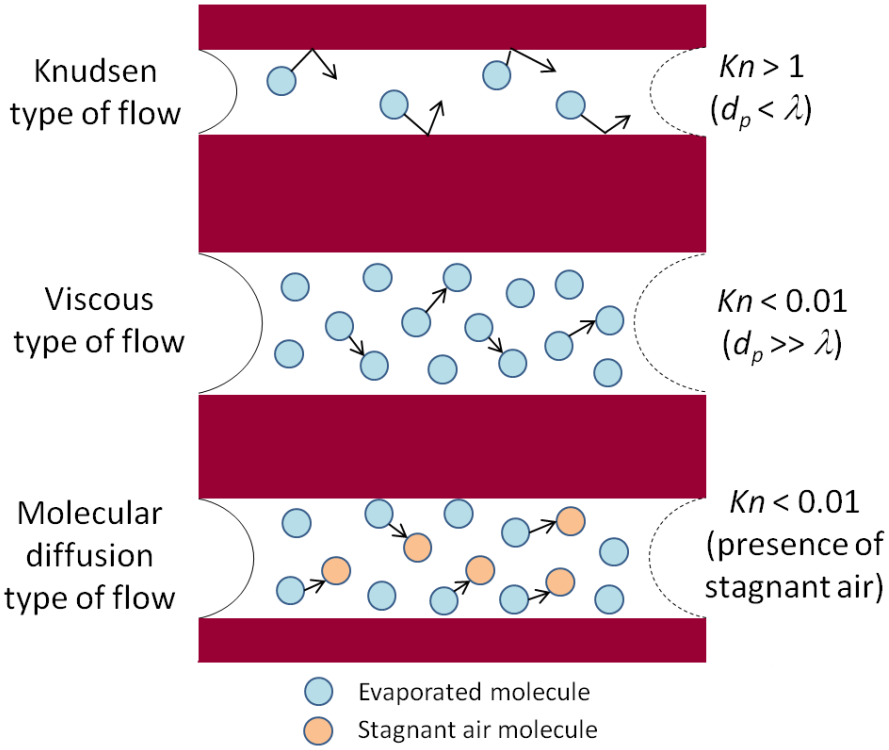

Fig. 1.1.3. Schema of the mass transport mechanisms through a pore of an MD membrane.

1.1.2.2 Heat transport

Simultaneously to the mass transport, the heat transfer through the membrane (Q_m) takes place during MD process by two main contributions: i) the latent heat associated to the vapor flux (Q_J) and ii) the heat loss by conduction following the Fourier´s low (Q_C):

$$Q_m = Q_J + Q_C \tag{1.1.4}$$

$$Q_m = J\,\Delta H_w + \frac{k_m}{\delta}\left(T_{f,m} - T_{p,m}\right) \tag{1.1.5}$$

where ΔH_w is the enthalpy of water vaporization, $T_{f,m}$ is the feed temperature at the membrane surface, $T_{p,m}$ is the permeate temperature at the membrane surface and k_m is the thermal conductivity of the membrane, which can be expressed as follows.

$$k_m = \varepsilon\, k_g + (1 - \varepsilon)\, k_s \tag{1.1.6}$$

where k_g and k_s are the thermal conductivities of the gas-filled pores and the solid matrix of the membrane, respectively.

1.1.2.3 Polarization phenomena

Both mass and heat transfer are affected by the temperature and concentration polarization effects, which reduce the efficiency of the MD process. Due to the heat transfer by conduction through the membrane and the applied fluid flow regimes, which are mostly laminar, the temperature at the membrane surface ($T_{m,f}$ and $T_{m,p}$) is different from that of the bulk fluids ($T_{b,f}$ and $T_{b,p}$), leading to a lower effective temperature gradient through the membrane. The same polarization phenomenon takes place with the concentration of the feed at the membrane surface ($C_{m,f}$), which is different from that at the bulk liquid solution ($C_{b,f}$). These phenomena affect the effective ΔP_v (i.e. MD driving force) and the permeate flux as consequence.

The temperature and concentration polarization coefficients (*TPC* and *CPC*, respectively) can be calculated by the following equations (1.1.7) and (1.1.8):

$$TPC = \frac{T_{m,f} - T_{m,p}}{T_{b,f} - T_{b,p}} \; 100 \tag{1.1.7}$$

$$CPC = \frac{C_{m,f}}{C_{b,f}} \tag{1.1.8}$$

Both phenomena can be simultaneously taken into consideration and expressed in a single coefficient, the vapor pressure polarization (*VPC*). It represents the percentage of the applied transmembrane driving force that contributes to the effective mass transport by the following equation:

$$VPC = \frac{\Delta P_{v,m}}{\Delta P_{v,b}} \; 100 \tag{1.1.9}$$

where $\Delta P_{v,m}$ is the vapor pressure difference between the feed and permeate at the membrane surface and $\Delta P_{v,b}$ is the bulk vapor pressure difference.

1.1.2.4 Membrane requirements

As described previously, both mass and heat transport depend directly on the membrane properties. Therefore, suitable MD membranes must meet specific characteristics that maximize the mass transport and minimize the heat transfer [1, 4, 6-8, 14]:

- The material of the membrane matrix must be hydrophobic and exhibits excellent thermal stability (i.e. temperatures as high as 100 °C), good chemical resistance to a wide variety of feed solutions and an adequate mechanical stability. It is highly recommended that the membrane surface be omniphobic in order to extend the MD applicability to other feed solutions with lower surface tension than water.

- Apart from the hydrophobicity of the material, the membrane should be highly wetting resistant (i.e. high liquid entry pressure, *LEP*). *LEP* is defined as the highest applied transmembrane pressure on a liquid solution before this penetrates into the pores. It should be as high as possible to prevent the wetting of the membrane pores, and be always greater than the applied MD operating pressure. In order to achieve a high *LEP*, the membrane should have a small maximum pore size, its material should have low surface energy or which is the same its surface should be very omniphobic (i.e. large contact angle to water and feed solutions).

- The pore size may be within several nanometers and few micrometers. This parameter affects mass transport (i.e. the permeate flux increases with the increase of r_p, and depends on the mechanism of mass transport, see C_m dependence in Eq. (1.1.3)). However, it is necessary a compromise between a high permeate flux and a high *LEP* (i.e. small maximum pore size means small mean pore size). Moreover, the pore size distribution should be as narrow as possible in order to prevent the wetting risk of the membrane.

- The tortuosity factor (i.e. deviation of the pore structure from straight cylindrical pores normal to the surface) should be low as it is inversely proportional to the MD membrane permeability (see Eq. (1.1.3)). This factor is difficult to measure and a value of two is commonly considered for permeate flux predictions.

- The thickness should be optimized as it is inversely proportional to the mass and heat transport by conduction through the membrane (see Eqs. (1.1.3) and (1.1.5)). The reduction of the membrane thickness leads to an increase of the permeate flux whereas the thermal driving force is also reduced due to the increase of the heat loss by conduction through the membrane. A balance between the mass and the heat transfer fluxes is needed to properly adjust the membrane thickness.

- The porosity of the membrane (i.e. void volume fraction accessible to MD vapor flux) should be as high as possible as long as its mechanical integrity is maintained to be packed in modules. High porosity reduces the thermal conductivity coefficient of the membrane and increases the mass transport (i.e. low heat loss by conduction through the membrane and high thermal driving force are obtained as can be seen in Eqs. (1.1.5) and (1.1.6) and Eq. (1.1.3), respectively).

- The thermal conductivity of the membrane should be as low as possible (see Eq. (1.1.5)). In order to meet this requirement, it is necessary that the membrane material has a low thermal conductivity and the membrane has a high porosity (see Eq. (1.1.6)). The thermal conductivity coefficients of the gases entrapped in the

pores are an order of magnitude smaller than that of the majority of the polymers used in membrane preparation. Most of the hydrophobic polymers have similar thermal conductivities. Therefore, high porosities are required to decrease the heat transfer by conduction through the membrane. This is perfectly in accordance with the MD permeability enhancement condition, Eq. (1.1.3).

- It is advisable that the feed surface of the membrane to be highly fouling resistance. MD fouling effect is not as strong as it is in pressure-driven membrane processes. However, membrane surface modification could be necessary if certain types of feed solutions must be treated.
- The membrane should have a long operating life with stable MD performance (i.e. permeate flux and selectivity).

The new MD membranes should fulfill all the aforementioned features to achieve optimal morphological structures that lead to high permeate fluxes and rejection factors together with high thermal efficiencies.

1.2 Membranes used in membrane distillation: preparation and characterization

1.2.1 Introduction

Membrane distillation (MD) technology has been receiving a great deal of interest since 2000 because of its important advantages as already described in detail in the previous chapter. In contrast to other widely used membrane technologies not only at laboratory scale but also at industrial level, e.g., the pressure-driven membrane processes, MD is based on a nonisothermal separation in which only volatile molecules are transported through microporous hydrophobic membranes as the driving force the partial vapour pressure of the species present in the feed aqueous solution [1]. In this technology, both heat and mass transfer take place simultaneously through the membrane and the driving force can be applied following different configurations: direct contact MD (DCMD), sweeping gas MD (SGMD), thermostatic SGMD (TSGMD), air gap MD (AGMD), liquid gap MD (LGMD) and vacuum MD (VMD) [1, 4, 5, 8] .

Although the application of MD technology is considered in different fields, providing good and valuable results, e.g., desalination, its commercial and industrial implementation is limited by some factors [1]. The most significant one is the unavailability of commercial membranes and modules specifically designed for MD in order to guarantee the long-term application of the process with stable permeability, high performance, low conductive heat transfer, and high resistance to scaling, fouling and wetting [1, 5, 19]. An area of emerging scientific research in membrane science and technology is the design and development of advanced membranes for MD. Figure 1.2.1 shows the growing interest on both MD technology, in general, and membrane engineering for MD in particular. Up to 31 December 2013, among the total studies published each year on MD, those reported on the development of membranes for MD varied between 6.5 and 37.8 % with an average value of 23.0 %.

As already outlined in our previous studies [1, 4], the key membrane characteristics of an adequate MD membrane are the high porosity, hydrophobicity, and liquid entry pressure (*LEP*) in the pores, narrow pore size distribution, optimum thickness, small tortuosity of pores, low thermal conductivity, good and long-term thermal stability, and excellent chemical resistances.

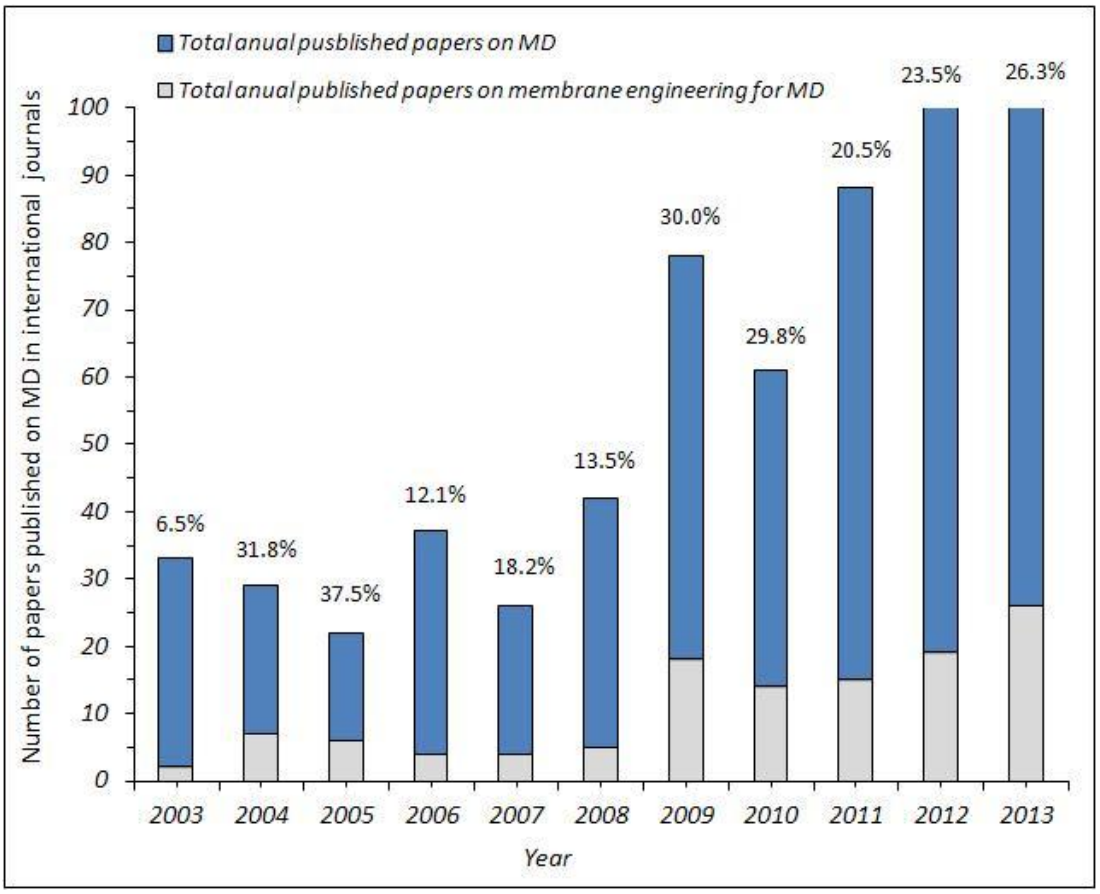

Fig. 1.2.1. Research interests in membrane distillation (MD) in general and membrane engineering for MD applications up to 31 December 2013.
This figure is an updated version of a figure adapted with permission from Khayet [4] ©2011 Elsevier B.V.

The MD performance not only depends on the membrane itself but it is also affected by the module design, the MD configuration and the applied operating conditions. Various types of membrane modules were proposed and tested in each MD configuration. Those are plate-and-frame modules, shell-and-tube or tubular modules, and spiral wound membrane modules. An adequate MD module should exhibit high membrane packing density, high permeate product rate, low temperature and concentration polarization effects, low fluid pressure drop, low external heat loss, etc. [1].

This chapter book gives a thorough report on the materials used so far for MD membrane fabrication and modification. Then, necessary membrane characterization techniques for MD are summarized and discussed. Different membrane modules proposed in MD are discussed. Finally, future trends and useful sources for more details are included.

1.2.2 Materials for membrane distillation (MD) membranes

Although it is believed that the membranes used in MD act only as a support of the vapor/liquid equilibrium and are not involved in mass transport, some interesting experimental and theoretical research studies [20-24] were performed on the effects of the membrane materials on the MD performance (i.e. selectivity) showing their influence in specific MD applications, treatment of aqueous solutions containing volatile organic compounds (VOCs) such as chloroform, alcohols and acids. The MD separation performance is not only based on vapor/liquid equilibrium of the involved components in the feed aqueous solution but also on the thermodynamics effects (affinity and interaction effects between these components and the membrane material) and kinetic effects (diffusion of these components through the membrane). Providing that the major application of MD is desalination and water is the major transferred component through the membrane, which should exhibit high porosity (i.e. void volume fraction), the major required characteristic of the membrane material is its high hydrophobicity. Therefore, mass transport through the membrane material is generally neglected.

In general, few porous and hydrophobic membranes prepared with different materials (polytetrafluoroethylene, PTFE; polypropylene, PP; polyvinylidene fluoride, PVDF) are available in the market (Gelman, Osmonics, Gore, Enka, Millipore, etc.) for their use in MD applications although these membranes are proposed for other membrane processes (microfiltration, MF and ultrafiltration, UF) [4]. These membranes are often selected based on their morphological characteristics and not on the material used for their preparation. The most selected ones are PTFE membranes. This selection is based on their higher hydropobicity and *LEP* of water inside the membrane pores, although PVDF exhibits a good processability in different solvents. PP and PTFE, however, can only be processed at temperatures higher than their melting temperature. PVDF membranes are usually prepared by the phase inversion method, whereas PP membranes by stretching and PTFE membranes by complicated extrusion, sintering, or stretching procedures. Table 1.2.1 summarizes the most used commercial membranes in MD together with different membranes fabricated or modified for MD process [1, 4, 5, 8].

As stated above, some worldwide research groups are focusing their investigations on the design, fabrication, and modification of membranes for MD. The materials for the preparation of MD membrane should be selected according to various criteria including their high chemical resistance to a wide number of compounds present in wastewaters, low cost, ease of manipulation and assembly, high thermal resistance, and low thermal conductivity. It must be pointed out that the most proposed MD membranes are polymeric and the most commonly used technique for their fabrication is the well-known simple phase inversion for

Table 1.2.1. Reported membrane distillation (MD) permeate fluxes of different types of commercial, fabricated and modified flat sheet (FS) and hollow fiber (HF) membranes.

Membrane	MD configuration	Feed solution composition	Feed inlet temperature (ºC)	Permeate flux (kg/m²h)	Reference
Commercial Millipore® PVDF: GVHP	DCMD	Distilled water	90.7	48.7	[25]
Commercial Millipore® PVDF: HVHP	Deaeration DCMD	Distilled water 14 - 25 wt% NaCl	80	67 59 - 40	[26]
Commercial Gelman® PTFE: TF200	DCMD	Distilled water	80.1	67.3	[25]
Commercial Gelman® PTFE: TF450	AGMD	30 g/L NaCl	71	51.1	[27]
Commercial Osmonics® Corporation PTFE: TS45	DCMD	0.6 g/L	60	80	[28]
PVDF FS composite	DCMD	3.5 wt% NaCl	80.5	47.6	[29]
PEI FS composite (SMM modified)	DCMD AGMD	Distilled water	80	41.6 14.9	[30]
PES FS (plasma modified)	DCMD	4 wt% NaCl	74.5	40.9	[31]
PVDF ENMs	DCMD	Distilled water 12 - 30 - 60 g/L NaCl	80	54.72 54 - 53 - 49	[32]
PVDF ENMs	AGMD	1 - 3.5 - 6 wt% NaCl	82	11.6-11.1-10.2	[33]
PVDF ENMs (heat-press posttreatment)	DCMD	3.5 wt% NaCl	50	21	[34]
PVDF ENMs (integrally modified)	DCMD	3.5 wt% NaCl	60	31.6	[35]
PVDF-HFP electrospun (hot pressed 2 layers)	DCMD	10 g/L table salt aqueous solution	65	20-22	[36]
Matrimid® ENMs	DCMD	Seawater	80	56	[37]
F-PT electrospun	DCMD	Red Sea water	80	85	[38]
Triple layer (H/h)[a] PVDF flat composite	AGMD	3.5 wt% NaCl	80	15.2	[39]
Commercial Accurel® PP S6/2 HF	DCMD	Tap water	90	33.3	[40]
Commercial Accurel® GmbH PP HF	DCMD	1.0 wt% NaCl	90	41.4	[41]
Modified PP MXFR 3 HF	DCMD	1.0 wt% NaCl	90	78.8	[41]
PVDF HF (additive AMAL)	DCMD VMD	Double distilled water	70 50	21.78 41.78	[42]
PVDF HF (ultrathin skin)	DCMD	3.5 wt.% NaCl	79.3	41.5	[43]
PVDF HF (macrovoid-free)	DCMD	3.5 wt% NaCl	80	67	[44]
PVDF HF (via TIPS)	DCMD	3.5 wt% NaCl	90	51.5	[45]
PVDF capillary HF	DCMD	1000 ppm NaCl	85	37.3	[19]
PVDF HF	VMD DCMD	9 wt% NaCl	65	~ 23.7 ~ 16	[46]
PVDF HF	DCMD	5 mg/L NaF	80	35.6	[47]
PVDF HF	DCMD	3.5 wt% NaCl	79.5	46.1	[48]
PVDF-PTFE HF	DCMD	3.5 wt% NaCl	79.5	40.4	[48]
PVDF/Cloisite clay HF	DCMD	3.5 wt% NaCl	81.5	79.2	[49]
PES HF (plasma modified)	DCMD	4 wt% NaCl	73.8	66.7	[31]
Alumina HF	VMD	4 wt% NaCl	80	42.9	[50]

Silicon nitride HF	VMD DCMD	4 wt.% NaCl	70	22.4 7.8	[51]
Dual-layer (H/h)[a] PVDF HF (clay particles in both layers)	DCMD	3.5 wt% NaCl	90.3	55.2	[52]
Dual-layer (H/h)[a] PVDF/PAN HF (clay particles)	DCMD	3.5 wt% NaCl	86	70.1	[53]
Dual-layer (H/h)[a] PVDF HF (graphite/MWCNTs in hydrophilic layer)	DCMD	3.5 wt% NaCl	80.4	66.9	[54]
Dual-layer (H/h)[a] PVDF HF (methanol additive in hydrophobic layer)	DCMD	3.5 wt% NaCl	80	83.4	[55]
Dual-layer (H/H)[b] PVDF HF (PTFE particles in outer layer)	DCMD	3.5 wt% NaCl	80	50.9	[56]
Dual-layer (H/H)[b] PVDF HF (higher desalination)	DCMD	3.5 wt% NaCl	79.8	98.6	[57]

[a]H/h: hydrophobic/hydrophilic.

[b]H/H: hydrophobic/hydrophobic.

flat sheet, tubular and hollow fiber (HF) membrane preparation [1]. In what follows, the suitable materials involved in this technique are described.

The polymer type directly affects the membrane hydrophobicity. Apart from the chemical nature of the polymer, its concentration in the dope solution is an important factor affecting the membrane characteristics. This effect was widely studied [58-60]. It was observed that the reduction of the polymer concentration improved the porosity, surface pore size and MD permeate flux. However, care must be taken because low polymer concentration reduced the membrane mechanical properties and the *LEP* in the membrane pores. The membrane structure changed from a finger-like structure to a sponge-like structure with the increase of the polymer concentration in the spinning solution due to the reduction of the coagulation rate [58].

The polymer-solvent interaction and solvent-nonsolvent interaction are also key parameters affecting the membrane structure. To select the most appropriate solvent(s) for a given polymer, these interactions are mainly evaluated by the solubility parameters, viscosity, diffusivity, and thermodynamic properties [61, 62]. Different single solvents such as N-methyl-2-pyrrolidone (NMP), N,N-dimethylformamide (DMF), N,N-dimethylacetamide (DMAC), triethyl phosphate (TEP), or mixed solvents such as NMP/tetrahydrofuran (THF), NMP/acetone [63], trimethyl phosphate/DMAC, TEP/DMAC have been considered.

Organic or inorganic additives are introduced in the polymer solution in order to modify the membrane morphology, induce pores in the membrane matrix, improve pores interconnections and, as a result, increase the MD performance. It is worth noting that the incorporation of additives in the polymer solution usually increases its viscosity [64] and

changes both the kinetic and the thermodynamic properties of the coagulation process affecting the final membrane structure. In order to study the polymer coagulation rate and the initiation time of phase separation different techniques can be employed, such as direct light microscopy observation [65, 66] or light transmittance experiment [65, 67, 68]. On the other hand, the solvent evaporation test can be determined gravimetrically by measuring the weight change of the cast film with time [69].

Different types of additives have been used for preparation of membranes for MD. These are inorganic salts (i.e lithium chloride, lithium perchlorate, etc.), polymeric additives (i.e polyvinylpyrrolidone, poly(ethylene glycol), PEG, etc.) or any other type of nonsolvent additive capable of increasing both the pore size and the porosity of the prepared membranes [42, 69-71].

Recently, fluoro-copolymers such as poly(vinylidene fluoride-co-tetrafluoroethylene) (P(VDF-co-TFE)), poly(vinylidene fluoride-co-chlorotrifluoroethylene) (P(VDF-co-CTFE)), poly(tetrafluroethylene-co-hexafluoropropylene) (FEP), poly(ethylene chlorotrifluoroethylene) (ECTFE), poly(vinylidene fluoride-co-hexafluoropropylene) (PVDF-HFP), Hyflon® AD, Teflon® AF and Cytop® have been proposed as novel materials for MD membrane fabrication [72]. PVDF-HFP shows higher hydrophobicity than PVDF due the hexafluoropropylene (HFP) group, which increases the fluorine content of the copolymer [71, 73]. Unlike PTFE, P(VDF-co-TFE) can be dissolved in common solvents and therefore it can be used for the preparation of phase inversion membranes [74]. ECTFE and FEP, which is a random copolymer of tetrafluoroethylene (TFE) with HFP, are easier to process than PTFE. Moreover, ECTFE is more hydrophobic than PTFE and exhibits excellent chemical and thermal stabilities than PVDF.

Another material, Matrimid®, has been used recently to prepare electrospun nanofibrous membranes (ENMs) for desalination by MD [37]. These membranes showed high water vapor flux and salt rejection factors (Table 1.2.1), attributed to their high void volume fraction, interconnectivity, and hydrophobicity.

Maab et al. [38] synthesized aromatic fluorinated polyoxadiazoles, polyoxadiazole copolymer, and fluorinated polytriazoles (F-PT) for the preparation of MD membranes by electrospinning and phase inversion. The prepared F-PT ENM exhibited the highest permeate flux obtained so far in the MD literature using ENMs with a salt rejection factor higher than 99.95% (Table 1.2.1).

Compared to the polymeric membranes, ceramic membranes can tolerate aggressive environments because of their excellent chemical, structural, and thermal stabilities. Metal oxides of alumina, zirconia, silica, and titania are commonly used materials in MD [50, 75]. The problem is that ceramic membranes are hydrophilic in nature and it is necessary to

modify them to be hydrophobic following different tedious surface modification techniques [51, 75]. Fang et al. [50] developed a novel hydrophobic porous alumina ceramic hollow fiber membrane by a phase inversion and sintering method for desalination by MD process. When using a feed salt aqueous solution of 4 wt% sodium chloride (NaCl) at 80 ºC and a vacuum pressure of 4 kPa applied in the lumen side of the hollow fibers, a water permeate flux as high as 42.9 L/m^{2}h was achieved with a salt rejection factor over 99.5 %, which was comparable to polymeric membranes (Table 1.2.1).

Different types of fluorinated surface modifying macromolecules (SMMs) were blended into hydrophilic polymers (polyetherimide, PEI, polysulfone, polyethersulfone, PES, etc.) to prepare porous composite hydrophobic/hydrophilic membranes for MD by phase inversion technique [30, 76-78]. During membrane formation, SMMs migrate to the polymer/air interface (i.e. top flat sheet membrane surface; Fig. 1.2.2) rendering it more hydrophobic. This type of membrane proved to be good membranes for DCMD [30] (Table 1.2.1) because they combine the low resistance to mass transport, achieved by the reduction of the water vapor transport path (i.e. thin hydrophobic top layer), and the low conductive heat loss through the whole membrane due to the thicker hydrophilic bottom layer [30, 77, 79]. Moreover, these membranes were successfully tested for processing low-and medium-level radioactive aqueous solutions by the MD process [80].

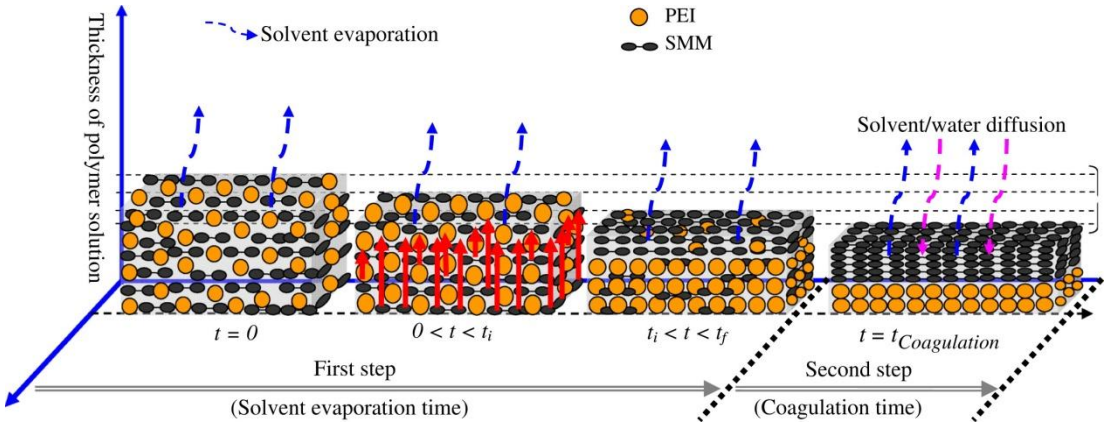

Fig. 1.2.2. Schematic illustration of surface modifying macromolecule (SMM) migration during the membrane formation.
Reprinted with permission from Essalhi and Khayet [30] ©2012 Elsevier B.V.

Nanoparticles (NPs) have been used as additives for fabrication of advanced membranes for MD. NPs have unique electronic, magnetic, optical, thermal, and mechanical stable properties, which improve the performances of membranes due to their small sizes and large surface area. In MD, the hydrophobic NPs are the most commonly used ones. For instance, PTFE NPs were selected because of their superior mechanical and physicochemical properties, high thermal stability, superhydrophobicity, and good stability in various types of

solvents. PTFE NPs have been blended into PVDF dope solutions, improving the hydrophobicity of the membrane [19, 48].

Clay particles [49, 52, 81], self-synthesized fluorinated silica particles [55], or calcium carbonate particles [82] have also been used as hydrophobic modifiers that enhance some membrane properties. For example, PVDF-Cloisite clay particles blending improved the tensile modulus and the long-term stability of hollow fiber membranes prepared by Wang et al. [49] and the hydrophobicity (i.e. contact angles around 150º), salt rejection factors (i.e. from 98.3 to 99.9%), and pore wetting prevention of the ENMs fabricated by Prince et al. [81].

In the case of dual-layer hydrophobic/hydrophilic membranes, thermally conductive NPs can be dispersed in the hydrophilic layer to study their effects on the heat transport by conduction through the hydrophilic layer, thermal efficiency, and permeate flux of these membranes. Su et al. [54] checked this effect embedding both graphite particles and multiwall carbon nanotubes (MWCNTs) into the hollow fiber hydrophilic layer formed by PVDF/polyacrylonitrile (PAN)/Cloisite NA^+, leading to a significant increase of the permeate flux (from 41.2 to 66.9 kg/m^2h, see Table 1.2.1).

1.2.3 Design and fabrication of MD membranes

Different membrane fabrication techniques were applied to prepare MD membranes depending on the considered materials and the designed membrane shape.

1.2.3.1 MD membrane fabrication techniques

MD membranes can be prepared by sintering, stretching, phase inversion, track-etching, and electrospinning. These techniques were already explained in detail elsewhere [1, 4, 83, 84]. Among them, the phase inversion is the most used technique. Some types of membranes are prepared combining different techniques. For example, Zhu et al. [85] prepared novel PTFE hydrophobic hollow fiber membranes by a cold pressing method including extrusion, stretching, and sintering.

Stretching is a solvent-free technique, in which membranes are made by extrusion of the polymer at a temperature close to its melting point coupled with a rapid stretching to form micropores [86]. This technique is suitable when using highly crystalline polymers. The crystallites in the partial crystalline polymer are aligned in the direction of drawing. The material's physical properties, such as its crystallinity, melting point, and tensile strength, together with the applied processing parameters affect considerably the final porous membrane structure and its properties. With this technique membranes with a relatively uniform porous structure and porosity of about 90% are prepared.

Phase inversion can be described as a demixing process in which the initially homogeneous polymer solution is transformed in a controlled way from a liquid to a solid phase. This technique can be used to prepare both asymmetric and symmetric porous membranes via different methods, namely, immersion precipitation (IP) or nonsolvent induced phase separation (NIPS), thermally induced phase separation (TIPS), vapor induced phase separation (VIPS), and evaporation induced phase separation (EIPS). IP (i.e. NIPS) and TIPS are the most commonly employed methods for MD membrane preparation [1].

In the IP or NIPS technique, the polymer is first dissolved in an appropriate solvent and the formed solution is then cast on a flat support. After a partial evaporation of the solvent (i.e. dry-wet phase inversion) or without allowing any solvent evaporation to occur, the cast film is immersed into a coagulant (i.e. nonsolvent) media. The polymer solution is separated spontaneously into two phases, a polymer-rich phase and a liquid-rich phase, via solvent-nonsolvent exchange phenomenon. Demixing takes place and the liquid phase becomes a solid polymeric film (i.e. membrane). During the evaporation step, a thin skin layer of solid polymer is formed at the top of the cast film due to the loss of solvent and the increase of the polymer concentration. Providing that this skin layer may govern the MD performance, it is advisable to optimize the solvent evaporation period.

To prepare MD membranes following the TIPS method, first a homogenous polymer/diluent solution is prepared at high temperature and then this is casted, extruded, or spun into a film or into any other shape. The precipitation step takes place via cooling the solution to a given demixing point, which depends on the type of the polymer solution. Finally, the diluents extraction results in the formation of pores in the solid matrix. This technique is applicable to a wide range of polymers, including those that cannot be used for formation of membranes via NIPS and semicrystalline polymers. Various research studies have been carried out on porous membrane preparation by TIPS using blends of hydrophobic polymer/diluents(s) systems [87, 88]. Very few MD membranes were prepared using this technique [45, 89].

In the track-etching technique, a polymeric film is irradiated with energetic heavy ions and subsequent etching, for example in acid or alkaline bath, leading to the formation of cylindrical pores with uniform pore size distribution [90, 91]. The membrane porosity is mainly controlled by the duration of radiation, while the pore size is related to the etching time and temperature [92]. It was observed that the membranes prepared with this technique have low porosities.

Electrospinning technique has been proposed recently to fabricate nanofibrous membranes for MD [32-34, 36, 81, 93]. This technique consists of a polymer solution-filled syringe connected to a flow rate-controlled pump and a metallic needle or spinneret, a high voltage

electric source, and a grounded collector. The application of a high electric potential in the range of kilovolts (kV) between the polymer solution drop at the metallic needle and the grounded collector transforms the spherical pedant drop into a conical shape. Under the presence of an electrostatic field and when the electrostatic potential overcomes the surface tension of the polymer drop, a charged liquid jet is formed and travels to the collector reducing its diameter through the air gap. The morphology of the produced nano/microfibers changes by varying the solution viscosity, electrical conductivity, surface tension, environmental conditions, applied electric potential, flow rate of the polymer solution, gap between the needle and the collector, etc. [1]. Interesting membrane characteristics required for MD process are provided by ENMs, especially the high hydrophobicity and the high thermal efficiency or which is the same low heat transfer, by conduction [94]. Another advantage of ENMs is their tailorable thickness. Essalhi and Khayet [32] prepared ENMs of different thicknesses by considering different electrospinning times.

Carbon nanotubes (CNTs) are also used to prepare membrane for MD due to its exceptional mechanical, electrical, and thermal properties. Self-supporting CNT bucky-paper (CNT-BP) membranes were fabricated by vacuum filtration [95, 96]. CNTs were first dispersed in isopropyl alcohol and then filtered through a PES membrane under vacuum. In this case, CNTs are held together by van der Waals force without the aid of any binding agent. These membranes exhibited promising properties adequate for MD such as a high hydrophobicity, high void volume fraction, high specific surface area, and relatively low heat transfer by conduction. Nevertheless, during MD testing, these CNT-BP membranes showed high permeate flux decline with time due to temperature polarization, delamination, and formation of microcracks.

By using CNTs, Gethard, Sae-Khow and Mitra [97] fabricated MD membranes by immobilizing CNTs in the pores of hydrophobic PVDF membranes. In this case CNTs were first dispersed in a polymer solution, which was then injected into the lumen of a conventional hollow fiber under a hydrostatic pressure [98]. Fig. 1.2.3 shows schematically the MD mechanism of transport in the presence of CNTs, which act as sorbents providing additional pathways for solute transport. Such membranes were robust, thermally stable, had higher permeate flux, and possessed high selectivity, preventing liquid penetration into the membrane pores. When CNTs were incorporated, an increment of 1.85 and 15 times in permeate flux and salt reduction was observed, respectively, for a salt aqueous solution (34 g/L) as feed [97].

1.2.3.2 Single hydrophobic layer and multilayered membranes for MD

Flat sheet and hollow fiber single layer hydrophobic membranes are the most considered in the design of membranes in MD. These are fabricated by the phase inversion technique as it is explained previously. The dry/jet wet spinning method is the most widely used fabrication

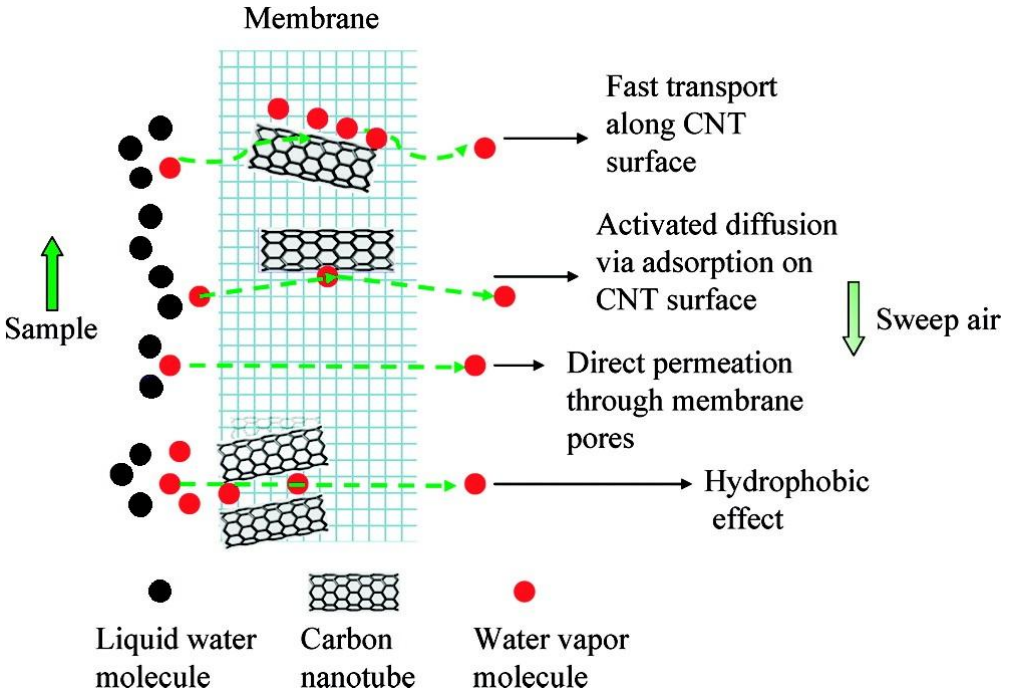

Fig. 1.2.3. Mechanism of transport of membrane distillation (MD) process in the presence of carbon nanotubes (CNTs).
Adapted with permission from Gethard et al. [97] ©2010 American Chemical Society.

method for hollow fiber membranes. The effects of different involved parameters associated with either the polymer solution or the fabrication technique on the MD performance were studied [1].

The influence of the phase inversion parameters such as the concentration of the polymer and the content of the additive (PEG) in the casting solutions, the solvent evaporation time, and the temperature of the coagulant on the structural characteristics and MD performance of the PVDF-HFP flat sheet membranes has been investigated using a statistical approach [99]. An experimental design was first performed and factorial linear models were developed to describe the main effects of factors on the MD responses (i.e. permeate flux and salt rejection factor). The increase of the polymer concentration, the coagulant temperature, and the solvent evaporation time improved the salt rejection factor but reduced the MD permeate flux. On the contrary, the enhancement of the additive (PEG) content in the PVDF-HFP casting solution exerted an inverse effect on the output responses. The prepared membrane using the determined optimum parameters exhibited an improved MD performance (i.e. the highest salt rejection factor 99.95%).

Single layer flat sheet membranes were also prepared by eletrospinning for the MD process. The properties of the polymer solution have the most significant influence on the ENM morphology and its structure. For example, the increase of the polymer concentration resulted in fibers with higher diameters, whereas low polymer concentrations promoted the

formation of beaded ENMs [60]. The fiber diameter decreased as the viscosity of the polymer solution was decreased and its electrical conductivity was increased [60]. The surface tension of the polymer solution also plays an important role in the formation of beads through the structure of ENMs. Moreover, the process parameters, such as the applied voltage, the flow rate of the polymer solution, and the distance between the needle tip and the collector, affect considerably the physical characteristics and morphology of the ENMs [1, 100].

After electrospinning, a heat posttreatment at temperatures below the material´s melting point is applied to improve the integrity and the mechanical strength of the ENMs. Heat-press posttreatment is also considered [34, 36]. Dry ENMs are pressed between two flat glass or metallic sheets in an oven to control the pressing temperature.

Although hollow fiber membrane fabrication is more complex than that of flat sheet membranes, various studies have been carried out on the preparation of hollow fiber membranes because of their various advantages, high packing density (i.e. surface area per unit volume) in modules, good flexibility in operation, mechanically self-supporting, easy to assemble in modules, etc. Different techniques are used to prepare hollow fiber membranes, TIPS, dry spinning, wet spinning and the most useful one, dry/wet spinning. The polymer solution composition, the internal and external coagulants, and all the spinning operational conditions, such as the spinneret dimensions, the bore coagulant flow rate, the dope extrusion rate, the take-up speed, and the air gap distance, affect the morphology, structure, and MD performance of the membranes [1]. For example, hollow fiber membranes with a single PVDF layer and good MD performance were prepared by the TIPS technique using a diluent mixture of γ-butyrolactone (γ-BL) and dioctyl phthalate (DOP) [45]. It was observed that the membrane prepared with the obtained optimal percentage of the polymer/mixed diluent system, 12.7 wt% of PVDF and 58.4 wt% of DOP in γ-BL, exhibited well-interconnected sponge-like structures and a good MD performance (i.e. 51.5 kg/m^2h permeate flux and 99.99% salt rejection factor when using 3.5 wt% NaCl aqueous solution at 90 ºC).

PVDF hollow membranes with an ultrathin skin layer and a porous support layer were prepared by Wang et al. [43] using ethylene glycol (EG) as an additive in the PVDF/NMP spinning solution. A good MD permeate flux, 41.5 kg/m^2h, was achieved (compared to the permeate fluxes lower than 10 kg/m^2h obtained for hollow fiber membrane prepared without EG) with a high NaCl rejection rejection factor, 99.99%, for a 3.5 wt.% NaCl feed aqueous solution. This result is attributed to the increase of the membrane porosity when EG was introduced.

The addition of the organophilic clay (Cloisite 20A) in the PVDF spinning solution resulted in high porosities (i.e. up to 90%) [49]. This highly porous structure improved the hollow fiber thermal insulation, reduced the vapor transport resistance, and improved the

thermal efficiency of the MD process. MD permeate fluxes as high as 79.2 kg/m^{2}h with 100% salt rejection factors for 3.5 wt% NaCl feed aqueous solution were achieved.

Both the fractional factorial design and the steepest ascent method were considered to fabricate hollow fiber membranes by the dry/wet spinning technique, taking into account seven spinning factors, namely, PVDF-HFP concentration, the PEG concentration, the air gap length, the temperature of both the internal and external coagulants, the temperature of the polymer solution, the flow rate of the internal coagulant, the take-up speed, and the pressure applied on the polymer solution [59]. The developed approach permitted the localization of the region of spinning conditions to produce hollow fiber membranes without defects. The followed approach proved to be effective for preparing defects-free single hydrophobic layer PVDF-HFP hollow fiber membrane. Recently, Song and Jiang [101] developed also an experimental design and a statistical analysis to identify the relationship between the hollow fiber membrane fabrication conditions and the membrane performance. Analysis of variance (ANOVA) showed that among the three considered fabrication variables (i.e. polymer concentration, additive concentration, and external coagulant composition), the concentration of the additive in the spinning solution had the most significant effects on the MD performance, while the external coagulant composition exerted the least impact.

All the previously noted spinning parameters can modify the geometrical parameters of the hollow fiber membranes (i.e. thickness, inner and outer diameters). However, these parameters are affected predominantly by the geometry of the used spinneret. The design of the spinneret plays a critical role in determining the molecular orientation and membrane morphology of the resultant hollow fiber membranes. A common spinneret design consists of a reservoir and an annular channel, which has a high annulus length per flow gap to ensure a stable flow of the polymer solution. Different spinneret designs and configurations are reviewed elsewhere [1, 102]. A double spinneret was used by Bonyadi and Chung [44] to prepare macrovoid-free PVDF hollow fiber membranes. In this case, the bore fluid, the dope solution, and the NMP solvent were simultaneously extruded through the inner, middle, and outer channels of the triple-orifice spinneret, respectively. Porous hollow fiber membranes with high outer surface porosity and without macrovoids through their cross-section structure were fabricated due to the introduction of the two-phase flow of the solvent and the dope solution along the air gap length. The obtained MD permeate flux of the prepared hollow fiber membranes was two to three times higher (i.e. water permeate flux of 67 kg/m^{2}h and a salt rejection factor higher than 99.9% for 3.5 wt% NaCl aqueous solution at 80 ºC) than those of the standard dry/jet wet-spun fibers prepared under similar conditions.

Composite membranes fabricated with different materials offer interesting possibilities for achieving some desired membrane characteristics for MD. Among this type of membranes, bilayered hydrophobic/hydrophilic porous composite membranes proved to be attractive for

direct contact MD. The hydrophobic layer is brought into contact with the feed aqueous solution while the hydrophilic layer is maintained in contact with the permeate liquid. Different techniques have been adopted to prepare composite membranes either by modifying the already existing membranes (i.e. coating, grafting, plasma surface modification, etc.) or in situ modification during membrane formation. One of the simplest methods is blending an SMM in a hydrophilic polymer solution and then preparing surface modified membranes by the phase inversion technique [30, 76-78]. During membrane formation, SMMs migrate to the polymer/air interface rendering it more hydrophobic. Hydrophobic porous layers of about 10 μm were prepared [79]. Another followed method to prepare hydrophobic/hydrophilic membranes is to cast a hydrophobic polymer solution onto a hydrophilic porous support [29] or vice versa, to cast a hydrophilic polymer solution onto a hydrophobic porous support [103]. This type of membranes showed high MD stability and durability.

Triple-layered MD membranes were also proposed for MD [1]. Prince et al. [39] prepared a triple layer flat sheet membrane consisting, as can be seen in Fig. 1.2.4, of a thin hydrophobic electrospun nanofibrous layer over the conventional cast PVDF microporous layer (i.e. a middle layer made by immersion precipitation method) in addition to the bottom hydrophilic polyethylene terephthalate (PET) support layer. The layers were attached to each other by heat treatment under pressure and solvent binding. The triple-layered membrane was compared to bilayered membrane (i.e. only the cast PVDF film on PET, without nanofibrous layer). The MD permeate flux, the salt rejection, and the long-term performance of the triple-layered membrane were found to be higher than those of the bilayered membrane being the permeate flux 1.5 times higher. It was observed that the triple-layered membrane could be used for more than 40 h MD operating time without detection of any significant change of the permeate quality. Nevertheless, the bilayered membrane could only be used for 10 h MD operating time before pore wetting. This result was attributed to the addition of the more hydrophobic character of the nanofibrous layer, higher water contact angle, and higher *LEP* values as compared to the bilayered membrane.

A great interest was devoted also to the fabrication of composite hollow fiber membranes for MD. The dual-layer hollow fiber membranes were fabricated by the dry/wet spinning process using a triple-orifice spinneret. The bore fluid was extruded through the central channel of the spinneret and both spinning solutions (i.e. hydrophobic and hydrophilic solutions) were circulated through its annular channels (middle and the outer) [52, 55]. For example, the inner dope solution was composed of PVDF/PAN/hydrophilic Cloisite NA^+/EG/NMP and the effect of adding methanol (MeOH) and fluorinated silica (FSi) particles into the outer dope solutions (PVDF/NMP) was studied [55]. It was observed that the formation of the thinner hydrophilic inner layer and less macrovoid structure resulted in

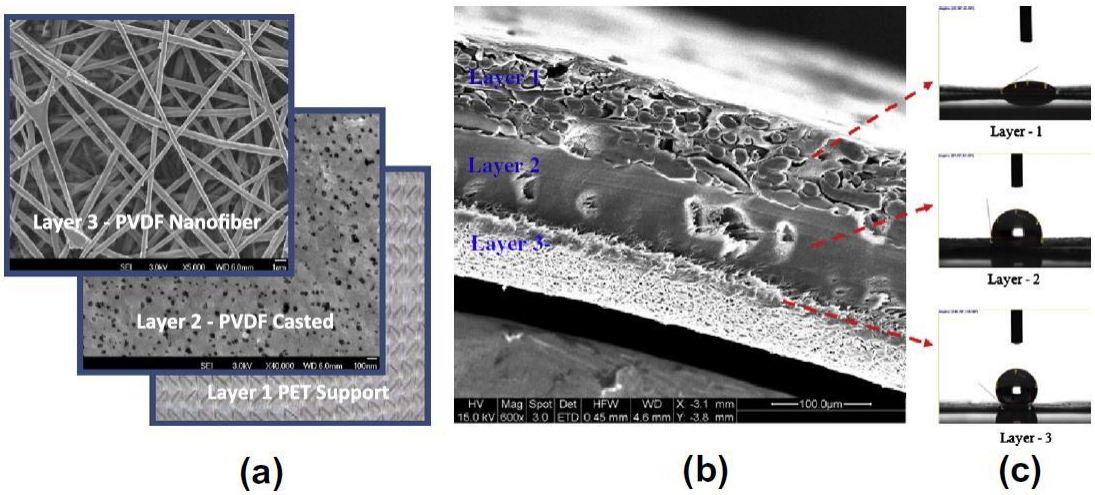

Fig. 1.2.4. SEM images of the triple layer membrane: (a) top surface, (b) cross-section, and (c) contact angle of each layer.
Reprinted with permission from Prince et al. [39] ©2013 Elsevier B.V.

an enhancement of the permeate flux (Fig. 1.2.5). DCMD permeate flux of 83.40 kg/m^{2}h and a separation factor higher than 99.99% (3.5 wt% NaCl as feed solution at 80 ºC) were achieved for the membrane spun with PVDF/MeOH/NMP as an outer layer. Another example is the addition of PTFE particles in the PVDF/NMP/EG dope solution to prepare the outer layer of the hollow fiber membranes, while the same polymer solution without PTFE particles was used for the inner layer [56]. A macrovoid-free morphology and a relatively thin outer layer were obtained when 30 wt% of PTFE particles was blended in the outer layer dope. A relatively high DCMD permeate flux, 50.9 kg/m^{2}h at 80 ºC, and 100% NaCl rejection factor were obtained. Better MD performance was obtained by Wang et al. [57] when the inner layer dope composition was formed by PVDF/NMP/EG/hydrophobic Cloisite 20A, and the outer layer dope contained the same materials except the hydrophobic Cloisite 20A, which were replaced by PTFE particles. The DCMD permeate flux was enhanced up to 98.6 kg/m^{2}h maintaining the NaCl separation factor higher than 99.98% for a 3.5 wt% NaCl aqueous solution used as feed.

Membrane surface coating is applied to improve the surface hydrophobicity of the membranes. The main drawback of this technique is the instability of the coated layer, which could be removed during the operation process due to the weak physical interaction between the membrane and the coated layer, and the high risk to close the pores and/or reduce their size. In some cases, chemical treatment or solid-vapor interaction crosslinking was applied. Surface grafting is advisable because the membrane surface is modified through the covalent attachment between the grafted chains and the membrane. In contrast to the physically surface coating method, covalent bonding interaction of graft chains on the membrane surface avoids their delamination, offering a long-term chemical stability of grafted chains.

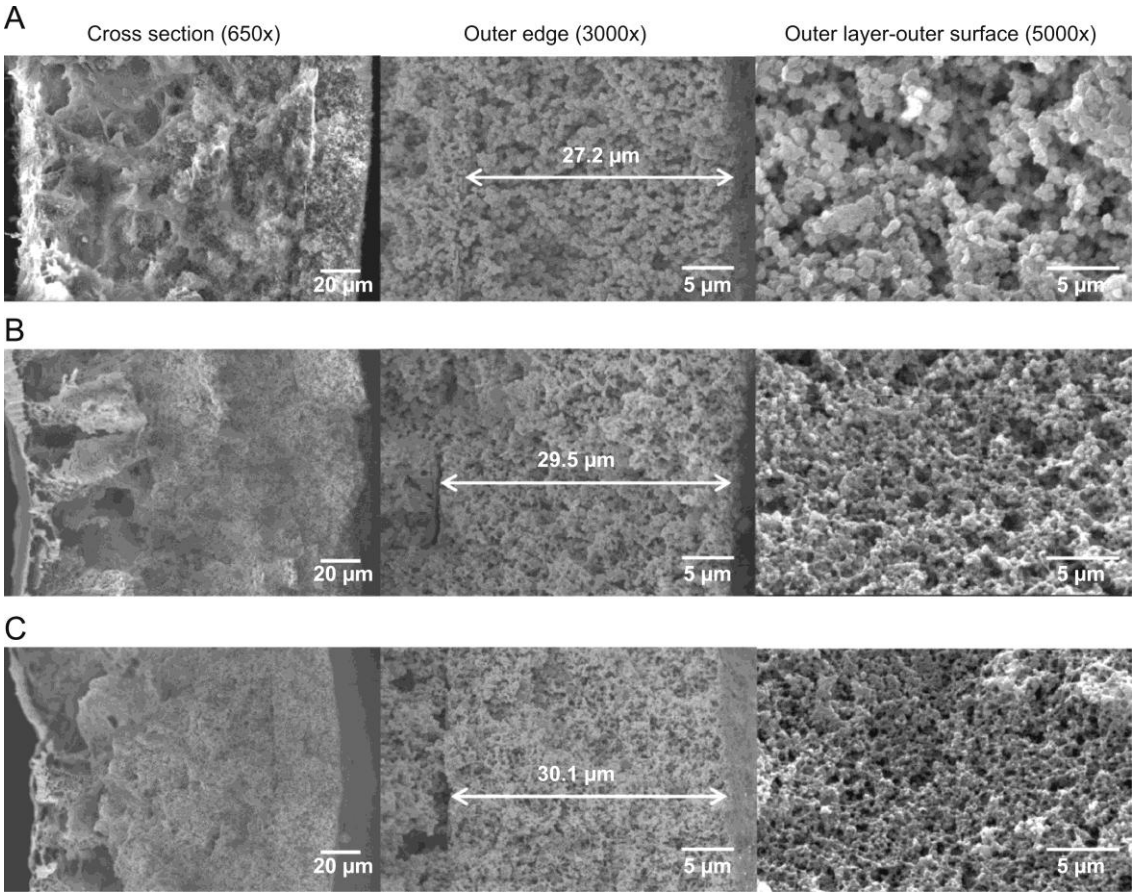

Fig. 1.2.5. Scanning electron microscopy (SEM) images of dual-layer hydrophobic/hydrophilic polyvinylidene (PVDF) hollow fiber membranes with different additives: (a) without additives, (b) with methanol (10 wt%) as additive, and (c) with methanol (10 wt%) and FSi particles (5 wt%) as additives.
Reprinted with permission from Edwie et al. [55] ©2012 Elsevier B.V.

Several surface-modified membranes have been prepared for MD technology. Self-supporting BP membranes were fabricated using CNTs and coated on both sides with a thin layer of PTFE by sputtering to increase both their hydrophobicity and their mechanical stability, without changing too much their average pore size and porosity [104]. The coated BPs were hot pressed on top of poly(ethylene) (PE) grid layer used as a mechanical support. Therefore, this composite membrane, which was successfully tested in MD, was composed of four layers (PTFE layer, CNTs BP, PTFE layer and PE support).

Superhydrophobic membranes, with water contact angles higher than 150º, have been fabricated for MD [35, 105, 106]. Razmjou et al. [105] prepared superhydrophobic membranes with a water contact angle of 163º for DCMD by developing a hierarchical structure with multilevel roughness. These were carried out by depositing TiO_2 nanoparticles on microporous PVDF membranes by means of a low temperature hydrothermal (LTH) technique. TiO_2 precursor was prepared by mixing anhydrous ethanol with 2,4-pentanedione,

perchloric acid, and titanium (IV) iso-propoxide and ultra-pure Milli-Q water. A separate solution of Pluronic F127 as templating agent in anhydrous ethanol was also prepared. Both solutions were first stirred separately and then mixed and stirred again. The coated membranes by TiO_2 were then fluorosilanized using 1H, 1H, 2H, 2H-perfluorododecyltrichlorosilane (FTCS) with a low surface energy. The FTCS–TiO_2–PVDF membranes showed good thermal and mechanical resistances. Two years later, Meng et al. [106] prepared porous PVDF membranes, which were coated using the same procedure developed by Razmjou et al. [105], but employing different templating agents (PEG, Pluronic F-127, Wacker IM-22, and cetyltrimethylammonium bromide). After the deposition of FTCS, all modified membranes were superhydrophobic. However, the structure, wettability, and DCMD desalination performance of the resultant coatings were dependent on the physical and chemical properties of the templating agent. Among the studied templating agents, PEG exhibited the best properties, with an optimum *LEP* and DCMD desalination performance.

Besides the TiO_2 coating method, there are other modification techniques for fabricating superhydrophobic membranes. Two types of PVDF nanofibrous membranes, integrally modified (I-PVDF) and surface-modified (S-PVDF), were fabricated by electrospinning followed by surface modification including poly-dopamine (PDA) surface coating to improve the adhesive force, silver nanoparticle deposition during chemical reduction to optimize the morphology and roughness of the membrane, and hydrophobic treatment with 1-dodecanethiol (Fig. 1.2.6). The difference between the integrally and surface modified membranes is the pre-activation by PDA. Wetting of the PVDF nanofibrous membrane was detected after 1 h of DCMD operation, although this membrane showed a high permeate flux of 35.7 L/m^{2}h. The I-PVDF nanofibrous membrane exhibited a similar permeate flux, 31.6 L/m^{2}h using a 3.5 wt% NaCl as a feed solution, while the feed and permeate temperatures were fixed at 60 ºC and 20 ºC, respectively. After integral modification, the obtained I-PVDF nanofibrous membrane was not wetted over the testing period of 8 h. For the S-PVDF nanofibrous membrane, the permeate flux was much lower than the original membrane (5.4 L/m^{2}h). This result may be attributed to the high mass transfer resistance induced by the dense modification layer on the membrane surface.

A simple method to fabricate superhydrophobic membranes for MD is via spraying a mixture of polydimethylsiloxane and a hydrophobic silica (SiO_2) nanoparticles on PVDF flat sheet membranes using an airbrush [107]. The DCMD permeate flux of all modified membranes was lower than that the originally used membrane because of the enhancement of the mass transfer resistance of the coated layer, which reduced the permeate flux from 32 to 14 kg/m^{2}h with the increase of silica content (from 0 to 1.5 wt%). Nevertheless, when using 3.5 wt% of NaCl aqueous solution as feed, the electrical conductivity of the produced water using the modified membrane was maintained in the range of 30–50 μS/cm, whereas that of

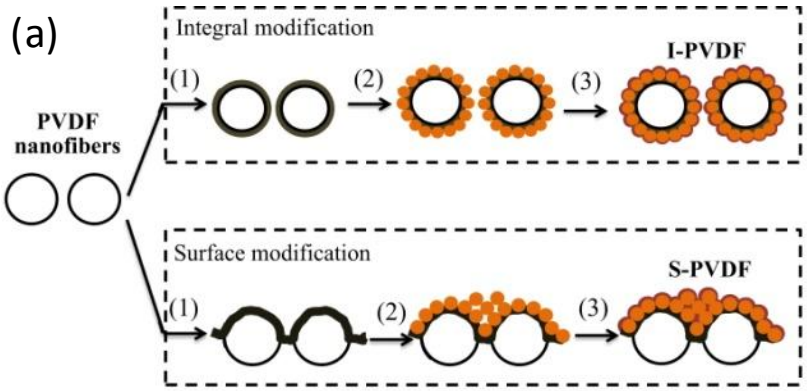

(1) PDA modification; (2) Silver nanoparticle coating; (3) 1-dodecanethiol hydrophobic modification

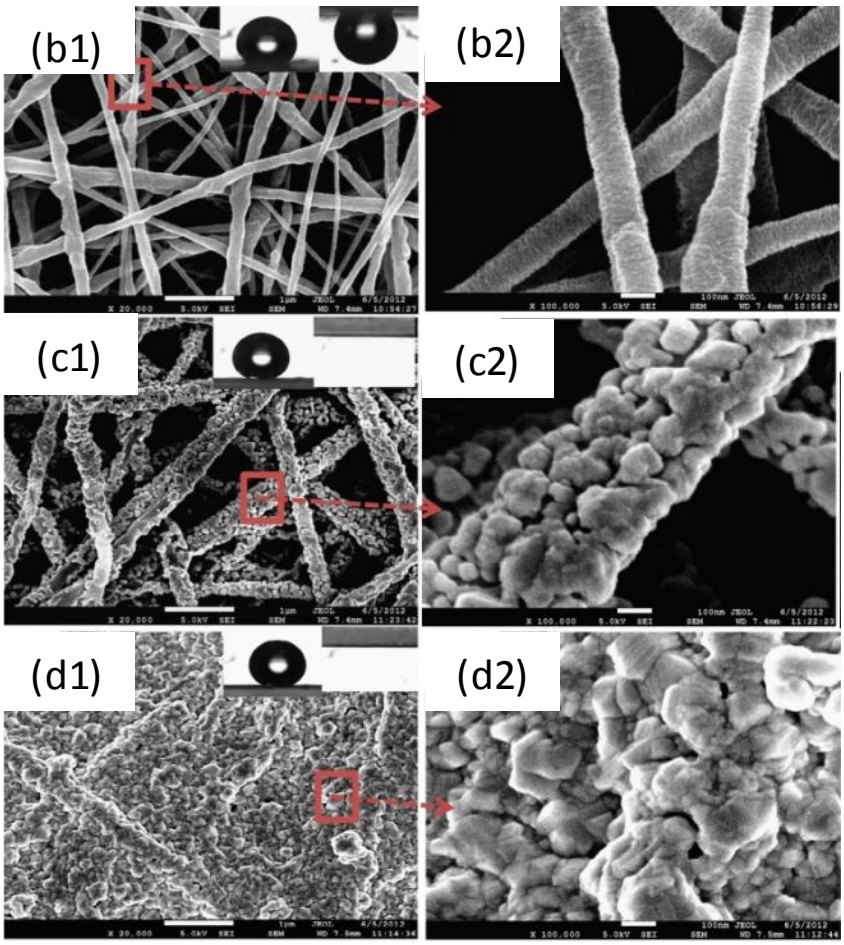

Fig. 1.2.6. (a) Schematic illustration of superhydrophobic polyvinylidene fluoride (PVDF) nanofibrous membrane preparation: (1) PDA modification; (2) silver nanoparticle coating; and (3) 1-dodecanethiol hydrophobic modification. Photographs are field emission scanning electron microscopy (FESEM) images of (b1) (b2) unmodified PVDF, (c1) (c2) I-PVDF, and (d1) (d2) S-PVDF nanofiber membranes.
Reprinted with permission from Liao, Wang and Fane [35] ©2013 Elsevier B.V.

the original membrane was increased sharply, indicating partial wetting of this membrane. In addition, after 180 h DCMD tests with 25 wt% NaCl feed aqueous solution, a slight decrease of the permeate flux of the modified membrane was observed maintaining the NaCl rejection factor above 99.99%, whereas the permeate flux of the original membrane showed a significant reduction with a lower NaCl rejection factor. Therefore, it was concluded that the modified membrane had an excellent antifouling property compared to the originally used membrane.

One of the main advantages of the plasma surface modification technique is to change the membrane surface wettability without affecting their bulk properties. Yang et al. [108] applied this technique using a P2i plasma and a chemical modification procedure by hydroxylation to prepare improved PVDF hollow fiber membranes for MD. Compared to the unmodified PVDF hollow fiber membrane, the modified membranes by the two procedures showed greater hydrophobicity, higher *LEP* values (i.e. 1.38 bar for the unmodified membrane and about 3.5 bar for the modified membranes), better mechanical strengths (i.e. enhancement of the strain at break from 98.6% for the unmodified membrane to 102.1% for the plasma and 121.94% for the chemically modified membranes), and smaller maximum pore sizes, which were reduced from 0.42 μm for the original membrane to 0.19 μm for the modified membranes. When using synthetic water, the produced water by the modified membranes over 1-month DCMD operation time had a high quality (i.e. electrical conductivity < 1 μS/cm). It was claimed that the chemically modified membrane had marginally better DCMD performance than the plasma-modified membrane.

The carbon tetrafluoride (CF_4) plasma surface modification technique has also been used to improve the membrane hydrophobicity due to the strong fluorination of the membrane surface by fluorine functional groups. Wei et al. [31] applied the CF_4 plasma modification technique to render the surface of asymmetric hydrophilic PES flat sheet and hollow fiber membranes hydrophobic and therefore suitable for MD applications. The performed DCMD experiments of both membrane types revealed high salt rejection factors (i.e. 99.97%) when 4 wt% NaCl aqueous solution was used as feed. The permeate fluxes of the modified hollow fiber membranes were about 50% higher than those of flat sheet membranes (i.e. 40.9 kg/m^{2}h for the flat sheet membrane obtained at 74.5 ºC feed temperature and 66.7 kg/m^{2}h for the hollow fiber membrane obtained at 73.8 ºC).

Ceramic membranes were also modified to be hydrophobic, employing different techniques. For example, silicon nitride (Si_3N_4) hollow fiber membranes were first prepared by a combined phase inversion and sintering method and then chemically modified by grafting fluoroalkylsilane for seawater desalination by MD [51]. Si_3N_4 is hydrophilic in nature due to the presence of the surface hydroxyl (–OH) groups. After surface modification, the water contact angle was increased from 56° to 136°. The modified Si_3N_4 hollow fiber membranes

exhibited satisfactory MD performance (i.e. salt rejection factors over 99% and permeate fluxes of 22.4 for vacuum MD, VMD, and 7.8 L/m^{2}h for DCMD when using 4 wt% NaCl feed aqueous solution) with a good long-term stability.

1.2.4 Characterization of MD membranes

The characterization techniques should be selected to analyze the proposed membrane and be sure whether it is suitable for a given MD application. Various characterization techniques for MD membranes were reported in [1]. These can be divided in as follows:

1.2.4.1 Membrane surface and bulk structure

Scanning electron microscopy (SEM) and field emission scanning electron microscopy (FESEM) provide a direct visualization of both the surface and the cross-section of the membrane. First, the sample should be fractured in liquid nitrogen and then sputter-coated with a thin layer of gold using an evaporator, which is necessary because the membrane is not an electrically conductive material. Special care must be taken because this previous sample preparation step can gives some artifacts or damage the membrane surface. Transmission electron microscopy is not usually applied in MD, but it is necessary if the membrane exhibits any kind of nanostructure or when nano-additives are used.

Atomic force microscopy (AFM) was used to characterize the surface of MD membranes. The main advantage of AFM compared to any other microscopy technique is that the samples do not need any previous preparation and the analysis of the membrane can be carried out at room temperature, in air or any liquid media. The AFM images are obtained using a tapping mode and then the captured images are treated as described elsewhere [109, 110]. Three-dimensional (3D) AFM images revealed that the surfaces of polymeric MD membranes possess nodule-like and valley-like structures (Fig. 1.2.7). The bright peaks represent nodules while the dark depressions or valleys are the pores. 3D AFM images also permit an estimation of the roughness not only of the top surface of flat sheet membranes but also the internal and external surfaces of hollow fiber membranes [30, 59, 111]. The followed methods to evaluate the mean roughness are explained elsewhere [110, 112].

1.2.4.2 Membrane porosity and pore size

The membrane porosity (ε) refers to its void volume fraction defined as the volume of the pores divided by the total volume of the membrane. In general, a membrane with a high porosity has high permeate flux and low conductive heat loss. The porosity is determined following the method described in previous studies [58, 112].

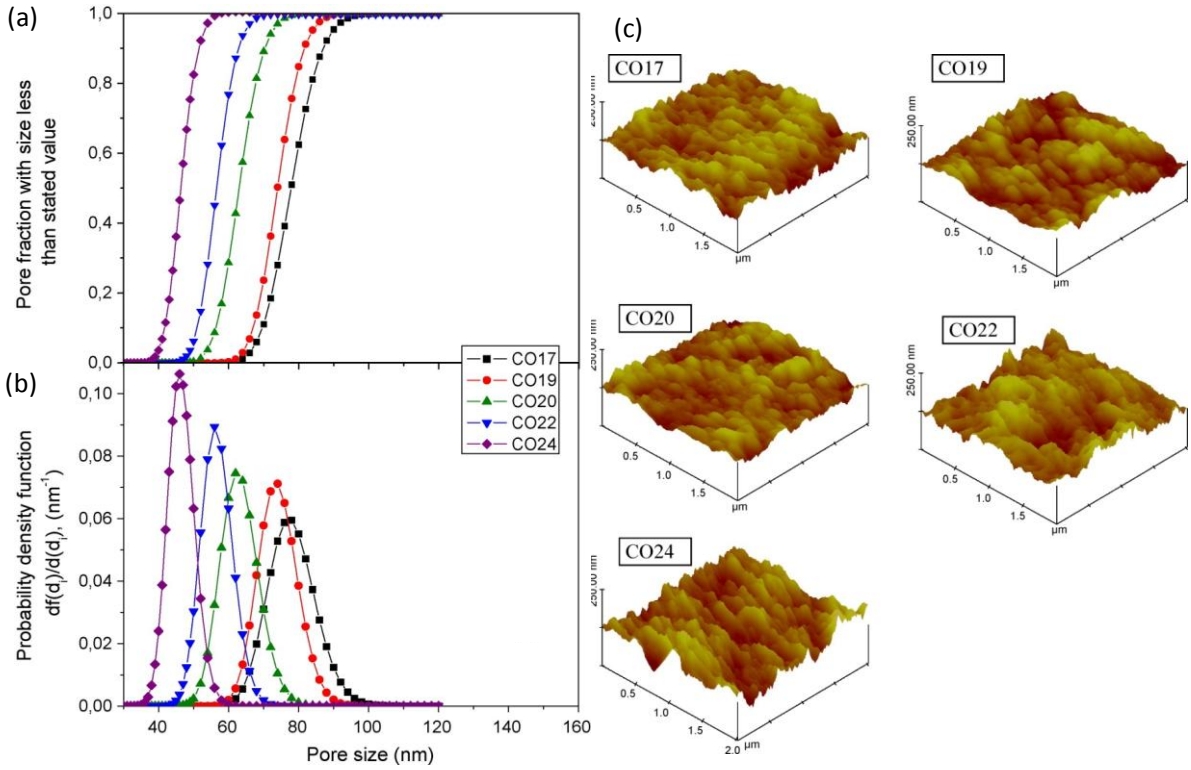

Fig. 1.2.7. Cumulative distribution of pore sizes (a) and probability density function (b) curves generated from the pore sizes obtained from atomic force microscopy (AFM) images (c) of the inner surfaces of the poly(vinylidene fluoride-co-hexafluoropropylene) (PVDF-HFP) hollow fiber membranes prepared with different copolymer concentrations.
Adapted with permission from García-Payo, Essalhi, and Khayet [58] ©2010 Elsevier B.V.

The effective porosity ($\varepsilon_e = \varepsilon/L_p$), which is defined as the ratio of the porosity and the effective pore length (L_p) that takes into consideration the pore tortuosity (τ), can be determined by gas permeation method together with the mean pore size of the membrane [112]. The pore tortuosity is the deviation of the pore structure from the straight line perpendicular to the membrane surface.

The mean pore size of the MD membranes, the maximum pore size and the pore size distribution are determined by the wet/dry flow method as described elsewhere [60, 113]. This method involves the displacement of liquid-filled membrane pores under different hydrostatic pressures using a gas, air, or nitrogen. First the gas permeation flow through a dry membrane is measured at different pressures obtaining the dry curve. Then, the membrane sample is wetted by a low surface tension liquid and the gas permeation flow is measured again at increasing transmembrane pressures to obtain the S-shaped wet curve. The mean pore size is determined from the intersection between the half-dry curve corresponding to 50% gas flow through the dry membrane sample and the wet curve. The half-dry curve is obtained mathematically as half of the dry curve. The maximum pore size is determined from the

lowest applied hydrostatic pressure on the wet membrane at which a permeate gas flow was observed. The Laplace equation taking into consideration the surface tension of the used wetting liquid is used as described in [1]. In addition, the cumulative distribution of pore size and pore size distribution can also be determined from the S-shaped wet curve.

Besides the gas permeation test and the wet/dry flow method, some microscopy techniques such SEM, FESEM, and AFM are also used to estimate the pore size and the pore size distribution of the MD membrane surface together with its porosity by means of computerized image analysis of the scanned images [1, 44, 114-116]. Calculations are based on encircling the pore surface area (S_{pore}) and from the obtained value the equivalent pore size (d_p) is then determined as

$$d_p = 2\sqrt{\frac{S_{pore}}{\pi}} \tag{1.2.1}$$

The surface mean pore size, its distribution and porosity of MD membranes were also determined by AFM [117]. A minimum number of pores, about 30, should be measured by inspecting line profiles on the scanned AFM images of each sample and at different locations of the membrane surface. If the obtained pore sizes fit to a log-normal distribution, a straight line is observed when plotting on log-normal probability paper the median ranks against the pore sizes arranged in an ascending order. If this condition is satisfied, the mean pore sizes and the corresponding geometric standard deviations can be calculated from the obtained straight line. The mean pore size corresponds to 50% of the cumulative number of pores while the geometric standard deviation is determined from the ratio of 84.13% of the cumulative number of pores to that of 50%. Finally, the cumulative distribution of pores and the probability density function can be obtained from these values as shown in Fig. 1.2.7. The corresponding surface porosity (ε_s), defined as the ratio between the area of the pores to the total membrane surface area, and the surface pore density, which is the number of pores per unit area, can be determined as described elsewhere [1, 112].

1.2.4.3 *LEP* of water in pores and hydrophobicity

The membrane *LEP* is the lowest applied transmembrane pressure on a liquid solution before this penetrates into the pores [113]. It is a key parameter to be known for an MD membrane before being applied in MD. A slight transmembrane pressure is applied first to the liquid solution for at least 10 min, and then the pressure is increased gradually until a first drop of the feed solution appears on the permeate side of the membrane. The corresponding applied pressure is the *LEP* value and must be as high as possible for MD membranes. It will be high for low maximum pore size and more hydrophobic membranes.

The water contact angle is the key parameter indicating whether an MD membrane is more hydrophobic than the other. In general, membranes with a water contact angle lower than 90º are considered hydrophilic, whereas membranes having higher water contact angle than 90º are considered hydrophobic. However, the measured water contact angle is affected by the membrane roughness (i.e. presence of pores) and should be corrected [118]. Optical contact angle meters are often used to measure the liquid contact angle of MD flat sheet membranes, for example, CAM200 [30, 60]. For MD hollow fiber membranes, tensiometers are used [52], for example, Sigma 701 Tensiometer from KSV instruments Ltd. This tensiometric method permits the determination of the liquid contact angle from the force measurement when the hollow fiber membrane is brought into vertical contact with the liquid. In general, the method is based on the forces of interaction among the liquid and the solid surface, the liquid surface tension, and geometry of the solid.

1.2.4.4 Thermal and mechanical properties

The MD membranes should exhibit good thermal stability up to 100 ºC. Differential scanning calorimetry (DSC) technique and thermogravimetric analysis are used to study the thermal properties of membranes and their thermal degradation. The melting temperature (T_m), the crystallization temperature (T_c), the enthalpy of melting (ΔH_m), the enthalpy of crystallization (ΔH_c), and the degree of crystallinity of MD membranes were determined (Fig. 1.2.8(a)) [60, 119]. Moreover, the thermal conductivity of the MD membrane must be as low as possible. In general, the thermal conductivity of MD membranes is calculated from the thermal conductivity of the used material and the void volume factor [4]. The method of Lees disc proved to be a quite good for measuring the thermal conductivity of MD membranes [1, 120].

It is not necessary for MD membranes to be mechanically resistant like the membranes used in the pressure-driven membrane separation processes (i.e. ultrafiltration, nanofiltration, and reverse osmosis). MD membranes only need to have adequate mechanical strength to be assembled in modules. The mechanical properties of MD membranes can be determined by tensile testing. For example, Essalhi and Khayet [60] employed this technique for PVDF ENMs, using an Instron dynamometer (Fig. 1.2.8(b)).

Other complementary techniques are used to characterize specific MD membranes, especially the modified ones. For example, X-ray photoelectron spectroscopy (XPS), X-ray diffraction and Fourier transform infrared spectroscopic analysis [1, 121, 122]. XPS analysis was used to determine the concentration of different chemical species (fluorine, nitrogen, oxygen, carbon, etc.) at the surface and through the cross-section of modified MD membranes.

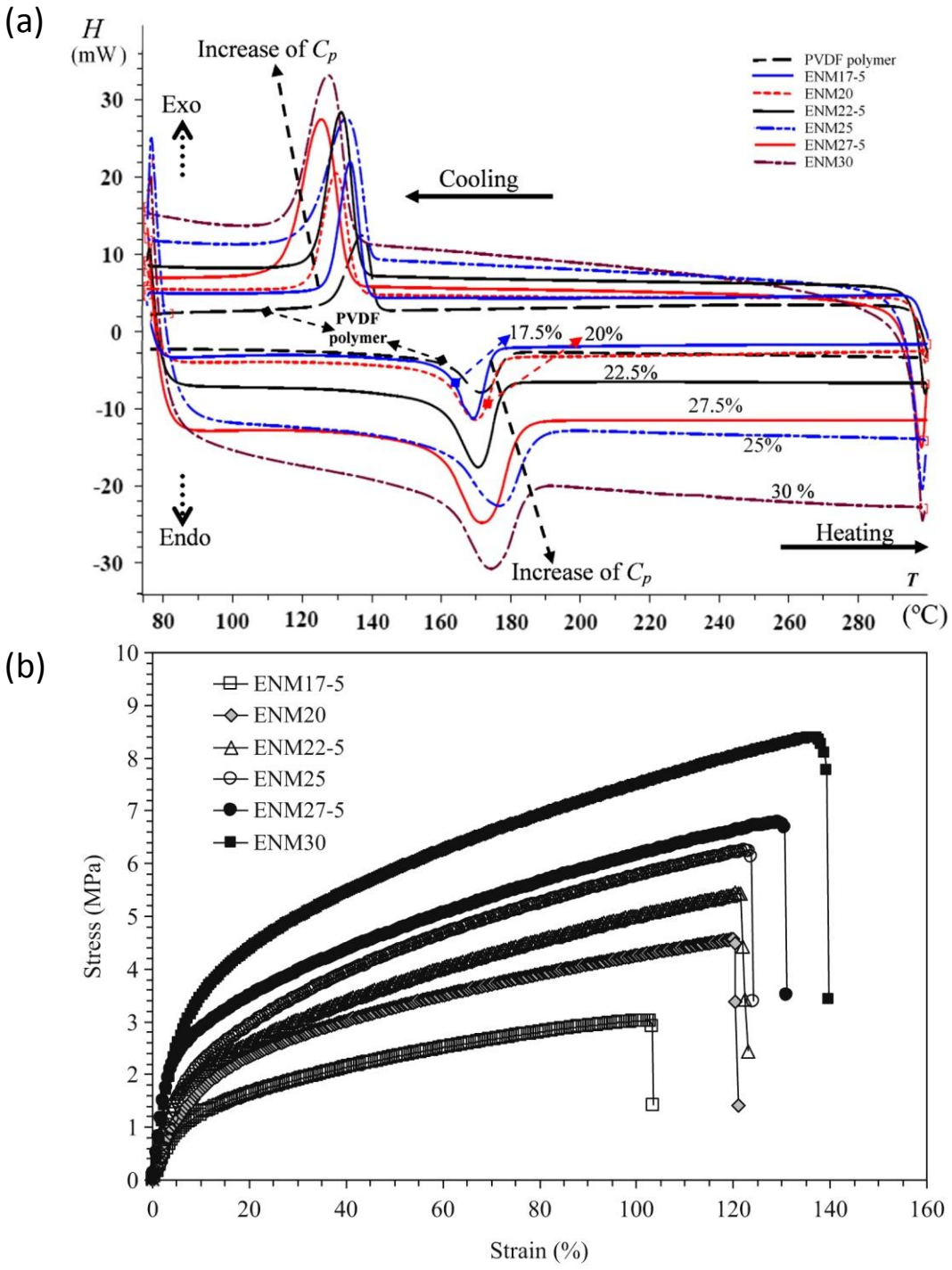

Fig. 1.2.8. (a) Differential scanning calorimetry (DSC) heating and cooling thermograms and b) stress-strain curves of the electrospun nanofibrous membranes (ENMs) prepared with different polyvinylidene fluoride (PVDF) concentrations in the electrospinning polymer solution.

1.2.5 MD membrane modules and testing of MD membranes

Different configurations and membrane modules were considered in MD technology as indicated in the previous chapter. Independently from the chosen MD configuration, the MD performance (i.e. permeate flux, solutes separation, and thermal efficiency) is predominantly dependent on the membrane characteristics. The MD configuration, the membrane module, and the applied operating conditions affect also MD permeate flux and thermal efficiency. The high feed temperature, low permeate temperature, high and turbulent flow rates, system isolation and heat recovery are some of the main operating conditions followed for an efficient MD process [1, 5, 8]. The type of the feed solution also affects the MD performance. When using a feed aqueous solution containing only nonvolatile solutes such as saline solutions, the reduction of the water vapor pressure together with the concentration polarization effect resulted in low MD permeate flux ([32] in Table 1.2.1). This effect is different if volatile solutes (e.g., alcohol in aqueous alcohol solution) are present in the feed solution because both water and solutes are transported through the membrane [123]. In this case special care must be taken in order to prevent membrane pore wetting for high concentrations of volatile solute(s).

There are many types of membrane modules that can be used in MD process. These should provide high flow rates of both the feed and permeate, high packing density, low pressure drop, high thermal stability, and heat recovery. The MD membrane modules can be divided as follows [1, 124]:

- *Plate and frame membrane modules:* There are different module designs considering specially the feed solution flow direction (i.e. tangential or radial). These are mostly employed at bench scale owing to their low packing density and easy cleaning, testing and membrane replacement. The plate and frame membrane module configuration, based on tangential flow to the surface of flat sheet membranes, is commercially attractive (Fig. 1.2.9(a)). Spacers are placed in this type of membrane modules and their membrane packing densities vary between 100 and 400 m^2/m^3.

- *Spiral wound membrane modules:* Flat sheet membranes and supports are assembled in spiral around a perforated central tube as plotted in Fig. 1.2.9(b). The liquid solution also flows tangentially to the membrane surface. This type of modules is considered the most suitable for commercial MD systems due to their higher packing densities, which vary between 300 and 1000 m^2/m^3 (Fig. 1.2.9(c)).

- *Tubular, capillary, and hollow fiber membrane modules:* The difference between tubular, capillary and hollow fiber membranes lies on the size of their diameters and therefore their packing density in modules. The diameters of tubular membranes range from 5 to 25 mm and their packing density is around 300 m^2/m^3. The diameters of the capillary membranes are between

1 and 3 mm and their packing density can go up to 1200 m^2/m^3, whereas the hollow fiber diameters are lower than 1 mm. The fibers are normally bundled and sealed inside a shell and tube module (i.e. tubular module). For an industrial/commercial view point, this type of module is attractive because of the high packing density achieved when hollow fiber membranes are used (500 - 9000 m^2/m^3). Their main drawbacks are fouling, which increases with the reduction of the diameters of the fiber membranes associated with the difficulties of cleaning, maintenance, reuse, and membrane replacement.

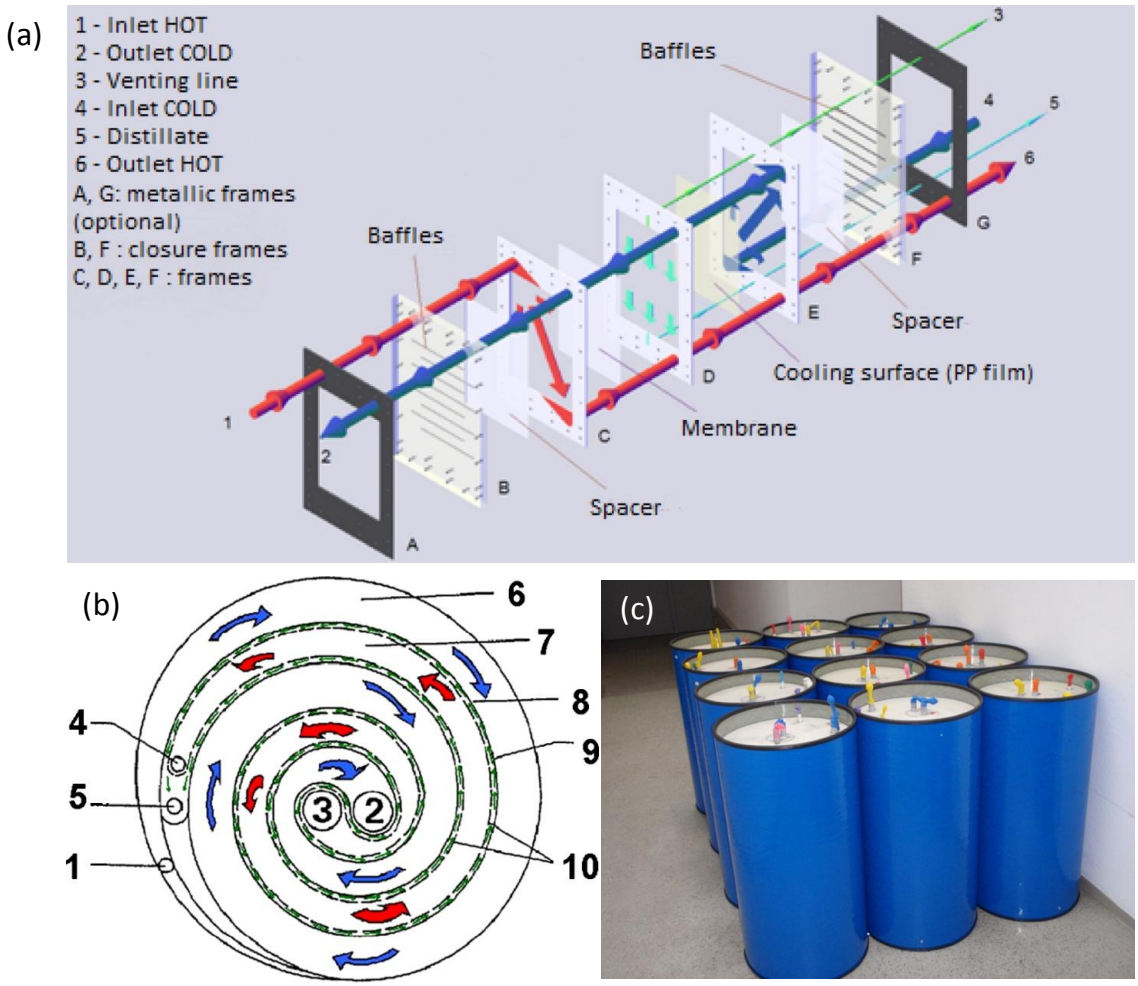

Fig. 1.2.9. Schemas of internal configuration of (a) plate and frame membrane module (Reprinted with permission from Cipollina et al. [125] ©2012 Elsevier B.V.) (b) Spiral would membrane module ((1) condenser inlet, (2) condenser outlet, (3) evaporator inlet, (4) evaporator outlet, (5) distillate outlet, (6) condenser channel, (7) evaporator channel, (8) condenser foil, (9) distillate channel, and (10) hydrophobic membrane); and (c) external shape of the spiral wound modules with 14 m^2 membrane area.
Reprinted with permission from Winter et al. [132] ©2011 Elsevier B.V.

Table 1.2.2 reports some commercial and patented MD membrane modules. The major application of these MD modules is desalination.

Table 1.2.2. Commercial and patented membrane distillation (MD) modules using different configurations.

Manufacturer	Membrane material (pore size)	Effective membrane area (m^2)	MD configuration	Permeate flux (kg/m^2h)	MD conditions[c]	Other module specifications[d]	References
PLATE AND FRAME MEMBRANE MODULES							
GE Osmonics SEPA CF	PTFE GE[a] (0.45 μm) PTFE MS[b] (0.45 μm)	0.014	DCMD	22.3 23.4	F: 10,000 mg/L NaCl; FR = 400 mL/min ΔT = 25ºC		[126]
Scarab development AB	PTFE (0.2 μm)	2.8	AGMD	6.5	Solar desalination pilot F: 1 g/L NaCl; ΔT = 65ºC	Dimensions: 63 cm width; 73 high; 17.5 thickness; 1 mm AG width	[127]
Keppel Seghers	-	9	AGMD	3.25	Compact single module: F: 35 g/L NaCl; F FR= 26 L/min F T = 80ºC; R T = 30ºC		[128]
	-			5.09	Three stages connected in series: F: 35 g/L NaCl; F FR = 19 L/min F T = 80ºC; R T= 30ºC		
Memsys	PTFE (0.2 μm)	1.88 (7 frames)	V-MEMD	8.7	2 stage system F: tap water C FR = 9 L/min; F T = 25ºC F FR = 1.5 L/min; C T = 25ºC VP = 65 mbar	Diesel heater driven H FR = 15 L/min; H T = 60ºC	[129]
		2.5 (9 frames)		6.4			
		5 (17 frames)		3.9			
Patent (US20100072135)	PTFE	3	DCMD	20.2	F: artificial sea water RT T = 55ºC; R F V = 0.04 m/s	4 sheets	[130]
SPIRAL WOUND MEMBRANE MODULES							
SEP GmbH	PTFE (0.2 μm)	4	DCMD	2.5-12.5	F: LLLW F T = 30-80ºC; P T = 5-30ºC F/P FR = 300-1500 kg/h	G-4.0-6-7 module Dimensions (ϕ x h) = 0.45 x 0.62 m	[131]

Continued

Fraunhofer ISE	PTFE (0.2 μm)	10	LGMD	1-2.5	Solar desalination F: tap water E T = 80ºC; CD T = 25ºC F FR = 200-500 kg/h	Spiral coil diameter = 0.28 m	[132]
Fraunhofer ISE	PTFE (0.2 μm)	10	LGMD (with deaeratiom)	1.2-3.0	F: tap water E T = 80ºC; CD T = 25ºC F FR = 200-500 kg/h VP = 40 mbar	Spiral coil diameter = 0.28 m	[133]
				3.77	F: tap water E T = 90ºC ; CD T = 20ºC F FR = 500 kg/h		
Patent (US4545862)	PTFE 5C.2 W. L. Gore & Associates, Inc. (0.45 μm)	5	DCMD	2.65	F: 40 g/L salt water F FR = 170 L/h	L = 19.5 m Diameter = 0.5 m	[134]
TUBULAR MEMBRANE MODULES							
Enka-Microdyn	PP (0.2 μm)	0.036	DCMD	4	F: 35 g/L NaCl F T = 70ºC ; P T = 15ºC F FR = 0.055 kg/s; P FR = 0.027 kg/s	Countercurrent flow module: MD020TP2N (3 tubes) PF = 0.5; L = 0.75 m	[135]
CAPILLARY AND HOLLOW FIBER MEMBRANE MODULES							
Microdyn	PP (0.2 μm)	0.1	VMD	3.6	F: Dist. Water; F T = 40ºC F V = 0.4 m/s; VP = 40 mbar	Capillary module: MD020CP2N 40 capillary fibers; L = 0.47 m	[136]
				6.1	F: Dist. Water; F T = 50ºC F V = 0.8 m/s; VP = 60 mbar		
				9.1	F: Dist. Water; F T = 60ºC F V = 0.8 m/s; VP = 90 mbar		
Microdyn	PP (0.2 μm)	0.1	DCMD	13	F: 35 g/L NaCl F T = 70ºC ; P T = 15ºC F FR = 0.055 kg/s; P FR = 0.027 kg/s	Countercurrent flow module: MD020CP2N (40 HF) PF = 0.7; L = 0.45 m	[135]
Enka Microdyn	PP (0.45 μm)	0.1	DCMD	1.38	F: 465 g/L dilute apple juice F FR = 300 L/h; P FR = 200 L/h F T = 28ºC; ΔT = 19ºC	Tube and shell module: MD-020-2N-CP (41 HF) PD = 70%; L = 0.45 m	[137]

Enka-Microdyn	PP (0.2 μm)	2	DCMD	5.5	F: 35 g/L NaCl F T = 70ºC ; P T = 15ºC F FR = 0.055 kg/s; P FR = 0.027 kg/s	Countercurrent flow module: MD080CO2N (467 HF) PF = 0.5; L = 1 m	[135]
Memstill®	-	-	LGMD	3.53	F: seawater;T_{top} = 74.3ºC Channel V = 0.035 m/s	M28 module (BS) L = 1.5 m; Width = 0.5 m	[138]
				2.45	F: seawater; T_{top} = 51.2ºC Channel V = 0.027 m/s	M31 module (BS) L = 1.5 m;Width = 0.5 m	
				3.78-1.94	F: seawater;T_{top} = 77-69ºC Channel V = 0.034-0.023 m/s	M32 module (BS) L = 1.5 m;Width = 0.5 m	

[a]Membrane Providers: GE: GE osmonics.

[b]Membrane Providers: MS: Membrane solutions.

[c,d]AG, air gap; BS, bench-scale; C, cooling; CD, condenser; E, evaporator; F, feed; FR, flow rate; H, heating; LLLW, liquid low-level radioactive waste; P, permeate; PD, packing density; PF, packing factor; R, refrigeration; RT, retentate; V, velocity; VP, vacuum pressure; V-MEMD, vacuum-multi-effect-membrane-distillation; h, module height; L, length; T, temperature; ΔT, temperature difference; ϕ, module diameter.

1.2.6 Conclusions and future trends

Although much progress has been made in the use of novel materials, sophisticated membrane fabrication and modification techniques, and a variety of membrane characterization tools and methods, a good commercial membrane and module still are not available in the market. In other words, MD membrane technology is still not fully developed for industrial implementation. There are some MD-specific areas that deserve further investigations to improve the water production rate, its long-term quality, thermal efficiency and to reduce energy consumption, for example, design of novel membranes and modules.

New promising materials including nano-additives are currently used for MD membrane preparation and some novel membranes have been developed at laboratory scale, e.g., bilayered flat sheet membranes, hollow fiber membranes, and electrospun nanofibrous membranes. It is important to look for specific and controlled membrane morphology and properties in order to improve the MD performance according to the type of water solution to be treated and the considered MD configuration. Novel membrane modules with high packing density, and better heat and mass transfer performance are required.

It is interesting to focus on the improvement of high salt concentration solution processing by MD (e.g., brines). This is one of the strongest and promising industrial applications of MD technology. Other techniques such as pressure-driven membranes processes cannot compete in this field. The integration of MD units to desalination plants generating brines could be very useful.

The use of MD for wastewater treatment is another area that it is less explored, especially when volatile compounds are present in wastewater. Specific membranes with very high *LEP* in pores and high fouling resistance are demanded.

1.2.7 Sources of further information and advice

Complete and specialized sources of further MD global information may be found in [1, 8, 139, 140]. For better understanding the MD mechanism of transport the recommended sources are [4, 141]. Further details on novel materials used for MD membrane fabrication might be found in [1, 72, 98, 142]. Different membrane fabrication methods are defined in [84] and especially described in [1] with all the fabrication parameters effects fully detailed for each method. Further information about commercial, single, and multilayered membranes fabricated for MD is summarized in [4]. Other membrane modification technologies are collected in [143]. Several techniques used for MD membranes characterization may be found in [1, 8, 100, 144]. Further sources for MD modules may be found in [8, 124]. Energy analysis and cost evaluation of MD technology are reported in [1, 135, 145].

1.3 Development of hollow fiber membranes: motivation and objectives

1.3.1 Motivation

A state-of-the-art of MD membranes is summarized in the previous section 1.2. Some novel membranes of different configurations as well as the techniques followed for their preparation and characterization are also described. It is worth noting that hollow fiber membrane is nowadays the most attractive membrane geometry for MD industrial implementation. Hollow fiber membranes usually exhibit a high packing density (i.e. large surface area per unit volume, 500 – 9000 m^2/m^3) in tubular modules, are mechanically self-supporting and versatile for diverse MD applications. Therefore, membranologists are making significant efforts to develop suitable hollow fiber membranes for MD technology [1, 4, 9, 57].

Different techniques are employed to prepare hollow fiber membranes such as thermally induced phase separation, dry spinning, wet spinning and the commonly used dry/wet spinning technique shown schematically in Fig. 1.3.1. It must be recognized that hollow fiber membrane preparation is more complex than that of flat-sheet membrane because much more operating parameters are involved simultaneously such as the spinning solution (composition and temperature), the spinneret (shape and dimension), the dope extrusion pressure, the gap type (length and humidity), the internal/external coagulant (composition, temperature and flow rate), the coagulation bath (composition and temperature), the fiber take-up speed, etc. All these parameters interact with each other, making difficult the control of the membrane morphology and its properties [1, 46, 59, 102, 146].

Due to the complexity of the hollow fiber membrane fabrication, membranes with different morphological structures are prepared in several research studies based on trial-and-error experiments. In fact, the understanding of hollow fiber membrane formation mechanism is very complicated and the preparation of a hollow fiber membrane with a given desirable structure remains a current challenge for the membrane community [102, 147]. The aim of this PhD Thesis is to study the effects of different spinning parameters on hollow fiber membrane morphology in order to better understand the formation mechanism of these membranes and try to develop a guideline that provides a proper MD membrane structure and minimize the number of experimental tests.

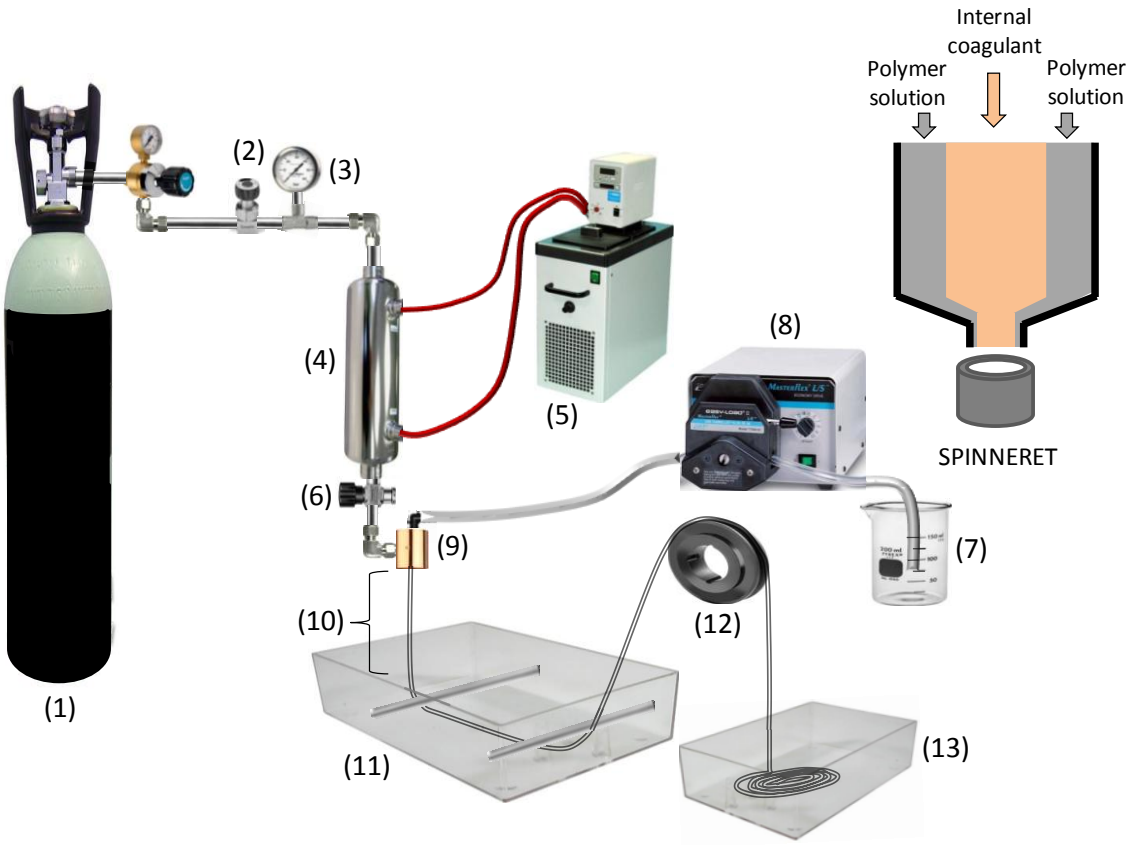

Fig. 1.3.1. Dry/wet spinning experimental set-up. (1) Nitrogen cylinder, (2) regulating pressure valve, (3) pressure gauge, (4) spinning dope tank, (5) thermostat, (6) dope valve, (7) bore liquid vessel, (8) bore liquid pump, (9) spinneret, (10) air gap, (11) coagulation bath, (12) wind-up drum and (13) fiber collection reservoir.

1.3.2 Objectives

In this PhD Thesis, the hollow fiber membranes have been prepared based on the dry/wet spinning technique focusing on the following spinning parameters:

- Spinning dope composition: solvent effect on the structural parameters and MD performance of polymeric membranes (Chapter 2).
- Nonsolvent composition: internal and external coagulant effects on the structural parameters and MD performance of polymeric hollow fiber membranes (Chapter 3).
- Spinneret and gap type: spinneret shape and wetting gap design effect on the structural parameters and MD performance of polymeric hollow fiber membranes (Chapter 4).

- Various spinning parameters and different inorganic suspensions: study of their simultaneous effects on the structural parameters and MD performance of ceramic hollow fiber membranes (Chapter 5).

First of all, before membrane preparation it is necessary to have an in-depth knowledge of the polymer-solvent-nonsolvent system selection. The dope solution (polymer, additive and solvent) and the nonsolvent composition affect considerably the membrane morphology, its structural characteristics and MD performance [9, 61, 146, 148]. The suitable materials for membrane preparation should be chosen after analyzing the viscosity and the surface tension of the dope solution as well as the polymer-solvent-nonsolvent interactions, the thermodynamic and kinetic evaluation using the appropriate characterization techniques [45, 69].

The majority of the used polymeric hollow fiber membranes for MD applications have been prepared with poly(vinylidene fluoride) (PVDF) [83]. This is a commercial polymer, easy to dissolve in common solvents and it is thermally and chemically resistant. Other than the main polymer, pore former additives such as inorganic salts, polymeric additives or even nanoparticles have been usually added to the dope solution in order to increase the porosity of the prepared membranes [9, 149, 150]. In the research studies included in this PhD Thesis the spinning solution used to prepare all the polymeric hollow fiber membranes has been formed by the copolymer poly(vinylidene fluoride-co-hexafluoropropylene) (PVDF-HFP) and the additive polyethylene glycol (PEG). The copolymer PVDF-HFP is an advisable material for MD membranes because of its excellent hydrophobic character owing to the embedment of the group hexafluoropropylene (HFP) to the main polymeric chain PVDF. Not only does the HFP incorporation improve the hydrophobic character of PVDF due to its fluorine content, but also the crystalline character of vinylidene fluoride (VDF) enhances the mechanical properties of the formed material [151]. It is important to highlight that despite the excellent promising properties of PVDF-HFP, it is not very used to prepare hollow fiber membranes for MD applications [58, 59].

It must be pointed out that the polymer must be soluble and the nonsolvent must be miscible in the chosen solvent. Usually, more porous membrane structure is obtained when better miscibility of the polymer in the solvent and higher mutual affinity between the solvent and nonsolvent are met. Before preparing the polymeric spinning dope, it is crucial to study the relative affinity (i.e. Hansen solubility parameter distance, R_{HSP}) between the components of the dope solution in order to select a suitable polymer-solvent-nonsolvent system [102, 152].

Besides other fabrication parameters, the solvent choice determines the success of the membrane preparation [61, 153]. In order to select a suitable solvent for a given polymer, the

affinity between polymer (P) and solvent (S) is analyzed by means of R_{HSP} (P-S). Once the appropriate materials are chosen, the rheological properties of the spinning solution are measured. Both viscosity and surface tension are important parameters that affect the thermodynamics and kinetics of the phase inversion in membrane formation process. Chapter 2 is focused on the selection of the adequate solvent or solvent mixture for the copolymer PVDF-HFP and the nonsolvent "water" for the preparation of MD hollow fiber membranes.

The affinity between nonsolvent (NS) and solvent (i.e. R_{HSP} (NS-S)) affects the demixing rate and influences to the final membrane structure. Kinetic and thermodynamic experiments are advisable to understand the membrane formation mechanism. The phase separation (i.e. thermodynamics) and the rates of solvent evaporation and polymer coagulation (i.e. kinetics) can be determined. The ternary phase diagram is a useful tool to analyze the thermodynamic of membrane precipitation permitting to figure out whether the demixing process is instantaneous or delayed. The thermodynamic experiment represents the thermodynamic stability of a dope solution when a nonsolvent is added permitting the determination of the nonsolvent content (i.e. cloud point) that the polymer system can tolerate before its precipitation. The kinetics of polymer coagulation does not only influence the ultimate structure of the membrane but also the time required for the membrane to solidify during the wet step [69, 102, 154].

Based on the conclusions drawn in Chapter 2, the best spinning solution of the carried out study has been used to prepare improved PVDF-HFP hollow fiber membranes with different nonsolvent mixtures (Chapter 3) used as internal (Chapter 3, 3.1) and external (Chapter 3, 3.2) coagulants. The main objective accomplished in Chapter 3 is the preparation of macro-void free, open-porous structure and skinless hollow fiber membranes that enhance the MD performance [43, 44, 48]. The effects of the addition of the solvent to the nonsolvent mixture on both the inner and outer coagulation power efficiency have been thoroughly studied via Hansen solubility parameter in order to understand the mechanism of formation of the prepared MD hollow fiber membrane. In order to prepare hollow fiber membranes using different external coagulant mixtures along the gap distance (i.e. wet/wet spinning technique) (Chapter 3, 3.2), it was necessary to design and fabricate a triple-orifice spinneret shown in Fig. 1.3.2.

The polymer-solvent-nonsolvent interactions as well as the thermodynamic and kinetic experiments have been always carried out prior hollow fiber preparation in order to phenomenologically predict the membrane morphology (Chapters 2 and 3). Various characterizations techniques have been used to study the suitability of the prepared membranes for MD application. The techniques often used has been scanning electron microscopy (SEM), optical microscopy, atomic force microscopy (AFM), water contact angle equipment, liquid entry pressure set-up, porometer and differential scanning calorimerter to

study the thermal properties. Finally, all membranes have been tested in desalination by DCMD.

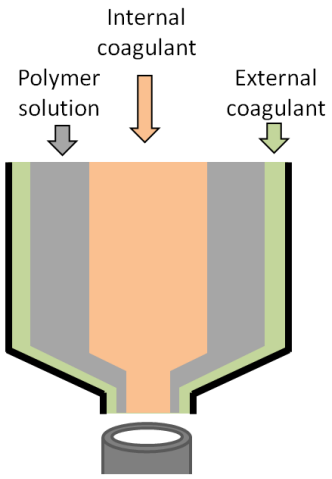

Fig. 1.3.2. Schematic diagram of the designed triple-orifice spinneret.

In addition to the unavailability of commercial/industrial membranes designed specifically for MD, another drawback of this process is the temperature and concentration polarization phenomena that induce severe reductions of the driving force (ΔP_v) of this process owing to the unavoidable presence of the boundary layers at the feed and permeate membrane sides. These effects can be mitigated by operating under a turbulent flow regime in the circulation channels (e.g. increase of fluid flow rates or use turbulence promoters such as spacers in channels) [4, 8, 155, 156]. A schema of the polarization phenomena in a hollow fiber membrane in DCMD configuration is shown in Fig. 1.3.3.

Temperature polarization (TP) phenomenon is covered in Chapter 4 using hollow fiber membranes with microstructured external surfaces. These have been prepared by wet/wet spinning technique using a micro-engineered triple-orifice spinneret (specifically designed for this study) or by spraying the outer surface of the nascent fiber using micro-jet nozzles. The corrugations built on the outer surface of the fiber could act as intrinsic turbulence promoters without the need to introduce any spacers in the membrane module or to increase the fluid circulation flow rates. Consequently, this method would permit to reduce the MD water production cost, increase its energy-efficiency and prevent wetting problem. The corrugated surface of the membrane has been visually inspected and the corresponding degree of corrugation has been determined by SEM and AFM. All prepared hollow fiber membranes have been tested in desalination by DCMD and thorough analysis of the effect of different microstructures on the membrane performance have been carried out in terms of TP phenomenon.

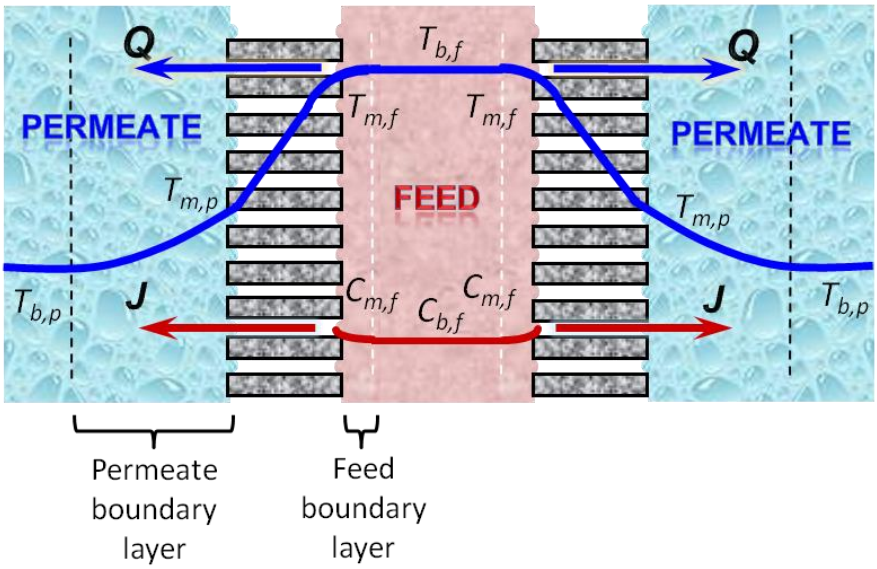

Fig. 1.3.3. Schematic diagram of temperature and concentration polarization phenomena in a hollow fiber membrane module used in DCMD.

The organic (polymeric) membranes have demonstrated to be more competitive in general than the inorganic (ceramic) membranes in MD application. It is easier and cheaper to prepare polymeric membranes that meet the MD membrane requirements. Furthermore, ceramic membranes must be modified to be hydrophobic before their use in MD process. However, it is interesting to fabricate suitable ceramic membranes for MD applications due to their superior mechanical, thermal and chemical properties compared to polymeric membranes. The excellent chemical characteristic of the ceramic membranes enables to treat a wider variety of feed solutions (i.e. extending the MD applicability) while their good thermo-mechanical stability allows to extend the membrane life because it can withstand the necessary cleaning treatment(s) for its further reuse after fouling. The majority of ceramic membranes used so far in desalination by MD are not hollow fibers and their MD performance is usually lower than that of polymeric membranes [14, 157, 158]. Therefore, attempts have been made in Chapter 5 to prepare ceramic hollow fiber membranes (i.e. alumina hollow fiber membranes) with different morphologies. These membranes have been modified to render them hydrophobic, characterized by different techniques and finally used in desalination by AGMD configuration.

References

[1] M. Khayet, T. Matsuura, Membrane Distillation: Principles and Applications. Elsevier, The Netherlands, 2011.

[2] J. Lee, C. Boo, W.H. Ryu, A.D. Taylor, M. Elimelech, Development of Omniphobic Desalination Membranes Using a Charged Electrospun Nanofiber Scaffold, ACS Appl. Mater. Interfaces 8 (2016) 11154-11161.

[3] C. Boo, J. Lee, M. Elimelech, Engineering Surface Energy and Nanostructure of Microporous Films for Expanded Membrane Distillation Applications, Environ. Sci. Technol. 50 (2016) 8112-8119.

[4] M. Khayet, Membranes and theoretical modeling of membrane distillation: a review, Adv. Colloid Interface Sci. 164 (2011) 56-88.

[5] H. Susanto, Towards practical implementations of membrane distillation, Chem. Eng. Process: Process Intensif. 50 (2011) 139-150.

[6] L. Eykens, K. De Sitter, C. Dotremont, L. Pinoy, B. Van der Bruggen, How To Optimize the Membrane Properties for Membrane Distillation: A Review, Ind. Eng. Chem. Res. 55 (2016) 9333-9343.

[7] Y. Zhang, Y. Peng, S. Ji, Z. Li, P. Chen, Review of thermal efficiency and heat recycling in membrane distillation processes, Desalination 367 (2015) 223-239.

[8] A. Alkhudhiri, N. Darwish, N. Hilal, Membrane distillation: A comprehensive review, Desalination 287 (2012) 2-18.

[9] P. Wang, T.-S. Chung, Recent advances in membrane distillation processes: Membrane development, configuration design and application exploring, J. Membr. Sci. 474 (2015) 39-56.

[10] M.R. Qtaishat, F. Banat, Desalination by solar powered membrane distillation systems, Desalination 308 (2013) 186-197.

[11] F. Macedonio, E. Drioli, A.A. Gusev, A. Bardow, R. Semiat, M. Kurihara, Efficient technologies for worldwide clean water supply, Chem. Eng. Process: Process Intensif. 51 (2012) 2-17.

[12] A. Chafidz, E.D. Kerme, I. Wazeer, Y. Khalid, A. Ajbar, S.M. Al-Zahrani, Design and fabrication of a portable and hybrid solar-powered membrane distillation system, J. Cleaner Product. 133 (2016) 631-647.

[13] P. Wang, T.S. Chung, A conceptual demonstration of freeze desalination-membrane distillation (FD-MD) hybrid desalination process utilizing liquefied natural gas (LNG) cold energy, Water research 46 (2012) 4037-4052.

[14] E. Drioli, A. Ali, F. Macedonio, Membrane distillation: Recent developments and perspectives, Desalination 356 (2015) 56-84.

[15] J.A. Sanmartino, M. Khayet, M.C. García-Payo, H. El Bakouri, A. Riaza, Desalination and concentration of saline aqueous solutions up to supersaturation by air gap membrane distillation and crystallization fouling, Desalination 393 (2016) 39-51.

[16] F. Edwie, T.S. Chung, Development of hollow fiber membranes for water and salt recovery from highly concentrated brine via direct contact membrane distillation and crystallization, J. Membr. Sci. 421-422 (2012) 111-123.

[17] F. Edwie, T.S. Chung, Development of simultaneous membrane distillation–crystallization (SMDC) technology for treatment of saturated brine, Chem. Eng. Sci. 98 (2013) 160-172.

[18] M. Essalhi, M. Khayet, Fundamentals of membrane distillation, in: A. Basile, A. Figoli, M. Khayet (Eds.) Pervaporation, Vapour Permeation and Membrane Distillation: Principles and Applications, Elsevier (Woodhead Publishing), Cambridge, 2015, pp. 277-316.

[19] M. Gryta, M. Barancewicz, Influence of morphology of PVDF capillary membranes on the performance of direct contact membrane distillation, J. Membr. Sci. 358 (2010) 158-167.

[20] Y. Fujii, S. Kigoshi, H. Iwatani, M. Aoyama, Selectivity and characteristics of direct contact membrane distillation type experiment. I. Permeability and selectivity through dried hydrophobic fine porous membranes, J. Membr. Sci. 72 (1992) 53-72.

[21] Y. Fujii, S. Kigoshi, H. Iwatani, M. Aoyama, Y. Fusaoka, Selectivity and characteristics of direct contact membrane distillation type experiment. II. Membrane treatment and selectivity increase, J. Membr. Sci. 72 (1992) 73-89.

[22] M. Khayet, T. Matsuura, Pervaporation and vacuum membrane distillation processes: modeling and experiments, AIChE Journal 50 (2004) 1697-1712.

[23] C.A. Rivier, M.C. García-Payo, I.W. Marison, U. von Stockar, Separation of binary mixtures by thermostatic sweeping gas membrane distillation: I. Theory and simulations, J. Membr. Sci. 201 (2002) 1-16.

[24] M.C. García-Payo, C.A. Rivier, I.W. Marison, U. von Stockar, Separation of binary mixtures by thermostatic sweeping gas membrane distillation: II. Experimental results with aqueous formic acid solutions, J. Membr. Sci. 198 (2002) 197-210.

[25] M. Khayet, A.O. Imdakm, T. Matsuura, Monte Carlo simulation and experimental heat and mass transfer in direct contact membrane distillation, International Journal of Heat and Mass Transfer 53 (2010) 1249-1259.

[26] R.W. Schofield, A.G. Fane, C.J.D. Fell, R. Macoun, Factors affecting flux in membrane distillation, Desalination 77 (1990) 279-294.

[27] M. Khayet, C. Cojocaru, Artificial neural network modeling and optimization of desalination by air gap membrane distillation, Sep. Purif. Technol. 86 (2012) 171-182.

[28] T.Y. Cath, V.D. Adams, A.E. Childress, Experimental study of desalination using direct contact membrane distillation: a new approach to flux enhancement, J. Membr. Sci. 228 (2004) 5-16.

[29] D. Hou, G. Dai, J. Wang, H. Fan, L. Zhang, Z. Luan, Preparation and characterization of PVDF/nonwoven fabric flat-sheet composite membranes for desalination through direct contact membrane distillation, Sep. Purif. Technol. 101 (2012) 1-10.

[30] M. Essalhi, M. Khayet, Surface segregation of fluorinated modifying macromolecule for hydrophobic/hydrophilic membrane preparation and application in air gap and direct contact membrane distillation, J. Membr. Sci. 417-418 (2012) 163-173.

[31] X. Wei, B. Zhao, X.M. Li, Z. Wang, B.Q. He, T. He, B. Jiang, CF4 plasma surface modification of asymmetric hydrophilic polyethersulfone membranes for direct contact membrane distillation, J. Membr. Sci. 407-408 (2012) 164-175.

[32] M. Essalhi, M. Khayet, Self-sustained webs of polyvinylidene fluoride electrospun nanofibers at different electrospinning times: 1. Desalination by direct contact membrane distillation, J. Membr. Sci. 433 (2013) 167-179.

[33] C. Feng, K.C. Khulbe, T. Matsuura, R. Gopal, S. Kaur, S. Ramakrishna, M. Khayet, Production of drinking water from saline water by air-gap membrane distillation using polyvinylidene fluoride nanofiber membrane, J. Membr. Sci. 311 (2008) 1-6.

[34] Y. Liao, R. Wang, M. Tian, C. Qiu, A.G. Fane, Fabrication of polyvinylidene fluoride (PVDF) nanofiber membranes by electro-spinning for direct contact membrane distillation, J. Membr. Sci. 425-426 (2013) 30-39.

[35] Y. Liao, R. Wang, A.G. Fane, Engineering superhydrophobic surface on poly(vinylidene fluoride) nanofiber membranes for direct contact membrane distillation, J. Membr. Sci. 440 (2013) 77-87.

[36] B.S. Lalia, E. Guillen-Burrieza, H.A. Arafat, R. Hashaikeh, Fabrication and characterization of polyvinylidenefluoride-co-hexafluoropropylene (PVDF-HFP) electrospun membranes for direct contact membrane distillation, J. Membr. Sci. 428 (2013) 104-115.

[37] L. Francis, H. Maab, A. AlSaadi, S. Nunes, N. Ghaffour, G.L. Amy, Fabrication of electrospun nanofibrous membranes for membrane distillation application, Desalin. Water Treat. 51 (2012) 1337-1343.

[38] H. Maab, L. Francis, A. Al-saadi, C. Aubry, N. Ghaffour, G. Amy, S.P. Nunes, Synthesis and fabrication of nanostructured hydrophobic polyazole membranes for low-energy water recovery, J. Membr. Sci. 423-424 (2012) 11-19.

[39] J.A. Prince, V. Anbharasi, T.S. Shanmugasundaram, G. Singh, Preparation and characterization of novel triple layer hydrophilic–hydrophobic composite membrane for desalination using air gap membrane distillation, Sep. Purif. Technol. 118 (2013) 598-603.

[40] M. Gryta, Influence of polypropylene membrane surface porosity on the performance of membrane distillation process, J. Membr. Sci. 287 (2007) 67-78.

[41] B.A. Li, K.K. Sirkar, Novel membrane and device for direct contact membrane distillation - based desalination process., Ind. Eng. Chem. Res. 43 (2004) 5300-5309.

[42] E. Drioli, A. Ali, S. Simone, F. Macedonio, S.A. Al-Jlil, F.S. Al Shabonah, H.S. Al-Romaih, O. Al-Harbi, A. Figoli, A. Criscuoli, Novel PVDF hollow fiber membranes for vacuum and direct contact membrane distillation applications, Sep. Purif. Technol. 115 (2013) 27-38.

[43] K.Y. Wang, T.S. Chung, M. Gryta, Hydrophobic PVDF hollow fiber membranes with narrow pore size distribution and ultra-thin skin for the fresh water production through membrane distillation, Chem. Eng. Sci. 63 (2008) 2587-2594.

[44] S. Bonyadi, T.S. Chung, Highly porous and macrovoid-free PVDF hollow fiber membranes for membrane distillation by a solvent-dope solution co-extrusion approach, J. Membr. Sci. 331 (2009) 66-74.

[45] Z. Song, M. Xing, J. Zhang, B. Li, S. Wang, Determination of phase diagram of a ternary PVDF/γ-BL/DOP system in TIPS process and its application in preparing hollow fiber membranes for membrane distillation, Sep. Purif. Technol. 90 (2012) 221-230.

[46] Y. Tang, N. Li, A. Liu, S. Ding, C. Yi, H. Liu, Effect of spinning conditions on the structure and performance of hydrophobic PVDF hollow fiber membranes for membrane distillation, Desalination 287 (2012) 326-339.

[47] D. Hou, J. Wang, C. Zhao, B. Wang, Z. Luan, X. Sun, Fluoride removal from brackish groundwater by direct contact membrane distillation, Journal of Environmental Sciences 22 (2010) 1860-1867.

[48] M.M. Teoh, T.S. Chung, Membrane distillation with hydrophobic macrovoid-free PVDF–PTFE hollow fiber membranes, Sep. Purif. Technol. 66 (2009) 229-236.

[49] K.Y. Wang, S.W. Foo, T.S. Chung, Mixed Matrix PVDF Hollow Fiber Membranes with Nanoscale Pores for Desalination through Direct Contact Membrane Distillation, Ind. Eng. Chem. Res. 48 (2009) 4474-4483.

[50] H. Fang, J.F. Gao, H.T. Wang, C.S. Chen, Hydrophobic porous alumina hollow fiber for water desalination via membrane distillation process, J. Membr. Sci. 403-404 (2012) 41-46.

[51] J.W. Zhang, H. Fang, J.W. Wang, L.Y. Hao, X. Xu, C.S. Chen, Preparation and characterization of silicon nitride hollow fiber membranes for seawater desalination, J. Membr. Sci. 450 (2014) 197-206.

[52] S. Bonyadi, T.S. Chung, Flux enhancement in membrane distillation by fabrication of dual layer hydrophilic–hydrophobic hollow fiber membranes, J. Membr. Sci. 306 (2007) 134-146.

[53] S. Bonyadi, T.S. Chung, R. Rajagopalan, A novel approach to fabricate macrovoid-free and highly permeable PVDF hollow fiber membranes for membrane distillation, AIChE Journal 55 (2009) 828-833.

[54] M. Su, M.M. Teoh, K.Y. Wang, J. Su, T.S. Chung, Effect of inner-layer thermal conductivity on flux enhancement of dual layer hollow fiber membranes in direct contact membrane distillation, J. Membr. Sci. 364 (2010) 278-289.

[55] F. Edwie, M.M. Teoh, T.S. Chung, Effects of additives on dual-layer hydrophobic–hydrophilic PVDF hollow fiber membranes for membrane distillation and continuous performance, Chem. Eng. Sci. 68 (2012) 567-578.

[56] M.M. Teoh, T.S. Chung, Y.S. Yeo, Dual-layer PVDF/PTFE composite hollow fibers with a thin macrovoid-free selective layer for water production via membrane distillation, Chem. Eng. J. 171 (2011) 684-691.

[57] P. Wang, M.M. Teoh, T.S. Chung, Morphological architecture of dual-layer hollow fiber for membrane distillation with higher desalination performance, Water research 45 (2011) 5489-5500.

[58] M.C. García-Payo, M. Essalhi, M. Khayet, Effects of PVDF-HFP concentration on membrane distillation performance and structural morphology of hollow fiber memebranes, J. Membr. Sci. 347 (2010) 209-219.

[59] M. Khayet, C. Cojocaru, M. Essalhi, M.C. García-Payo, P. Arribas, L. García-Fernández, Hollow fiber spinning experimental design and analysis of defects for fabrication of optimized membranes for membrane distillation, Desalination 287 (2012) 146-158.

[60] M. Essalhi, M. Khayet, Self-sustained webs of polyvinylidene fluoride electrospun nano-fibers: Effects of polymer concentration and desalination by direct contact membrane distillation, J. Membr. Sci. 454 (2014) 133-143.

[61] A. Bottino, G. Camera-Roda, G. Capanelli, S. Murani, The formation of microporous polyvinylidene difluoride membranes by phase separation, J. Membr. Sci. 57 (1991) 1-20.

[62] A. Bottino, G. Capanelli, S. Murani, A. Turturro, Solubility Parameters of Poly(vinylidene fluoride), Journal of Polymers Science: Part B: Polymer Physics 26 (1988) 785-794.

[63] Y.K. Ong, N. Widjojo, T.S. Chung, Fundamentals of semi-crystalline poly(vinylidene fluoride) membrane formation and its prospects for biofuel (ethanol and acetone) separation via pervaporation, J. Membr. Sci. 378 (2011) 149-162.

[64] D. Hou, J. Wang, D. Qu, Z. Luan, X. Ren, Fabrication and characterization of hydrophobic PVDF hollow fiber membranes for desalination through direct contact membrane distillation, Sep. Purif. Technol. 69 (2009) 78-86.

[65] D.Y. Xing, N. Peng, T.S. Chung, Investigation of unique interactions between cellulose acetate and ionic liquid [EMIM]SCN, and their influences on hollow fiber ultrafiltration membranes, J. Membr. Sci. 380 (2011) 87-97.

[66] L. Setiawan, L. Shi, W.B. Krantz, R. Wang, Explorations of delamination and irregular structure in poly(amide-imide)-polyethersulfone dual layer hollow fiber membranes, J. Membr. Sci. 423-424 (2012) 73-84.

[67] W.Z. Lang, J.P. Shen, Y.T. Wei, Q.Y. Wu, J. Wang, Y.J. Guo, Precipitation kinetics, morphologies, and properties of poly(vinyl butyral) hollow fiber ultrafiltration membranes with respect to polyvinylpyrrolidone molecular weight, Chem. Eng. J. 225 (2013) 25-33.

[68] Y.K. Ong, T.S. Chung, High performance dual-layer hollow fiber fabricated via novel immiscibility induced phase separation (I2PS) process for dehydration of ethanol, J. Membr. Sci. 421-422 (2012) 271-282.

[69] A.C. Sun, W. Kosar, Y. Zhang, X. Feng, A study of thermodynamics and kinetics pertinent to formation of PVDF membranes by phase inversion, Desalination 309 (2013) 156-164.

[70] J.C. Fontananova, A. Jansen, E. Cristiano, E. Curcio, E. Drioli, Effect of additives in the casting solution on the formation of PVDF membranes, Desalination 192 (2006) 190-197.

[71] S. Wongchitphimon, R. Wang, R. Jiraratananon, L. Shi, C.H. Loh, Effect of polyethylene glycol (PEG) as an additive on the fabrication ofpolyvinylidene fluoride-co-hexafluropropylene (PVDF-HFP) asymmetricmicroporous hollow fiber membranes, J. Membr. Sci. 369 (2011) 329-338.

[72] Z. Cui, E. Drioli, Y.M. Lee, Recent progress in fluoropolymers for membranes, Prog. Polym. Sci. 39 (2014) 164-198.

[73] L. Shi, R. Wang, Y. Cao, Effect of the rheology of poly(vinylidene fluoride co-hexafluropropylene) (PVDF-HFP) dope solutions on the formation of microporous hollow fibers used as membrane contactors, J. Membr. Sci. 344 (2009) 112-122.

[74] C. Feng, B. Shi, G. Li, Y. Wu, Preparation and properties of microporous membrane from poly(vinylidene fluoride-co-tetrafluoroethylene) (F2.4) for membrane distillation, J. Membr. Sci. 237 (2004) 15-24.

[75] S. Cerneaux, I. Strużyńska, W.M. Kujawski, M. Persin, A. Larbot, Comparison of various membrane distillation methods for desalination using hydrophobic ceramic membranes, J. Membr. Sci. 337 (2009) 55-60.

[76] M. Khayet, T. Matsuura, Application of surface modifying macromolecules for the preparation of membranes for membrane distillation, Desalination 158 (2003) 51-56.

[77] M. Khayet, J.I. Mengual, T. Matsuura, Porous hydrophobic/hydrophilic composite membranes: Application in desalination using direct contact membrane distillation, J. Membr. Sci. 252 (2005) 101-113.

[78] D.E. Suk, T. Matsuura, H.B. Park, Y.M. Lee, Development of novel surface modified phase inversion membranes having hydrophobic surface-modifying macromolecule (nSMM) for vacuum membrane distillation, Desalination 261 (2010) 300-312.

[79] M. Khayet, T. Matsuura, J. Mengual, Porous hydrophobic/hydrophilic composite membranes: Estimation of the hydrophobic-layer thickness, J. Membr. Sci. 266 (2005) 68-79.

[80] M. Khayet, Treatment of radioactive wastewater solutions by direct contact membrane distillation using surface modified membranes, Desalination 321 (2013) 60-66.

[81] J.A. Prince, G. Singh, D. Rana, T. Matsuura, V. Anbharasi, T.S. Shanmugasundaram, Preparation and characterization of highly hydrophobic poly(vinylidene fluoride) – Clay nanocomposite nanofiber membranes (PVDF–clay NNMs) for desalination using direct contact membrane distillation, J. Membr. Sci. 397-398 (2012) 80-86.

[82] D. Hou, J. Wang, X. Sun, Z. Ji, Z. Luan, Preparation and properties of PVDF composite hollow fiber membranes for desalination through direct contact membrane distillation, J. Membr. Sci. 405-406 (2012) 185-200.

[83] F. Liu, N.A. Hashim, Y. Liu, M.R.M. Abed, K. Li, Progress in the production and modification of PVDF membranes, J. Membr. Sci. 375 (2011) 1-27.

[84] B.S. Lalia, V. Kochkodan, R. Hashaikeh, N. Hilal, A review on membrane fabrication: Structure, properties and performance relationship, Desalination 326 (2013) 77-95.

[85] H. Zhu, H. Wang, F. Wang, Y. Guo, H. Zhang, J. Chen, Preparation and properties of PTFE hollow fiber membranes for desalination through vacuum membrane distillation, J. Membr. Sci. 446 (2013) 145-153.

[86] F. Sadeghi, S.H. Tabatabaei, A. Ajji, P.J. Carreau, Effect of PVDF characteristics on extruded film morphology and porous membranes feasibility by stretching, J. Polym. Sci. Polym. Phys. 47 (2009) 1219-1229.

[87] S. Rajabzadeh, T. Maruyama, T. Sotani, H. Matsuyama, Preparation of PVDF hollow fiber membrane from a ternary polymer/solvent/nonsolvent system via thermally induced phase separation (TIPS) method, Sep. Purif. Technol. 63 (2008) 415-423.

[88] M. Gu, J. Zhang, X. Wang, H. Tao, L. Ge, Formation of poly(vinylidene fluoride) (PVDF) membranes via thermally induced phase separation, Desalination 192 (2006) 160-167.

[89] J.M. Li, Z.K. Xu, Z.M. Liu, W.F. Yuan, H. Xiang, S.Y. Wang, Y.Y. Xu, Microporous polypropylene and polyethylene hollow fiber membranes. Part 3. Experimental studies on membrane distillation for desalination, Desalination 155 (2003) 153-156.

[90] M. Khayet, J.I. Mengual, Zakrzewska-Trznadel, Direct contact membrane distillation for nuclear desalination. Part I: review of membranes used in membranes distillation and methods for their characterization., Int. J. Nuclear Desalination 1 (2005) 435-449.

[91] M. Buczkowski, B. Sartowska, D. Wawszczak, W. Starosta, Radiation resistance of track etched membranes, Radiation Meas. 34 (2001) 597-599.

[92] M. Grasselli, N. Betz, Making porous membranes by chemical etching of heavy-ion tracks in β-PVDF films, Nucl. Instrum. Meth. B 236 (2005) 501-507.

[93] M. Khayet, M.C. García-Payo, Nanostructured Flat Membranes for Direct Contact Membrane Distillation. PCT/ES2011/000091, WO/2011/117443, in, 2011.

[94] M. Essalhi, M. Khayet, Self-sustained webs of polyvinylidene fluoride electrospun nanofibers at different electrospinning times: 2. Theoretical analysis, polarization effects and thermal efficiency, J. Membr. Sci. 433 (2013) 180-191.

[95] L. Dumée, K. Sears, J. Schütz, N. Finn, C. Huynh, S. Hawkins, M. Duke, S. Gray, Characterization and evaluation of carbon nanotube Bucky-Paper membranes for direct contact membrane distillation, J. Membr. Sci. 351 (2010) 36-43.

[96] L. Dumée, S. Gray, M. Duke, K. Sears, J. Schütz, N. Finn, The role of membrane surface energy on direct contact membrane distillation performance, Desalination 323 (2013) 22-30.

[97] K. Gethard, O. Sae-Khow, S. Mitra, Water Desalination Using Carbon-Nanotube-Enhanced Membrane Distillation, Appl. Mater. Interfaces 3 (2011) 110-114.

[98] M. Bhadra, S. Mitra, Nanostructured membranes in analytical chemistry, Trends in Analytical Chemistry 45 (2013).

[99] M. Khayet, C. Cojocaru, M.C. García-Payo, Experimental design and optimization of asymmetric flat-sheet membranes prepared for direct contact membrane distillation, J. Membr. Sci. 351 (2010) 234-245.

[100] L.D. Tijing, J.S. Choi, S. Lee, S.H. Kim, H.K. Shon, Recent progress of membrane distillation using electrospun nanofibrous membrane, J. Membr. Sci. 453 (2014) 435-462.

[101] Z.W. Song, L.Y. Jiang, Optimization of morphology and perf ormance of PVDF hollow fiber for direct contact membrane distillation using experimental design, Chem. Eng. Sci. 101 (2013) 130-143.

[102] N. Peng, N. Widjojo, P. Sukitpaneenit, M.M. Teoh, G.G. Lipscomb, T.-S. Chung, J.-Y. Lai, Evolution of polymeric hollow fibers as sustainable technologies: Past, present, and future, Prog. Polym. Sci. 37 (2012) 1401-1424.

[103] P. Peng, A.G. Fane, X. Li, Desalination by membrane distillation adopting a hydrophilic membrane, Desalination 173 (2005) 45-54.

[104] L. Dumée, J.L. Campbell, K. Sears, J. Schütz, N. Finn, M. Duke, S. Gray, The impact of hydrophobic coating on the performance of carbon nanotube bucky-paper membranes in membrane distillation, Desalination 283 (2011) 64-67.

[105] A. Razmjou, E. Arifin, G. Dong, J. Mansouri, V. Chen, Superhydrophobic modification of TiO2 nanocomposite PVDF membranes for applications in membrane distillation, J. Membr. Sci. 415-416 (2012) 850-863.

[106] S. Meng, J. Mansouri, Y. Ye, V. Chen, Effect of templating agents on the properties and membrane distillation performance of TiO2-coated PVDF membranes, J. Membr. Sci. 450 (2014) 48-59.

[107] J. Zhang, Z. Song, B. Li, Q. Wang, S. Wang, Fabrication and characterization of superhydrophobic poly (vinylidene fluoride) membrane for direct contact membrane distillation, Desalination 324 (2013) 1-9.

[108] X. Yang, R. Wang, L. Shi, A.G. Fane, M. Debowski, Performance improvement of PVDF hollow fiber-based membrane distillation process, J. Membr. Sci. 369 (2011) 437-447.

[109] M. Khayet, The effects of air gap length on the internal and external morphology of hollow fiber membranes, Chem. Eng. Sci. 58 (2003) 3091-3104.

[110] M. Khayet, M.C. García-Payo, F.A. Qusay, K.C. Khulbe, C.Y. Feng, T. Matsuura, Effects of gas gap type on structural morphology and performance of hollow fibers, J. Membr. Sci. 311 (2008) 259-269.

[111] M.C. García-Payo, M. Essalhi, M. Khayet, L. García-Fernández, K. Charfi, H. Arafat, Water desalination by memebrane distillation using PVDF-HFP hollow fiber membranes, Membr. Water Treat. 1 (2010) 215-230.

[112] M. Khayet, C.Y. Feng, K.C. Khulbe, T. Matsuura, Preparation and characterization of polyvinylidene fluoride hollow fiber membranes for ultrafiltration, Polymer 43 (2002) 3879-3890.

[113] M. Khayet, T. Matsuura, Preparation and characterization of polyvinylidene fluoride membranes for membrane distillation, Ind. Eng. Chem. Res. 40 (2001) 5710-5718.

[114] M. Qtaishat, M. Khayet, T. Matsuura, Novel porous composite hydrophobic/hydrophilic polysulfone membranes for desalination by direct contact membrane distillation, J. Membr. Sci. 341 (2009) 139-148.

[115] M. Qtaishat, D. Rana, M. Khayet, T. Matsuura, Preparation and characterization of novel hydrophobic/hydrophilic polyetherimide composite membranes for desalination by direct contact membrane distillation, J. Membr. Sci. 327 (2009) 264-273.

[116] Z.D. Hendren, J. Brant, M.R. Wiesner, Surface modification of nanostructured ceramic membranes for direct contact membrane distillation, J. Membr. Sci. 331 (2009) 1-10.

[117] M. Khayet, K. Khulbe, T. Matsuura, Characterization of membranes for membrane distillation by atomic force microscopy and estimation of their water vapor transfer coefficients in vacuum membrane distillation process, J. Membr. Sci. 238 (2004) 199-211.

[118] M. Khayet, M. Vázquez Álvarez, K.C. Khulbe, T. Matsuura, Preferential surface segregation of homopolymer and copolymer blend films, Surf. Sci. 601 (2007) 885-895.

[119] X. Tian, X. Jiang, B. Zhu, Y. Xu, Effect of the casting solvent on the crystal characteristics and pervaporative separation performances of P(VDF-co-HFP) membranes, J. Membr. Sci. 279 (2006) 479-486.

[120] M.C. García-Payo, M.A. Izquierdo-Gil, Thermal resistance technique for measuring the thermal conductivity of thin microporous membranes, J. Phys. D: Appl. Phys. 37 (2004) 3008-3016.

[121] J.B. Xu, S. Lange, J.P. Bartley, R.A. Johnson, Alginate-coated microporous PTFE membranes for use in the osmotic distillation of oily feeds, J. Membr. Sci. 240 (2004) 81-89.

[122] Y.J. Kim, C.H. Ahn, M.O. Choi, Effect of thermal treatment on the characteristics of electrospun PVDF−silica composite nanofibrous membrane, Eur. Polym. J. 46 (2010) 1957-1965.

[123] M.C. García-Payo, M.A. Izquierdo-Gil, C. Fernandez-Pineda, Air gap membrane distillation of aqueous alcohol solutions, J. Membr. Sci. 169 (2000) 61-80.

[124] C.K. Chiam, R. Sarbatly, Vacuum membrane distillation processes for aqueous solution treatment—A review, Chem. Eng. Process: Process Intensif. 74 (2013) 27-54.

[125] A. Cipollina, M.G. Di Sparti, A. Tamburini, G. Micale, Development of a Membrane Distillation module for solar energy seawater desalination, Chem. Eng. Res. Des. 90 (2012) 2101-2121.

[126] N. Dow, J. Khang, M. Duke, J. Li, S.R. Gray, E. Ostarcevic, Membrane distillation of brine wastes, in: Water Quality Research Australia. Research report 63, 2008.

[127] E. Guillén-Burrieza, J. Blanco, G. Zaragoza, D.C. Alarcón, P. Palenzuela, M. Ibarra, W. Gernjak, Experimental analysis of an air gap membrane distillation solar desalination pilot system, J. Membr. Sci. 379 (2011) 386-396.

[128] E. Guillén-Burrieza, G. Zaragoza, S. Miralles-Cuevas, J. Blanco, Experimental evaluation of two pilot-scale membrane distillation modules used for solar desalination, J. Membr. Sci. 409-410 (2012) 264-275.

[129] K. Zhao, W. Heinzl, M. Wenzel, S. Büttner, F. Bollen, G. Lange, S. Heinzl, N. Sarda, Experimental study of the memsys vacuum-multi-effect-membrane-distillation (V-MEMD) module, Desalination 323 (2013) 150-160.

[130] J.H. Hanemaaijer, A.E. Jansen, J. Van Medevoort, H. De Jon, E. Van Sonsbeek, P.J.J. Koele Engelbert, J.W. Assink, Membrane distillation method for the purification of a liquid, in, United States, 2010.

[131] G. Zakrewska-Trznadel, M. Harasimowicz, A.G. Chmielewski, Concentration of radioactive components in liquid low-level radioactive waste by membrane distillation, J. Membr. Sci. 163 (1999) 257-264.

[132] D. Winter, J. Koschikowski, M. Wieghaus, Desalination using membrane distillation: Experimental studies on full scale spiral wound modules, J. Membr. Sci. 375 (2011) 104-112.

[133] D. Winter, J. Koschikowski, S. Ripperger, Desalination using membrane distillation: Flux enhancement by feed water deaeration on spiral-wound modules, J. Membr. Sci. 423-424 (2012) 215-224.

[134] W.L. Gore, R.W. Gore, D.W. Gore, Desalination device and process, in, United States, 1985.

[135] S. Al-Obaidani, E. Curcio, F. Macedonio, G. Diprofio, H. Alhinai, E. Drioli, Potential of membrane distillation in seawater desalination: Thermal efficiency, sensitivity study and cost estimation, J. Membr. Sci. 323 (2008) 85-98.

[136] A. Criscuoli, M.C. Carnevale, E. Drioli, Modeling the performance of flat and capillary membrane modules in vacuum membrane distillation, J. Membr. Sci. 447 (2013) 369-375.

[137] F. Laganà, G. Barbieri, E. Drioli, Direct contact membrane distillation: modelling and concentration experiments, J. Membr. Sci. 166 (2000) 1-11.

[138] A.E. Jansen, J.W. Assink, J.H. Hanemaaijer, J. van Medevoort, E. van Sonsbeek, Development and pilot testing of full-scale membrane distillation modules for deployment of waste heat, Desalination 323 (2013) 55-65.

[139] M.S. El-Bourawi, Z. Ding, R. Ma, M. Khayet, A framework for better understanding membrane distillation separation process, J. Membr. Sci. 285 (2006) 4-29.

[140] E. Curcio, E. Drioli, Membrane distillation and related operations: A review, Sep. Pur. Rev. 34 (2005) 35-86.

[141] K.W. Lawson, D.R. Lloyd, Membrane distillation, J. Membr. Sci. 124 (1997) 1-25.

[142] P.S. Goh, A.F. Ismail, B.C. Ng, Carbon nanotubes for desalination: Performance evaluation and current hurdles, Desalination 308 (2013) 2-14.

[143] N. Hilal, M. Khayet, C.J. Wright, Membrane modification: technology and applications., CRC Press. Taylor & Francis Group, Boca Raton,U.S.A., 2012.

[144] M. Khayet, Membrane distillation, in: N.N. Li, A.G. Fane, W.S.W. Ho, T. Matsura (Eds.), Advanced Membrane Technology and Applications, John Wiley & Sons, New Jersey, 297-370, 2008.

[145] M. Khayet, Solar desalination by membrane distillation: Dispersion in energy consumption analysis and water production costs (a review), Desalination 308 (2013) 89-101.

[146] C.Y. Feng, K.C. Khulbe, T. Matsuura, A.F. Ismail, Recent progresses in polymeric hollow fiber membrane preparation, characterization and applications, Sep. Purif. Technol. 111 (2013) 43-71.

[147] P.S.T. Machado, A.C. Habert, C.P. Borges, Membrane formation mechanism based on precipitation kinetics and membrane morphology: flat and hollow fiber polysulfone membranes, J. Membr. Sci. 155 (1999) 171-183.

[148] M. Mulder, Basic Principles of Membrane Technology, Kluwer Academic Publishers, 1996.

[149] C. Feng, R. Wang, B. Shi, G. Li, Y. Wu, Factors affecting pore structure and performance of poly(vinylidene fluoride-co-hexafluoro propylene) asymmetric porous membrane, J. Membr. Sci. 277 (2006) 55-64.

[150] L. Shi, R. Wang, Y. Cao, D.T. Liang, J.H. Tay, Effect of additives on the fabrication of poly(vinylidene fluoride-co-hexafluropropylene) (PVDF-HFP) asymmetric microporous hollow fiber membranes, J. Membr. Sci. 315 (2008) 195-204.

[151] Z. Cui, E. Drioli, Y.M. Lee, Recent progress in fluoropolymers for membranes, Prog. Polym. Sci. 39 (2014) 164-198.

[152] C.M. Hansen, Hansen solubility parameters: A User´s Handbook. 2nd ed. CRC Press, Taylor & Francis Group, Boca Ratón, FL, 2nd ed ed., 2007.

[153] M.L. Yeow, Y.T. Liu, K. Li, Morphological Study of Poly(vinylidene fluoride) Asymmetric Membranes: Effects of the Solvent, Additive, and Dope Temperature, J. Applied Polym. Sci. 92 (2004) 1782-1789.

[154] P.v.d. Witte, P.J. Dijkstra, J.W.A.v.d. Berg, J. Feijen, Phase separation processes in polymer solutions in relation to membrane formation, J. Membr. Sci. 117 (1996) 1-31.

[155] Y.M. Manawi, M.A.M.M. Khraisheh, A.K. Fard, F. Benyahia, S. Adham, A predictive model for the assessment of the temperature polarization effect in direct contact membrane distillation desalination of high salinity feed, Desalination 341 (2014) 38-49.

[156] X. Yang, R. Wang, A.G. Fane, Novel designs for improving the performance of hollow fiber membrane distillation modules, J. Membr. Sci. 384 (2011) 52-62.

[157] L.F. Dumée, S. Smart, M.C. Duke, S.R. Gray, Next generation membranes for membrane distillation and future prospects, in: A. Basile, A. Figoli, M. Khayet (Eds.) Pervaporation, Vapour Permeation and Membrane Distillation: Principles and Applications, Elsevier (Woodhead Publishing), Cambridge, 2015, pp. 415-447.

[158] M. Lee, Z. Wu, R. Wang, K. Li, Micro-structured alumina hollow fibre membranes – Potential applications in wastewater treatment, J. Membr. Sci. 461 (2014) 39-48.

2

Polymeric hollow fiber membranes:

Solvent effect on the structural properties and MD performance

Poly(vinylidene fluoride-hexafluoropropylene), PVDF-HFP, hollow fiber membranes were prepared by the dry/wet spinning technique, maintaining all the parameters the same except the solvent used to prepare the polymer solution. Different solvents namely, single *N,N*-dimethyl acetamide (DMAC) and different mixed solvents, DMAC and trimethyl phosphate (TMP) as well as *N,N*-dimethyl formamide (DMF) and TMP were employed. The relative affinity of the PVDF-HFP and the solvent(s) and the thermodynamic and kinetic aspects responsible for membrane formation were investigated and related with the structure of the prepared hollow fiber membranes. The structural and morphological properties of the hollow fiber membranes as well as the necessary parameters to be known for a membrane proposed for direct contact membrane distillation (DCMD) were studied by different characterization techniques. It was observed that an increase of TMP ratio in the solvents mixture resulted in a decrease of the finger-like structure of the external layer, an increase of the pore sizes of the hollow fibers and the DCMD permeate flux enhancement as consequence. When changing DMAC by DMF a thicker hollow fiber membrane was obtained and the DCMD was decreased due partly to the formation of macro-voids in the middle layer of the hollow fiber membrane.

Effects of mixed solvents on the structural morphology and membrane distillation performance of PVDF-HFP hollow fiber membranes

2.1 Introduction

Membrane distillation (MD) is a non-isothermal separation process in which only molecules in vapour phase are transported through a porous and hydrophobic membrane. Recently, MD has received an increasing and special attention (design and fabrication of novel membranes and modules, coupling MD installations to renewable energy systems, development of theoretical models and optimization of MD plants, etc.) [1,2]. The permeability, wetting resistance, long-term stability, energy efficiency and solute rejection or separation factors of MD process are dependent on membrane properties [1-3]. Moreover, the membrane pore structure and morphology play a significant role on the mass and heat transport properties in MD as well as on the mechanical strength of the membrane. During last seven years, membrane fabrication and its performance improvement received a progressive attention by various worldwide research groups, with special interest in hollow fiber membranes due to their high membrane surface area per unit volume resulting in a high permeate production rate, good flexibility in operation, mechanically self-supporting and are easily assembled into modules [1,2,4-11].

Most hollow fiber membranes are prepared by the dry/wet spinning technique although it is a complex process that involves many operating parameters (dope composition, pressure applied on the dope solution, temperature, air gap distance between the spinneret and the external coagulant, nature of the internal and external coagulants, flow rate of the internal coagulant, structure and dimensions of the spinneret, fiber take-up speed, etc.) [12-18]. The morphology, mechanical properties and the performance of hollow fibers are affected by various spinning conditions. The interaction effects between the spinning parameters also play an important role to obtain an optimum hollow fiber membrane [12,19,20]. Therefore, it is not an easy task to identify the adequate spinning conditions for a given polymer. Moreover, up to date understanding the mechanisms of hollow fiber membrane formation is rather qualitative than quantitative.

Recently, the copolymer poly(vinylidene fluoride-co-hexafluoropropylene) (PVDF-HFP) has received much attention as a highly promising material for membrane fabrication for various membrane processes [21-28]. Fluorine content of PVDF-HFP is higher than that of poly(vinylidene fluoride) (PVDF) due to hexafluoropropylene (HFP) group, which makes PVDF-HFP more hydrophobic than PVDF. As a consequence, PVDF-HFP is a potential candidate in applications requiring membranes with higher hydrophobicity such as MD technology.

The reduction of the copolymer concentration in the spinning solution is one of the explored options to improve the membrane permeability but mechanical strength might be sacrificed [20,24,28]. Additives or pore formers are often used. Shi et al. [22,23] used polyvinylpyrrolidone (PVP), lithium chloride (LiCl) and glycerol as additives for fabrication of PVDF-HFP hollow fibers. It was found that the prepared fibers presented different structures with different additives. LiCl or glycerol addition made the resultant membranes exhibit a narrower pore size distribution than that fabricated with the additive PVP. The hydrophobic property of the membranes was affected by three additives in the sequence of PVP > LiCl > glycerol. Moreover, the use of mixed additives, LiCl with Tween 80, and PVP with glycerol, resulted in the development of finger-like macro-voids [27]. Feng et al. [24] reported on the preparation of PVDF-HFP flat sheet asymmetric membranes for direct contact membrane distillation (DCMD) and studied the effects on pore structure and permeate performance of different factors such as polyethylene glycol (PEG) molecular weight, type of additive (i.e. PEG or glycerol), temperature of the external coagulant and its type. Cao et al. [29] used dibutyl phthalate (DBP), PEG and PVP as additives for preparation of PVDF-HFP membranes. The membranes prepared with DBP and PEG exhibited an asymmetric structure and relatively small pore sizes; whereas nearly symmetric and microporous structures were observed when PVP was used as additive. PEG was also used by Hwang et al. [30] and found that the morphology of the PVDF-HFP membranes changed considerably with the composition of the polymer and solvent. Recently, Wongchitphimon et al. [31] revealed that the addition of PEG in PVDF-HFP/ *N*-methyl-2-pyrrolidone (NMP) solution resulted in a system thermodynamically less stable in reaction with water, promoting rapid phase demixing in the phase inversion process. When 3 wt% PEG was added in the polymer solution, it was observed an increase in the dimension of finger-like macro-voids of the membrane with the increase of PEG molecular weight from 200 to 600 and 6000 kDa, enhancing therefore the membrane water permeability .

It is clear that the kinetic parameters of a polymer solution such as the exchange rate between solvent and nonsolvent as well as the thermodynamic parameters such as the polymer-solvent interaction, solvent–nonsolvent interaction are necessary to understand in order to explain and predict a membrane structure [13,32]. For instance, the selection of the

solvent necessary to prepare the polymer solution plays a key role in membrane fabrication. The thermodynamic interaction between the polymer and solvent (i.e. the compatibility between the polymer and solvent) does not only affect the ternary phase diagram (solvent-polymer-nonsolvent) but also the kinetics pore growth [33,34]. As a result, the morphology and performance of the membrane may be predicted and controlled by selecting the appropriate solvent(s). Besides, by evaporating the solvent from the outer surface of the as-spun hollow fiber through the dry phase, air gap between the spinneret and the external coagulation bath, the cross section structure of the membrane can be modified.

Although it is well known that polymer coagulation is due to solvent exchange with nonsolvent affecting considerably the formed membrane structure, with the exception of few early studies, experimental measurements of the solvent-nonsolvent exchange rate and the additive leaching rate during polymer coagulation are very scarce. Recently, some studies appeared on the kinetics of polymer coagulation, but they are mainly focused on ternary systems formed by PVDF, a single solvent and a nonsolvent [33-36]. However, no study is found on the effects of mixed solvents on PVDF or PVDF-HFP hollow fiber membrane structure.

Yeow et al. [37] compared the morphology of flat sheet PVDF membranes prepared with different solvents, NMP, *N,N*-dimethyl formamide (DMF), *N,N*-dimethyl acetamide (DMAC) and triethyl phosphate (TEP). The scanning electron microscopy (SEM) images of these membranes showed a symmetrical sponge-like structure through the whole membrane thickness without cavities when using TEP (i.e. the poorest solvent), but the membrane prepared with the solvent NMP exhibited irregular macro-voids beneath the top skin layer. In the case of the solvents DMF and the strongest solvent DMAC, the PVDF membrane cross-sectional structure exhibited similar short finger-like structure with sponge substrates indicating a slow exchange rate between the solvent and nonsolvent.

Ong et al. [38], by preparing flat sheet asymmetric PVDF membranes with the solvents mixtures (NMP/tetrahydrofuran (THF) or NMP/acetone) and evaporation of the solvents THF and acetone, observed other than the formation of a dense skin top layer the suppression of macro-voids from the cross-section of the membrane. Li et al. [39] also used mixed solvents to prepare PVDF flat sheet membranes and found that the membrane prepared with 60 wt% of trimethyl phosphate (TMP) and 40 wt% of DMAC exhibited the highest permeate flux but a low salt rejection factor. Recently, Li et al. [40] used a dual coagulation process to further improve the PVDF membrane hydrophobicity and prevent the formation of the dense skin layer of flat sheet membranes. The solution casting film was first immersed for 30 s in a mixture of water and the (TEP–DMAC) solution (i.e. the first coagulation bath) followed by immersion in water (i.e. the second coagulation bath). An increase of the TEP–DMAC content in water changed the morphological structure of the

membrane from an asymmetric structure with a dense top layer to a symmetric structure with a skinless top layer, while the pore size distribution turned to be narrower. Moreover, by increasing the mass ratio of TEP to DMAC in the polymer solution, the dense top layer of the membrane surface decreased significantly.

The purpose of this study is to investigate the effects of the solvent type on the PVDF-HFP hollow fiber membrane structure, membrane parameters and DCMD performance. Single (DMAC) and mixed solvents (DMAC/TMP and DMF/TMP) have been considered. Attempts are made to correlate the solvent(s) used to prepare the spinning solutions to the characteristics and final DCMD performance of PVDF-HFP hollow fiber membranes.

2.2 Experimental

2.2.1 Materials

The spinning solutions were prepared from the copolymer poly(vinylidene fluoride-co-hexafluoropropylene) (PVDF-HFP; M_w = 455,000 g/mol), the solvents *N,N*-dimethyl formamide (DMF), *N,N*-dimethyl acetamide (DMAC) and trimethyl phosphate (TMP) and the nonsolvent additive poly(ethylene glycol) (PEG; M_w = 6000 g/mol). Isopropyl alcohol (IPA) was used as a wetting liquid for the measurements of the void volume fraction and sodium chloride (NaCl) to prepare the salt aqueous feed solutions for DMCD experiments. All these chemicals were purchased from Sigma-Aldrich Chemical Co, except NaCl that was purchased from Panreac.

2.2.2 Preparation and characterization of the spinning solutions

5 wt.% of the nonsolvent additive (PEG) was first dissolved in 76 wt.% of the solvent(s) at 42 ºC and 100 rpm using a magnetic stirrer (IKA, RCT basic). Based on the conclusions drawn by Li et al. [39], the used solvent was DMAC, its mixture with TMP at different ratios (40 and 60 wt.%) and the mixture TMP/DMF (40 wt.%) as indicated in Table 2.1. After getting an homogenous mixture, 19 wt.% of PVDF-HFP was added to this mixture and the whole solution was introduced in a thermal bath (Stuart SBS40) maintained at 42 ºC under an orbital shaker until the whole copolymer was totally dissolved.

2.2.2.1 Thermodynamic experiment: cloud point

It is convenient to study the ternary phase diagram in order to understand the thermodynamic behavior of a given phase inversion membrane formation process. Thermodynamic analysis reveals the effects of interaction of blend components during their mixing/demixing steps. The ternary phase diagram was plotted for the used system copolymer/single or mixed solvents/nonsolvent. The cloud point of this system was

determined for each spinning solution by turbidimetric titration method at the same temperature used for preparation of hollow fiber membranes (42 ºC). It is known that the cloud point depends on the temperature [36]. The nonsolvent water, 20 µl, was added stepwise in the PVDF-HFP spinning solution by means of a burette and a gentle stirring using a magnetic stirrer (IKA, RCT basic) at 250 rpm. The necessary quantity of water turning the spinning solution turbid is assigned as the cloud point.

Table 2.1. Composition of the spinning solutions, PVDF-HFP (19 wt%)/PEG (5 wt%)/Solvent (76 wt%), their viscosity and surface tension.

Dope solutions	Solvents			Viscosity (mPa s)	Surface tension (mN/m)
	DMF (%)	DMAC (%)	TMP (%)		
DMF60	60		40	3956 ± 51	33.72 ± 0.17
DMAC100		100		3030 ± 79	33.68 ± 0.14
DMAC60		60	40	4942 ± 66	31.74 ± 0.07
DMAC40		40	60	5792 ± 62	30.45 ± 0.20

2.2.2.2 Kinetic experiments: solvent evaporation and PVDF-HFP coagulation

Asymmetric hollow fiber membranes exhibiting a thin and relatively dense skin layer and a more open porous substrate are commonly produced by the dry/wet spinning technique. The skin layer is mainly due to the partial solvent evaporation involved in the dry phase inversion step through the air gap between the spinneret and the external coagulation bath. Therefore, kinetic studies on the rate of solvent evaporation in the dry step and the solvent-nonsolvent exchange rate in the wet step are essential to understand and subsequently control the membrane structure.

Solvent evaporation study was carried out by casting a flat sheet PVDF-HFP film on a glass plate at 42 ºC and recording the weight change with time of the cast film together with the glass plate. In this test, the same PVDF-HFP solutions prepared for fabrication of hollow fiber membranes were used. All the flat sheet films were fabricated following the same procedure under the same operating conditions.

The solvent-nonsolvent exchange rate of the PVDF-HFP solutions was studied by light transmittance test. The set-up consists of a low-pressure sodium (LPS) employed as light source. The casting PVDF-HPF solution was immersed in a water coagulation bath and the evolution of the transmitted light was detected by a photodiode at wavelength of 589 nm. The coagulation rate of the PVDF-HFP in the coagulation bath was determined by the obtained

normalized light transmittance curve over time. The normalized light transmittance was calculated as follows [41]:

$$T_{norm} = \frac{T - T_{min}}{T_{max} - T_{min}} \quad (2.1)$$

where T_{norm} is the normalized light transmittance, T_{min} is the minimum transmittance and T_{max} is the maximum transmittance.

2.2.2.3 Viscosity and surface tension of the spinning solutions

The viscosity of the spinning solution was measured by a Digital Viscometer (Brookfield, Model DV-I+) using a cylindrical sample container, which permits to keep constant the temperature of the spinning solution by a thermostat (Techne, Model TU-16D). In this study, the viscosity was measured at 42 ºC with the LV1 spindle at 1 rpm and a shear rate of 0.22 s^{-1}.

The surface tension of the spinning solution was determined at room temperature by the pendant drop shape analysis using an optical contact angle meter (CAM 200) and a stainless steel needle having an outer diameter of 1.832 mm. The drop volume of all samples was kept constant at 12.4 μL.

2.2.3 Preparation of hollow fiber membranes and their characterization

The dry/wet spinning technique was employed to prepare the hollow fiber membranes as described elsewhere [28]. Table 2.2 summarizes the spinning parameters, which were maintained the same except the solvent used to prepare the spinning solutions. After spinning, the fabricated hollow fiber membranes were stored in water bath at room temperature for 48 h to remove the residual solvent. Subsequently, the hollow fiber membranes were dried at room temperature before characterization tests.

The inner and outer diameters of the prepared PVDF-HFP hollow fiber membranes were measured by means of an optical microscope (OLYMPUS BX60M) with a precision of ± 1 μm. The internal structure of the membranes was studied by the field emission scanning electron microscope (FESEM, JEOL Model JSM-6335F). The samples were first fractured in liquid nitrogen and then sputter-coated with a thin layer (5 nm) of gold using an evaporator (EMITECH K550 X) for one minute under 25 mA.

The void volume fraction (i.e. porosity, ε) was determined following the method described in previous studies [28,42].

Table 2.2. Spinning parameters of PVDF-HFP hollow fiber membranes.

Parameters	Operating conditions
Inner and outer diameter of the spinneret	d_i = 1.0 mm / d_e = 2.4 mm
Extrusion pressure (kPa)	60
Polymeric solution flow rate (m^3/s)	$2.8\ 10^{-8}$
Polymeric solution temperature (ºC)	42
Bore fluid	Distilled water
Bore fluid flow rate (m^3/s)	$3.2\ 10^{-7}$
External coagulant	Tap water
Bore fluid and external coagulation temperature (ºC)	42
Air gap distance (m)	0.275
Take-up speed (m/s)	0.16
Post-treatment	Tap water

The roughness, the mean pore size and the pore size distribution of both the internal and external surfaces of the PVDF-HFP hollow fibers were studied by atomic force microscopy (AFM). The AFM images were obtained using a tapping mode Nanoscope III equipped with 1553D scanner (Digital Instruments Inc., Santa Barbara, Ca). The same tip was used to scan the surfaces of all samples and all captured images were treated in the same way as described elsewhere [15,16]. The followed methods to evaluate the mean roughness and the mean pore size and determine the pore size distribution were explained in detail in [16,42].

The liquid entry pressure (*LEP*) in the membrane pores is the highest applied transmembrane pressure on a liquid solution before this penetrates into the pores [28,43]. This is an important parameter to be known for a given membrane before its use in any MD application. In fact, *LEP* must be as high as possible. In this study, a salt aqueous solution (NaCl, 3 wt%) was used to determinate the *LEP* using the experimental set-up schematized in Fig. 2.1. Four hollow fibers having a length of about 8 cm were assembled in a stainless steel tube with an epoxy resin. One side of the fibers was closed while the other side was connected to the outlet of a pressurized tank (SARTORIUS, SM 16249). The module was submerged in a container filled with distilled water as shown in Fig. 2.1. After the pressurized tank was filled with the salt aqueous solution, a slight pressure was applied on the hollow fiber membrane for at least 20 min. Subsequently, the applied pressure was increased stepwise by means of a pressure valve. In order to register a correct electrical conductivity by a conductivity meter (EUTECH Instruments, ECCON1103K), distilled water was stirred using a magnetic stirrer

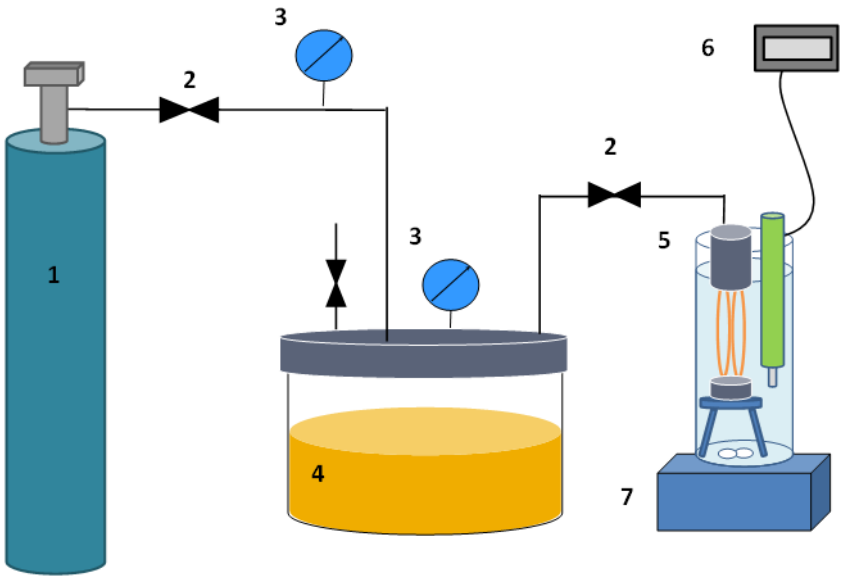

Fig. 2.1. Experimental *LEP* set-up for salt aqueous solutions. (1) Nitrogen tank; (2) regulating pressure valve; (3) pressure gauge; (4) salt solution vessel; (5) hollow fiber module; (6) electrical conductivity meter; (7) magnetic stirrer.

(EYELA RC-2). When the salt solution enters the membrane pores, a change in the electrical conductivity of water in the container is detected. These measurements were performed using three different samples for each PVDF-HFP hollow fiber membrane.

A gas-liquid displacement Porometer (POROLUX™ 100, Porometer) was also used to determine pore size of the hollow fiber membranes. First, a wet curve was obtained by measuring the air flow rate as a function of the difference applied transmembrane pressure using a sample previously submerged in a wetting liquid (POREFIL®, Porometer). Subsequently, a dry curve was obtained following the same procedure. The mean pore size was then determined using both wet and dry curves with the computer software (POROLUX100, Porometer) as described elsewhere [44]. Additionally, the mean pore size and the effective porosity (ε/L_p) were evaluated from the dry curve only following the gas permeation method described elsewhere [42]. ε/L_p is defined as the ratio of the porosity and the effective pore length that takes into account the tortuosity of the membrane pores.

Differential Scanning Calorimetry (DSC) tests were performed with a Mettler-Toledo DSC 1, STAR^e System. The measurements were carried out in a nitrogen atmosphere at flow rate of 20 ml/min. Samples from 3.21 to 4.35 mg were placed in standard aluminum pans of 100 µl capacity. The samples were heated at a rate of 15 °C/min from 35 °C to 200 °C and then cooled down at the same speed. The melting (T_m) and the crystallization (T_c) temperatures correspond to the minimum and maximum peaks of the obtained curves, respectively; while the enthalpy of melting (ΔH_m) and enthalpy of crystallization (ΔH_c) were obtained from the

area of the endothermic and exothermic peaks, respectively. The degree of the crystallinity of the samples was estimated as follows:

$$\chi_c(\%) = \frac{\Delta H_m}{\Delta H_m^{\,o}} \times 100 \tag{2.2}$$

where $\Delta H_m^{\,o}$ is the standard fusion enthalpy for a 100% crystalline polymer, which is 104.7 J/g for PVDF-HFP [45,46].

2.2.4 Direct contact membrane distillation experiments

DCMD experiments were carried out using the experimental set-up shown in Fig. 2.2 Tubular PVDF-HFP hollow fiber membrane modules were first prepared. Six hollow fiber membranes were cut and packed in a stainless-steel shell-and-tube module using epoxy resin at both ends. The effective length of the hollow fiber membranes is 20 cm. The feed and permeate circulated tangentially to the membrane in a counter-current way. The feed solution was circulated through the lumen side of the membrane module, while the permeate (distilled water) was circulated through its shell side. Both the feed and permeate circulated through the membrane module by means of a double-head peristaltic pump (5) (Watson Marlow 323). First, DCMD experiment was carried out using distilled water as feed to check if there is any loss of water in the set-up. Subsequently, DCMD experiments were carried out using a salt aqueous solution (NaCl, 3 wt.%) as feed. The permeate flow rate was determined from the registered mass of produced water over time using a precision balance (10) (Gibertini Europe 3000) connected to a computer (11). The permeate flux was calculated based on the inner fiber surface area. The feed and permeate temperatures were controlled by means of a heating (3) (Techne, model TE-8D) and a cooling (4) (Polysciences, model 6206T) thermostats, respectively. The feed and permeate containers were connected to the corresponding thermostats by glass heat exchangers. Pt-100 probes (7) were installed at both the inlets and outlets of the membrane modules and were connected to the computer (11) using own software developed by our research group that recorded the values of both the mass of produced water and temperatures automatically every 30 s. The feed inlet temperature was varied from 50 to 80 ºC while the permeate inlet temperature was kept at 25 ºC. The feed flow rate (circulated through the lumen side of the membrane module) was kept at 13.8 ± 1.2 kg/h, whereas the permeate circulated through the shell side was kept at 20.7 ± 0.6 kg/h. The membrane module and all tubes were insulated. At the beginning and the end of each DCMD experiment, samples of both the feed and permeate were extracted to measure their electrical conductivity by a conductivity meter (Metrohm model 712) and then determine the salt concentration and the salt rejection factor.

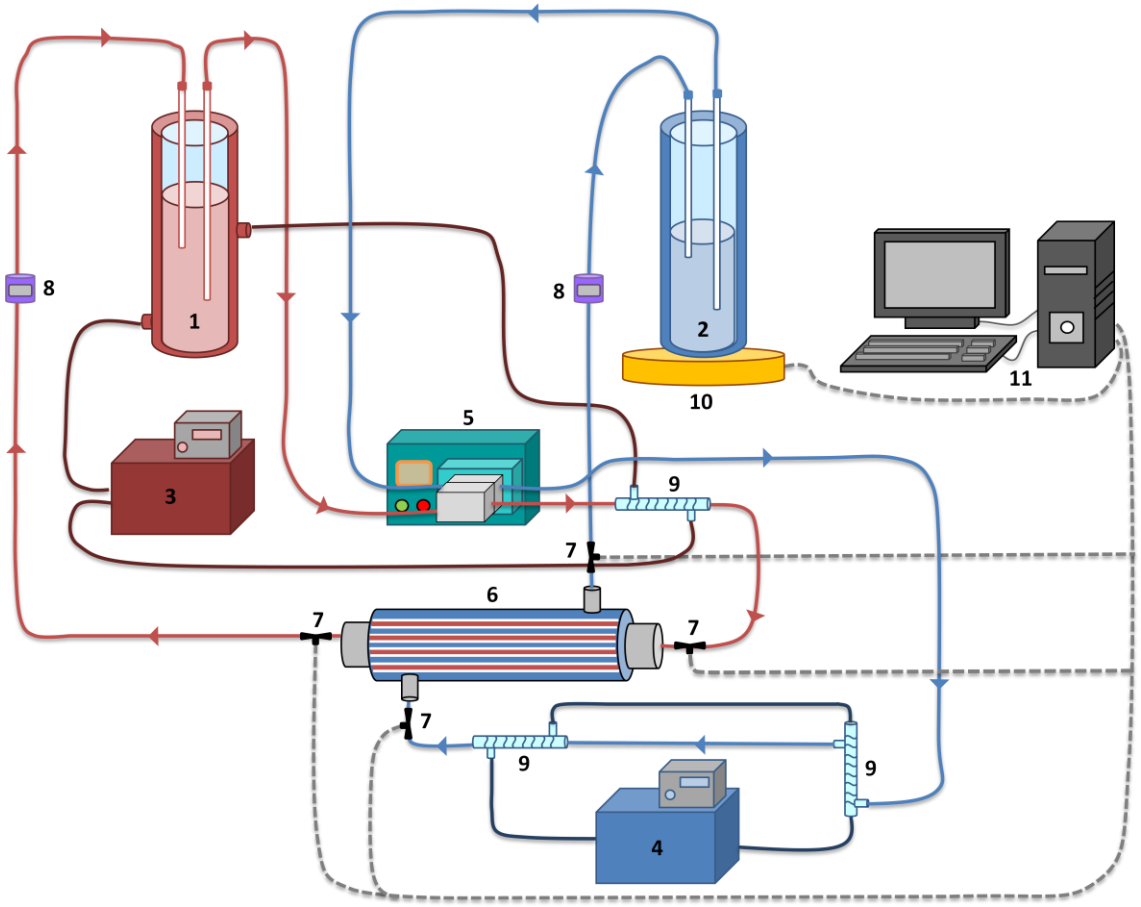

Fig. 2.2. Experimental set-up for direct contact membrane distillation (DCMD): (1) Feed; (2) permeate; (3) heating thermostat; (4) cooling thermostat; (5) double head peristaltic pump; (6) hollow fiber membrane module; (7) Pt-100 probes; (8) flow meter; (9) glass heat exchangers; (10) precision balance; (11) computer.

2.3 Results and discussions

2.3.1 Spinning solution characterization

2.3.1.1 PVDF-HFP/mixed solvent/PEG interactions

The relative affinity of PVDF-HFP and the solvent or the mixtures of solvents can be assessed using the Hansen's solubility parameter, *HSP*, (δ_t), which includes a polar component (δ_p), a dispersion force component (δ_d), and a hydrogen bonding component (δ_h) [47]. Since materials with similar values of δ_t are likely to be miscible, the interaction between PVDF-HFP and the solvent can be defined as *HSP* distance (R_{HSP}) following the equation [47]:

$$R_{HSP} = \left[4\left(\delta_{ds} - \delta_{dc}\right)^2 + \left(\delta_{ps} - \delta_{pc}\right)^2 + \left(\delta_{hs} - \delta_{hc}\right)^2\right]^{1/2} \quad (2.3)$$

where the subscripts *s* and *c* refer to the single solvent or the mixture of solvents and the copolymer PVDF-HFP, respectively. The lower is the distance R_{HSP}, the better is the solvent. *HSP* of solvents mixture can be calculated with the volume fraction weighted average of *HSP* components [48]:

$$\left[\delta_{dm}, \delta_{pm}, \delta_{hm}\right] = \left[a\,\delta_{d1} + b\,\delta_{d2}, a\,\delta_{p1} + b\,\delta_{p2}, a\,\delta_{h1} + b\,\delta_{h2}\right]/(a+b) \quad (2.4)$$

where the subscripts 1 and 2 are for each single solvent present in the mixture, *m* is the solvents mixture, and *a* and *b* are the volume fraction of the different solvents in the mixture. Table 2.3 lists the solubility parameters of PVDF-HFP [49], PEG [31], DMAC, DMF and TMP [47]. It can be seen that the value of R_{HSP} for the pair P-S (PVDF-HFP and DMAC or mixtures of DMAC and TMP) is smaller than those of DMF and TMP indicating that the affinity of PVDF-HFP with DMAC is better than that with the other studied solvents. In conclusion, DMAC demonstrated to be the strongest solvent to PVDF-HFP. The value of R_{HSP} for the pair (P-S) increased with the increase of the TMP amount in the solvent mixture. This means a less interaction of the PVDF-HFP copolymer chains with the solvents mixture making easier the diffusion of the solvent from the spinning solution. As summarized in Table 2.3, no significant change was detected in the R_{HSP} values for water-solvent (W-S) interaction for the spinning solutions DMAC100, DMAC60 and DMAC40. However, when DMAC was changed by DMF in the solvent mixture, R_{HSP} (P-S) was enhanced whereas R_{HSP} (W-S) was reduced improving further the affinity between water and the solvents and making easier the interdiffusion between water and the solvent(s) during coagulation process.

The viscosity of the spinning solution is also an important parameter exerting a strong influence on the interdiffusion of solvent and nonsolvent during the coagulation process and therefore affecting the kinetics of the phase inversion during membrane formation. It is believed that an enhancement of the viscosity reduced the coagulation rate of the polymer solution [39]. Table 2.1 presents the obtained viscosity of the studied spinning solutions. The order of magnitude of these values is the same as that of PVDF-HFP at 23 °C [31] and PVDF [35] solutions measured at 25 °C. As the amount of TMP was increased in the solvents mixture a significant enhancement of the viscosity was observed resulting in a high resistance to water/solvent interdiffusion during PVDF-HFP membrane formation. Moreover, a reduction of the viscosity of the spinning solution was observed when changing DMAC with DMF favoring the water/solvent exchange during PVDF-HFP coagulation.

As it is summarized in Table 2.1, the surface tension of the spinning solution decreased with increasing the amount of TMP in the DMAC mixture and it is higher for DMF60 than for DMAC60. These results are attributed partly to the higher surface tension of the corresponding used solvent(s) (e.g. the surface tension of DMF is higher than that of DMAC).

Table 2.3. Solubility parameters of the solvents, the solvents mixture, the additive PEG, the nonsolvent water and PVDF-HFP with their HSP distances (R_{HSP}) and diffusion coefficients of the solvents.

Material	Solubility parameters ($MPa^{1/2}$)			R_{HSP} [a] ($MPa^{1/2}$)		Diffusion coefficients (10^6 cm^2/s) [52]
	δ_D	δ_P	δ_H	P-S [b]	W- S [c]	D_m
DMF [47]	17.4	13.7	11.3	9.8	31.3	12.8
DMAC [47]	16.8	11.5	10.2	7.2	32.5	11.8
TMP [47]	16.7	15.9	10.2	10.4	32.2	8.6
Water [47]	15.5	16	42.3	---	---	
PEG [31]	15.3	9.6	8.5	---	---	
PVDF-HFP [49]	15.3	7.2	5.3	---	---	
DMF60[d]	17.2	14.5	10.9	9.9	31.6	
DMAC100 [d]	16.8	11.5	10.2	7.2	32.5	
DMAC60 [d]	16.8	13.0	10.2	8.1	32.3	
DMAC40 [d]	16.7	13.9	10.2	8.8	32.3	

[a] Calculated using Eq. (2.3).

[b] P-S: PVDF-HFP-solvent interaction.

[c] W-S: water-solvent interaction.

[d] Calculated using Eq. (2.4).

Decreasing the surface tension of the polymer solution reduced the die-swell effect at the exit of the spinneret. Moreover, it was verified that increasing the polymer solution viscosity also minimized the die-swell effect [50]; and high die swell resulted in greater outer and inner fiber diameters [51]. This statement is applicable for the hollow fiber membranes DMAC60and DMAC40, when the concentration of TMP was increased; and for DMF60 and DMAC60, when the solvent DMF was changed to DMAC. In both cases (i.e. increase of the TMP concentration from 40 to 60 wt% and use of DMAC instead of DMF) the viscosity was increased whereas the surface tension was decreased as can be seen in Table 2.1. Both led to a decrease of the die-swell effect and both the inner and outer fiber diameters were reduced considerably (Table 2.5). For the hollow fiber membranes DMAC100 and DMAC60, no clear relationship can be obtained if the standard errors of the diameters are considered.

The surface tension effect may be related with the die-swell and fiber diameters as a consequence, but this effect can be counterbalanced by the elongational stress along the air gap distance due to gravitational force. In this study, as it will be explained later on, it was

found greater fiber diameters and thickness of the membrane DMF60 prepared with higher surface tension spinning solution than the membrane DMAC60 (Table 2.5).

2.3.1.2 Thermodynamic and kinetics experiments

Figure 2.3 shows the developed ternary phase diagram representing phase separation of the studied spinning solutions prepared with different solvents. The stronger is the solvent power, the greater is the amount of nonsolvent (water in this study) required to induce PVDF-HFP precipitation. When the amount of TMP in the solvent mixture was increased, the cloud point shifted away from the PVDF-HFP/PEG – water axis towards the PVDF-HFP/PEG - solvent axis. This effect was more pronounced when DMF was used instead DMAC. The amount of water required for PVDF-HFP coagulation (i.e. cloud point) decreased following the order (the thermodynamically less stable spinning solution): DMF60 < DMAC40 < DMAC60 < DMAC100. This result agrees with the reported values of R_{HSP} for the pair (P-S) in Table 2.3. The thermodynamic results indicate that the increase of the TMP rate in the spinning solution and the use of the solvent DMF instead of DMAC both cause an earlier phase separation. It is known that the morphological structure of a membrane precipitated by liquid/liquid demixing depends on the position of the polymer solution in the ternary phase diagram and for the polymer concentration above the critical point demixing occurs by nucleation of the polymer lean phase resulting in a porous structure, which will be more or less open depending on the time available for droplets coalescence. However, when the polymer concentration is low, demixing takes place by nucleation of the polymer-rich phase giving rise to a latex-type structure. The structure of the hollow fiber membranes prepared in this study with different types of solvents will be explained based on the obtained SEM images taking into consideration this phenomenon.

The kinetics of solvent evaporation can be described quantitatively. Sun et al. [34] reported that the temperature and film-casting thickness affected the solvent evaporation rate significantly. In this study both parameters were maintained constant and only the effect of the mixed solvents was investigated. The partial evaporation of the solvent from the surface of the nascent membrane in the dry step (along the air gap in the case of hollow fiber spinning) affects not only the outer skin layer of the as-spun fiber but also the polymer coagulation from the inner wet side of the fiber. Figure 2.4 shows the relative quantity of the evaporated solvent $((W_0 - W_t)/(W_0 - W_\infty))$ versus time. W_0 is the initial weight of the cast film plus the glass plate at time 0, W_t is the weight at time t and W_∞ is the final weight, when the solvent is completely evaporated. The following empirical equation was proposed to describe solvent evaporation during the early stage of the dry step for membrane formation by the dry/wet phase inversion method [53]:

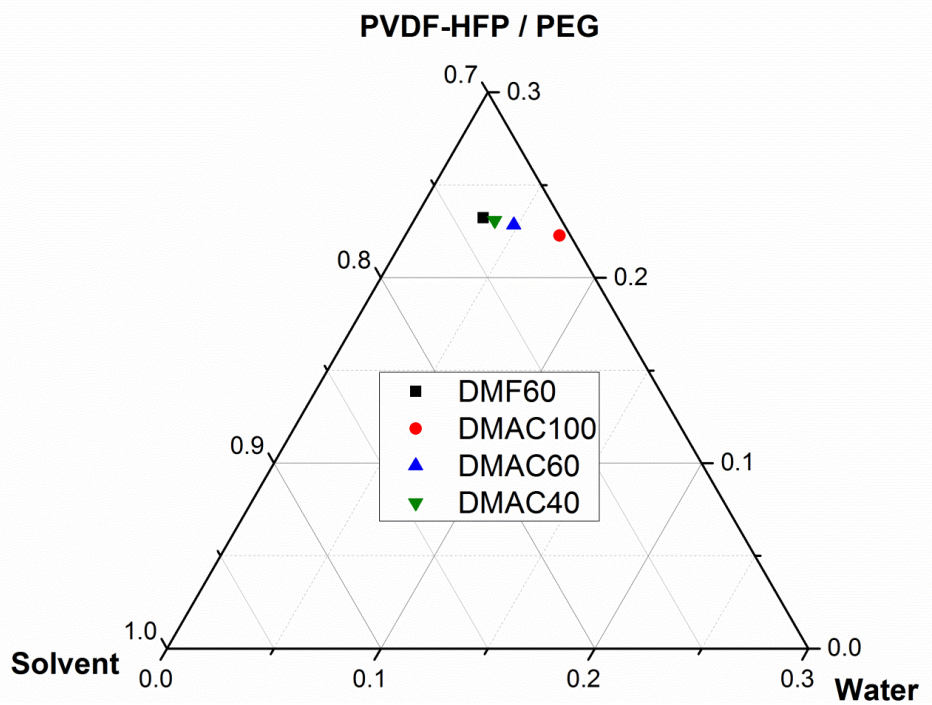

Fig. 2.3. Ternary phase diagram of the (PVDF-HFP/PEG)/solvent (single and mixed solvents)/water systems.

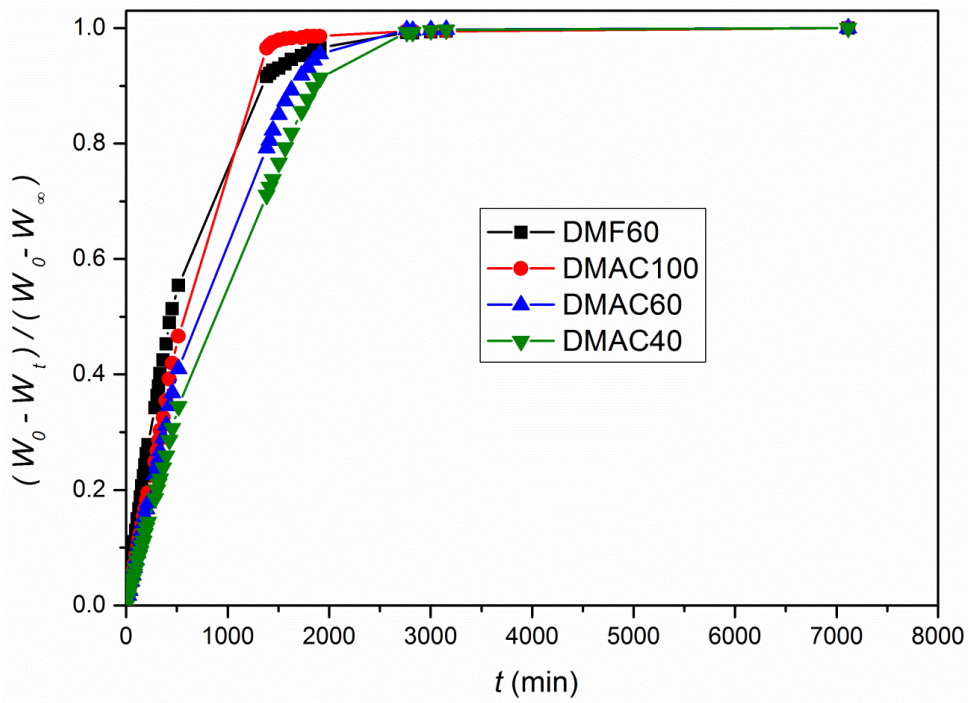

Fig. 2.4. Experimental data of the weights variation $(W_0\text{-}W_t)/(W_0\text{-}W_\infty)$ of different spinning solutions with solvent(s) evaporation time.

$$\frac{W_0 - W_t}{W_0 - W_\infty} = 1 - \exp\left(-b\,t^m\right) \tag{2.5}$$

where b is an empirical parameter indicating how sooner the solvent starts to evaporate while m represents the rate of solvent evaporation.

Table 2.4 presents the obtained empirical parameters (m and b) of the spinning solutions prepared with different solvents. The reasonably good linear fit in Fig. 2.5 indicates that Eq. (2.5) is suitable to describe the solvent evaporation during the early stage of the dry step for hollow fiber membrane formation. It can be seen that when the quantity of TMP in the solvents mixture was increased the parameter m decreased indicating a reduction of the solvent evaporation rate. However, no significant changes were detected for the parameter b concluding that the amount of TMP in the solvents mixture did not affect the onset time of solvent evaporation. Castellari and Ottani [54] stated that the mass transfer within the polymeric cast film, during the solvent evaporation step, was a combination of both solvent diffusion and polymer contraction. Taking into consideration that the diffusion coefficient (D_m in Table 2.3) of TMP is lower than that of DMAC, the lowest m value was obtained for the DMAC40 cast film prepared with the highest amount of TMP (see Table 2.4). When DMF was used as solvent instead of DMAC, the parameter b for the spinning solution DMF60 was found to be greater than that for the solution DMAC60, resulting in a quick initial solvent evaporation time when using DMF. This may be attributed partly to the lower boiling point of DMF (153 ºC) compared to that of DMAC (165 ºC) or which is the same the higher vapor pressure of the solvent DMF.

The dynamics of wet phase inversion was characterized by the solvent/nonsolvent exchange rate, which could give information on the structural morphology of the membrane. Faster solvent/nonsolvent exchange rate promotes the formation of finger-like structure or even macro-voids. Figure 2.6 illustrates the demixing curves of the studied spinning solutions by light transmittance. As it can be seen in Fig. 2.6, the phase inversion kinetic of the PVDF-HFP spinning solutions showed three stages. The normalized transmittance decreased slowly in the first stage, then it is quickly decreased in the second stage and finally it reduced slightly

Table 2.4. Empirical parameters (m and b in Eq. (2.5)) of the PVDF-HFP spinning solutions.

Spinning solution	m	b (10^{-4} min^{-m})
DMF60	1.0377 ± 0.0050	12.229 ± 0.048
DMAC100	1.1163 ± 0.0096	5.515 ± 0.037
DMAC60	1.0847 ± 0.0071	5.798 ± 0.029
DMAC40	1.0395 ± 0.0099	5.965 ± 0.042

in the third stage approaching an asymptotic transmittance value. The same trend was observed previously by Li et al. [39,40]. The first stage indicated a delay of the nonsolvent (water) penetration in the cast PVDF-HFP film. This effect can be attributed to the hydrophobic nature of this copolymer that delays the penetration of water during phase separation process [41]. However, no full delay was observed because the normalized transmittance did not maintain the same value to unity but it declined to approximately 0.8 attributed to the presence of the hydrophilic polymer, PEG, in the spinning solution. For this reason, this period was termed the first stage instead of "time lag". Lang et al. [55] also observed this effect when a hydrophilic polymer, perfluorosulfonic acid (PFSA), was added in the PVDF/DMAC solution. A perfect delayed demixing curve with its time lag period was obtained when PFSA was not added in the PVDF/DMAC solution.

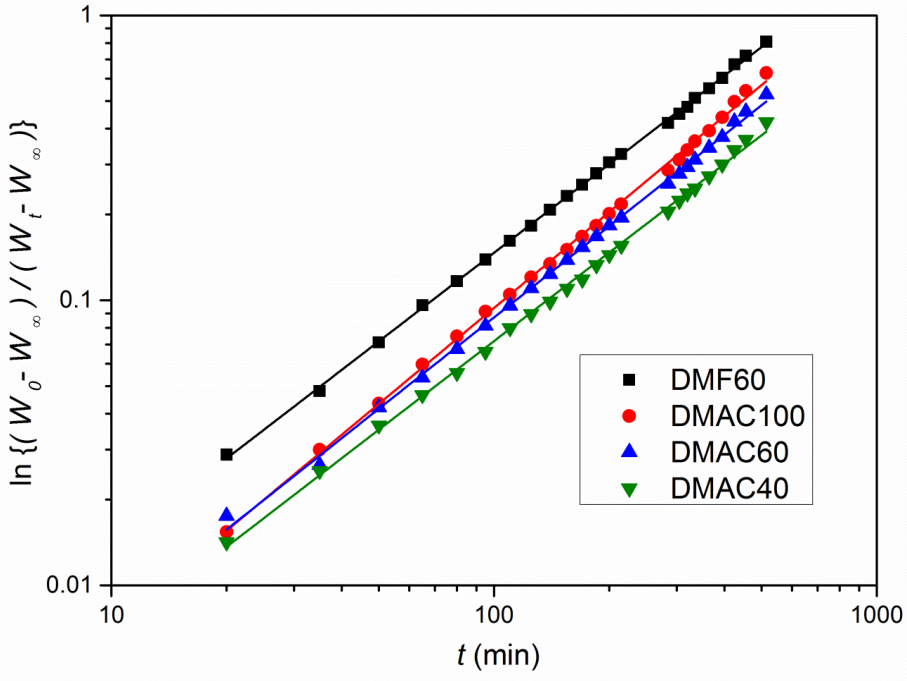

Fig. 2.5. Logarithmic plot of $\ln\left[(W_0\text{-}W_\infty)/(W_t\text{-}W_\infty)\right]$ versus time for the data shown in Fig. 2.4.

The registered period of the first stage increased with the use of the solvent DMAC and with the increase of TMP amount in the solvents mixture (DMAC/TMP). Moreover, it can be seen in Fig. 2.6 that the demixing rate declined with the increase of the amount of TMP in the solvents mixture. In addition, the coagulation rate of the spinning solution prepared with DMF (DMF60) was found to be the highest. These coagulation kinetic experiments agreed well with the solvent diffusion coefficients (Table 2.3) and the viscosity of the spinning solutions (Table 2.1). The highest diffusion coefficient corresponds to the solvent DMF, whereas the smallest one is for the solvent TMP. These mean a faster exchange rate between water and DMF and a slower water-solvent exchange when TMP was employed. As it was

stated earlier, the coagulation rate also depends strongly on the viscosity of the spinning solutions. The more viscous is the spinning solution, the lower is the PVDF-HFP coagulation rate. This effect has been observed when increasing the TMP amount in the solvent mixture and when changing DMF by DMAC. The solubility parameter difference and the thermodynamic results were both related with the initiation of the PVDF-HFP coagulation process, being able to conclude that the use of DMF and the increase of the TMP concentration in the solvent mixture may result in an earlier PVDF-HFP precipitation because less quantity of water was required (i.e. lower cloud point, Fig. 2.3).

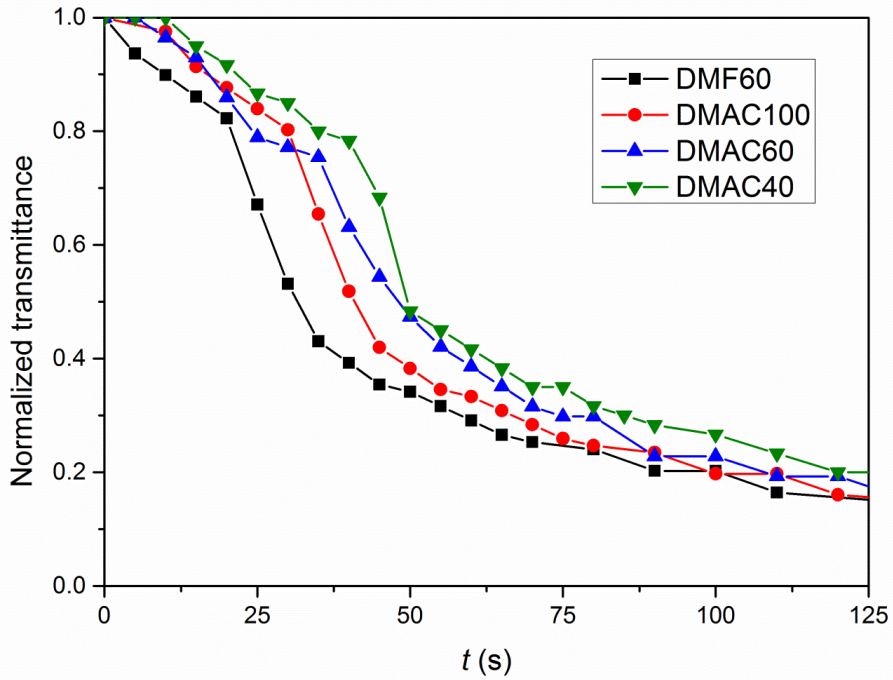

Fig. 2.6. Coagulation experiments of the spinning solutions prepared with different solvents.

2.3.2 Hollow fiber membrane characterization

2.3.2.1 Effects of the solvent(s) on the internal structure of the PVDF-HFP hollow fibers

The cross-sectional structure of the PVDF-HFP hollow fiber membranes were studied by SEM. Figure 2.7 shows the evolution of the cross-section structure of the hollow fiber membranes depending on the type of the used solvent(s). All membranes exhibit a common overall structure, which is a sponge-like structure in the middle layer and a finger-like structure in the internal and external layers of the hollow fiber membranes. The observed SEM membrane morphology confirms that the hollow fibers were formed by nucleation of the copolymer lean phase resulting in a porous structure. Larger and longer tear-drop macro-voids between the inner layer and sponge-like structure in the middle layer can be observed in the

hollow fibers prepared with the mixture of the solvents DMF/TMP. These macro-voids disappeared in the middle layer of the hollow fiber membranes when DMAC was used instead DMF in the solvent mixtures. In the case of flat sheet PVDF membranes prepared with different solvents mixtures, Li et al. [39] also observed that the increase of the solubility parameter difference between the polymer and the solvent, the weaker solvent power, the lower cloud point and the higher viscosity, lead to a slow polymer coagulation rate and avoid the formation of macro-voids and finger-like structures. Macro-voids can also be reduced to parallel finger-like structure or disappear and even turn to sponge-like structure with the increase of the copolymer concentration in the spinning solution [28]. It is worth noting that, in general the formation of macro-voids is an undesirable structure for MD [6,12,56]. Macro-voids can cause a weak mechanical strength, facilitate pore wetting and therefore reduce the long-term use of the membrane. For long-term performance application it is better to use membranes exhibiting a sponge-like structure through its cross-section [1,12,13]. When the TMP content in DMAC was increased, the sponge-like structure in the middle layer became thicker, whereas the finger-like structure formed at the outer side of the hollow fiber prepared with DMAC/TMP was decreased. Furthermore, the finger-like structure of the internal layer became slightly longer and narrower with the increase of TMP rate in the solvent mixture DMAC/TMP.

The observed changes of the structural morphology of the PVDF-HFP hollow fiber membranes can be associated to the previously reported characteristics of the spinning solutions based on the solubility parameters, thermodynamic tests, viscosity, coagulation rate and evaporation kinetic experiments. Elimination of macro-voids from the cross-section structure may be due to the increase of the viscosity of the spinning solution when using DMAC solvent instead of DMF (DMF60 and DMAC60 in Table 2.1). It has been demonstrated that increasing the dope viscosity is the main approach to suppress macro-voids from the cross-section of phase inversion membranes [56]. Furthermore, based on the calculated R_{HSP} (P-S) values, the best solvent is DMAC; whereas based on the calculated R_{HSP} (W-S) values, the highest solvent-water affinity corresponds to the spinning solution prepared with DMF. Therefore, the solvent DMF has less affinity towards the copolymer PVDF-HFP and better affinity to water than DMAC, facilitating in this case the interdiffusion between water and the solvent(s) during hollow fiber coagulation. The PVDF-HFP coagulation rate is faster and earlier when the solvent DMF was used as solvent, as it can be predicted also from the coagulation kinetics (see Fig. 2.6) and from the evaporation kinetics (see parameter *b* in Table 2.4) and the thermodynamic results (see Fig. 2.3), respectively. These lead to the formation of bigger fingers in the inner layer ended by macro-voids inside the cross-section as can be seen in Fig. 2.7 for the membrane DMF60.

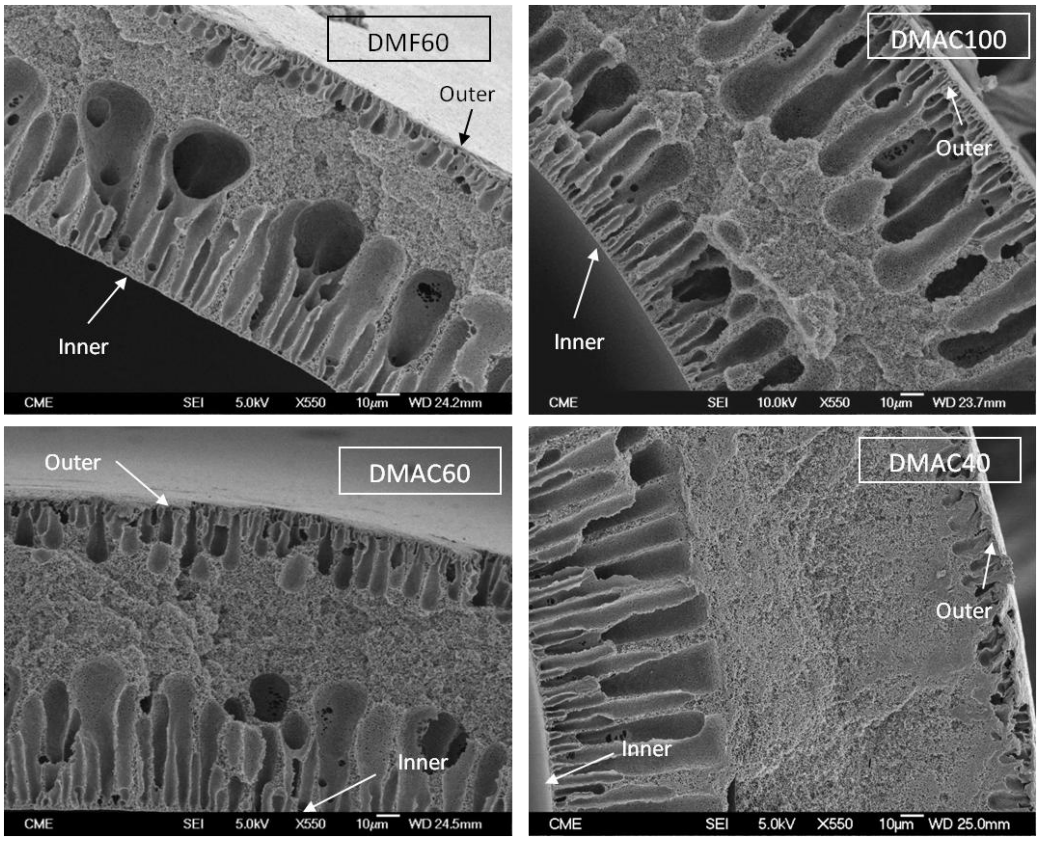

Fig. 2.7. SEM images of the cross-section morphology of the PVDF-HFP hollow fiber membranes prepared with different solvents.

Among all the PVDF-HFP spinning solutions considered in this study (see Table 2.1), the one prepared with the solvent mixture DMAC/TMP with the maximum TMP content in DMAC has the highest viscosity. Therefore, by increasing the TMP ratio in the solvent mixture, both the viscosity of the spinning solution and the R_{HSP} (P-S) increased and the cloud point declined affecting the kinetics of the phase inversion during membrane formation process. As a result, a larger sponge-like structure was obtained for higher TMP ratio.

The observed longer and narrower finger-like structure of the internal layer with the increase of TMP concentration in the dope solution can be due to the cloud point reduction (Fig. 2.3) and the increase of R_{HSP} (P-S) (Table 2.3). The lower coagulation (i.e. cloud point) and the higher R_{HSP} (P-S) both induced a deeper nonsolvent diffusion to the spinning solution and an easier solvent extraction from the spinning solution.

The SEM images were analyzed by UTHSCSA ImageTool 3.0 to determine the thickness of the finger-like and sponge-like structures of the different layers. The sponge-like structure in the middle layer represents 27%, 43% and 53% of the total thickness of the hollow fiber membranes DMAC100, DMAC60 and DMAC40, respectively. As it has been mentioned earlier, a macro-void free structure is desirable in membrane processes. Therefore, the

membranes DMAC60 and DMAC40 exhibited better structure than the other prepared hollow fiber membranes with similar materials PVDF-HFP/PEG/DMAC, having cross-section structures containing a high percentage area covered by macro-voids (i.e. 63 - 76%) [20].

For PVDF polymer, Li et al. [39,40] observed a delayed demixing hindering the development of finger-like structure when using the solvents mixture having the poorest solvent power. Similar result is obtained in this study when increasing the amount of TMP in the in the solvent mixture (DMAC/TMP) (i.e. increase of R_{HSP} (P-S)). In addition, a weaker solvent power and a higher solution viscosity mainly enhanced the shrinkage of the membranes [39]. The areas of the membranes were measured before and after the evaporation test, obtaining reductions of their areas of (i.e. shrinkage) of 32%, 35% and 41% for DMAC100, DMAC60 and DMAC40, respectively. Higher shrinkage of the membranes and lower solvent evaporation rate (see the parameter *m* in Table 2.4) resulted in denser and more wrinkled skin-layer [17], which acted as a resistive barrier between the coagulation bath and the interior region of the membrane [57]. Consequently, a delayed demixing was detected with the increase of TMP amount in the solvents mixture (i.e. first stage period of the coagulation curves in Fig. 2.6 became longer) and the thickness of the finger-like structure of the external layer of the hollow fiber membranes decreased. The finger like structure layer of the external surface represents 34%, 19% and 6% of the total thickness of the hollow fiber membranes for DMAC100, DMAC60 and DMAC40, respectively.

2.3.2.2 Effects of the solvent(s) on the morphological characteristics of the PVDF-HFP hollow fibers

The internal and external diameters as well as the thickness of the prepared PVDF-HFP hollow fiber membranes are summarized in Table 2.5. No clear trends were detected for the effects of TMP content on both the thickness and the diameters, which were not changed significantly. Among all PVDF-HFP hollow fiber membranes, DMAC60 is the thinnest one. The thickness of all prepared hollow fiber membranes are thicker than those prepared under similar spinning conditions in our previous study [28]. For example, if the membrane DMAC100 is compared to the membrane CO19 (PVDF-HFP (19 wt%)/PEG (3 wt%)/ DMAC) in [28], it can be seen a decrease in both the inner and outer diameters and an increase of the thickness (more than two times). This can be attributed to the higher amount of PEG used in this study, 5 wt% instead of 3 wt%, as described elsewhere [26]. The thickness enhancement may be attributed to the viscosity of the dope solution, which increased with increasing PEG concentration in the dope solution (i.e. increase of the shear stress of the dope solution within the spinneret).Both the inner and outer diameters as well as the thickness of the PVDF-HFP hollow fiber membrane prepared with DMF (DMF60) were greater than

those of the membrane prepared with DMAC (DMAC60). These results may be attributed to the surface tension of the spinning solution, which is higher for DMF/TMP (DMF60) compared to DMAC/TMP (DMAC60). Moreover, the higher thickness of the membrane DMF60 compared to the membrane DMAC60 can also be explained admitting that the same quantity of copolymer is more closely packed in a spongy structure than in an asymmetric structure containing macro-voids [59-61].

The void volume fraction (ε) of the hollow fiber membranes is shown in Table 2.5. No clear trend was detected for the void volume fraction in relation with the TMP content in the solvent mixture, and the membranes DMAC100 and DMAC40 exhibited the highest void volume fraction values. Similar ε values were reported in previous studies for PVDF and PVDF-HFP hollow fiber membranes [6,8,14,28]. However, the ε values obtained in this study are higher than those presented by Khayet et al. [20,42] for PVDF (lower than 43%) and PVDF-HFP (lower than 60%) hollow fiber membranes.

The measured *LEP* values of the hollow fiber membranes are also shown in Table 2.5. These *LEP* values are greater than those reported by Khayet el al. [20] for PVDF-HFP hollow fiber membranes, which are between 0.25 and 0.75 10^5 Pa, and lower *LEP* values than the majority of PVDF hollow fiber membranes prepared by Khayet et al. [42]. The highest *LEP* value in this study was obtained for the membrane DMAC100 and it is similar to those obtained by García-Payo et al. [28] when it is compared with the same PVDF-HFP concentration and the same single solvent DMAC (CO19 membrane in [28]). Therefore, among all prepared PVDF-HFP hollow fiber membranes it may be expected a small maximum pore size of this membrane. For the membranes prepared with TMP mixed solvent (DMAC40, DMAC60 and DMF60), the *LEP* value decreased by half that of DMAC100.

The SEM image of the cross-section of the membrane DMF60 showed macro-voids in the middle layer. The formation of these macro-voids could facilitate membrane wetting, decreasing the corresponding *LEP* value. The lower *LEP* of the hollow fiber membranes prepared with the mixed solvent DMAC/TMP (DMAC60 and DMAC40) compared to that

Table 2.5. Diameters, thickness, void volume fraction and *LEP* of PVDF-HFP hollow fibers membranes.

Membrane	Inner diameter (μm)	Outer diameter (μm)	Thickness (μm)	Void volume fraction (ε %)	*LEP* (10^5 Pa)
DMF60	1515 ±130	1800 ± 100	141 ± 19	67.3 ± 2.4	0.95 ± 0.06
DMAC100	1310 ± 70	1610 ± 80	150 ± 50	72.5 ± 1.1	2.04 ± 0.04
DMAC60	1470 ± 100	1700 ± 130	113 ± 16	65.1 ± 2.2	1.00 ± 0.05
DMAC40	1190 ± 180	1550 ± 150	180 ± 40	70.9 ± 1.2	1.04 ± 0.04

of DMAC100 may be attributed to the main difference observed for the external layer structure. DMAC100 had longer and bigger fingers, while the membranes DMAC60 and DMAC40 had shorter and narrower fingers in their external layer. The finger-like structure of the outer surface of the membrane DMAC100 may hinder the exit of the wetting liquid and therefore it is necessary to apply more hydrostatic pressure before water flows out of this membrane. On the other hand, the *LEP* values of the membranes DMAC60 and DMAC40 are almost similar and lower than that of DMAC100, due to the shorter and narrower fingers of the outer structure. In general, judging from the obtained *LEP* values, all prepared membranes in this study can be used in MD.

Figures 2.8 and 2.9 show the 3D AFM images of the inner and outer surfaces of the PVDF-HFP hollow fiber membranes, respectively. AFM images reveal that the surfaces of all membranes possess smooth nodule-like and valley-like structures. The bright peaks represent

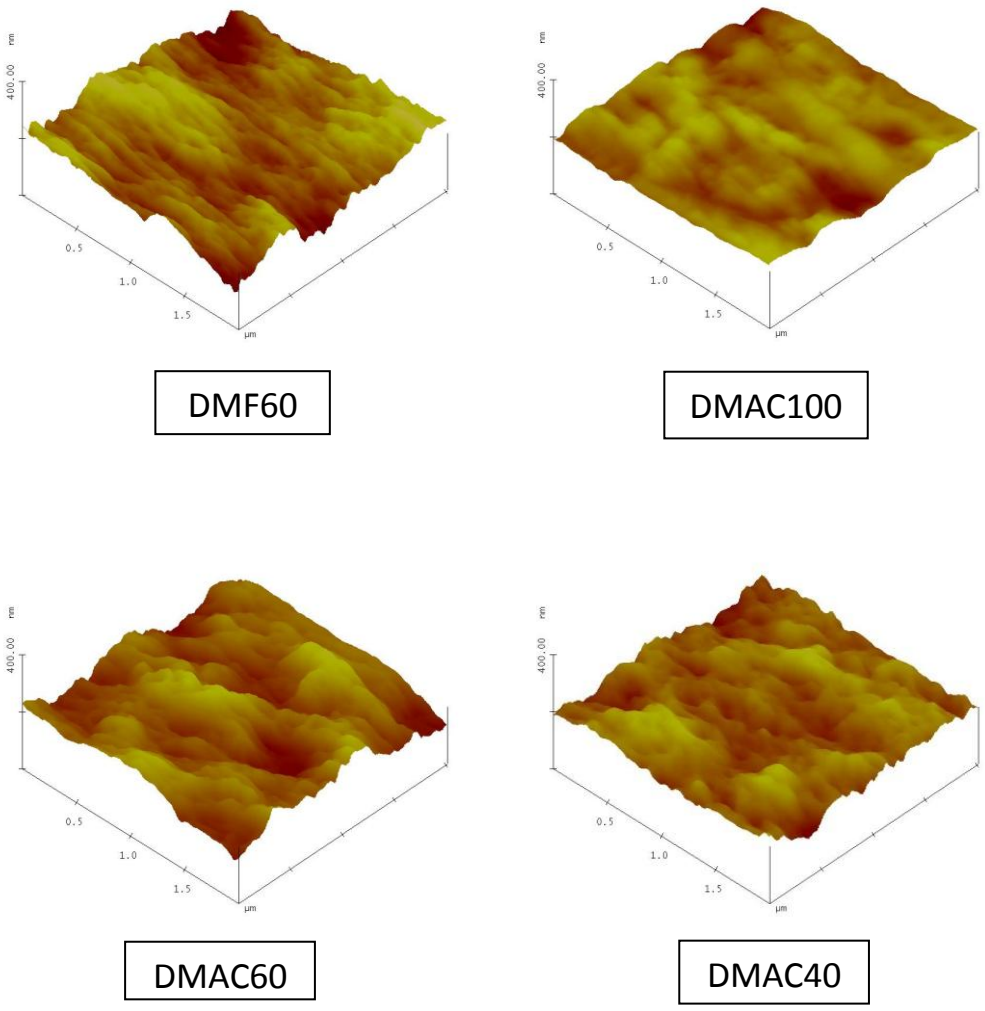

Fig. 2.8. 3D AFM images of the inner surfaces of the PVDF-HFP hollow fiber membranes prepared with different solvents.

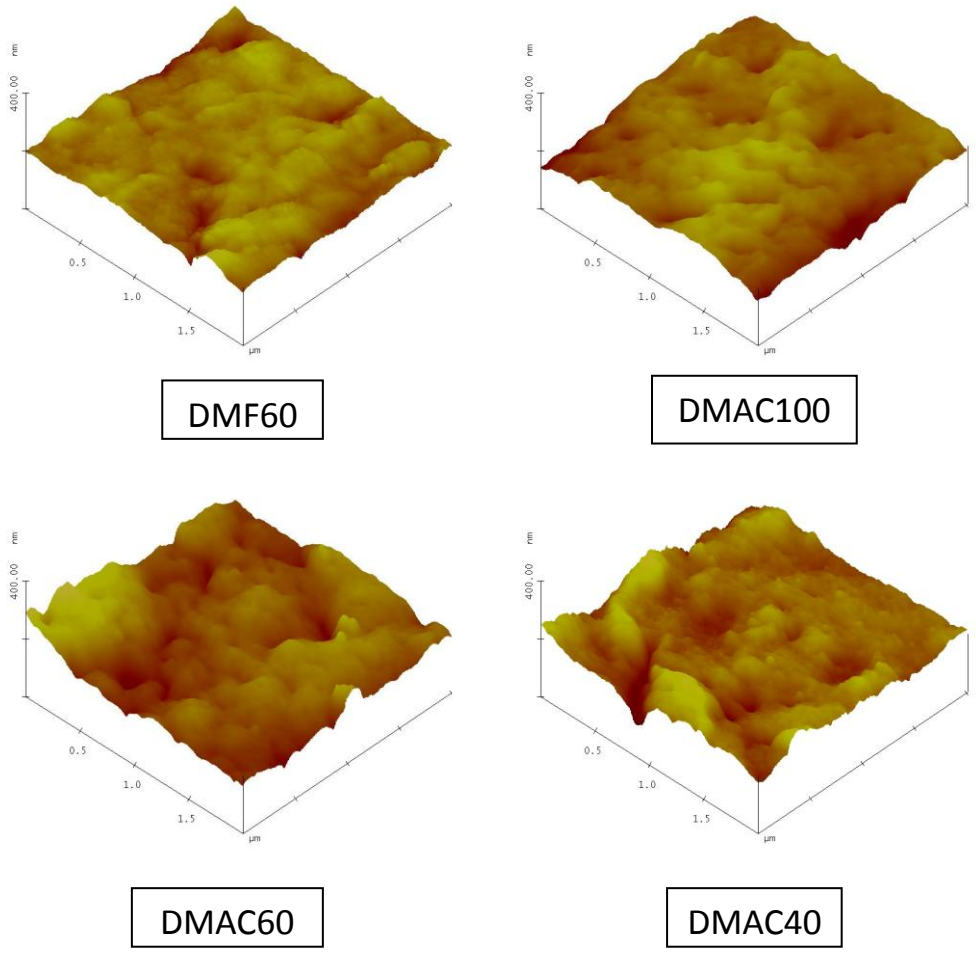

Fig. 2.9. 3D AFM images of the outer surfaces of the PVDF-HFP hollow fiber membranes prepared with different solvents.

nodules and the dark depressions (i.e. valleys) are pores. 3D AFM images also permit to estimate the roughness of both the internal and external surfaces of the membranes. The obtained mean roughness parameters (minimum, maximum and average values) are summarized in Table 2.6, being all the values similar to those of other hollow fiber membranes [20,26,28,42]. The mean roughness of both the inner and outer surfaces decreased when DMF (DMF60) was used instead DMAC (DMAC60). Moreover, the mean roughness of the internal surfaces of the membranes DMF60 and DMAC60 was similar to the mean roughness of their external surfaces. It is worth noting that no clear trend was detected between the mean roughness of the inner surfaces and the increase of the TMP content in the solvent mixture. This may be due to the slight change in the R_{HSP} values for the pair W-S. However, an increase of TMP concentration results in a small and gradual enhancement of the mean roughness of the outer surfaces. As it was stated previously, this effect can be related to the shrinkage of the membrane, which enhanced with the increase of the TMP amount in the

Table 2.6. Minimum, maximum and average mean roughness parameter, R_a, together with the corresponding standard deviation of the internal and external surfaces of the PVDF-HFP hollow fibers prepared with different solvents (scan range considered 2 μm × 2 μm).

Membrane	R_a (nm), inner surface			R_a (nm), outer surface		
	Minimum	Maximum	Average	Minimum	Maximum	Average
DMF60	10.0	22.2	15.7 ± 4.1	8.1	22.4	15.7 ± 5.0
DMAC100	10.2	15.4	12.6 ± 1.9	12.6	23.5	17.1 ± 3.0
DMAC60	11.6	28.0	20.2 ± 4.4	16.9	25.9	21.6 ± 3.3
DMAC40	13.9	18.6	15.8 ± 2.0	15.8	29.9	22.5 ± 4.3

solvent mixture. A higher shrinkage of the membranes resulted in dense and wrinkled surface [17] and consequently a rougher outer surface of the hollow fiber membranes.

The mean pore sizes and their corresponding geometric standard deviations of both the inner and outer surfaces of the hollow fibers are summarized in Table 2.7. The mean pore sizes of the surfaces of other PVDF-HFP and PVDF hollow fiber membranes were found to be similar or even greater than the values of the membranes prepared in this study [20,26,28,42]. Figures 2.10 and 2.11 show the cumulative pore size distributions and the probability density function curves. The pore size distributions of the internal and external surfaces (Figs. 2.10 and 2.11) of the membranes prepared with mixed solvents (DMAC/TMP or DMF/TMP) were found to be narrower than those of the hollow fibers fabricated with a single solvent, DMAC (membrane DMAC100). It was observed a slight increase of the mean pore size of the external surfaces of the hollow fibers when TMP content in the solvent mixture was increased. This result may be attributed partly to the decrease of the solvent(s) evaporation rate, which increases the pore size of the outer membrane surface. Among all prepared hollow fibers the smallest mean roughness and mean pore size of the outer surface correspond to the membrane DMF60. When comparing the membranes DMAC60 and DMF60, the observed smaller mean pore size and mean roughness of the membrane DMF60 may be explained based on the high value of its parameter *b* (see Table 2.4) and the lowest observed shrinkage (i.e. 26%) from the solvent evaporation kinetic results, indicating an earlier solvent evaporation and the subsequent formation of a thicker and smoother skin-layer. By changing the solvent DMAC to DMF, no clear tendency was found for the pore sizes of the inner surfaces of the hollow fiber membranes. The mean pore size decreased and then increased with the TMP content in the solvents. The membrane DMAC60 exhibited the smallest mean pore size.

Table 2.7. Mean pore size, μ_p, and geometric standard deviation, σ_p, of the internal and external surfaces of the PVDF-HFP hollow fiber membranes determined by AFM images analysis.

Membrane	Inner surface		Outer surface	
	μ_p (nm)	σ_p (nm)	μ_p (nm)	σ_p (nm)
DMF60	69.38	1.09	63.71	1.09
DMAC100	71.11	1.12	64.76	1.11
DMAC60	65.38	1.09	66.76	1.08
DMAC40	69.20	1.09	67.31	1.07

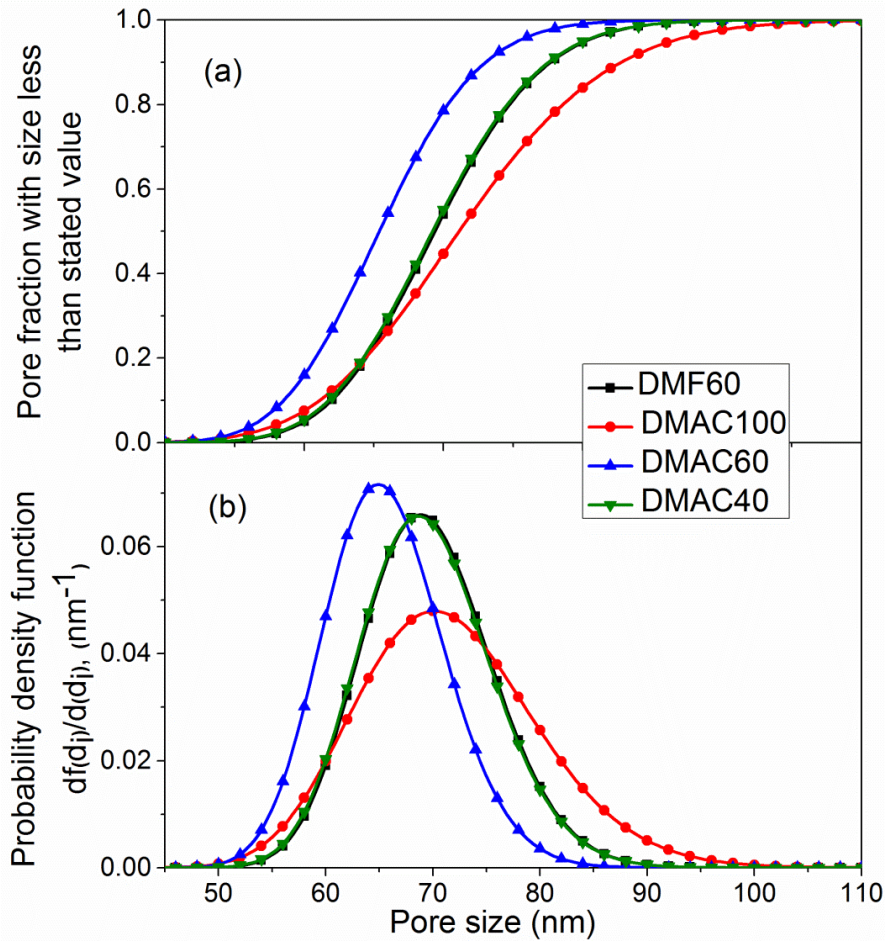

Fig. 2.10. Cumulative pore size (a) and probability density function (b) curves generated from the pore sizes obtained from AFM images of the inner surfaces of the PVDF-HFP hollow fiber membranes prepared with different solvents.

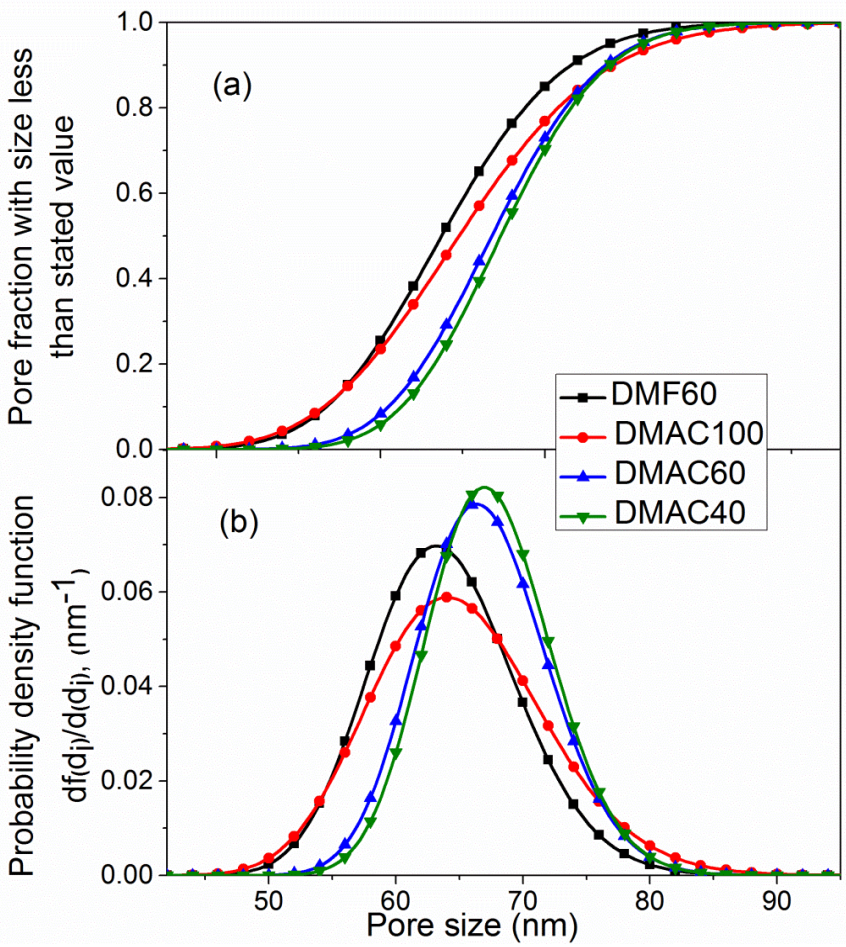

Fig. 2.11. Cumulative pore size (a) and probability density function (b) curves generated from the pore sizes obtained from AFM images of the outer surfaces of the PVDF-HFP hollow fiber membranes prepared with different solvents.

Table 2.8. Mean pore radius, r_p, and effective porosity, ε/L_p, of the PVDF-HFP hollow fiber membranes determined from wet and dry curves obtained by Porometry test.

Membrane	Wet curve	Dry curve	
	r_p (nm)	r_p (nm)	ε/L_p (m^{-1})
DMAC100	114.8 ± 1.1	121 ± 6	277 ± 29
DMAC60	141.8 ± 1.1	141 ± 4	276 ± 19
DMAC40	188.7 ± 1.1	177 ± 3	193± 7

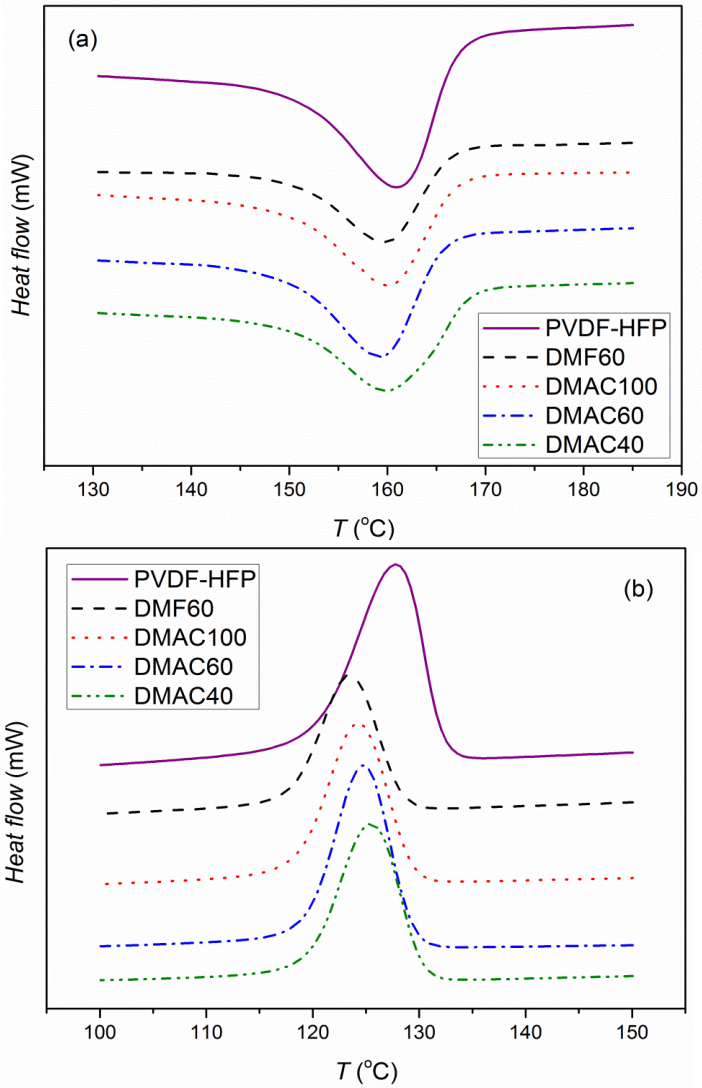

Fig. 2.12. DSC thermograms, (a) heating and (b) cooling of the copolymer PVDF-HFP and the PVDF-HFP hollow fiber membranes prepared with different solvents.

Table 2.9. Melting temperature (T_m), crystallization temperature (T_c), enthalpy of melting (ΔH_m), enthalpy of crystallization (ΔH_c) and crystallinity (X_c) of the PVDF-HFP copolymer and the hollow fiber membranes prepared with different solvents.

Sample	Heating process		Cooling process		Crystallinity X_c (%) [a]
	$\Delta H_m \pm 0.5$ (J/g)	$T_m \pm 0.15$ (°C)	$\Delta H_c \pm 0.5$ (J/g)	$T_c \pm 0.15$ (°C)	
PVDF-HFP	29.0	161.41	29.4	128.00	27.68
DMF60	28.0	159.53	23.7	123.85	26.76
DMAC100	29.7	160.18	29.8	124.17	28.36
DMAC60	29.9	159.42	31.1	124.94	28.52
DMAC40	32.7	159.69	32.2	125.43	31.23

[a] Calculated using Eq. (2.2).

The mean pore sizes (r_p) obtained from the wet curve (porometry method) and the dry curve (gas permeation method) together with the effective porosity (ε/L_p) of the PVDF-HFP hollow fiber membranes are summarized in Table 2.8. Because of the low mechanical properties of the membrane DMF60 having large and long tear-drop macro-voids, these tests cannot be carried out using this membrane. Taking into account the standard deviation, the mean pore sizes determined by the two methods are quite similar for all PVDF-HFP hollow fiber membranes. Moreover, it can be seen a greater mean pore size for the hollow fiber membrane prepared with higher TMP content in the solvents mixture. However, the lowest effective porosity was found for the hollow fiber membrane prepared with the highest TMP concentration in the solvents mixture. It is worth quoting that the effective porosity reported by Tang et al. [14] for PVDF hollow fiber membranes prepared with the solvent DMAC are similar to those presented in Table 2.8. The thermal properties of the PVDF-HFP hollow fiber membranes were studied by DSC and the obtained thermograms are presented in Fig. 2.12. Table 2.9 summarizes the melting temperature (T_m), the crystallization temperature (T_c), the enthalpy of melting (ΔH_m) and the enthalpy of crystallization (ΔH_c). In general, if the standard deviations are taking into consideration, all the obtained transition peaks of the membranes as well as T_m, T_c, ΔH_m and ΔH_c are almost similar to those of the copolymer PVDF-HFP. It was observed that the crystallinity of the studied PVDF-HFP hollow fiber membranes is lower than that of the PVDF hollow fiber membranes, which is in the range 40-50% [18,38,41]. Moreover, the obtained crystallinity values in this study agree with those obtained by Tian et al. [58] for flat sheet PVDF-HFP membranes prepared with DMAC or acetone. Providing that both T_m and T_c of the PVDF-HFP hollow fiber membranes are much higher than the DCMD operating temperatures, these membranes will maintain their thermal stability during DCMD processing.

2.3.3 DCMD performance

The DCMD performance of the fabricated hollow fibers with different solvents was carried out as stated previously. Distilled water and NaCl aqueous solution (3 wt%) were used as feed. As it was expected the permeate flux (J) of all membranes increased exponentially, following an Arrhenius type of dependence, with the feed temperature (T_{feed}). Figure 2.13 shows as an example the DCMD permeate flux of the PVDF-HFP hollow fiber membranes (DMF60) as a function of different feed temperatures maintaining the permeate temperature at 25 ºC. In addition, as it is well known in MD, when the salt solution (3 wt.%) was used as feed the permeate fluxes are lower than the permeate flux obtained for feed distilled water. For sake of comparison, Figure 2.14 shows the permeate fluxes of all hollow fiber membranes prepared with different solvents. The obtained DCMD permeate fluxes are similar to those of other PVDF-HFP hollow fiber membranes [20,26]. As it can be seen in Fig. 2.14, the type of solvent affects the characteristics of the PVDF-HFP hollow fiber membranes and their

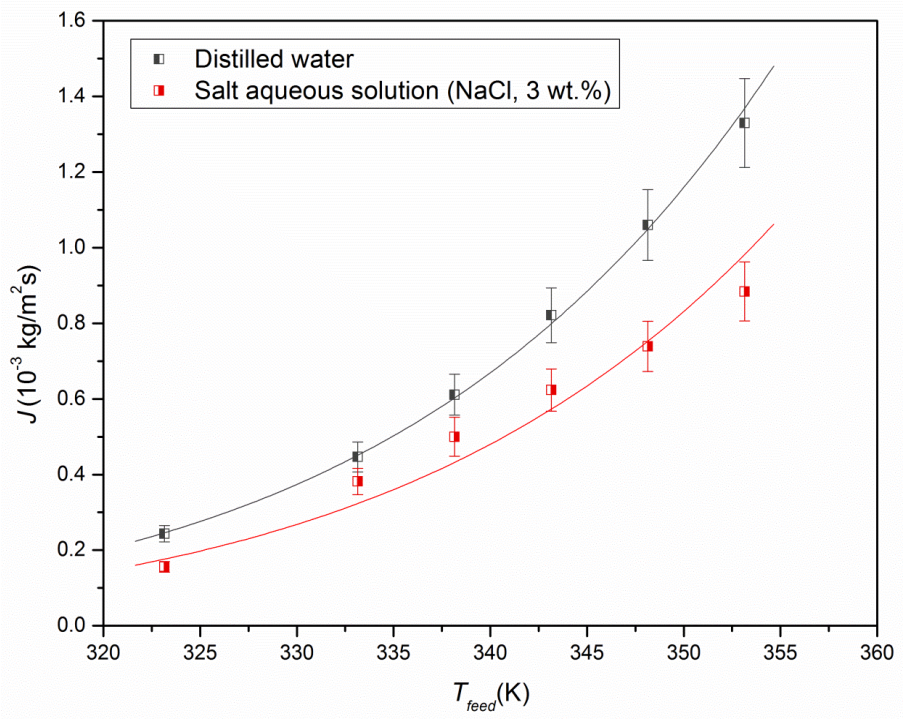

Fig. 2.13. Effect of the feed inlet temperature on the DCMD permeate flux of the membrane DMF60. The permeate temperature was kept at 25 °C.

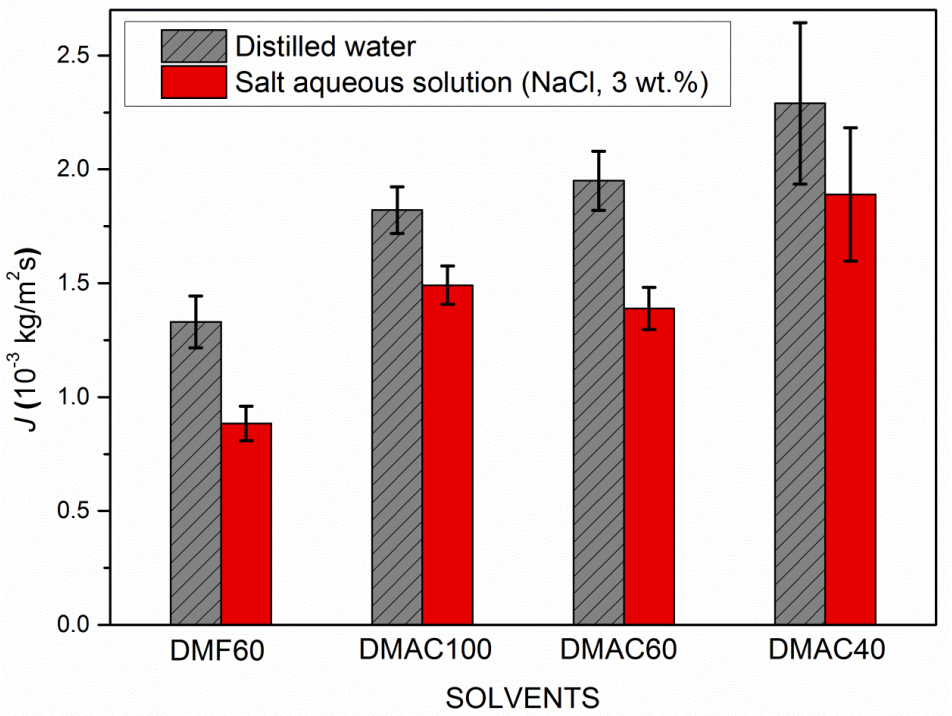

Fig. 2.14. DMCD permeate flux of the PVDF-HFP hollow fiber membranes prepared with different solvents. (Feed temperature = 80 °C; Permeate temperature = 25 °C).

DCMD permeate flux as a consequence. The hollow fiber membrane (DMAC60) prepared with the solvent DMAC exhibited higher DCMD permeate flux than the membrane (DMF60) prepared with the solvent DMF. As it is discussed previously, compared to the membrane DMF60, the membrane DMAC60 exhibits thicker internal sponge-like structure with fewer macro-voids (see Fig. 2.7), lower thickness, higher mean roughness of both the outer and inner surfaces and similar porosity. These justify the higher DCMD permeate flux of the membrane DMAC60 compared to the membrane DMF60. On the other hand, DCMD permeate flux was increased with increasing TMP concentration in the solvent mixture, due the formation of a thicker sponge-like structure in the membrane cross-section, a higher mean roughness of the external surface and a bigger mean pore size. Larger mean pore size usually corresponds to higher permeate flux [6].

The permeate flux reduction factor (*FRF*) represents the permeate flux difference when the salt aqueous solution (J_{NaCl}) was used as feed instead of distilled water (J_w) and defined as

$$FRF\ (\%) = \frac{(J_w - J_{NaCl})}{J_w} \times 100 \tag{2.6}$$

The highest *FRF* value corresponds to the membrane DMF60 (33.5%) whereas the lowest *FRF* value was obtained for the membrane DMAC40 (17.5%). A quality membrane must exhibit a high desalination performance with a low *FRF*. When changing DMF by DMAC in the solvent mixture, the *FRF* value decreased due partly to the increase of both the internal and external mean roughness, which reduced the concentration polarization effect. All the above indicated results corroborate that DMAC is better solvent than DMF for the preparation of PVDF-HFP hollow fiber membranes. Another parameter that must be taken into account is the salt rejection factor. The obtained values were 99.65%, 99.30%, 99.80%, and 99.35% for DMF60, DMAC100, DMAC60, DMAC40, respectively. The highest salt rejection factor was achieved for the membrane DMAC60, which corresponds to the lowest mean pore size of the inner surface.

2.4 Conclusions

The type of solvent affects both the characteristics and the DCMD permeate flux of the PVDF-HFP hollow fiber membrane prepared by the dry/wet spinning technique. By choosing an adequate solvent or solvents mixture with the aid of the results obtained by the different spinning solutions characterization techniques the internal structure of the hollow fiber membrane may be predicted for preparation of a high MD membrane performance.

The type of the used solvent(s) completely changed the spinning solution characteristics. The selected solvent modified the solvent-copolymer-nonsolvent interaction and consequently

dictated the kinetic and the thermodynamic precipitation of the membrane formation. These affected the morphological characteristics of the hollow fiber membranes and the MD performance. The thicker the sponge-like structure of the hollow fiber membrane, the higher the MD permeate flux is.

Macro-voids disappeared from the cross-section of the hollow fiber membranes when DMAC was used instead DMF because DMAC is better solvent for PVDF-HFP than DMF. DMAC leads to higher viscosity, thermodynamic stability and lower coagulation rate. The onset time of the solvent evaporation clearly decreased when DMAC was used instead DMF rendering the external layer less dense with higher mean roughness and greater outer surface mean pore size. When the solvent was changed from DMF to DMAC, both the DCMD permeate flux and the salt (NaCl) rejection factor were enhanced because of the thicker internal sponge-like structure, the lower thickness and the higher mean roughness of both the outer and inner surfaces.

The hollow fibers prepared with the mixed solvents, DMF/TMP and DMAC/TMP in this study, exhibited narrow pore size distributions but low *LEP* results.

When the TMP concentration in the solvents mixture was increased, the affinity between PVDF-HFP and the solvent(s) decreased, whereas the viscosity of the spinning solutions was increased. Furthermore, the solvent(s) evaporation rate and the coagulation rate of PVDF-HFP became slow and the thickness of the finger-like structure of the external layer was reduced (i.e. the formation of a thicker sponge-like structure in the membrane cross-section). Higher mean roughness of the external surface and greater mean pore sizes were obtained when the TMP amount in the solvent mixture was higher. These results lead to higher DCMD permeate fluxes for the PVDF-HFP hollow fiber membranes prepared with more amount of TMP in the solvents mixture. The solvent DMAC was found to be better solvent than DMF and the increase of TMP content enhanced the desalination performance of the PVDF-HFP hollow fiber membrane.

References

[1] M. Khayet, T. Matsuura, Membrane Distillation. Principles and Aplications, Elsevier (2011).

[2] M. Khayet, Membranes and theoretical modeling of membrane distillation: A review, Adv. Colloid Interface Sci. 164 (2011) 326–339.

[3] M. Gryta, M. Barancewicz, Influence of morphology of PVDF capillary membranes on the performance of direct contact membrane distillation, J. Membr. Sci. 358 (2010) 158–167.

[4] L. Song, B. Li, K. Sirkar, J. Gilron, Direct contact membrane distillation-based desalination: novel membranes, devices, larger-scale studies, and a model, Ind. Eng. Chem. Res. 46 (8) (2007) 2307–2323.

[5] M. Essalhi, M. Khayet, Surface segregation of fluorinated modifying macromolecule for hydrophobic/hydrophilic membrane preparation and application in air gap and direct contact membrane distillation, J. Membr. Sci. 417–418 (2012) 163–173.

[6] M.M. Teoh, T.S. Chung, Membrane distillation with hydrophobic macrovoid-free PVDF–PTFE hollow fiber membranes, Sep. Purif. Technol. 66 (2009) 229–236.

[7] M.C. García-Payo, M. Essalhi, M. Khayet, Preparation and characterization of PVDF–HFP copolymer hollow fiber membranes for membrane distillation, Desalination, 245 (2009) 469-473.

[8] D.Y. Hou, J. Wang, D. Qu, Fabrication and characterization of hydrophobic PVDF hollow fiber membranes for desalination through direct contact membrane distillation, Sep. Purif. Technol. 69 (2009) 78–86.

[9] K.Y. Wang, T.S. Chung, M. Gryta, Hydrophobic PVDF hollow fiber membranes with narrow pore size distribution and ultra-thin skin for the fresh water production through membrane distillation, Chem. Eng. Sci. 63 (2008) 2587–2594.

[10] X. Yang, R. Wang, L. Shi, A.G. Fane, M. Debowski, Performance improvement of PVDF hollow fiber-based membrane distillation process, J. Membr. Sci. 369 (2011) 437–447.

[11] P. Wang, M.M. Teoh, T.S. Chung, Morphological architecture of dual-layer hollow fiber for membrane distillation with higher desalination performance, Water Res. 45 (17) (2011) 5489–5500.

[12] C.Y. Feng, K.C. Kulbe, T. Matsuura, A.F. Ismail, Review. Recent progresses in polymeric hollow fiber membrane preparation, characterization and applications, Sep. Puri. Tech. 111 (2013) 43–71.

[13] N. Peng, N. Widjojo, P. Sukitpaneenit, M.M. Teoh, G.G. Lipscomb, T.S. Chung, J.Y. Lai, Evolution of polymeric hollow fibers as sustainable technologies: past, present and future, Prog. Polym. Sci. 37 (2012) 1401–1424.

[14] Y. Tang, N. Li, A. Liu, S. Ding, C. Yi, H. Liu, Effect of spinning conditions on the structure and performance of hydrophobic PVDF hollow fiber membranes for membrane distillation, Desalination 287 (2012) 326–339.

[15] M. Khayet, The effects of air gap length on the internal and external morphology of hollow fiber membranes, Chem. Eng. Sci. 58 (2003) 3091–3104.

[16] M. Khayet, M.C. García-Payo, F.A. Qusay, K.C. Khulbe, C.Y. Feng, T. Matsura, Effects of gas gap type on structural morphology and performance of hollow fibers, J. Membr. Sci. 311 (2008) 259–269.

[17] X.Y. Wang, L. Zhang, D.H. Sun, Q.F. An, H.L. Chen, Effect of coagulation bath temperature on formation mechanism of poly(vinylidene fluoride) membrane, J. Appl. Polym. Sci. 110 (2008) 1656–1663.

[18] S.H. Choi, F. Tasselli, J.C. Jansen, G. Barbieri, E. Drioli, Effect of the preparation conditions on the formation of asymmetric poly(vinylidene fluoride) hollow fibre membranes with a dense skin, J. Eur. Polym. 46 (2010) 1713–1725.

[19] X. Yang, H. Yu, R. Wang, A.G. Fane, Optimization of microstructured hollow fiber design for membrane distillation applications using CFD modeling, J. Membr. Sci. 421–422, (2012) 258–270.

[20] M. Khayet, C. Cojocaru, M. Essalhi, M.C. García-Payo, P. Arribas, L. García-Fernández, Hollow fiber spinning experimental design and analysis of defects for fabrication of optimized membranes for membrane distillation, Desalination 287 (2012) 146–158.

[21] C.S. Feng, B.L. Shi, G.M. Li, Y.L. Wu, Preparation and properties of microporous membrane from poly(vinylidene fluoride-co-tetrafluoroethylene) (F2.4) for membrane distillation, J. Membr. Sci. 237 (2004) 15–24.

[22] L. Shi, R. Wang, Y. Cao, D.T. Liang, J.H. Tay, Effect of additives on the fabrication of poly(vinylidene fluoride-co-hexafluropropylene) (PVDF-HFP) asymmetric microporous hollow fiber membranes, J. Membr. Sci. 315 (2008) 195–204.

[23] L. Shi, R. Wang, Y. Cao, C. Feng, D.T. Liang, J.H. Tay, Fabrication of poly(vinylidene fluoride-co-hexafluropropylene) (PVDF-HFP) asymmetric microporous hollow fiber membranes, J. Membr. Sci.305 (2007) 215–225.

[24] C. Feng, R. Wang, B. Shi, G. Li, Y. Wu, Factors affecting pore structure and performance of poly(vinylidene fluoride-co-hexafluoropropylene) asymmetric porous membrane, J. Membr. Sci.277 (2006) 55–64.

[25] G.C. Li, P. Zhang, H.P. Zhang, L.C. Yang, Y.P. Wu, A porous polymer electrolyte based on P(VDF-HFP) prepared by a simple phase separation process, Electrochem. Comm. 10 (2008) 1883–1885.

[26] M.C. García-Payo, M. Essalhi, M. Khayet, L. García-Fernández, K. Charfi, H. Arafat, Water desalination by membrane distillation using PVDF-HFP hollow fiber membranes, Membrane Water Treatment 1 (2010) 215–230.

[27] L. Shi, R. Wang, Y. Cao, Effect of the rheology of poly(vinylidene fluoride co-hexafluropropylene) (PVDF-HFP) dope solutions on the formation of microporous hollow fibers used as membrane contactors, J. Membr. Sci. 344 (2009) 112–122.

[28] M.C. García-Payo, M. Essalhi, M. Khayet, Effects of PVDF-HFP concentration on membrane distillation performance and structural morphology of hollow fiber membranes, J. Membr. Sci. 347 (2010) 209–219.

[29] J.H. Cao, B.K. Zhu, Y.Y. Xu, Structure and ionic conductivity of porous polymer electrolytes based on PVDF-HFP copolymer membranes, J. Membr. Sci. 281 (2006) 446–453.

[30] Y.J. Hwang, S.K. Jeong, K.S. Nahm, A.M. Stephan, Electrochemical studies on poly(vinylidene fluoride-hexafluoropropylene) membranes prepared by phase inversion method, Eur. Polym. J. 43 (2007) 65–71.

[31] S. Wongchitphimon, R. Wang, R. Jiraratananona, L. Shi, C.H. Loh, Effect of polyethylene glycol (PEG) as an additive on the fabrication of polyvinylidene fluoride-co-hexafluropropylene (PVDF-HFP) asymmetric microporous hollow fiber membranes, J. Membr. Sci. 369 (2011) 329–338.

[32] P. van de Witte, P.J. Dijkstra, et al., Phase separation processes in polymer solutions in relation to membrane formation, J. Membr. Sci. 117 (1996) 1–31.

[33] Z. Song, M. Xing, J. Zhang, B. Li, S. Wang, Determination of phase diagram of a ternary PVDF/γ-BL/DOP system in TIPS process and its application in preparing hollow fiber membranes for membrane distillation, Sep. Puri. Tech. 90 (2012) 221–230.

[34] A.C. Sun, W. Kosar, Y. Zhang, X. Feng, A study of thermodynamics and kinetics pertinent to formation of PVDF membranes by phase inversion, Desalination 309 (2013) 156–164.

[35] A. Mansourizadeh, A.F. Ismail, Preparation and characterization of porous PVDF hollow fiber membranes for CO_2 absorption: Effect of different non-solvent additives in the polymer dope, Int. J. Greenh. Gas Control 5 (2011) 640–648.

[36] M.L. Yeow, Y.T. Liu, K. Li, Isothermal Phase Diagrams and Phase-Inversion Behavior of Poly(vinylidene fluoride)/Solvents/Additives/Water Systems, J. Appl. Polym. Sci. 90 (2003) 2150–2155.

[37] M.L. Yeow, Y.T. Liu, K. Li, Morphological Study of Poly(vinylidene fluoride) Asymmetric Membranes: Effects of the Solvent, Additive, and Dope Temperature, J. Appl. Polym. Sci. 92 (2004) 1782–1789.

[38] Y.K. Ong, N. Widjojo, T.S. Chung, Fundamentals of semi-crystalline poly(vinylidene fluoride) membrane formation and its prospects for biofuel (ethanol and acetone) separation via pervaporation, J. Membr. Sci. 378 (2011) 149–162.

[39] Q. Li, Z.L. Xu, L.Y. Yu, Effects of Mixed Solvents and PVDF Types on Performances of PVDF Microporous Membranes, J. Appl. Polym. Sci. 115 (2010) 2277–2287.

[40] Q. Li, Z.L. Xu, M. Liu, Preparation and characterization of PVDF microporous membrane with highly hydrophobic surface, Polym. Adv. Technol. 22 (2011) 520–531.

[41] Y.K. Ong, T.S. Chung, High performance dual-layer hollow fiber fabricated via novel immiscibility induced phase separation (I^2PS) process for dehydration of ethanol, J. Membr. Sci., 421-422 (2012) 271–282.

[42] M. Khayet, C. Feng, K.C. Khulbe, T. Matsuura, Preparation and characterization of polyvinylidene fluoride hollow fiber membranes for ultrafiltration, Polymer 43 (2002) 3879–3890.

[43] M.C. García-Payo, M.A. Izquierdo-Gil, C. Fernández-Pineda, Wetting study of hydrophobic membranes via liquid entry pressure measurements with aqueous alcohol solutions, J. Colloid Interface Sci. 230 (2002) 420–431.

[44] M. Essalhi, M. Khayet, Self-sustained webs of polyvinylidene fluoride electrospun nanofibers at different electrospinning times: 1. Desalination by direct contact membrane distillation, J. Membr. Sci., 433 (2013) 167-179].

[45] X. Tian, X. Jiang, Poly (vinylidene fluoride-co-hexafluoropropene) (PVDF-HFP) membranes for ethyl acetate removal from water, J. Hazard. Mater. 153 (2008) 128–135.

[46] M. Tazaki, R. Wada, M. Okabe, T. Homma, Crystallization and gelation of poly (vinylidene fluoride) in organic solvents, J. Appl. Polym. Sci. 65 (8) (1997) 1517–1524.

[47] C.M. Hansen, Hansen solubility parameters: a user´s handbook. 2nd ed. CRC Press, Taylor & Francis Group (2007).

[48] S. Abbott, C.M. Hansen, H. Yamamoto, Hansen Solubility Parameters in Practice - Complete with software, data, and examples, 3rd ed. Ebook: Hansen-solubility.com (2010).

[49] J.E. Mark (Ed.), Polymer Data Handbook, Oxford University Press (1999).

[50] N. Widjojo, T.S. Chung, D.Y. Arifin, M. Weber, V. Warzelhan, Elimination of die swell and instability in hollow fiber spinning process of hyperbranched polyethersulfone (HPES) via novel spinneret designs and precise spinning conditions, Chem. Eng. J. 163 (2010) 143-153.

[51] C.C. Pereira, R. Nobrega, C.P. Borges, Spinning process variables and polymer solution effects in the die-swell phenomenon during hollow fiber membranes formation, Brz. J. Chem. Eng. 17 (2000) 4–7.

[52] A. Bottino, G. Camera-Roda, G. Capannelli, S. Munari, The formation of microporous polyvinylidenedifluoride membranes by phase separation, J. Membr. Sci. 57 (1) (1991) 1–20.

[53] R.Y.M. Huang, X. Feng, Studies on solvent evaporation and polymer precipitation pertinent to the formation of asymmetric polyetherimide membranes, J. Appl. Polym. Sci. 57 (1995) 613–621.

[54] C. Castellari, S. Ottani, Preparation of reverse osmosis membranes. A numerical analysis of asymmetric membrane formation by solvent evaporation from cellulose acetate casting solutions, J. Membr. Sci. 9 (1981) 29–41.

[55] W.Z. Lang, Z.-L. Xu, H. Yang, W. Tong, Preparation and characterization of PVDF-PFSA blend hollow fiber UF membrane, J. Membr. Sci. 288 (2007) 123-131.

[56] N. Peng, T.S. Chung, K.Y. Wang, Macrovoid evolution and critical factors to form macrovoid-free hollow fiber membranes, J. Membr. Sci. 318 (2008) 363–372.

[57] A.F. Ismail, L. P. Yean, Review on the development of defect-free and ultrathin-skinned asymmetric membranes for gas separation through manipulation of phase inversion and rheological factors, J. Appl. Polym. Sci. 88 (2003) 442-451.

[58] X. Tian, X. Jiang, B. Zhu, Y. Xu, Effect of the casting solvent on the crystal characteristics and pervaporative separation performances of P(VDF-*co*-HFP) membranes, J. Membr. Sci. 279 (2006) 479–486.

[59] N. Vogrin, C. Stropnik, V. Musil, M. Brumen, The wet phase separation: the effect of cast solution thickness on the appearance of macrovoids in the membrane forming ternary cellulose/acetone/water system, J. Membr. Sci. 207 (2002) 139-141.

[60] D. Li, T.S. Chung, J. Ren, R. Wang, Thickness dependence of macrovoid evolution in wet phase-inversion asymmetric membranes, Ind. Eng. Chem. Res. 43 (2004) 1553-1556.

[61] N. Widjojo, T.S. Chung, Thickness and air gap dependence of macrovoid evolution in phase-inversion asymmetric membranes, Ind. Eng. Chem. Res. 45 (2006) 7618-7626.

3

Polymeric hollow fiber membranes:

Nonsolvent effect on the structural properties and MD performance

3.1 Mechanism of formation of hollow fiber membranes for membrane distillation: 1. Inner coagulation power effect on morphological characteristics

3.2 Mechanism of formation of hollow fiber membranes for membrane distillation: 2. Outer coagulation power effect on morphological characteristics

3.1 Mechanism of formation of hollow fiber membranes for membrane distillation: 1. Inner coagulation power effect on morphological characteristics

Abstract

Hollow fiber membrane morphology and inner surface structure were analyzed based on the thermodynamic and kinetics of the phase inversion process. Different nonsolvent mixtures formed by *N,N*-dimethyl acetamide (DMAC) and distilled water were considered. By means of Hansen solubility parameters, lower interaction between the nonsolvent and the mixed solvent (DMAC/trimethyl phosphate, TMP) was observed when greater amount of DMAC was added in the nonsolvent. The spinning solution became thermodynamically more stable and kinetically showed slower coagulation rates, being both related to the resultant membrane formation. In this first study poly(vinylidene fluoride-co-hexafluoropropylene) (PVDF-HFP) hollow fiber membranes were prepared by the dry/wet spinning technique employing the above cited nonsolvent mixtures as an internal coagulant. Their effect on the internal structure of the membrane evolved towards a more open-porous inner surface when increasing the solvent content in the bore liquid. Various characterization techniques were used in order to analyze the adequacy of these membranes for desalination by direct contact membrane distillation (DCMD). It was found that all the properties together with the permeability of the hollow fibers improved when the coagulation power of the nonsolvent was reduced.

3.1.1 Introduction

Membrane distillation (MD) is a non-isothermal process applied mainly to remove non-volatile solutes such as salts from water. Its driving force is the transmembrane water vapor pressure and the most commonly used MD configuration is direct contact membrane distillation (DCMD) [1]. However, one of the main drawbacks of this process is the unavailability of commercial membranes that meet all the MD requirements [2]. Therefore, the design of MD membranes is nowadays an attractive research topic [3-5], despite the great difficulty associated with understanding the mechanism of membrane formation [6]. Some of

the main requirements of an adequate MD membrane are the high hydrophobicity, low thermal conductivity and high porosity [1-3].

Cui et al. [7] reported different hydrophobic fluoropolymers and copolymers that can be employed as suitable materials for MD membranes preparation, such as the well known and commonly used polyvinylidene fluoride (PVDF) [8, 9]. Fluoropolymers exhibit excellent properties as materials for a membrane for MD including thermal and chemical resistances [7]. The copolymer poly(vinylidene fluoride-co-hexafluoropropylene) (PVDF-HFP) stands out for its excellent hydrophobic character due to the hexafluoropropylene (HFP) group embedment, as confirmed by several researchers [10, 11]. Not only does the HFP incorporation improve the hydrophobic character of PVDF due to its fluorine content, but also the crystalline character of vinylidene fluoride (VDF) enhances the mechanical properties of the formed material [7]. Therefore, PVDF-HFP is an advisable copolymer to consider for the preparation of MD membranes as confirmed elsewhere [12-14]. The polymeric matrix selection is also important in terms of thermal conductivity. Nevertheless, there is not much difference between the thermal conductivity coefficients of the majority of the available hydrophobic polymers. That is why the heat transfer by conduction through the membrane must be reduced by enhancing the void volume fraction (i.e. porosity) [2]. High porosity always induces high MD permeability, as it has been confirmed in several studies [1, 2, 13]. Trying to pursue this objective, it is advised by several membranologists to introduce in the dope solution pore former additives such as polyvinylpyrrolidone (PVP), lithium chloride (LiCl), glycerol, polyethylene glycol (PEG), etc [12, 15].

Besides the aforementioned MD membrane main properties, a proper morphology also plays a key role on membrane performance. It would be enhanced if macro-void free structure, skinless and open-porous surfaces conform the membrane morphology [8, 9, 16]. First, in order to obtain the desired structure, it is necessary to analyze the membrane formation process via the thermodynamic and kinetics of the phase inversion, and to understand the consequence of the variation of each fabrication parameter [6, 17-20]. This is even more complicated for hollow fiber membrane preparation, because dry/wet spinning technique involves many fabrication parameters, which directly affect membrane morphology. One of the advantages of using MD hollow fiber membranes is the high packing density that can be easily achieved in tubular membrane modules [1-3].

Several hollow fiber preparation parameters such as spinning dope composition, spinneret dimensions, extrusion pressure, air gap distance, temperatures of the dope and coagulants solutions, coagulants flow rate and composition, take-up speed, etc., can modify the membrane structure [1, 21-23]. Although it has been already studied the effect of solvent/water mixture as nonsolvent on the membrane characteristics [24, 25], no study is found when the coagulant interacts with a mixed solvent instead of a single solvent for

preparing PVDF-HFP hollow fiber membranes. The solvents mixture is formed by two solvents, one is the same main solvent of the nonsolvent aqueous mixtures, and therefore different interaction forces compete between each other simultaneously. The nonosolvent-solvent exchange type during the phase inversion strongly affects hollow fiber membrane morphology and properties as well as membrane performance by MD process. In the first part of this study the solvent-nonsolvent interaction effect on the PVDF-HFP hollow fiber membrane formation mechanism and consequently on its structural cross-section and inner surface morphology have been deeply and exhaustively investigated.

3.1.2 Experimental

3.1.2.1 Materials

The copolymer poly(vinylidene fluoride-co-hexafluoropropylene) (PVDF-HFP; M_w = 455,000 g/mol), the solvents *N,N*-dimethyl acetamide (DMAC) and trimethyl phosphate (TMP) and the additive poly(ethylene glycol) (PEG; M_w = 6000 g/mol) were used to prepare the spinning solution and were all purchased from Sigma-Aldrich. Isopropyl alcohol (IPA, Sigma-Aldrich) and POREFIL® (Porometer) were employed as wetting liquids for the measurements of the void volume fraction and porometry, respectively. Sodium chloride (NaCl) was employed to prepare the salt aqueous feed solutions for DMCD experiments and it was purchased from Panreac.

3.1.2.2 Preparation of hollow fiber membranes

The dry/wet spinning was the fabrication technique employed to prepare all the hollow fiber membranes in this study as it was described elsewhere [26, 27]. First, a unique spinning solution was prepared as follows. 5 wt% of the additive (PEG) was first dissolved in 76 wt% of the solvents mixture at 42 ºC and 100 rpm using a magnetic stirrer (IKA, RCT basic), and after getting an homogenous mixture, 19 wt% of PVDF-HFP was added to this mixture. Then, the whole solution was introduced in a thermal bath (Stuart SBS40) maintained at 42 ºC under an orbital shaker until the whole copolymer was totally dissolved. The solvents mixture used to prepare this spinning solution was 40 wt% DMAC and 60 wt% TMP. This mixture was chosen based on the conclusions drawn in our previous study [17].

Table 3.1.1 summarizes the spinning parameters, which were maintained the same except the type of the internal coagulant. After spinning, in order to remove the residual solvents, the fabricated hollow fiber membranes were stored in water bath at room temperature for 48 h. Subsequently, the hollow fiber membranes were dried at room temperature before characterization tests. Several mixtures of DMAC and distilled water were used as internal coagulant, employing the following ratios: 0, 20, 40, 50 and 60 wt% of DMAC. The

corresponding fabricated hollow fiber membranes are termed here after 1IND0, 1IND20, 1IND40, 1IND50 and 1IND60, respectively.

Table 3.1.1. Spinning parameters of PVDF-HFP hollow fiber membranes.

Parameters	Operating conditions
Spinneret: 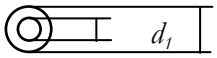	d_1= 1.0 mm / d_2= 2.4 mm
Extrusion pressure (kPa)	60
Polymeric solution temperature (ºC)	42
Internal coagulant	DMAC/distilled water
Internal coagulation temperature (ºC)	42
Internal coagulant flow rate (m^3/s)	$2.7\ 10^{-7}$
Air gap distance (m)	0.275
Liquid coagulation bath	Tap water
Liquid coagulation bath temperature (ºC)	42

3.1.2.3 Spinning solution characterization prior to membrane fabrication

Physical properties: surface tension, viscosity and Hansen solubility parameters

The surface tension of the spinning solution was measured at room temperature by the pendant drop shape analysis. An optical contact angle meter (CAM 200) and a stainless steel needle with an outer diameter of 1.832 mm were employed to carry out the measurement, keeping constant the drop volume at 12.4 μL for all the samples.

The viscosity of the spinning solution was determined by a Digital Viscometer (Brookfield, Model DV-I+) using the SC4-31 spindle at 4 rpm and a cylindrical sample container. The temperature of the spinning solution was maintained constant at 42 ºC (i.e. the same temperature considered to prepare the hollow fiber membrane) by a thermostat (Techne, Model TU-16D).

Copolymer/solvent/nonsolvent interactions were analyzed via Hansen solubility parameter (*HSP*) distance (R_{HSP}), as it was explained in detail by Hansen [28] and described elsewhere [17]. This parameter informs about the relative affinity between the PVDF-HFP and the solvent, represented by R_{HSP} (P-S); and between nonsolvent (DMAC/water coagulant mixtures) and the mixed solvent, represented by R_{HSP} (NS-S_m). These R_{HSP} values were calculated from the following equations:

$$R_{HSP}(P - S) = \sqrt{4\left(\delta_{d_P} - \delta_{d_S}\right)^2 + \left(\delta_{p_P} - \delta_{p_S}\right)^2 + \left(\delta_{h_P} - \delta_{h_S}\right)^2} \quad (3.1.1)$$

$$R_{HSP}(NS - S_m) = \sqrt{4\left(\delta_{d_{NS}} - \delta_{d_{S_m}}\right)^2 + \left(\delta_{p_{NS}} - \delta_{p_{S_m}}\right)^2 + \left(\delta_{h_{NS}} - \delta_{h_{S_m}}\right)^2} \quad (3.1.2)$$

Before R_{HSP} calculation, it is necessary to know the *HSP* components, which includes the polar component (δ_p), the dispersion force component (δ_d), and the hydrogen bonding component (δ_h) [28]. In Table 3.1.2, the *HSP* components of all the pure substances are listed [10, 28, 29], as well as the obtained values of both solvent mixture (S_m) and nonsolvent mixtures (NS), which were calculated from the following equations (3.1.3) and (3.1.4), respectively [17, 30]:

$$\left[\delta_{d_{S_m}}, \delta_{p_{S_m}}, \delta_{h_{S_m}}\right] = \left[a\,\delta_{d1} + b\,\delta_{d2} + c\,\delta_{d3},\ a\,\delta_{p1} + b\,\delta_{p2} + c\,\delta_{p3},\ a\,\delta_{h1} + b\,\delta_{h2} + c\,\delta_{h3}\right]/(a + b + c) \quad (3.1.3)$$

where the subscripts 1, 2 and 3 are for each compound present in the solvent mixture (i.e. DMAC, TMP and PEG) and *a, b* and *c* are the volume fraction of the different compounds in the solvent mixture.

$$\left[\delta_{d_{NS}}, \delta_{p_{NS}}, \delta_{h_{NS}}\right] = \left[d\,\delta_{d1} + e\,\delta_{d2},\ d\,\delta_{p1} + e\,\delta_{p2},\ d\,\delta_{h1} + e\,\delta_{h2}\right]/(d + e) \quad (3.1.4)$$

where the subscripts 1 and 2 are for each compound present in the nonsolvent mixture (i.e. DMAC and water) and *d* and *e* are the volume fraction of the different compounds in the nonsolvent mixture.

It is important to highlight that in this study, the additive PEG was also considered as compound in the solvents mixture, together with DMAC and TMP. This additive was treated as solvent (instead of a polymer) for copolymer/solvent/nonsolvent interactions [31, 32] and for thermodynamic experiments analysis [33]. The authors of these mentioned research studies considered that nonsolvent additives and solvents may be considered as unique component. Furthermore, this fact was confirmed via Fourier transform infrared spectroscopy (FTIR); which showed that after phase inversion, other than the solvents, PEG was completely removed from the membrane matrix.

As it is mentioned previously, the proportions of the nonsolvent mixture (DMAC/water) used as internal coagulant were changed for each spinning process. Therefore, R_{HSP} (NS-S_m) was the main parameter considered for comparisons and analysis. The lower is the distance R_{HSP} (NS-S_m), the weaker is the coagulant.

Table 3.1.2. Solubility parameters of the solvents, the solvents mixture, the additive PEG, the nonsolvent (water and DMAC/water mixtures) and PVDF-HFP with their *HSP* distances (R_{HSP}).

Material type	Code	Composition: material (wt%)			Solubility parameters ($MPa^{1/2}$)			R_{HSP} ($MPa^{1/2}$) [16, 27]	
		Compound 1	Compound 2	Compound 3	δ_D	δ_P	δ_H	P-S [b]	NS- S_m [c]
Copolymer (P)	PVDF-HFP [28]	---	---	---	15.3	7.2	5.3	---	---
Additive	PEG [10]	---	---	---	15.3	9.6	8.5	---	---
Solvents	DMAC [27]	---	---	---	16.8	11.5	10.2	7.2	---
	TMP [27]	---	---	---	16.7	15.9	10.2	10.4	---
Solvent mixture (S_m)	DMAC40 [a]	DMAC (40%)	TMP (60%)	PEG (5%)	16.7	13.6	10.1	8.5	---
Nonsolvent (NS)	Water (D0)	DMAC (0%)	Water (100%)	---	15.5	16	42.3	---	32.4
	D20	DMAC (20%)	Water (80%)	---	15.8	15	35.5	---	25.5
	D40	DMAC (40%)	Water (60%)	---	16	14.1	28.9	---	18.9
	D50	DMAC (50%)	Water (50%)	---	16.2	13.7	25.7	---	15.6
	D60	DMAC (60%)	Water (40%)	---	16.3	13.2	22.5	---	12.5
	D70	DMAC (70%)	Water (30%)	---	16.4	12.8	19.4	---	9.3
	D80	DMAC (80%)	Water (20%)	---	16.5	12.3	16.3	---	6.3

[a] Calculated using Eq. (3.1.1).

[b] P-S: PVDF-HFP-solvent interaction.

[c] NS-S_m: nonsolvent-mixed solvent interaction.

Thermodynamic experiment: cloud point

The thermodynamic behavior during phase inversion membrane formation process can be studied by the ternary phase diagram, where the system copolymer/solvent/nonsolvent was analyzed. The quantity of nonsolvent required to induce copolymer precipitation (i.e. cloud point) was plotted for the same spinning solution (i.e. same copolymer and mixed solvent) but for different nonsolvents (DMAC/water mixtures at different rates). The cloud point was measured by turbidimetric titration method [34]. 50 μl of each nonsolvent mixture was added stepwise to the spinning solution, keeping constant the stirring at 150 rpm and the temperature at 42 ºC by a magnetic stirrer (IKA, RCT basic) until the dope solution became permanently turbid.

Kinetics experiment: copolymer coagulation

The solvent-nonsolvent exchange rate and the coagulation initiation of the spinning solution were studied by light transmittance test. The experimental device consists of a light-emitting diode (LED) tube lamp employed as light source and a set of Light Dependence Resistances (LDRs) as light detector. The spinning solution was cast and immersed in different nonsolvent (DMAC/water) coagulation baths and the transmitted light evolution was registered by a multimeter (KEITHLEY 199 SYSTEM DMM/SCANNER) connected to a computer. The whole set-up was designed, calibrated and automated by our research group. Both phase inversion initiation and coagulation rate of PVDF-HFP in each coagulation bath were determined by the resultant transmittance curve over the time.

3.1.2.4 Characterization of hollow fiber membranes

The morphology of the prepared membranes was studied by the field emission scanning electron microscope (FESEM, JEOL Model JSM-6335F). Previously, the samples were fractured in liquid nitrogen and then sputter-coated (BALZERS SCD 004) with a thin layer (~15 nm) of gold under 20 mA.

The inner and outer diameters of the hollow fibers were measured by an optical microscope (OLYMPUS BX60M) with a precision of ± 1 μm. Both, the void volume fraction (i.e. porosity, ε) and the liquid entry pressure (*LEP*) in the membrane pores were determined following the methods described in previous studies [35, 36]. The porosity of the membranes was measured by the pycnometer gravimetric method as it was explained in detail elsewhere [37]. In this case, *LEP* measurement was carried out using the procedure and set-up schematized in [17]. The *LEP* results inform about membrane hydrophobicity and its applicability in MD process. The transmembrane operating hydrostatic pressure during MD experiment must be always lower than the *LEP* value, in order to avoid wetting problems.

Another parameter related to the hydrophobic character of the membranes is the water contact angle. Both inner and outer surface contact angles of hollow fiber membranes were measured at room temperature, (30 ± 1) °C, following the method described by Zhang et al. [38] based on surface tension effects.

The bubble pore size, the mean pore size and the smallest pore size of all the prepared hollow fiber membranes, as well as the cumulative filter flow curves were determined via gas-liquid displacement Porometer and its corresponding computer software (POROLUX™ 100, Porometer). POREFIL® (Porometer) was used as the wetting liquid. The whole followed procedure was described elsewhere [17, 39, 40].

Atomic force microscopy (AFM) was the technique employed to study the mean pore size, the pore size distribution and the roughness of both internal and external surfaces of the prepared hollow fibers. Nanoscope III equipped with 1553D scanner (Digital Instruments Inc., Santa Barbara, Ca) in a tapping mode, provided images, which were treated and analyzed following the same procedure detailed elsewhere [26, 35, 40-42].

The melting (T_m) and the crystallization (T_c) temperatures as well as the enthalpy of melting (ΔH_m) and enthalpy of crystallization (ΔH_c) were obtained from the endothermic and exothermic peaks, respectively; which were determined by the Differential Scanning Calorimetry (DSC) (Mettler-Toledo DSC 1, STAR^e System). The measurements were carried out from 3.25 to 3.73 mg samples that were placed in standard aluminum pans of 100 μl capacity in a nitrogen atmosphere at a flow rate of 60-70 ml/min. The same speed was employed for both heating and cooling at a rate of 15 °C/min from 60 °C to 200 °C. The degree of the crystallinity of the samples was estimated as stated in other studies [17, 43, 44].

The mechanical properties of the hollow fiber membranes were determined at room temperature using an Instron dynamometer (model 3366), according to ASTM D 3379-75 specifications. A load cell of 50 N with a cross-head speed of 80 mm/min and an initial length of the fiber sample of 50 mm were employed. The tensile test of each membrane was repeated for five samples, and the corresponding characteristics were calculated as the average of the five measurements.

3.1.2.5 Direct contact membrane distillation experiments

DCMD experiments were carried out using the experimental set-up and the procedure described in detail in [17]. Briefly, six PVDF-HFP hollow fibers were assembled in a shell-and-tube module with an effective length of 20 cm. The feed and permeate circulated tangentially to the membrane in a counter-current way. The feed solution was circulated through the lumen side of the membrane, while the permeate (distilled water) was circulated through the shell side of the module. First, prior to the DCMD experiments, a checking leak

test was carried out by circulating distilled water through both the lumen and shell sides of the membrane module at the same temperature confirming that no mass was registered during at least five hours. Subsequently, DCMD experiments were performed with distilled water and a salt aqueous solution (NaCl, 3 wt%) as feed solutions. The feed inlet temperature was 80 °C and that of the permeate was 25 °C. The feed flow rate was kept at 13.8 ± 1.2 kg/h, and the permeate at 20.7 ± 0.6 kg/h. The permeate flux was calculated based on the mass of water produced over time and the inner fiber surface area. The salt rejection factor was determined measuring the electrical conductivity of both the feed and permeate extracted at the beginning and at the end of each DCMD experiment.

3.1.3 Results and discussions

3.1.3.1 Spinning solution characterization prior to membrane fabrication

Physical properties: surface tension, viscosity and Hansen solubility parameters

The surface tension obtained for the used dope solution in this study was (30.45 ± 0.20) mN/m. This is an important characteristic parameter to be considered as it affects the hollow fiber diameters and its thickness as consequence. The spinning solution viscosity is related to the kinetics of the phase inversion process, during solvent and nonsolvent interdiffusion. The viscosity of the dope solution prepared for this study was (3688 ± 81) mPa s, which is in the same order of magnitude as other used PVDF-HFP spinning dope solutions in other studies [10, 11, 15].

As it is summarized in Table 3.1.2 and represented in Fig. 3.1.1(a), the value of R_{HSP} for the pair nonsolvent and solvents mixture (NS-S_m) linearly decreased when DMAC amount in the nonsolvent mixture (DMAC/water) increased. This means that the interaction between nonsolvent and solvent was reduced with the increase of DMAC content, making the solvent-nonsolvent interdiffussion during the phase inversion process slower. It is because the coagulant became weaker when the quantity of solvent increased in DMAC/water mixture as Xu et al. [24] described.

Figure 3.1.1(a) also shows the intersection between R_{HSP} (P-S_m) value for the pair PVDF-HFP and DMAC40 and the R_{HSP} (NS-S_m) curve, which represents the DMAC limit concentration in the nonsolvent mixture for coagulation power effectiveness. The corresponding R_{HSP} (NS-S_m) of the nonsolvent mixtures D70 and D80 were almost equal or even smaller than R_{HSP} (P-S_m), respectively. It means that the mixture D70 could hardly been able to induce the phase inversion of the copolymer, being impossible its coagulation if the nonsolvent D80 was used. The conclusions obtained from the Hansen solubility analysis

could predict the possibility/impossibility of a membrane phase inversion formation according the polymer/solvent/nonsolvent interactions.

ΔR_{HSP} (NS-S) dependence on the DMAC concentration in the nonsolvent mixture is shown in Fig. 3.1.1(b). ΔR_{HSP} (NS-S) represents the difference between the R_{HSP} value for the pair nonsolvent mixture and mixed solvent (NS-S_m) and the R_{HSP} value for the pair nonsolvent mixture and each individual solvent (NS-S_i). This parameter was calculated from the following equation:

$$\Delta R_{HSP}(NS - S)_i = R_{HSP}(NS - S_m) - R_{HSP}(NS - S_i) \quad (3.1.5)$$

where the subscript *i* is for each solvent, DMAC or TMP.

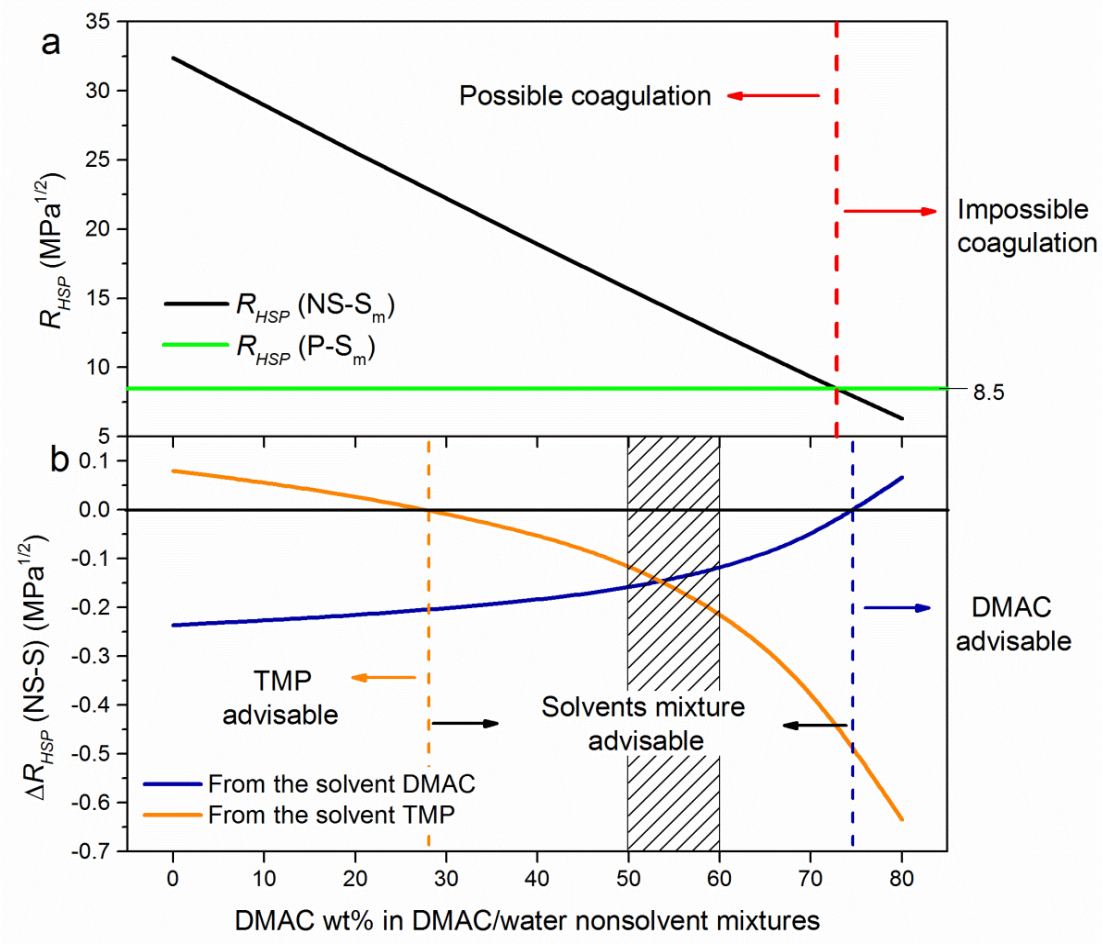

Fig. 3.1.1. Effect of the DMAC content in DMAC/water nonsolvent mixtures (a) on the R_{HSP} (NS-S_m) and (b) on the ΔR_{HSP} (NS-S).

Interesting conclusions can be drawn from Fig. 3.1.1(b). Nonsolvent-solvent affinity improved when the solvents mixture was used instead of each solvent individually. This was expressed as the negative values of the calculated parameter ΔR_{HSP} (NS-S) (i.e. R_{HSP} (NS-S_m) < R_{HSP} (NS-S_i)). ΔR_{HSP} (NS-S) < 0 were obtained for all the DMAC concentrations in the nonsolvent mixture ranging from 28 to 75 wt% approximately, for both DMAC and TMP solvents. However, for DMAC concentrations below 28 wt% in the nonsolvent, using the TMP as individual solvent would enhance the nonsolvent-solvent affinity; and for DMAC concentrations higher than 75 wt% in the nonsolvent, DMAC would be more advisable to use as a single solvent (i.e. in both cases ΔR_{HSP} (NS-S) > 0). On the other hand, in the concentration range 28 – 75 wt% DMAC, $|\Delta R_{HSP}(\text{NS-S})_{TMP}| < |\Delta R_{HSP}(\text{NS-S})_{DMAC}|$ for DMAC content in the nonsolvent lower than 50 wt% and $|\Delta R_{HSP}(\text{NS-S})_{TMP}| > |\Delta R_{HSP}(\text{NS-S})_{DMAC}|$ for DMAC content greater than 60 wt%, as shown Fig. 3.1.1(b). Therefore, for low concentrations of DMAC in the nonsolvent below 50 wt%, R_{HSP} (NS-S_m) is closer to R_{HSP} (NS-S_{TMP}) than to R_{HSP} (NS-S_{DMAC}). This means that for these DMAC concentrations, TMP is the predominant solvent of the mixture that intervenes more in the NS-S_m interaction. An opposite but more pronounced behavior was observed for higher concentrations of DMAC (above 60 wt%), concluding that the solvent DMAC is the predominant solvent of the mixture influencing the NS-S_m interaction. Furthermore, the calculated values of ΔR_{HSP} (NS-S) for each solvent were similar for DMAC concentrations in the nonsolvent mixture between 50 and 60 wt%. This indicates that in this range both solvents represented a similar power for nonsolvent-solvent interaction and their influences on the nonsolvent would be compensated. Consequently, slower NS-S_m exchange rate occurred, resulting in the most promising conditions for an appropriate membrane design as porous and sponge-like structure could be obtained.

Thermodynamic and kinetics experiments

The thermodynamic of the spinning solution during the phase inversion process was represented in the ternary phase diagram (see Fig. 3.1.2). In this study, a unique dope solution was analyzed; however, the nonsolvent solution was changed increasing the amount of DMAC in DMAC/water mixture. It was observed that when the content of DMAC in water was increased, the cloud point shifted away from PVDF-HFP – solvent axis towards PVDF-HFP – nonsolvent axis; and this effect was much more pronounced for the highest DMAC concentrations (70 and even more for 80%). It means that larger quantity of nonsolvent was needed for PVDF-HFP precipitation. The results of these thermodynamic experiments agrees with the R_{HSP} (NS-S_m) trend in Fig. 3.1.1(a), showing that increasing the amount of DMAC in water, the nonsolvent become weaker and consequently the coagulation process starts later. Xu et al. [45] observed the same direction displacement of the binodal line when the content

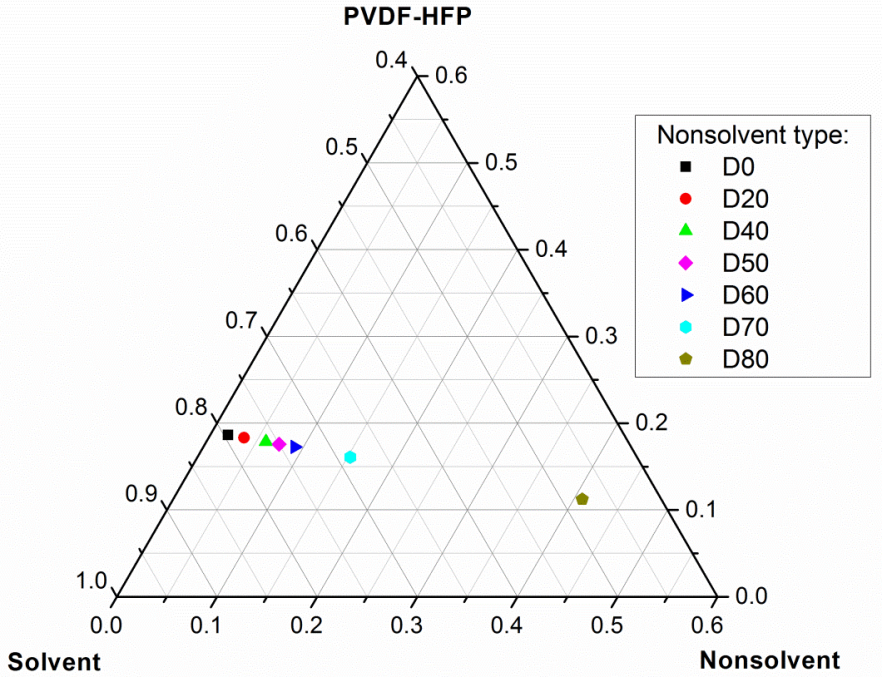

Fig. 3.1.2. Ternary phase diagram of the copolymer/solvent/nonsolvent systems.

of DMAC in the nonsolvent increased for the system poly(ether imide) (PEI)/DMAC/DMAC+water. This result showed a delayed demixing phase separation process when greater quantity of DMAC was used in the internal coagulant.

The kinetics experiments were carried out via light transmission test, employing the same dope solution and changing the nonsolvent mixture. The obtained demixing curves are represented in Fig. 3.1.3. The curves show the appearance of three different stages during the coagulation process as it was also reported by Li et al. [31, 46]. In the first stage there is a slight decrease of the transmittance, showing a delay in the nonsolvent penetration into the copolymeric cast film. In the second stage, the curve´s slope changes abruptly indicating the beginning and the rate of the demixing process. Finally, in the third stage the transmittance reduces approaching an asymptotic transmittance value indicating the end of the demixing process. By increasing the quantity of DMAC in the nonsolvent mixture, the registered time for the first stage became longer and the slope of the curve in the second stage decreased. These mean that due to the weaker coagulant, the initiation of the phase inversion was delayed and the coagulation rate became slower, being the three stages indistinguishable when the highest percentage of DMAC (60 wt%) was used in the nonsolvent mixture. This result is related to the solubility parameter difference and the thermodynamic results (i.e. the lower R_{HSP} (NS-S_m) is the longer the time to occur the cloud point is and the slower the coagulation is too). Both parameters indicated that increasing the amount of DMAC in the nonsolvent mixture the coagulation started later and the process was slower. Similar light transmittance´s curves tendency (i.e. lower precipitation rate) was obtained by Zhang et al. [47] when polyvinyl

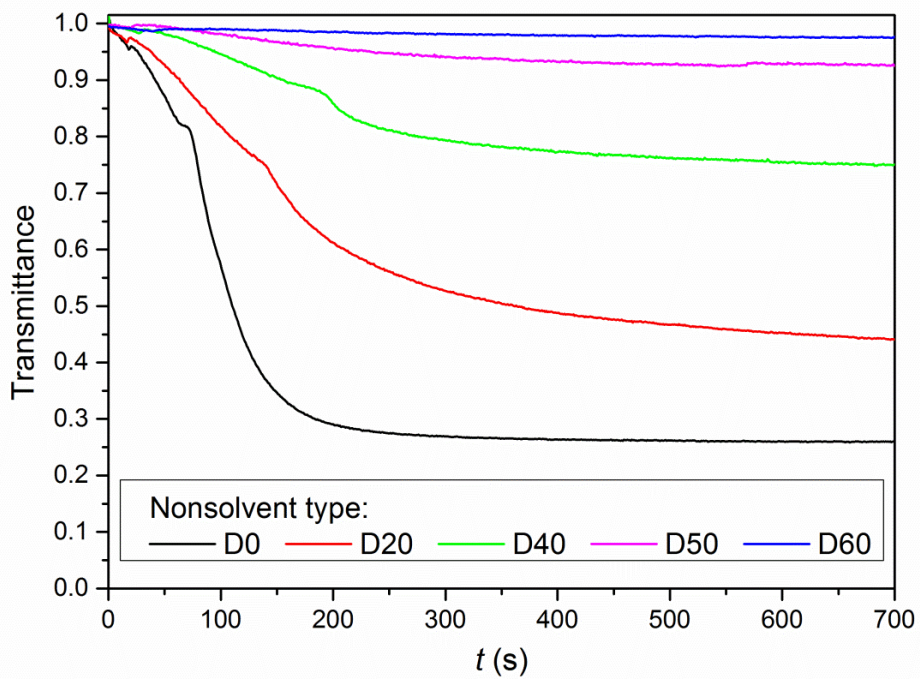

Fig. 3.1.3. Coagulation experiments of the spinning solution for different nonsolvent mixtures (DMAC/water in different proportions).

butyral (PVB) dope solutions came into contact with DMAC/water coagulation baths. Machado et al. [6] who studied the membrane formation mechanism of flat-sheet polysulfone (PSf) membranes explained that increasing the solvent concentration in the coagulation bath diminished the driving force responsible to leach out the solvent from the polymeric solution, inducing longer liquid-liquid demixing process as consequence.

It is to be noted that when employing higher quantities of DMAC (i.e. 70 and 80 wt%) in the nonsolvent DMAC/water mixture for light transmittance experiments, it was impossible to observe membrane phase inversion. This may be attributed to the extremely weakness properties of these coagulants when higher quantity of DMAC (over 60 wt%) was used in DMAC/water nonsolvent mixture. As it was predicted by R_{HSP} (NS-S_m) results (see the limit concentration of coagulation at Fig. 3.1.1(a)) and the cloud point experiments, with both mixtures the copolymer in the dope solution tends to be dissolved instead of coagulating. From the qualitative model developed for flat-sheet polymeric membranes by Machado et al. [6], the precipitation rate greatly decreased tending to dissolve the polymer for very high solvent concentration in the coagulation bath. Therefore, in light of all the previous characterization results, it was concluded that preparing PVDF-HFP hollow fiber membranes under the same experimental conditions and employing these mixed coagulants (i.e. D70 and D80) would be impossible. This was experimentally verified using these mixtures as bore liquids to prepare hollow fiber membranes. It was observed that the nonsolvent mixture D70 used as the internal coagulant of the spinning process was not able to form the hollow fiber

membrane shape although phase inversion was occurred. Nevertheless, the copolymer coagulation was impossible using D80 as the bore liquid and the phase inversion did not take place.

3.1.3.2 Hollow fiber membrane characterization

Morphology of the hollow fiber membranes prepared with different internal coagulants

The cross-section and the internal surface of the hollow fiber membranes were analyzed by SEM and the corresponding images can be seen in Fig. 3.1.4. These illustrate the effect of the internal coagulant by analyzing the evolution of the internal structure of the membranes prepared with different internal coagulants (i.e. different amount of DMAC in DMAC/water mixtures). In general, all the membranes present common asymmetric cross-section morphology, a sponge-like structure in the middle and a finger-like structure in the external and/or internal layers. When water was used as a bore fluid, long fingers ended by voids grew from the inner layer to the middle of the fiber cross-section, while short fingers appeared in the outer layer. Increasing DMAC concentration in DMAC/water mixture modified both the cross-section and the inner surface structure of the membranes. The fingers of the outer layer became longer while the fingers of the inner layer became shorter, changing therefore the thickness of the middle sponge-like structure. This effect on membrane morphology was also observed by Xu et al. [24] when low concentrations of DMAC (i.e. 0, 10, 20 and 30 wt%) in water were used as internal coagulant for the fabrication of the PVDF hollow fibers. Besides the structure of the PVDF-HFP membranes prepared for the present study, from SEM images a thinner hollow fiber cross-section was detected for the membranes prepared with higher DMAC content in the DMAC/water mixture. This will be explained in the following section.

Porous inner surfaces were observed for all the fabricated membranes. The largest internal surface pore sizes were observed for the membranes 1IND50 and 1IND60, when the greatest amounts of DMAC were used in the bore liquid, as it will be confirmed by means of AFM analysis. The thermodynamic experiment results could explain the skinless inner surfaces of the prepared hollow fibers [45]. When DMAC concentration in the internal coagulant was increased, the cloud point was greater. This means that more quantity of nonsolvent can be incorporated to the dope solution, resulting in a greater amount of solvent in the nascent inner layer of the hollow fiber during the spinning process. The solvent inflow from the bore liquid may decrease the local polymer concentration on the inner interface, preventing the formation of the dense skin-layer and obtaining a more open-porous inner surface structure [25, 48]. It is worth quoting that a skinless and open microporous inner surface of the PSf hollow fiber

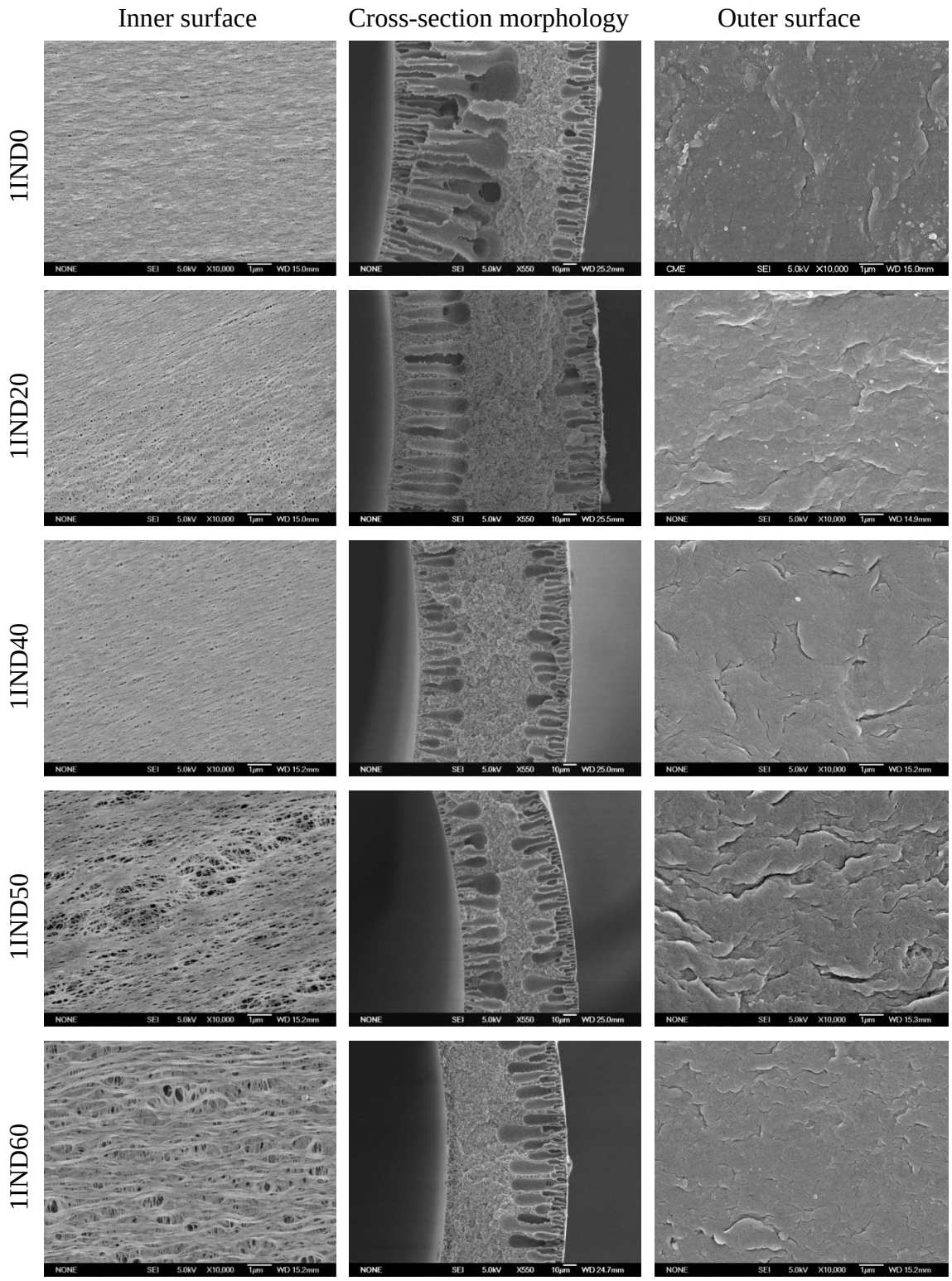

Fig. 3.1.4. SEM images of the cross-section morphology and the inner and outer surfaces of the hollow fiber membranes prepared with different concentrations of DMAC in water as internal coagulants.

membranes was detected by Rahbari-sisakht et al. [25] when 1-Methyl-2-pyrrolidone (NMP)/water mixture was used as the bore liquid. By increasing the NMP content from 50 to 90 wt%, the inner surface became more porous with larger pores. Zhang et al. [47] also observed a porous inner surface structures of PVB hollow fibers, when high solvent amounts were added in the internal coagulants. Furthermore, as it can be seen in Fig. 3.1.4, all the inner surfaces exhibited a stretched morphology due to the gravity force that elongated the fiber along the gap distance. This stretching effect was more pronounced when increasing the DMAC concentration in the bore liquid. The nascent hollow fibers prepared with a high amount of DMAC in the internal coagulant were not coagulated very fast along the air gap leading to a great stretching effect of the hollow fiber.

As it can be seen in Fig. 3.1.4, all the outer surfaces of the PVDF-HFP hollow fibers presented similar dense skin-layer as a consequence of the dry phase inversion step of the spinning process (i.e. solvent evaporation along the air gap distance) [48-50]. The aforementioned consequences of the higher cloud point also explained the larger fingers observed at the outer layer of the fiber when DMAC content in the internal coagulant mixture was increased. By increasing the DMAC concentration in the bore liquid the nascent membrane was less coagulated along the gap distance. Then, when the hollow fiber reached the water bath, the coagulation process became faster and the inflow of water from the outer layer of the membrane induced the formation and growth of longer fingers from the external layer.

It is worth noting that the fingers of the internal layer disappeared when the highest quantity of DMAC (i.e. 60 wt%) was used, resulting in the most spongy inner layer (see 1IND60 cross-section in Fig. 3.1.4) and the most open-porous inner surface structure (see 1IND60 inner surface in Fig. 3.1.4). Therefore, it may be expected a higher MD performance for the membrane 1IND60 [8, 18, 23, 51]. It is well known that a sponge-like structure corresponds to a lower coagulation rate whereas a finger-like structure represents a faster solvent-nonsolvent exchange during the coagulation process [17, 24, 35, 46]. The observed changes of the inner structure of the hollow fibers are related with the characteristics of the dope solution discussed previously. The solubility parameter distance between the nonsolvent and the solvents mixture (R_{HSP} (NS-S_m)) was decreased while the cloud point was increased and the coagulation rate was slower when the quantity of DMAC in DMAC/water mixture was increased. In other words the internal coagulant became weak with less interaction with the solvent, delaying the precipitation initiation and slowing down the coagulation during the phase inversion process [24, 52]. Wang et al. [9] also justified the formation of the sponge-like structure near the inner skin of the PVDF hollow fiber membranes by the delayed phase inversion, caused by the use of the bore liquid mixture, NMP/water (80:20).

Structural properties of hollow fiber membranes prepared with different internal coagulants

Table 3.1.3 summarizes the inner and outer diameters as well as the thickness of all the prepared hollow fiber membranes in this study. There is no clear effect on either the internal or external diameters when the amount of DMAC is increased. However, as it was observed from SEM cross-section images (Fig. 3.1.4), the thickness of the membranes certainly decreased. For 1IND50 and 1IND60 membranes, the thickness was half that of the 1IND0. Shi et al. [11] observed the same effect for the PVDF-HFP hollow fiber membranes. This result may be attributed to the decrease of the bore liquid coagulation power, when a greater solvent quantity was considered. These weaker internal coagulant mixtures were able to precipitate the spinning solution very slowly, as it was predicted by the dope solution characterization experiments, and through the air gap distance due to the stretching of the fiber that was not completely coagulated, the thickness was reduced as consequence.

The void volume fraction or porosity and *LEP* measurements of the hollow fiber membranes are shown in Table 3.1.3. The porosity of the membranes increased while the *LEP* decreased when larger amount of DMAC in water was used as internal coagulant mixture. The hollow fiber membrane 1IND0 was out of these trends. This is attributed to the large and numerous fingers of the inner layer that ended by voids in the middle of the fiber cross-section. These induced a higher porosity and a lower *LEP* as it was indicated in [16]. The fiber prepared with the highest amount of DMAC (i.e. membrane 1IND60) resulted to be the most porous membrane. This was justified due to the above mentioned open-porous structure of the inner layer (see SEM cross-section morphology, Fig. 3.1.4). The void volume fraction of this membrane was greater than the highest value obtained by García-Payo et al. [13] for the PVDF-HFP hollow fiber membrane prepared with the lowest copolymer

Table 3.1.3. Diameters, thickness, void volume fraction, *LEP* and contact angles of hollow fiber membranes prepared with different amounts of DMAC in water as internal coagulants.

Membrane	Inner diameter (μm)	Outer diameter (μm)	Thickness (μm)	Void volume fraction (ε %)	*LEP* (10^5 Pa)	Inner contact angle (º)	Outer contact angle (º)
1IND0	1190 ± 180	1550 ± 150	180 ± 40	66.0 ± 2.4	1.02 ± 0.06	152.2 ± 1.3	95.8 ± 0.4
1IND20	994 ± 96	1332 ± 94	169 ± 28	53.0 ± 0.7	3.93 ± 0.20	147.5 ± 1.8	99.1 ± 0.4
1IND40	1360 ± 170	1630 ± 160	133 ± 30	62.5 ± 0.5	2.85 ± 0.21	142.6 ± 0.7	89.2 ± 0.7
1IND50	1120 ± 150	1310 ± 150	99 ± 24	76.3 ± 2.2	1.69 ± 0.19	157.7 ± 1.6	90.0 ± 0.6
1IND60	1180 ± 110	1380 ± 110	96 ± 17	78.4 ± 0.8	1.35 ± 0.34	149.8 ± 0.6	89.4 ± 0.6

concentration (i.e.17 wt%). A similar effect was detected by Rahbari-sisakht et al. [25] when a mixed bore liquid (NMP/water) was employed for PSf membrane fabrication. The overall porosity increased from 62.0% to 71.7 % when a 50 wt% of NMP was employed instead of water.

As it can be observed in Fig. 3.1.4, when DMAC content in the bore liquid was increased the inner surface pore size became larger and bigger fingers were detected in the external layer of the fiber cross-section. These explain the decrease of the *LEP* with the DMAC content in the bore liquid. It is worth noting that the obtained *LEP* values were higher than 1 bar, confirming that all the prepared membranes can be applied in MD technology. These *LEP* values are in the same range as that reported for other PVDF-HFP fibers used for DCMD [13] but higher than those determined for all the PVDF-HFP hollow fiber membranes considered for the experimental design developed by Khayet et al. [21].

Both inner and outer contact angle measurements are also collected in Table 3.1.3. No clear trend was observed between these values and the internal coagulant mixtures used for hollow fiber membrane preparation. However, it can be observed that the inner contact angles were much larger than outer contact angles. The same result was observed by Zhang et al. [38] for fluorinated hydrocarbon hollow fiber when using the same contact angle measurement procedure. The very high inner contact angles obtained in this study show that the inner layers of theses fibers have similar hydrophobicity to the polytetrafluoroethylene (PTFE) flat-sheet membrane reported by Zhang et al. [53]. The obtained results for the outer contact angles can be compared to the dynamic contact angles of other fibers measured by a tensiometer. All the membranes prepared in this study have similar outer contact angles to those of other PVDF-HFP hollow fibers [10], but higher than the water contact angle of the PVDF commercial membrane analyzed by Shi et al. [11]. This result confirms the hydrophobic character enhancement of the PVDF-HFP membrane due to the HFP group addition to the PVDF chain.

The pore sizes of the hollow fiber membranes obtained by means of Porometry test are shown in Table 3.1.4. These values were higher than the average pore size of the PVDF-HFP hollow fiber membranes prepared by Wongchitphimon et al. [10]. When the amount of DMAC in the internal coagulant mixture was increased, the bubble pore size was gradually increased, while both the mean and smallest pore sizes became significantly bigger for the fibers prepared with the highest amount of DMAC in water as inner coagulant. This means that not only greater pore sizes were obtained, but also pore size distributions were wider, as shown in Fig. 3.1.5 when higher amount of DMAC was used in the internal coagulant. A similar effect was observed by Zhang et al. [54] for the yttria-stabilized zirconia (YSZ) fibers pore size distributions when NMP/water mixtures with higher amount of solvent were used as internal coagulants. The narrowest pore size distribution corresponded to the membrane

prepared with pure water as nonsolvent. This was also observed in this study for PVDF-HFP hollow fibers. The mean pore size of the aforementioned YSZ membranes and the PSf hollow fibers prepared by Rahbari-sisakht et al. [25] also increased with increasing the NMP content in the bore liquid.

Table 3.1.4. Bubble pore size, mean pore size, and smallest pore size of the hollow fiber membranes prepared with different amounts of DMAC in water as internal coagulants determined by gas-liquid porosimetry.

Membrane	Bubble pore size (nm)	Mean pore size (nm)	Smallest pore size (nm)
1IND0	566 ± 6	403 ± 3	356 ± 2
1IND20	586 ± 6	488 ± 4	400 ± 3
1IND40	819 ± 13	474 ± 4	403 ± 3
1IND50	1273 ± 30	656 ± 8	492 ± 4
1IND60	1989 ± 74	711 ± 9	528 ± 5

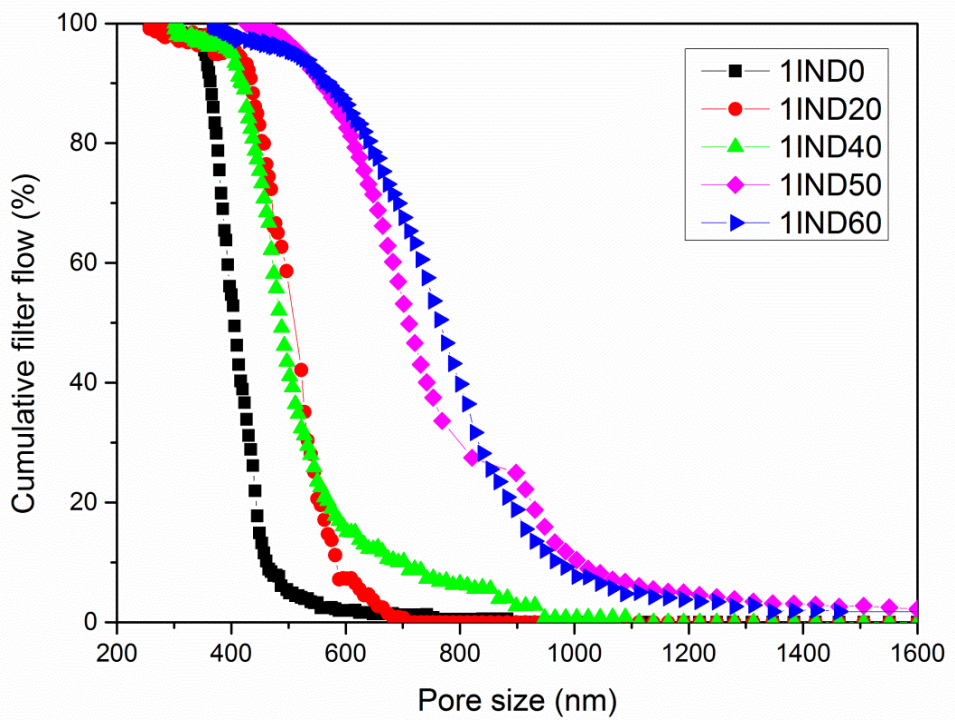

Fig. 3.1.5. Cumulative filter flow of the hollow fiber membranes prepared with different DMAC concentrations in water as internal coagulants.

Figure 3.1.6 shows the 3D AFM images of the inner surface of the hollow fiber membranes prepared with different internal coagulant mixtures and Table 3.1.5 summarizes the roughness of both the inner and outer surfaces of hollow fibers. No tendency was detected for the mean roughness of the outer surface. If the standard deviations are taken into account, all the values can be considered similar, which is in accordance with the presence of the skin-layer in the external surfaces of all the prepared membranes (see Fig. 3.1.4) as discussed earlier. Similar roughness values were obtained for the outer surface of other PVDF-HFP hollow fiber membranes, which were also prepared with a large air gap distance [13, 55]. Nevertheless, the inner surface of the membranes became significantly rougher when increasing the DMAC quantity in the bore liquid (DMAC/water mixture) up to 60 wt% (see 1IND60 in Fig. 3.1.6). This effect on the fiber surface roughness may be related to the open-pore, sponge inner layer structure, and formation of bigger nodules.

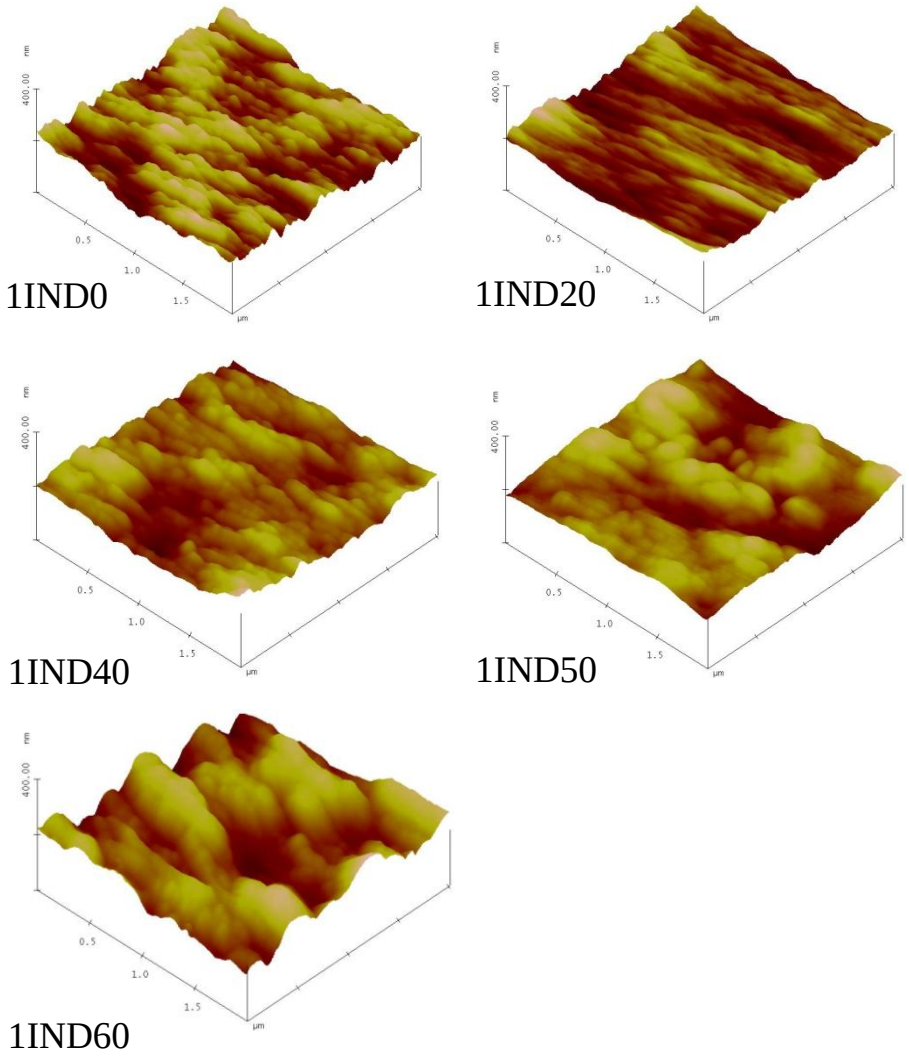

Fig. 3.1.6. 3D AFM images of the inner surfaces of the hollow fiber membranes prepared with different concentrations of DMAC in water as internal coagulants.

Table 3.1.5. Minimum, maximum and average mean roughness parameter, R_a, together with the corresponding standard deviation of the internal and external surfaces of the hollow fibers prepared with different concentrations of DMAC in water as internal coagulants (scan range considered 2 μm × 2 μm).

Membrane	R_a (nm) Inner surface			R_a (nm) Outer surface		
	Minimum	Maximum	Average	Minimum	Maximum	Average
1IND0	13.4	17.4	16.0 ± 1.2	16.7	26.3	21.0 ± 4.0
1IND20	7.3	11.5	9.1 ± 1.3	16.0	24.1	19.4 ± 3.0
1IND40	9.5	14.6	12.0 ± 2.0	15.3	22.6	18.4 ± 2.5
1IND50	10.2	20.8	13.7 ± 2.8	17.9	25.2	21.4 ± 2.6
1IND60	20.0	26.1	22.8 ± 2.1	11.8	25.3	16.0 ± 4.0

The mean pore size and the corresponding standard deviation of the inner surfaces were analyzed (Table 3.1.6). All these values were higher than those determined for the inner surface of other PVDF-HFP hollow fiber membranes prepared with different copolymer concentrations and distilled water as a bore liquid [13]. Greater pores were found on the internal surface of the membranes prepared with higher amounts of DMAC (50 and 60 wt%) in the bore liquid. This result was previously observed from the corresponding SEM surface images (see Fig. 3.1.4). Figure 3.1.7 shows the cumulative pore size distributions and the probability density functions of the corresponding surfaces. It can be seen that the curves of the membranes 1IND50 and 1IND60 shift towards bigger surface pore sizes coinciding with the mean values presented in Table 3.1.6.

Table 3.1.6. Mean pore size, μ_p, and geometric standard deviation, σ_p, of the internal surfaces of the hollow fiber membranes prepared with different concentrations of DMAC in water as internal coagulants.

Membrane	μ_p (nm)	σ_p (nm)
1IND0	85.23	1.09
1IND20	89.91	1.10
1IND40	86.04	1.07
1IND50	98.53	1.07
1IND60	100.44	1.10

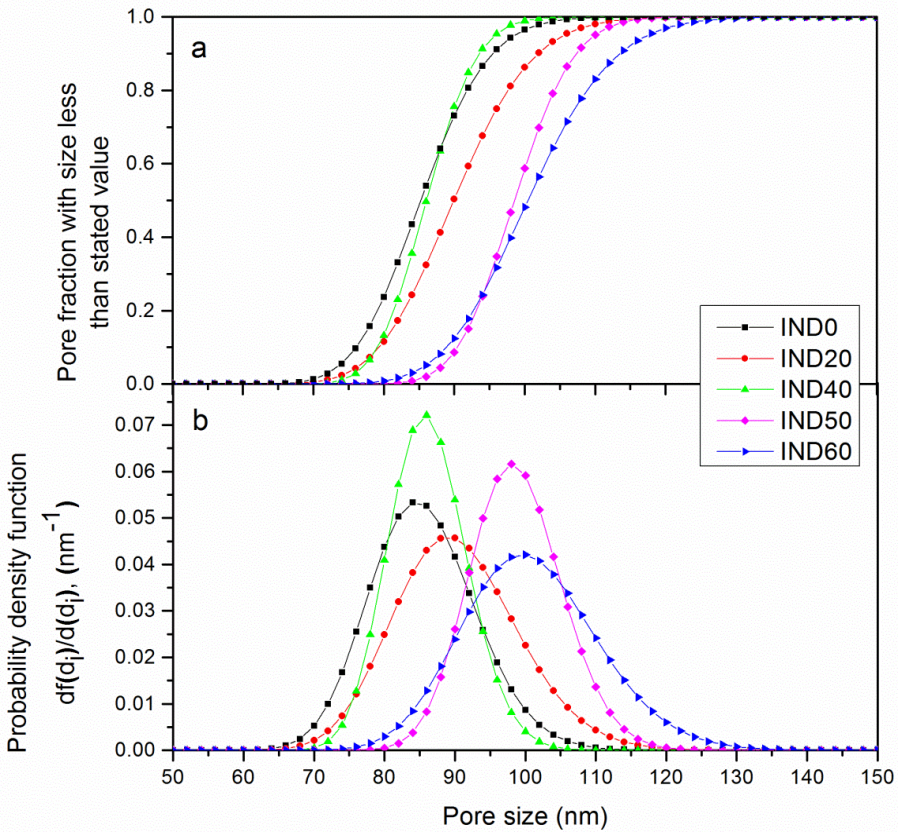

Fig. 3.1.7. Cumulative pore size (a) and probability density function (b) curves generated from the pore sizes obtained from AFM images of the inner surfaces of the hollow fiber membranes prepared with different DMAC concentrations in water as internal coagulants.

Figure 3.1.8 and Table 3.1.7 summarize the thermal properties of the hollow fiber membranes measured by DSC. Both melting and crystallization temperatures and the corresponding enthalpies, of the hollow fiber membranes fabricated with different internal coagulants, were found to be similar to each other and to the copolymer, PVDF-HFP. This result proved that the bore liquid did not affect either the thermal properties or the crystallinity of the membranes. The melting temperatures as well as the corresponding enthalpies fell within the data range of PVDF-HFP, included in Handbook of Polymers [56], 125 – 164 °C and 36 – 65 J/g, respectively. It is to point out that the maximum DCMD operating temperature considered in this study was 80 °C, much lower than both T_m and T_c obtained for all PVDF-HFP hollow fiber membranes; ensuring that the fibers did not suffer any thermal deterioration during DCMD process.

MD technology does not require the use of membranes with very high mechanical properties compared to other pressure-driven membrane processes (Microfiltration, Ultrafiltration, Nanofiltration and Reverse Osmosis). The transmembrane hydrostatic pressure applied in MD is smaller. However, it is important to know the mechanical characteristics of the membranes in order to guarantee a good packing of the membranes in modules [1, 3]. The

obtained stress-strain experiments are plotted in Fig. 3.1.9 and from these curves the main mechanical parameters were calculated (see Table 3.1.8). The Young´s modulus (*E*) represents the stiffness of the hollow fiber membranes. The *E* parameter values summarized in Table 3.1.8 were higher than those reported by Shi et al. [11] and Wongchitphimon et al. [10] for other PVDF-HFP hollow fiber membranes. By increasing the DMAC concentration in the internal coagulant mixture, *E* was reduced and the membranes became more elastic. This effect may be related to the increase of fiber´s porosity (see Table 3.1.3), facilitating the polymeric chains movement during the stress-strain experiments. The same behavior was detected by Shi et al. [11] when PVP was added into the PVDF-HFP spinning solution.

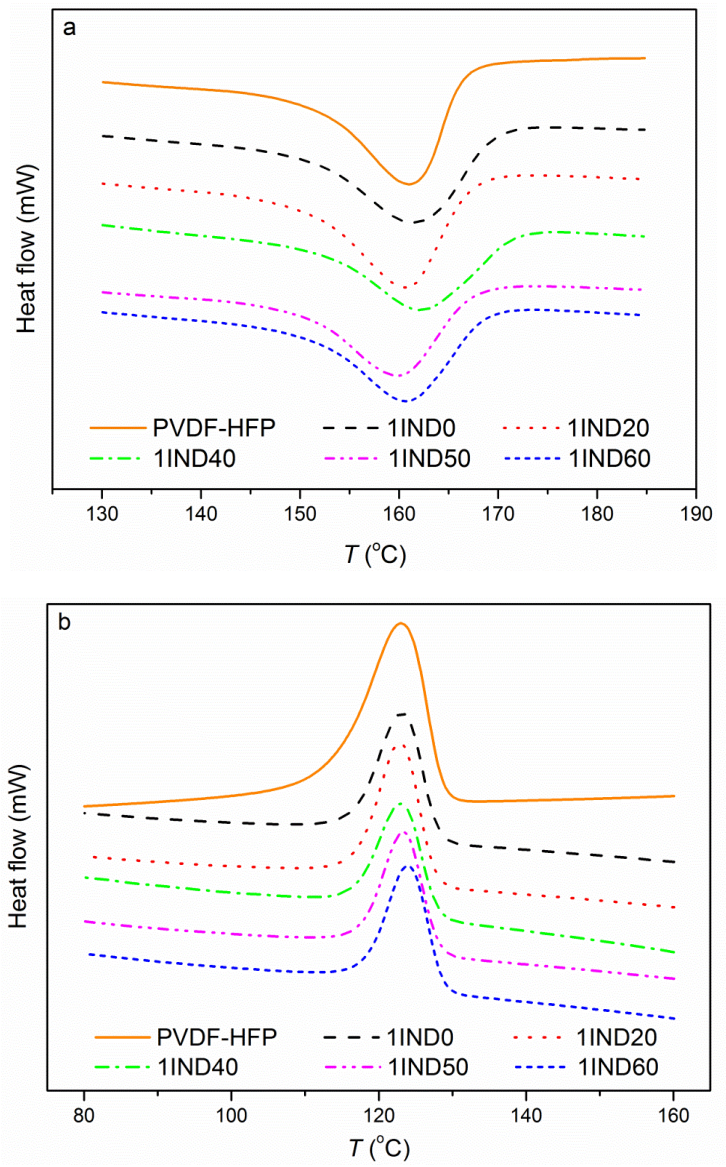

Fig. 3.1.8. DSC thermograms, (a) heating and (b) cooling of the copolymer PVDF-HFP and the hollow fiber membranes prepared with different concentrations of DMAC in water as internal coagulants.

Table 3.1.7. Melting temperature (T_m), crystallization temperature (T_c), enthalpy of melting (ΔH_m), enthalpy of crystallization (ΔH_c) and crystallinity (X_c) of the copolymer PVDF-HFP and the hollow fiber membranes prepared with different DMAC concentrations in water as internal coagulants.

Sample	Heating process		Cooling process		Crystallinity X_c (%)
	$\Delta H_m \pm 0.5$ (J/g)	$T_m \pm 0.15$ (°C)	$\Delta H_c \pm 0.5$ (J/g)	$T_c \pm 0.15$ (°C)	
PVDF-HFP	45.7	160.98	45.4	123.00	43.6
1IND0	45.5	161.49	45.5	123.48	43.4
1IND20	45.6	160.71	45.4	123.00	43.6
1IND40	45.2	162.18	45.3	123.21	43.2
1IND50	45.3	159.97	45.5	123.48	43.3
1IND60	45.4	160.69	45.6	124.25	43.4

Nevertheless, the E parameter obtained for the membrane prepared with the highest amount of DMAC in the bore liquid (1IND60) did not follow this tendency, it was higher than the Young´s modulus of the hollow fiber 1IND50. In fact, these two membranes had similar porosities. Hence, it may be the change in membrane morphology the responsible of the elasticity difference. As it can be observed in Fig. 3.1.4, the fiber 1IND60 is totally free of fingers at the inner layer and exhibits larger sponge-like structure along its cross-section than the membrane 1IND50, making the fiber a little more rigid [15]. The yield and the tensile stress at break were also analyzed, and both were decreased when the amount of DMAC was higher in the internal coagulant. These results indicate the reduction of the stress held before leaving the elastic region and fracture. The observed decrease of tensile stress at break may be due to the thickness decrease (see Table 3.1.3) when a weaker coagulant was used as a bore liquid [5, 39]. However, for both membranes, 1IND50 and 1IND60, with a similar thickness, the yield and the tensile stress at break of 1IND60 were slightly higher than those of the membrane 1IND50. This might be attributed to the inner layer sponge-like structure of 1IND60 and to its stronger and better interconnected inner surface. It is worth noting that all the prepared PVDF-HFP membranes had a tensile stress at break similar or even higher than the reported value of other hollow fibers [10, 11, 15, 57]. The strain at break of the hollow fiber membranes decreased following the same tendency than the tensile stress at break. These values were all lower than the strain at break data of PVDF-HFP fibers reported in other studies [10, 11, 15] but higher than the strain at break of the PVDF commercial hollow fiber (i.e. 128 ± 16 %), tested by Shi et al [11]. It was stated that the observed ductile behavior improvement of all the PVDF-HFP fibers compared with PVDF ones was due to the amorphous group HFP embedment in the PVDF polymeric structure [11].

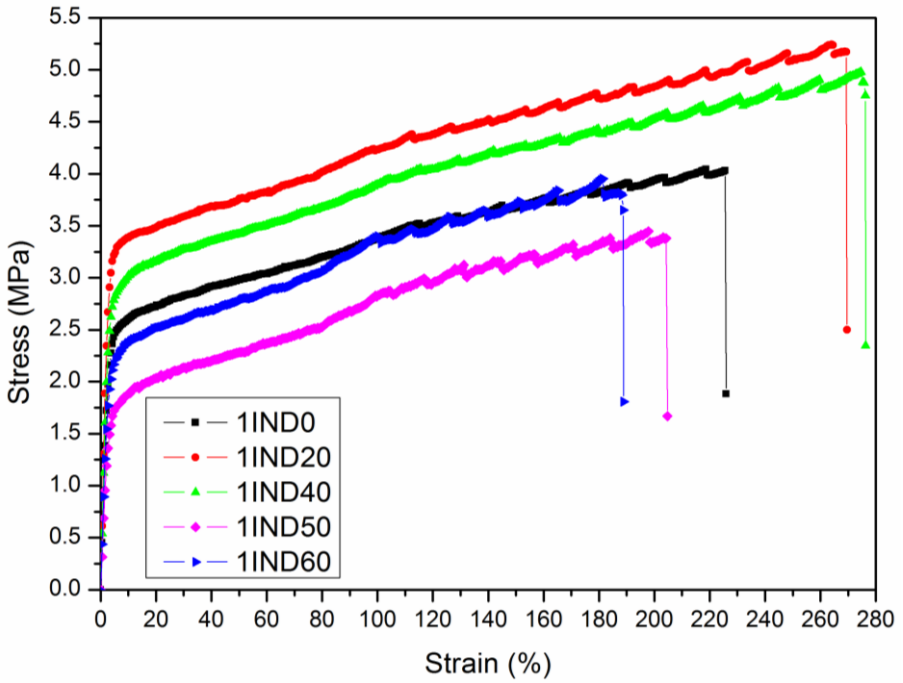

Fig. 3.1.9. Stress-strain curves of the hollow fiber membranes prepared with different DMAC amounts in water as internal coagulants.

Table 3.1.8. Mechanical properties (Young´s modulus, E; yield stress, σ_y; tensile stress at break, σ_b and strain at break, ε_b) of the hollow fiber membranes prepared with different DMAC concentrations in water as internal coagulants.

Membrane	E (MPa)	σ_y (MPa)	σ_b (MPa)	ε_b (%)
1IND0	103 ± 9	1.83 ± 0.09	4.26 ± 0.20	230 ± 23
1IND20	135 ± 9	2.41 ± 0.02	5.4 ± 0.5	267.3 ± 2.8
1IND40	117 ± 7	2.27 ± 0.23	5.0 ± 0.4	269 ± 10
1IND50	62 ± 6	1.15 ± 0.08	3.30 ± 0.07	212 ± 11
1IND60	87 ± 3	1.55 ± 0.14	3.70 ± 0.21	195 ± 9

3.1.3.3 DCMD experiments of hollow fiber membranes prepared with different internal coagulants

In order to compare the DCMD performance of the prepared membranes, the permeate fluxes (J) and the salt rejection factors (α) are presented in Fig. 3.1.10. As it was expected, the obtained permeate fluxes when distilled water was used as feed were higher than those corresponding to the feed salt aqueous solution (NaCl, 3 wt%) and all hollow fiber membranes exhibited good salt rejection factors. It is worth noting the good fabrication

reproducibility of the hollow fiber membranes prepared in this study. It was confirmed by SEM that the membranes prepared in different batches had the same morphology, and as it is shown in Fig. 3.1.10, the obtained DCMD permeate fluxes are within the error range. The permeate fluxes presented in Fig. 3.1.10 were greater than the maximum DCMD fluxes reported for other PVDF-HFP hollow fiber membranes (i.e. 1.3 kg/m^{2}h for distilled water as feed at 45 °C and a permeate temperature of 20 °C; 6.5 kg/m^{2}h for distilled water as feed at 80 °C and a permeate temperature of 25 °C; 5.4 kg/m^{2}h for 3 wt% NaCl feed solution at 80 °C and a permeate temperature of 25 °C) [13, 55]. According to the membrane characterization results and the obtained DCMD fluxes, it can be concluded that the use of a mixed internal coagulant improves the hollow fiber morphology, properties and DCMD performance, as consequence. The permeate flux enhancement was not very noticeable when water was changed for 20 wt% DMAC/water or 40 wt% DMAC/water mixtures as internal coagulants. Practically similar DCMD permeate fluxes were obtained for the membranes, 1IND20 and 1IND40, which was totally in accordance with their similar main characteristics such as cross-section structure, inner surface morphology, and mean pore size. However, a sharp increase of the permeate flux was observed when the highest amounts of DMAC (50 and 60 wt%) were used in the bore liquid mixture (DMAC/water). The permeate fluxes of the membranes

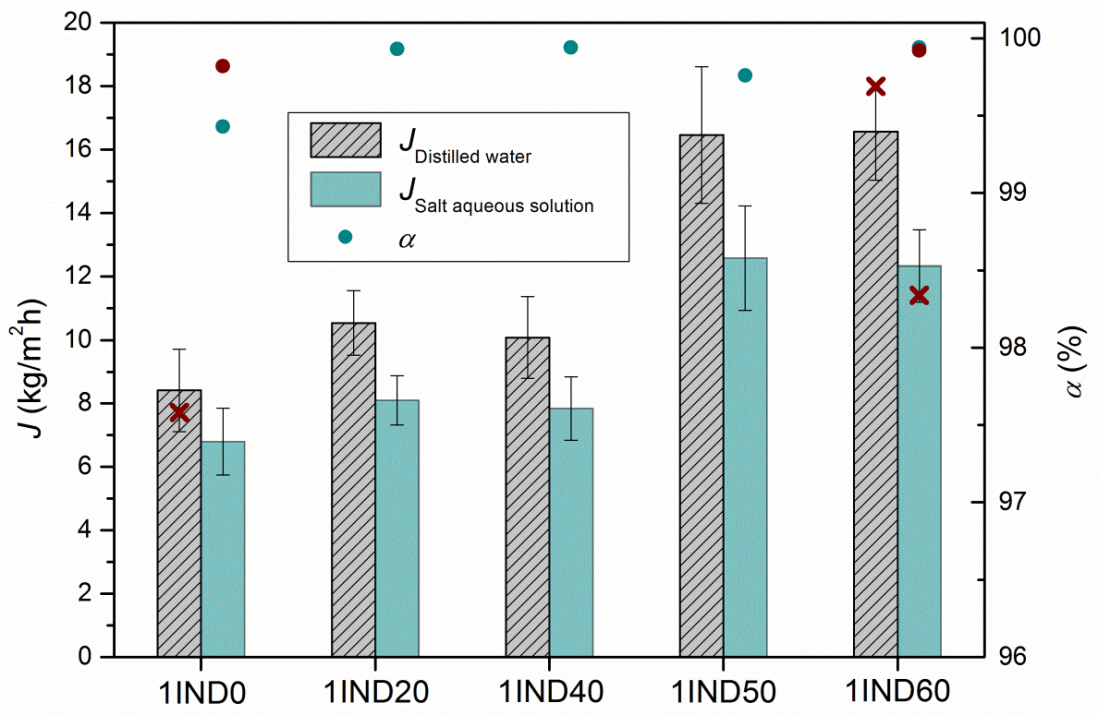

Fig. 3.1.10. DMCD permeate flux and salt rejection factor of the hollow fiber membranes prepared with different DMAC amounts in water as internal coagulants. (Feed temperature = 80 °C; Permeate temperature = 25 °C). **X** represents the DCMD permeate flux and ● the salt rejection factor of hollow fiber membranes prepared in different batches.

1IND50 and 1IND60 were almost doubled due to various reasons. Compared to the membrane 1IND0, the thickness of 1IND50 and 1IND60 membranes decreased around 50%, the porosity became nearly a 20% higher, and the pore sizes were approximately a 70% greater. Furthermore, these hollow fibers had more open porous inner surfaces with larger pores, and especially the membrane 1IND60 exhibited a thicker sponge-like structure more open at the immediately inner layer with a higher mean roughness of the inner surface. All the aforementioned characteristics totally justified the observed greater permeate fluxes of these two hollow fiber membranes, 1IND50 and 1IND60 [5, 13, 16, 17]. These DCMD permeate fluxes were similar to those exhibited by the optimal PVDF-HFP hollow fiber membrane developed by a statistical experimental design (i.e. 13.5 kg/m^2h for 3 wt% NaCl feed aqueous solution at 75 °C and a permeate temperature of 20 °C) [21]. It is necessary to highlight that these hollow fiber membranes had excellent salt rejection factors, 99.76% (1IND50) and 99.94% (1IND60) although their maximum pore size were greater than that of the other fibers.

3.1.4 Conclusions

The selection of the nonsolvent type for PVDF-HFP hollow fiber membrane preparation strongly affected the membrane morphology, its structural characteristics, and DCMD performance. It was demonstrated that the morphology of these fibers was determined by the quantity of DMAC in water used as an internal coagulant for their preparation. As it was predicted by the spinning solution characterization techniques, the resultant membrane morphology directly depends on the nonsolvent-solvent interactions and thermodynamic and kinetics of membrane phase inversion. The usefulness and validity of the Hansen solubility parameter distance analysis prior membrane preparation was demonstrated. This procedure can be applied to any phase inversion membrane prepared with different spinning solutions and coagulants minimizing therefore the number of the experiments.

It was observed that the higher was the quantity of DMAC in the nonsolvent mixture, the weaker was the internal coagulant, and the earlier and slower was the phase inversion of the membrane. Therefore, more porous inner surfaces with larger pore sizes were formed and the finger-like structure of the inner layer was reduced or even disappeared forming an open-spongy structure when the greatest content of DMAC was used in the bore liquid.

Other structural characteristics of the hollow fibers were enhanced when the solvent concentration was increased in the internal coagulant such as the lower thickness, higher porosity, larger pore size, narrower inner surface pore size distribution and higher inner surface roughness. The larger bubble pore sizes resulted in lower *LEP* values.

In general, all the prepared membranes exhibited adequate thermal and mechanical properties for MD application. The most significant improvements were obtained for the hollow fibers prepared with the highest concentrations of DMAC in the bore liquid mixtures. The corresponding membranes (1IND50 and 1IND60) were the thinnest and the most porous with the largest pore sizes, leading to the greatest DCMD permeate fluxes and maintaining high salt rejection factors during desalination by DCMD. These results might be even improved if the skin-layer could be removed from the outer surface of these PVDF-HFP hollow fiber membranes. This is the main objective of the next research study [58].

3.2 Mechanism of formation of hollow fiber membranes for membrane distillation: 2. Outer coagulation power effect on morphological characteristics

Abstract

Poly(vinylidene fluoride-co-hexafluoropropylene) (PVDF-HFP) hollow fiber membranes with porous and skinless outer surfaces were prepared for desalination by direct contact membrane distillation (DCMD). *N,N*-dimethyl acetamide (DMAC)/distilled water mixtures extruded from the outermost channel of the spinneret were employed as external coagulants along the gap of the spinning process. During membrane formation, various types of interactions studied via Hansen solubility parameters were identified at the outer layer of the nascent fiber. Several characterization techniques and DCMD experiments were carried out in order to analyze the effects of the wet gap on the membrane morphology, properties and desalination performance. The skin-layer was avoided and permeate flux was enhanced when using the DMAC/water mixtures as the external coagulants. Increasing the concentration of DMAC in the nonsolvent mixture weakened the external coagulation power and the outer layer morphology of the fiber became more porous with larger surface pore sizes. Open-porous inner surface, skinless outer layer and spongy cross-section were observed for the hollow fiber membranes prepared with the highest amounts of DMAC in water, 50 and 60 wt%, used simultaneously as internal and external coagulants. The hollow fiber membrane prepared with the coagulant mixture 50 wt% DMAC in water exhibited good mechanical properties and excellent MD membrane characteristics, leading to the highest DCMD permeate flux with a good salt rejection factor.

3.2.1 Introduction

Membrane engineering is an important key step for obtaining good morphological characteristics of membrane distillation (MD) membranes. Several studies have demonstrated the membrane structural morphology effects on both the permeate flux and separation factor of this separation process [2, 3, 5].

Hydrophobic polymeric hollow fiber membranes are commonly prepared by the dry/wet spinning technique, whose operating parameters affect considerably the final structure of the

membrane [1, 21-23]. It was observed that the formation of the fiber´s inner layer structure was mainly determined by the bore liquid composition. By changing the type of the bore liquid it was possible to prepare porous inner surfaces [24, 25, 59]. However, the majority of the hollow fibers described in the open literature prepared by the dry/wet technique have a dense skin on the outer layer. Its formation starts with the nascent fiber´s path across de air gap distance (i.e. dry step of the spinning process) due to the forced-convective evaporation of the volatile solvents contained in the dope solution; and then completely formed when finally immersed in the nonsolvent coagulation bath [48]. Solvent evaporation increases the polymer concentration at the outermost layer of the fiber compared to that of the bulk of the spinning solution. Additionally, faster solvent outflow in comparison to the nonsolvent inflow inside the coagulation bath also induced the formation of the skin-layer [48, 60].

The denser structure of the outer surface of the hollow fiber membranes induces lower external surface porosity, higher vapor transport resistance and lower MD permeate flux as consequence [8, 9]. Therefore, it is necessary to improve the outer surface morphology trying to avoid the outer skin-layer formation. Previous studies have analyzed different options to reduce the thickness of the membrane´s external layer and to obtain more porous surfaces. When the air gap distance was reduced, Clausi and Koros [48] and Tsai et al. [49] were able to reduce the skin-layer thickness of the polyimide and polysulfone (PSf) hollow fiber membranes, respectively. The temperature and composition of the coagulation bath are other fabrication parameters that affect the membrane formation mechanism. Wang et al. [61] prepared poly(vinylidene fluoride) (PVDF) membranes by immersing the casting dope solution in de-ionized water coagulation bath at different temperatures (15, 25 and 60 °C). It was observed much shrinkage and denser top surfaces for lower coagulation bath temperatures. By adding solvent into the coagulation bath, the phase inversion rate slows down and porous surfaces could be obtained. Wijmans et al. [62] determined the minimum concentration of solvent in the water coagulation bath required to obtain porous top layers of flat-sheet membranes for various polymer/solvent/nonsolvent systems. Yu et al. [63] used the mixture *N,N*-dimethyl formamide (DMF) and water at different ratios (from 0 to 60% of DMF) in the coagulation bath for the preparation of polyacrylonitrile (PAN) hollow fiber membranes via dry/wet spinning technique. The formation of the outer skin-layer was very slow for 60% of DMF in water leading to observable pores on the external surface of the corresponding hollow fiber membrane. Other researchers [8, 64] preferred to use a triple-orifice spinneret to extrude a solvent from the outer channel of the spinneret. He et al. [64] and Bonyadi and Chung [8] employed this technique to prepare PSf and PVDF hollow fiber membranes, respectively. Pure *N*-methylpyrrolidone (NMP) solvent was used in these studies observing porous outer surfaces.

In our previous study [59], hollow fiber membranes were prepared using different nonsolvent mixtures (solvent/water) as internal coagulant. It was observed that these hollow fibers presented a sponge inner layer and skinless and porous inner surface structure, resulting in an improved DCMD performance. This can be enhanced if the formed dense skin-layer at the outer side of the hollow fiber membrane is removed. It is well known that the dry step of the spinning process is the responsible for the formation of the dense outer surface [33, 48, 50]. The main objective of this study is the change of the outer layer structure from dense skin to open-porous morphology. Two different options have been followed in order to solve the aforementioned drawback: i) eliminating the air gap distance between the spinneret and the liquid coagulation bath and ii) changing the gap type from dry to wet, using different nonsolvent mixtures (solvent/water) as external coagulants through the gap distance. Following these strategies, the solvent evaporation step that occurs through the air gap would be prevented and the polymer concentration on the external interface could be controlled by the solvent outflow and nonsolvent inflow relative ratio [64, 65]. In line with previous research studies [17, 59, 65], the selection of the polymer/solvent/nonsolvent system and the thermodynamic and the kinetics of the phase inversion process play a critical role on the final morphological structure of the membrane. In other words, the solvent-nonsolvent interaction represents the key control factor of the skin-layer thickness. Finally, trying to benefit from the advantages of employing the nonsolvent mixtures as internal and external coagulants, hollow fiber membranes have been prepared using simultaneously the same coagulant solution as both internal and external coagulants.

3.2.2 Experimental

3.2.2.1 Materials

The spinning solution was composed by the solvents *N,N*-dimethyl acetamide (DMAC) and trimethyl phosphate (TMP), the additive poly(ethylene glycol) (PEG; M_w = 6000 g/mol) and the copolymer poly(vinylidene fluoride-co-hexafluoropropylene) (PVDF-HFP; M_w = 455,000 g/mol). All these reagents were purchased from Sigma-Aldrich. Isopropyl alcohol (IPA, Sigma-Aldrich) was used as the wetting liquid for the void volume fraction or porosity measurements. The sodium chloride (NaCl) was employed as the salt of the aqueous feed solutions of DCMD experiments, and it was purchased from Panreac.

3.2.2.2 Preparation and characterization of hollow fiber membranes and direct contact membrane distillation experiments

The spinning solution was composed by 19 wt% of the copolymer PVDF-HFP, 5 wt% of the additive PEG and 76 wt% of the solvent mixture combining 40 wt% of DMAC and 60

wt% of TMP. The selection of the dope solution, its preparation procedure and some properties such as viscosity, surface tension and the thermodynamic and kinetics experiments were explained in [59]. More information about the copolymer PVDF-HFP can be found in [7, 59]. The hollow fibers were prepared by the dry/wet spinning technique, as described elsewhere [26, 27]. The spinning parameters are summarized in Table 3.2.1 and the prepared membranes are identified in Table 3.2.2 according to the considered fabrication parameters.

The prepared hollow fiber membranes were characterized by means of the following techniques: scanning electron microscope (FESEM, JEOL Model JSM-6335F), optical microscope (OLYMPUS BX60M), water contact angles, liquid entry pressure, mechanical properties (Instron dynamometer, model 3366), mean pore size (POROLUX^{TM} 100, Porometer), atomic force microscopy (Nanoscope III equipped with 1553D scanner (Digital Instruments Inc., Santa Barbara, Ca)), thermal properties (Differential Scanning Calorimetry (DSC), Mettler-Toledo DSC 1, STAR^{e} System) and direct contact membrane distillation (DCMD). All the characterization procedures were detailed in the previous study [59]. In this case, the mean pore size of the prepared hollow fiber membranes was obtained by the gas permeation method described elsewhere [35] and using the dry curve obtained from the porometry test.

Table 3.2.1. Spinning parameters of the PVDF-HFP hollow fiber membranes.

Parameters	**Operating conditions**
Spinneret : 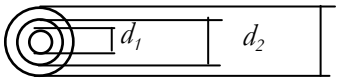	d_1= 1.0 mm / d_2= 2.4 mm / d_3= 3.4 mm
Extrusion pressure (kPa)	60
Polymeric solution temperature (ºC)	42
Internal coagulant	DMAC/distilled water
Internal coagulation temperature (ºC)	42
External coagulant	DMAC/distilled water
Internal and external coagulant flow rate (m^3/s)	2.7 10^{-7}
External coagulation temperature (ºC)	Room temperature
Liquid coagulation bath	Tap water
Liquid coagulation bath temperature (ºC)	42

Table 3.2.2. Membranes prepared in this study.

Membrane name	Internal coagulant (wt%)		Gap: type/distance (m)	External coagulant (EC)	
	DMAC	Water		DMAC	Water
IND0 (GAP 0)[a]	0	100	0	---	
2IND0	0	100	Air/0.275	---	
2OUTD0	0	100	EC/0.275	0	100
2OUTD20	0	100	EC/0.275	20	80
2OUTD40	0	100	EC/0.275	40	60
2OUTD60	0	100	EC/0.275	60	40
2IND50OUTD50	50	50	EC/0.275	50	50
2IND60OUTD60	60	40	EC/0.275	60	40

[a]All the hollow fiber membranes were prepared using the double spinneret described in Table 3.2.1 except the membrane called IND0 (GAP 0), which was prepared employing the single spinneret detailed in [59].

3.2.3 Results and discussions

3.2.3.1 Air gap elimination

The first step considered in order to remove the skin-layer from the outer surface of the hollow fibers was to prepare the membrane IND0 (GAP 0), eliminating the air gap distance. For instance, Clausi and Koros [48] and Tsai et al. [49] prepared membranes with thinner skin-layer when the air gap distance was reduced.

The outer surface SEM image of the membrane IND0 (GAP 0) (see Fig. 3.2.1) shows the presence of a dense skin-layer. Several studies described that the skin-layer formation is the result of a high polymer concentration at the external side of the membrane compared with that in the sublayer. The local polymer concentration increase can be caused by an extremely quick phase inversion induced by a strong nonsolvent in the coagulation bath [8, 60, 64]. In our case, the observed non-porous outer surface of the membrane IND0 (GAP 0) was the consequence of using a water quench bath. When the nascent fiber was just immersed in the coagulation bath, the solvent outflow was faster than the relative nonsolvent inflow, leading to a great enhancement of the polymer concentration and consequently a dense outer layer [60, 65]. Li et al. [46] also observed a dense top surface of the prepared flat-sheet PVDF membrane, when water was used as coagulation bath and no evaporation time was employed for the phase inversion process.

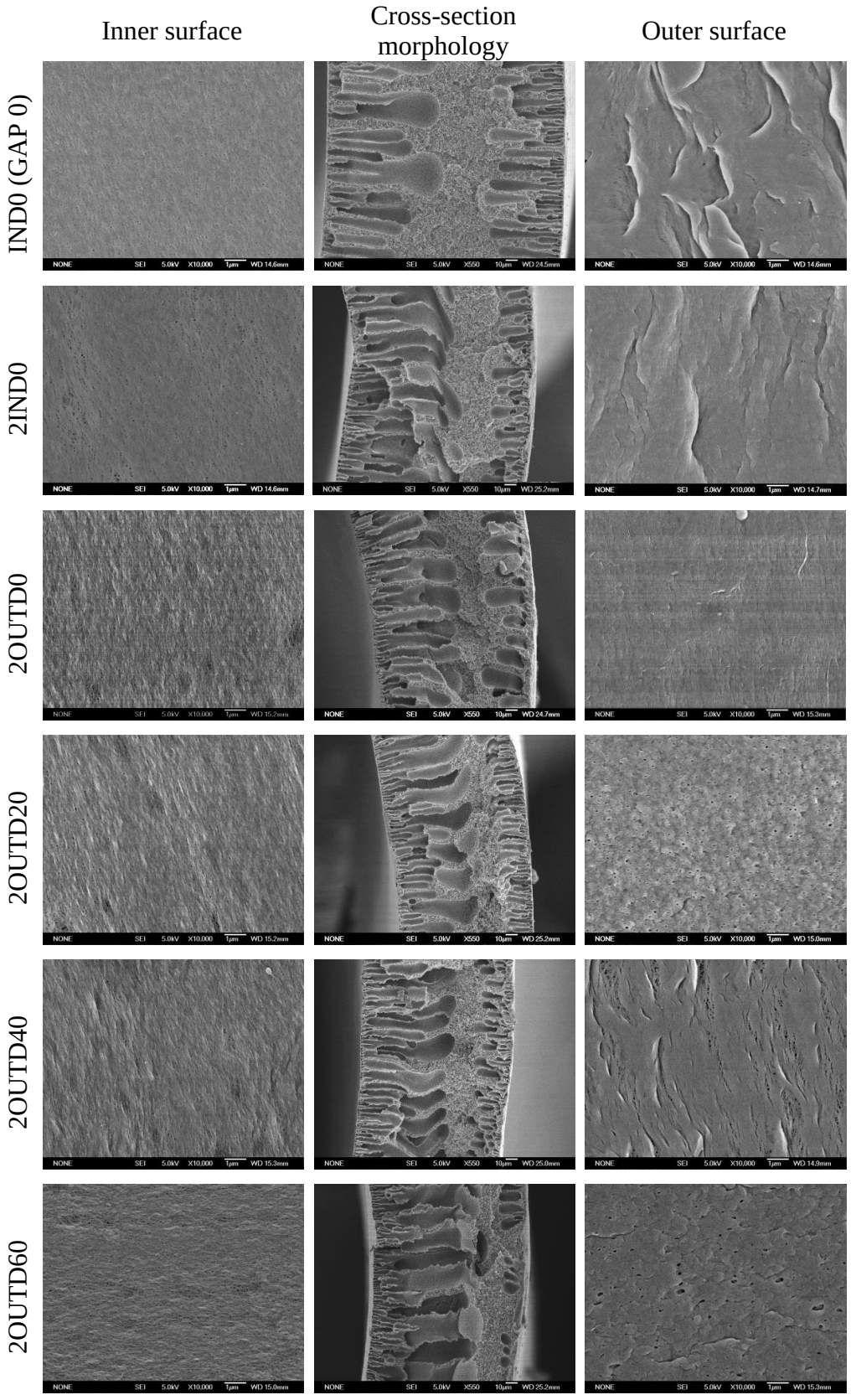

Fig. 3.2.1. SEM images of the cross-section morphology and the inner and outer surface of the prepared hollow fiber membranes.

It can be observed that the hollow fiber membrane IND0 (GAP 0) was the thickest membrane prepared in this study. By removing the air gap distance, the gravity force that is normally exerted on the spun fiber was declined, reducing therefore fiber elongation stress during membrane fabrication [26]. Due to this effect, the hollow fiber membrane IND0 (GAP 0) exhibited the largest thickness, (260 ± 30) μm, and the lowest tensile stress and strain at break in this study, (2.47 ± 0.13) MPa and (72 ± 7) %, respectively. Tsai et al. [49] who confirmed the decrease of the PSf hollow fiber membranes tensile stress as a consequence of the air gap distance reduction, explained this effect by a lack of orientation of the polymer chains. The porosity of IND0 (GAP 0) was (77.4 ± 0.3) %, leading to an elastic hollow fiber with a Young´s modulus of (71.7 ± 0.9) MPa. The resultant DCMD permeate fluxes were (8.6 ± 0.6) kg/m^{2}h and (7.0 ± 0.5) kg/m^{2}h, for feed distilled water and salt aqueous solution (NaCl, 3 wt%), respectively. Taking into account all the observed membrane characteristics for the hollow fiber membrane IND0 (GAP 0), it can be concluded that the total suppression of the air gap distance was an unsuccessful route to obtain porous hollow fiber external layer and to improve the DCMD performance. Hence, hollow fiber membrane preparation with a minimum gap distance was required. It can also guarantee adequate mechanical properties and inner regular contours (i.e. circular shape) without deformations as reported by Shi et al. [11].

3.2.3.2 External coagulant effect

For safety consideration, water quench bath is commonly used in the dry/wet spinning technique to remove all remaining solvent(s) in the formed fiber and to complete the coagulation step. However, it is not advisable if porous outer layer is required as it yields skinned membranes [62]. A coagulation bath composed by a mixture of solvent and nonsolvent would be a solution to obtain skinless outer surfaces [62, 63]. This decreased both the polymer concentration at the outer layer and the phase inversion rate. However, the large amount of solvent(s) discharged would make this alternative not viable for environmental and economic reasons [64]. In order to reduce the solvent waste, He et al. [64] and Bonyadi and Chung [8] proposed using a triple-orifice spinneret with a solvent in the outer channel to fabricate hollow fiber membranes with highly porous external surfaces.

In the present research study, the following step to remove the outer skin-layer was the preparation of hollow fiber membranes with a wet gap distance, applying as an external coagulant different DMAC/water mixtures along this gap (see Table 3.2.2). For this purpose, a doubled spinneret (i.e. triple-orifice spinneret) was designed and fabricated (see dimensions in Table 3.2.1), maintaining the same outflow diameters for bore liquid and copolymeric solution (i.e. d_1 and d_2, respectively) as those of the single spinneret used to prepare the hollow fiber membrane IND0 (GAP 0) and the membranes reported in previous study [59]. First, the hollow fiber membrane 2IND0 was prepared in order to check that the resultant hollow fiber

was similar to the membrane 1IND0 prepared in our previous study [59], under the same conditions but with the single spinneret. It is important to do this verification for further comparisons or improvements between both groups of hollow fiber membranes (i.e. inner coagulation power effect [59] and outer coagulation power effect). It was confirmed the similarity of the membrane 2IND0 to the fiber 1IND0 in terms of morphology (see 2IND0 cross-section in Fig. 3.2.1) and characteristics such as inner and outer diameters, thickness, *LEP*, and inner and outer surface roughness. Consequently, very close DCMD permeate fluxes were obtained for both hollow fibers (i.e. (10.2 ± 0.5) and (7.3 ± 0.4) kg/m^{2}h for the membrane 2IND0; and (8.4 ± 1.3) and (6.8 ± 1.0) kg/m^{2}h for the membrane 1IND0 [59], when distilled water and salt aqueous solution were used as feed, respectively).

Type of the gap between spinneret and coagulation bath: dry versus wet

Figure 3.2.1 shows similar fiber cross-sections when the gap type was modified from dry to wet. However the outer surfaces of the fibers changed significantly, from dense to porous (i.e. compare the morphology of the membrane 2IND0 with that of the fibers 2OUTD in Fig. 3.2.1). Bonyadi and Chung [8] observed a similar behavior at the external surface of the PVDF hollow fiber membranes, when comparing the fibers prepared under an air gap distance with those fabricated with NMP solvent circulated through the outside orifice of the spinneret.

The use of the external coagulant along the gap distance (i.e wet gap) during membrane fabrication induced the following main changes on the fibers (compare the characteristics of the fibers 2OUTD with those of the membrane 2IND0 in Tables 3.2.3-3.2.5): greater diameters and lower thicknesses, larger mean pore sizes and slightly worse mechanical properties.

The surface tension of the nascent fiber at the exit of the spinneret was higher when a wet gap was used instead of a dry gap to prepare the hollow fiber membranes. All the considered nonsolvent liquids as external coagulants, with different amounts of DMAC in DMAC/water mixtures, have higher surface tension values (between 72 and 75.4 mN/m) [66] than that of the spinning solution (30.45 ± 0.20) mN/m [59]. It is well known that higher surface tension at the exit of the spinneret intensifies the die-swell effect. This justifies the observed larger diameters of the hollow fibers [17, 67].

The larger mean pore size and the slightly weaker mechanical properties could be the consequence of removing the dense skin-layer from the outer surface. Specially, the decrease of the thickness and the increase of the mean pore size resulted in greater hollow fiber DCMD permeate fluxes. Bonyadi and Chung [8] also determined larger average pore size and higher DCMD flux, induced mainly by the high surface porosity.

Morphology of the hollow fiber membranes prepared with different external coagulant mixtures

First, it is necessary to identify and calculate the different interactions between solvent, nonsolvent mixtures and water that take place at the outer layer of the nascent fiber during the spinning process (see Fig. 3.2.2). The affinity between components can be calculated via Hansen solubility parameter (*HSP*) distance (R_{HSP}), as described in previous studies [17, 59]. The effects of DMAC concentration in DMAC/water nonsolvent mixtures on the R_{HSP} are shown in Fig. 3.2.2(b). Three types of interactions occur during the formation of the outer structure of the fibers (see Fig. 3.2.2(a)): (i) along the gap distance different nonsolvent (NS) mixtures interact with the mixed solvent (S_m) of the spinning solution at the outer surface of the nascent fiber (see R_{HSP} (NS-S_m) in Fig. 3.2.2(b)); (ii) when the fiber reaches the coagulation bath, the water (W) interacts with the nonsolvent mixture accumulated on the outermost layer of the membrane (see R_{HSP} (NS-W) in Fig. 3.2.2(b)) but the NS-S_m affinity may be also taken into account in this step; and (iii) instantaneously after NS-W interaction took place, the mixed solvent of the spinning solution is exchanged with the water of the coagulation bath (see R_{HSP} (W-S_m) in Fig. 3.2.2(b)). As it can be observed in Fig. 3.2.2(b), the nonsolvent mixtures with larger quantities of DMAC have more affinity to the mixed solvent of the dope solution (i.e. lower R_{HSP} (NS-S_m)) and less affinity to the water of the coagulation bath (i.e. higher R_{HSP} (NS-W)). It shows the opposite behavior of these interactions, which coexist when the fiber is just immersed into the water coagulation bath. The intersection of both lines was found to be around 48 wt% of DMAC in water of the nonsolvent mixture. Therefore, this is the amount of DMAC for which the interactions between nonsolvent and mixed solvent and between nonsolvent and water are compensated. For concentrations of DMAC lower than 48 wt%, it can be seen that R_{HSP} (NS-S_m) is greater than R_{HSP} (NS-W), which means that the affinity of the nonsolvent mixtures with the water is better than that with the mixed solvent. In this DMAC concentration range, the water of the coagulation bath would facilitate the NS extraction. However, for DMAC rates higher than 48 wt%, the affinity preference of the nonsolvent mixture is inverted (i.e R_{HSP} (NS-S_m) < R_{HSP} (NS-W)), being better the affinity of the nonsolvent with the mixed solvent. In this concentration range, the water of the coagulation bath would make difficult the nonsolvent outflow from the dope solution. Furthermore, it is worth noting that the highest R_{HSP} of this study corresponds to the pair W-S_m. It means that the strongest interaction occurs when water comes in contact with the solvents mixture.

Figure 3.2.1 shows the SEM cross-section images of the hollow fibers prepared with different external coagulant mixtures. These membranes have a common asymmetric structure, longer finger-like structure in the internal layer, shorter finger-like structure in the external layer and sponge-like structure in the middle of the cross-section. The large finger-like

structure observed at the inner layer was formed due to the quick phase inversion caused by distilled water, the strong coagulant for PVDF-HFP used as a bore liquid. When water was used as external coagulant (2OUTD0 membrane), big fingers-like ellipses were formed in the outer layer of the fiber. Using DMAC/water mixture as the external coagulant, the fingers of the outer layer became thinner (see 2OUTD20 cross-section of Fig. 3.2.1) and by increasing the DMAC amount in the external coagulant the number of fingers at the external layer were reduced, leading to a slight spongier outer layer. A more sponge-like structure was observed at the external layer of the fiber when the nonsolvent mixture used as external coagulant had the maximum amount of DMAC (i.e. 60 wt%). Only some small fingers-like tears appeared in the outer layer of the membrane 2OUTD60.

Outer surfaces of the hollow fibers prepared with different external coagulant mixtures are also shown in Fig. 3.2.1. Porous external surfaces with bigger pores were observed when DMAC concentration in the external coagulant was increased, as it will be also confirmed by AFM analysis. Although the membrane 2OUTD60 shows the largest outer surface pores, its SEM external surface does not seem to be very porous. On the other hand, all the inner surfaces of the prepared hollow fiber membranes (see Fig. 3.2.1) presented the same porous structure to that of the hollow fiber 1IND0 [59], which was also fabricated using distilled water as internal coagulant.

The obtained evolution of the fiber outer layer during the wet gap spinning process (see Fig. 3.2.2), may be explained as follows. When the fiber is crossing the gap distance, the main interaction occurs between the nonsolvent external coagulant and the mixed solvent of the dope solution (see Fig. 3.2.2(a), i). As it can be seen in Fig. 3.2.2(b) (R_{HSP} (NS-S_m), the increase of DMAC content in the nonsolvent mixture could reduce the polymer concentration at the outer layer facilitating the phase separation [8, 64]. Lower polymer concentration could be obtained when higher quantity of DMAC was added in the nonsolvent mixture used as external coagulant. When the fiber reaches the water coagulation bath another interaction appears between the strong coagulant, water, and the nonsolvent mixture (see Fig. 3.2.2(a), ii). By increasing the quantity of DMAC in the external coagulant mixture, the affinity of water with the nonsolvent was reduced (i.e higher R_{HSP} (NS-W)), compensating ever more the coexistent opposite interaction between the nonsolvent and the mixed solvent (see Fig. 3.2.2(b)) and leading to smoother outer surface as consequence. However, the effect of the external coagulant on the outer surface of the fiber was different when 60 wt% of DMAC in water was used as nonsolvent mixture. For this concentration, the nonsolvent affinity preference was inverted, being the NS-W exchange more difficult than that of NS-S_m. It means that the water inflow from the coagulation bath could be hindered, giving a rougher and a little bit denser outer surface (see 2OUTD60 in Fig. 3.2.1). Finally the water of the coagulation bath was exchanged by the mixed solvent (see Fig. 3.2.2(a), iii), constituting the

final structure of the hollow fiber membrane. The residual solvent was finally removed from the fiber by the strongest coagulation power of water (i.e. the highest R_{HSP} (W-S_m) value). This could explain the small finger-like tears that appeared at the outer layer of the membrane 2OUTD60.

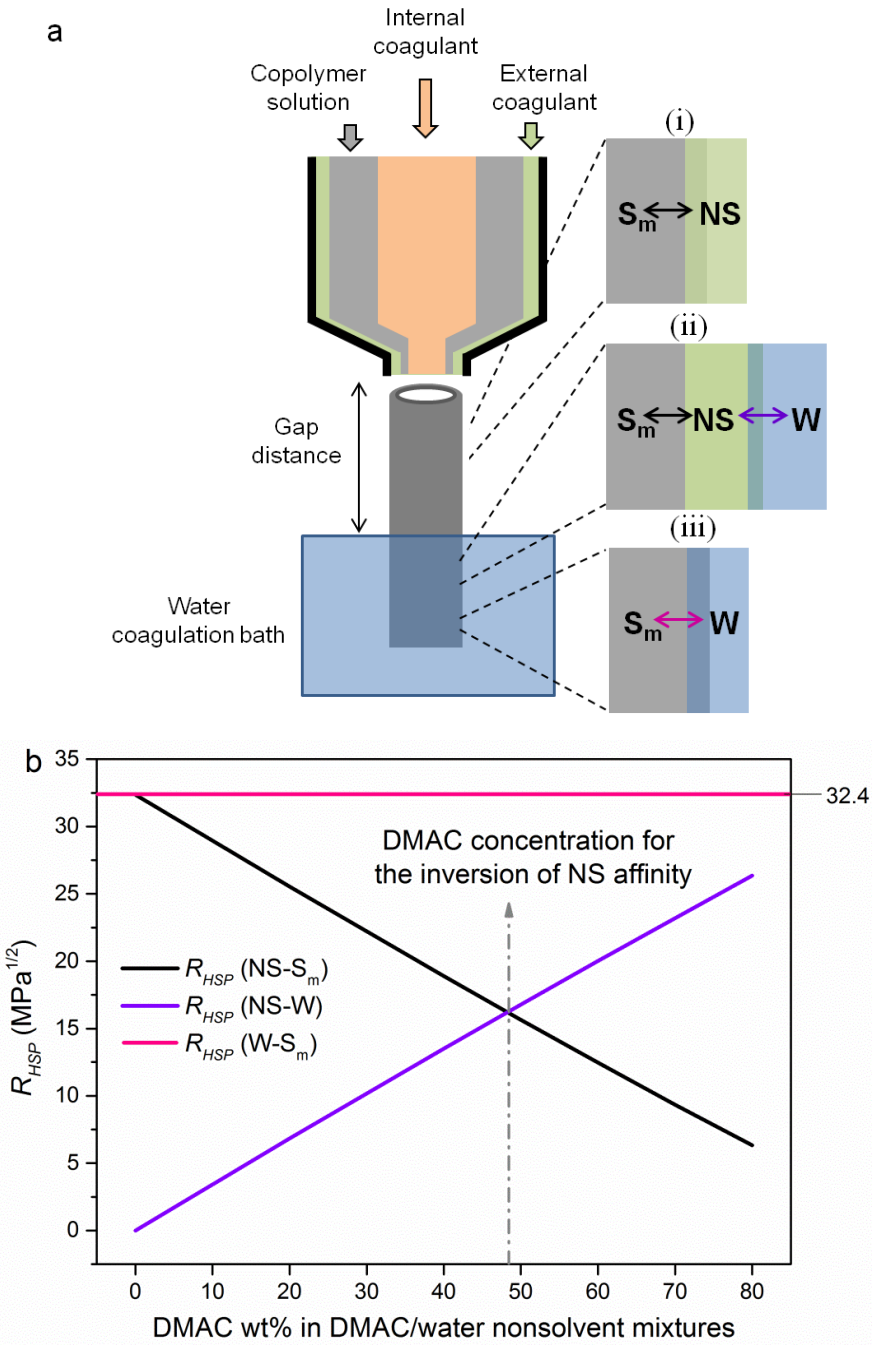

Fig. 3.2.2. Interactions on the outer layer of the nascent hollow fiber membrane (a) identification and (b) R_{HSP} calculation versus DMAC concentration in DMAC/water nonsolvent mixtures.

Structural properties and DCMD experiments of the hollow fiber membranes prepared with different external coagulant mixtures

Both the inner and outer diameters as well as the thickness of all the hollow fibers prepared with wet gap composed by different DMAC/water mixtures as external coagulants were the same taking into account the standard deviations (see Table 3.2.3). However, a clear decreasing trend was detected in the void volume fraction when DMAC concentration was increased in the external coagulant. This may be attributed to the reduction of the number of fingers at the outer layer of the fiber cross-section (Fig. 3.2.1). However, all the porosity values were similar or higher than those reported for other PVDF-HFP hollow fiber membranes by Shi et al. [68] and Khayet et al. [21], respectively. No clear trends were determined for either the inner or outer water contact angles (see Table 3.2.3). All of them were higher than 90°, showing the hydrophobic character of these membranes, and were similar to those obtained for the hollow fibers prepared in our previous study [59].

Figure 3.2.3 shows the tensile stress–strain experiments of the hollow fibers prepared in this study. The mechanical properties of these membranes were determined and the corresponding parameters are summarized in Table 3.2.4. The stiffness and the tensile stress and strain at break of these fibers were lower than those of the majority of the membranes prepared in our previous study [59]. However, the tensile stress at break values of the hollow fibers prepared in this study were similar to those obtained by Shi et al. [15] for PVDF-HFP hollow fiber membranes. The large finger-like structure observed at the inner layer of all the

Table 3.2.3. Diameters, thickness, void volume fraction and inner and outer water contact angles of the prepared hollow fiber membranes.

Membrane	Inner diameter (μm)	Outer diameter (μm)	Thickness (μm)	Void volume fraction (ε %)	Inner contact angle (°)	Outer contact angle (°)
IND0 (GAP 0)	1680 ± 110	2200 ± 140	260 ± 30	77.4 ± 0.3	143.5 ± 0.4	91.3 ± 1.8
2IND0	1025 ± 50	1420 ± 80	195 ± 21	73.0 ± 1.4	143.3 ± 0.2	91.5 ± 1.4
2OUTD0	1240 ± 120	1566 ± 110	160 ± 30	75.7 ± 0.9	139.0 ± 0.8	96.0 ± 0.4
2OUTD20	1290 ± 70	1610 ± 70	157 ± 16	78.6 ± 1.7	147.1 ± 1.3	93.8 ± 0.5
2OUTD40	1270 ± 90	1589 ± 80	158 ± 19	73.5 ± 1.2	142.3 ± 1.8	92.1 ± 1.5
2OUTD60	1280 ± 90	1590 ± 90	156 ± 19	67.8 ± 1.2	144.5 ± 1.6	94.8 ± 2.2
2IND50OUTD50	1640 ± 220	1770 ± 220	67 ± 17	83.3 ± 4.7	153.8 ± 1.3	97.9 ± 2.7
2IND60OUTD60	1010 ± 250	1050 ± 190	17 ± 7	-	-	-

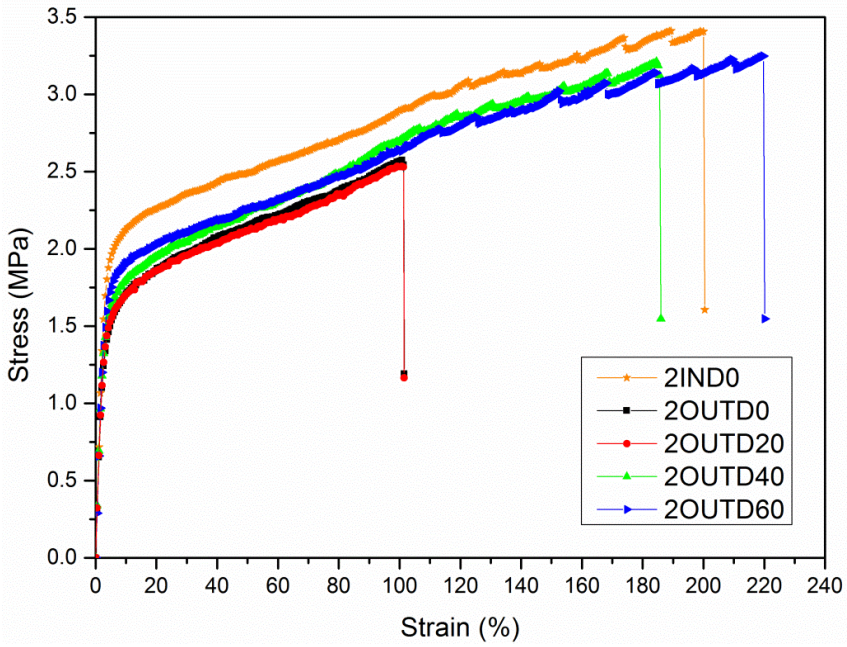

Fig. 3.2.3. Stress-strain curves of the hollow fiber membranes prepared under different external conditions.

Table 3.2.4. Mechanical properties (Young´s modulus, E; yield stress, σ_y; tensile stress at break, σ_b and strain at break, ε_b) of the prepared hollow fiber membranes.

Membrane	E (MPa)	σ_y (MPa)	σ_b (MPa)	ε_b (%)
IND0 (GAP 0)	71.7 ± 0.9	1.17 ± 0.03	2.47 ± 0.13	72 ± 7
2IND0	70 ± 3	1.29 ± 0.14	3.22 ± 0.17	214 ± 18
2OUTD0	63.2 ± 1.8	1.05 ± 0.04	2.71 ± 0.20	106 ± 6
2OUTD20	65 ± 3	1.05 ± 0.09	2.65 ± 0.20	103 ± 12
2OUTD40	62 ± 8	1.17 ± 0.23	3.09 ± 0.17	184 ± 11
2OUTD60	63 ± 8	1.23 ± 0.26	3.28 ± 0.05	228 ± 12
2IND50OUTD50	71 ± 13	2.35 ± 0.27	4.98 ± 0.14	253 ± 73
2IND60OUTD60	89 ± 14	2.75 ± 0.02	13.3 ± 1.4	434 ± 25

PVDF-HFP hollow fibers in this study (see cross-section morphologies in Fig. 3.2.1) may be the cause of the lower E values [11]. Moreover, the skinless outer surface could justify the low results of both the tensile stress and strain at break. No meaningful change was detected in Young´s modulus (E) of the hollow fiber membranes prepared with different nonsolvent mixtures along the wet gap. Nevertheless, the membranes prepared with more DMAC amounts in the external coagulant mixture, showed greater yield and tensile stress at break as

well as larger strain at break. It can be seen that the membranes prepared with water and 20 wt% of DMAC in water as external coagulants (i.e. 2OUTD0 and 2OUTD20, respectively) exhibited the same results if the standard deviations were taken into consideration. However, by increasing the DMAC content in the nonsolvent mixture from 20 to 60 wt%, the yield stress, tensile stress and strain at break of the fibers were enhanced. These could be due to the outer surface aspect of the fibers, which became more compact (see outer surfaces in Fig. 3.2.1) with the increase of DMAC in the external coagulant mixture. Yu et al. [63] detected that the fabricated PAN hollow fiber membranes enhanced their tensile strength with the DMF content in the coagulation bath. It is worth noting that all mechanical properties of the membrane 2OUTD60, except its Young´s modulus, tended to be close to the values obtained for the hollow fiber 2IND0, which was prepared under a dry gap. As it can be seen in Fig. 3.2.1, despite the large pores of the external surface of the hollow fiber 2OUTD60, this surface is slightly compact and dense, and it tends to resemble the outer surface of the membrane 2IND0.

The high elasticity and the low strain at break of the membranes prepared under the wet gap justify the impossibility of an accurate characterization of these membranes by various techniques such as the *LEP* and the wet/dry porometry test. In both experiments, the hollow fiber membranes work under hydrostatic pressures and suffer an irreversible deformation ended by its fracture. For the *LEP* measurements, it was determined that all the values were between 0.5 and 1 bar.

The pore sizes of the hollow fibers prepared with different external coagulants could not be measured via the wet/dry porometry test. Gas permeation method was used in this case. It is worth quoting that the maximum applied pressure for this experiment was 0.8 bar, because it was observed that for pressures greater than 1 bar the relationship between the gas flow and the applied pressure was no longer linear. The mean pore sizes obtained by the gas permeation test are shown in Table 3.2.5. Similar values for the membranes prepared with different amounts of DMAC in the external coagulant mixture were obtained if standard deviations had taken into account. These mean pore sizes were all larger than those determined by Wongchitphimon et al. [10] for other PVDF-HFP hollow fiber membranes.

The outer surfaces of the hollow fiber membranes prepared with different DMAC/water mixtures as external coagulant were analyzed by AFM. The 3D images of the outer surfaces are shown in Fig. 3.2.4, and the corresponding roughness and pore sizes are summarized in Tables 3.2.6 and 3.2.7, respectively. Similar roughness values were observed for both the inner and outer surfaces when the concentration of DMAC in water was increased from 20 to 40 wt% in the external coagulant. However, higher inner and outer surface roughness was detected for the membrane prepared with 60 wt% of DMAC in water as nonsolvent (D60).

Table 3.2.5. Mean pore size of the prepared hollow fiber membranes determined by the gas permeation test.

Membrane	Mean pore size (nm)
IND0 (GAP 0)	269 ± 18
2IND0	294 ± 19
2OUTD0	570 ± 60
2OUTD20	480 ± 80
2OUTD40	450 ± 50
2OUTD60	390 ± 50
2IND50OUTD50	770 ± 130

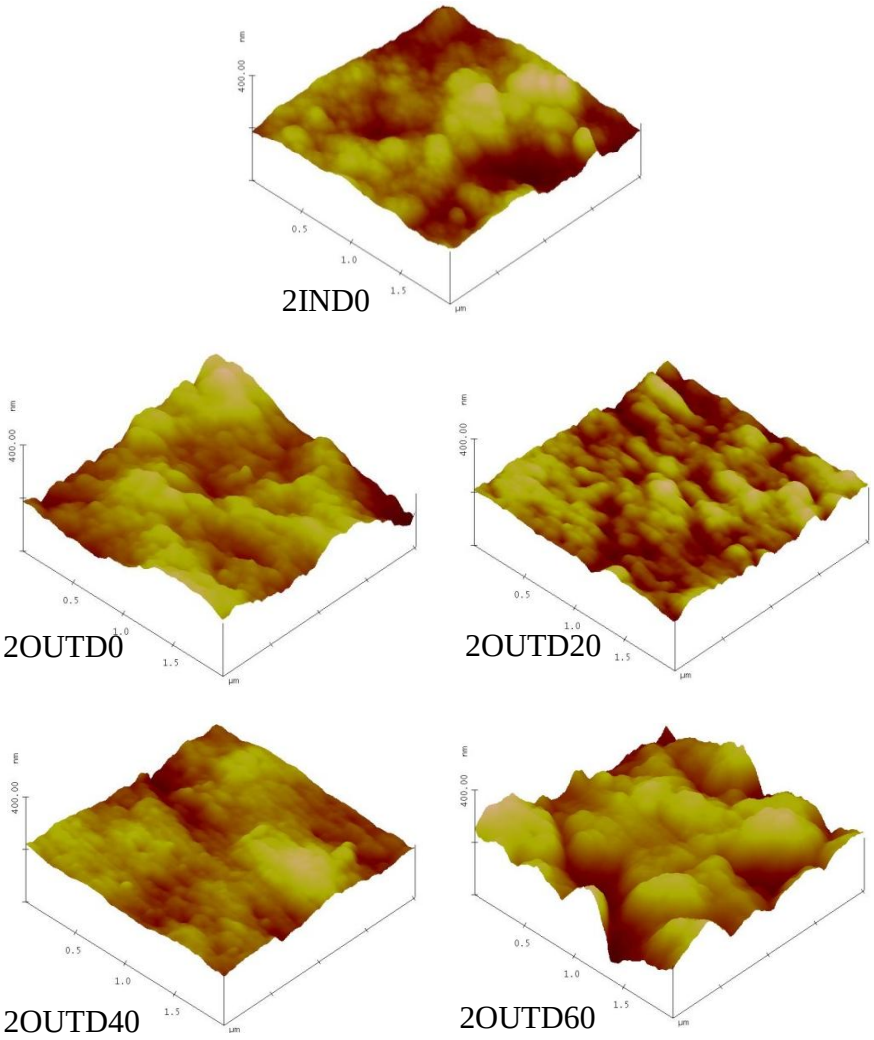

Fig. 3.2.4. 3D AFM images of the outer surfaces of the hollow fiber membranes prepared under different external conditions.

Table 3.2.6. Minimum, maximum and average mean roughness parameter, R_a, together with the corresponding standard deviation of the internal and external surfaces of the prepared hollow fiber membranes (scan range considered 2 μm × 2 μm).

Membrane	R_a (nm) Inner surface			R_a (nm) Outer surface		
	Minimum	Maximum	Average	Minimum	Maximum	Average
IND0 (GAP 0)	16.1	20.5	18.0 ± 1.6	15.8	28.5	22.0 ± 5.0
2IND0	14.4	20.3	16.8 ± 2.0	14.3	24.2	17.9 ± 3.0
2OUTD0	20.2	25.4	22.9 ± 2.0	16.5	22.8	19.9 ± 2.3
2OUTD20	17.1	24.5	20.7 ± 2.8	8.1	15.9	10.7 ± 2.2
2OUTD40	16.8	27.2	20.3 ± 5.0	7.9	12.5	10.2 ± 1.7
2OUTD60	24.3	32.7	28.5 ± 2.5	25.3	37.7	32.4 ± 5.0
2IND50OUTD50	8.5	11.6	9.8 ± 1.0	7.5	11.7	9.3 ± 1.5
2IND60OUTD60	10.7	15.9	13.3 ± 2.0	6.3	11.7	8.9 ± 1.6

Table 3.2.7. Mean pore size, μ_p, and geometric standard deviation, σ_p, of the internal and external surfaces of the prepared hollow fiber membranes determined by AFM images analysis.

Membrane	Inner surface		Outer surface	
	μ_p (nm)	σ_p (nm)	μ_p (nm)	σ_p (nm)
IND0 (GAP 0)	99.21	1.08	108.74	1.07
2IND0	84.89	1.06	96.76	1.07
2OUTD0	-	-	97.95	1.06
2OUTD20	-	-	86.22	1.06
2OUTD40	-	-	94.17	1.06
2OUTD60	-	-	125.02	1.09
2IND50OUTD50	207.29	1.10	146.09	1.10
2IND60OUTD60	268.53	1.19	218.09	1.11

The great affinity between the mixed solvent and D60 nonsolvent type (used as external coagulant) made the finger-like structure grew from the inner towards the outer layer (see 2OUTD60 cross-section of Fig. 3.2.1), leading to a slightly rougher inner surface. The lower affinity of D60 nonsolvent with water of the coagulation bath made it difficult for the NS-W to exchange at the outer interface of the fiber, forming a more compact and denser outer surface. This effect could explain the significant increase of the outer surface roughness of the membrane 2OUTD60. The pore size of the outer surface of the fiber increased when higher DMAC amount was used in the external coagulant mixture (see Table 3.2.7). Larger pores could be obtained as a consequence of using a weaker nonsolvent as external coagulant along the gap distance. Furthermore, by using the highest concentration of DMAC in the external coagulant mixture the outer surface pore size distribution became wider, as shown by the membrane 2OUTD60 in Fig. 3.2.5. Yu et al. [63] also observed slower hollow fiber coagulation with the increase of DMF amount in the coagulation bath, while the pores were detected at the surface for the highest DMF percentage.

The thermal properties of the prepared hollow fibers were almost the same, as it can be seen in Table 3.2.8 and Fig. 3.2.6. The external coagulant type did not affect the thermal characteristics of the membranes, which were similar to those of the copolymer PVDF-HFP

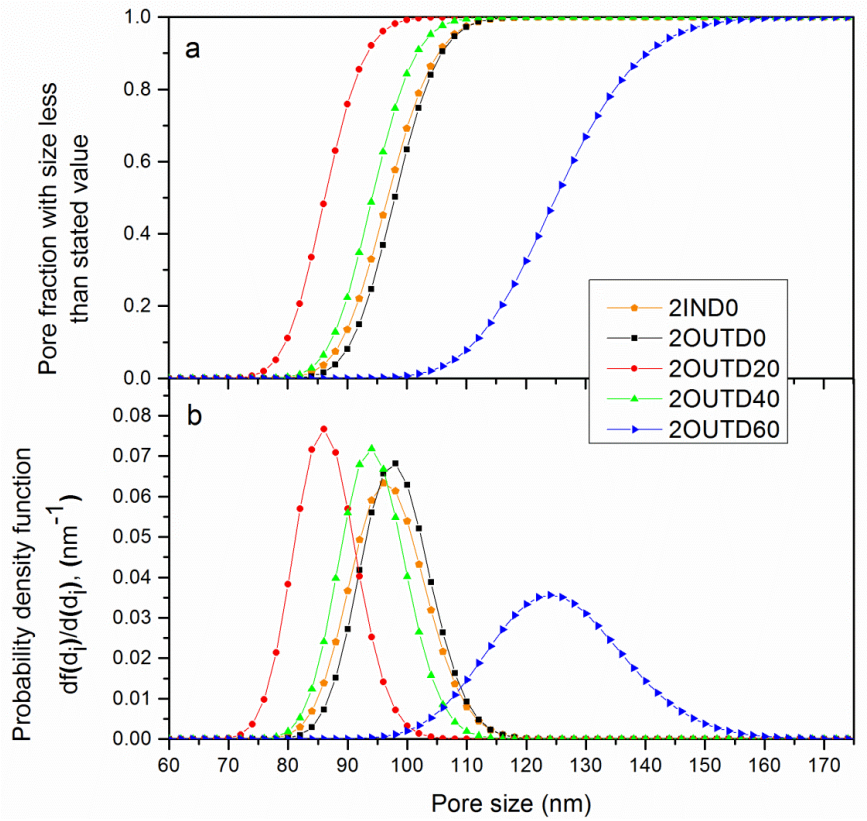

Fig. 3.2.5. Cumulative pore size (a) and probability density function (b) curves generated from the pore sizes obtained from the AFM images of the outer surfaces of the hollow fiber membranes prepared under different external conditions.

ones reported elsewhere [59]. The melting and crystallization temperatures were high enough to work with these membranes under the operational temperatures applied for DCMD experiments.

The DCMD permeate fluxes (J) and the salt rejection factors (α) of the hollow fiber membranes prepared with different external coagulants are shown in Fig. 3.2.7. When using distilled water as feed solution the obtained permeate fluxes were higher than those corresponding to salt aqueous feed solution (NaCl, 3 wt%). These DCMD permeate fluxes were all greater than the highest values reported for other PVDF-HFP hollow fiber membranes (i.e. 1.3 kg/m^{2}h for distilled water used as feed at 45 ^{o}C and a permeate temperature of 20 ^{o}C; 6.5 kg/m^{2}h for distilled water used as feed at 80 ^{o}C and a permeate temperature of 25 ^{o}C; and 5.4 kg/m^{2}h for 3 wt% NaCl feed solution at 80 ^{o}C and a permeate temperature of 25 ^{o}C) [13, 55]. No significant change was detected for the permeate fluxes obtained by the membranes 2OUTD20 and 2OUTD40. The greatest DCMD permeate fluxes were obtained for the hollow fiber membranes prepared with water (D0) and D60 mixture as external coagulants (see Fig. 3.2.7). These results were in accordance with the properties of the 2OUTD0 and 2OUTD60 membranes: high roughness, high porosity of the membrane 2OUTD0 and large outer surface pore size of the membrane 2OUTD60. The maximum salt rejection factor was obtained for the membrane prepared with 60 wt% of DMAC in the external coagulant mixture, 99.91%. It can be concluded that the hollow fiber membrane 2OUTD60 exhibited the best DCMD performance of all the membranes prepared with different external coagulants.

Table 3.2.8. Melting temperature (T_m), crystallization temperature (T_c), enthalpy of melting (ΔH_m), enthalpy of crystallization (ΔH_c) and crystallinity (X_c) of the prepared hollow fiber membranes.

Membrane	Heating process		Cooling process		Crystallinity X_c (%)
	$\Delta H_m \pm 0.5$ (J/g)	$T_m \pm 0.15$ (^{o}C)	$\Delta H_c \pm 0.5$ (J/g)	$T_c \pm 0.15$ (^{o}C)	
IND0 (GAP 0)	45.5	161.94	45.6	123.53	43.4
2IND0	45.7	158.86	45.5	124.47	43.6
2OUTD0	45.3	158.92	45.4	124.01	43.3
2OUTD20	45.4	158.24	45.4	124.35	43.4
2OUTD40	45.2	157.91	45.2	124.64	43.2
2OUTD60	45.2	158.01	45.3	124.58	43.2
2IND50OUTD50	43.1	157.91	42.9	124.62	41.2
2IND60OUTD60	38.5	158.46	38.6	124.56	36.7

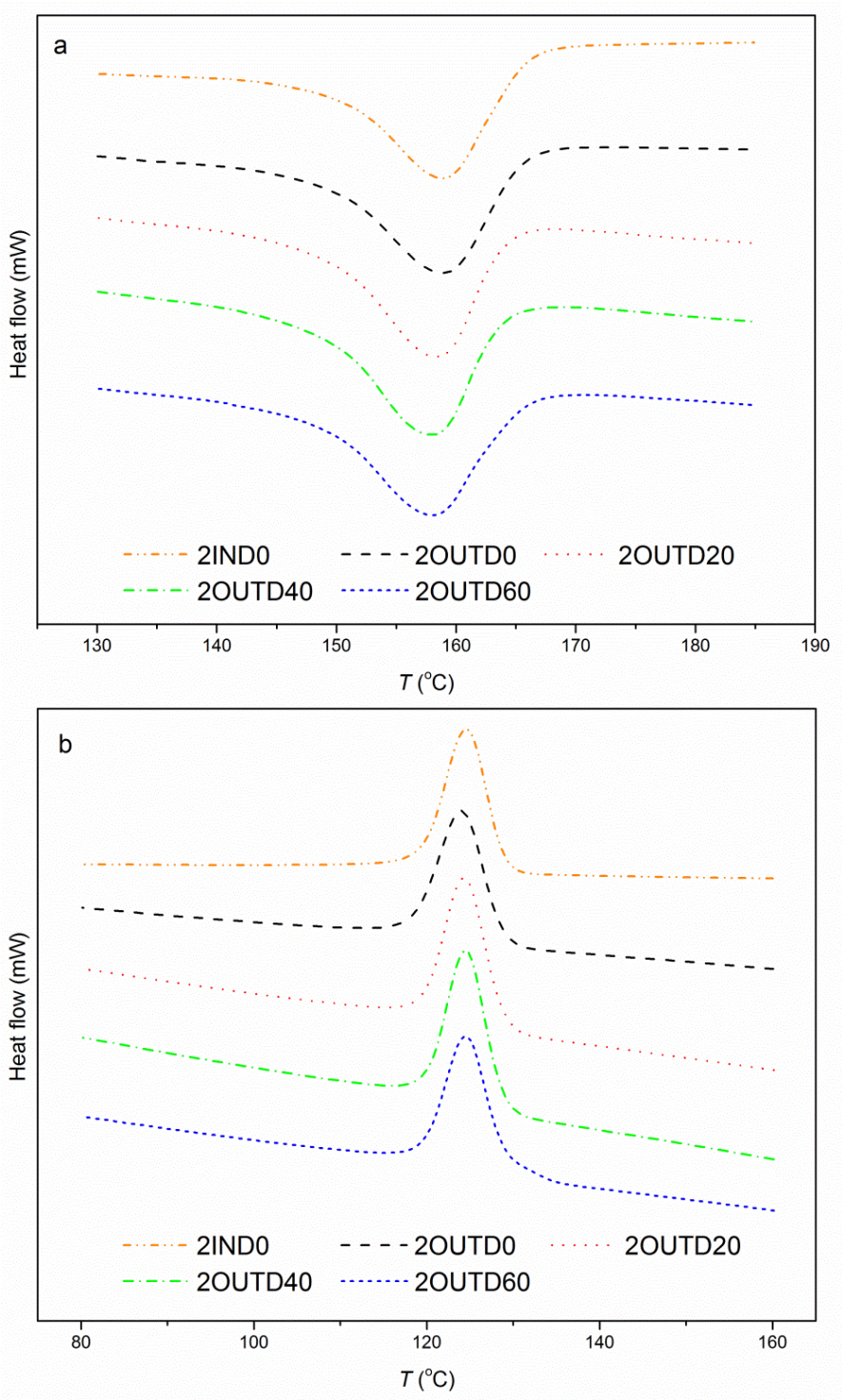

Fig. 3.2.6. DSC thermograms, (a) heating and (b) cooling of the hollow fiber membranes prepared under different external conditions.

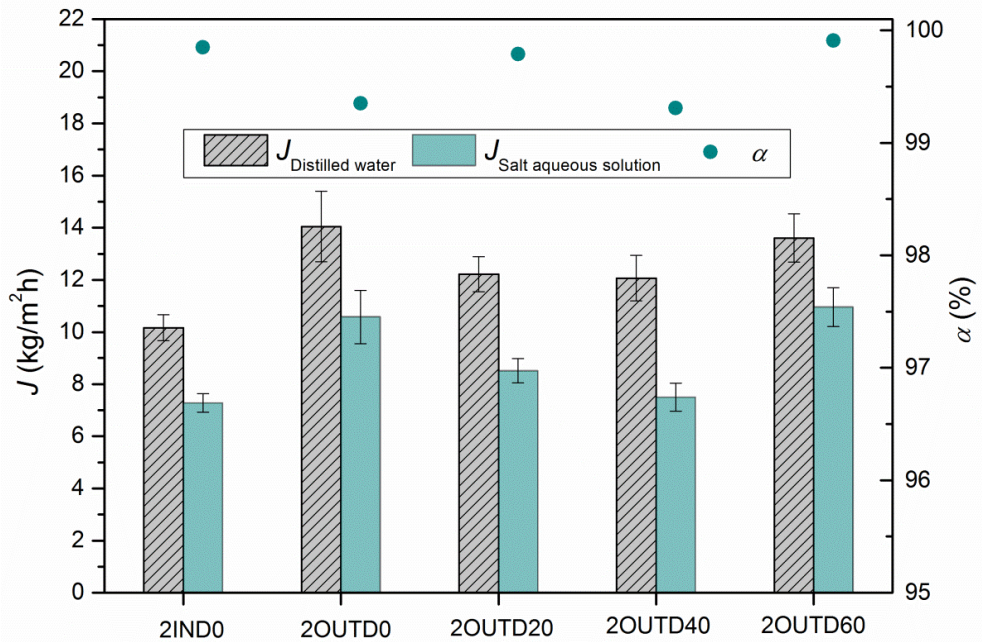

Fig. 3.2.7. DMCD permeate flux and salt rejection factor of the hollow fiber membranes prepared under different external conditions. (Feed temperature = 80 °C; Permeate temperature = 25 °C).

3.2.3.3 Simultaneous internal and external coagulant mixtures

After analyzing separately the effects of DMAC addition in the internal and external coagulants, it can be concluded that the DCMD performance of the hollow fiber membranes was improved. It is worth noting that the most noticeable enhancement was obtained when these nonsolvents mixtures were employed as internal coagulant. Increasing the DMAC concentration in the internal coagulant improved the hollow fiber membranes morphologies, the structural characteristics and the DCMD performances, doubling the permeate flux when 50 and 60 wt% of DMAC were used in the internal coagulation mixture [59]. In addition, using a wet gap composed by different mixed external coagulants instead of a dry gap also enhanced the DCMD permeate flux. However, it was the hollow fiber membrane prepared with 60 wt% of DMAC in water as external coagulant, which exhibited the best performance among all the membranes prepared under a wet gap. Therefore, in order to consider the benefits of both effects, DMAC/water mixtures with the highest available amounts of DMAC (50 and 60 wt%) were used simultaneously as inner and outer coagulants to prepare hollow fiber membranes.

Morphology of the hollow fiber membranes prepared with simultaneous internal and external coagulant mixtures

Figure 3.2.8 shows the cross section, inner and outer surfaces of the hollow fibers prepared with the same mixture 50 wt% DMAC/50 wt% water (D50) and 60 wt% DMAC/40 wt%

water (D60) as internal and external coagulants (i.e. membranes 2IND50OUTD50 and 2IND60OUTD60, respectively). Both coagulants were simultaneously extruded through the spinneret, so they can act on the nascent fiber at the same time, providing similar effect on the inner and outer layer, and probably leading to symmetric cross-sections, as consequence. When the nonsolvent D50 was used only as a bore liquid, short fingers were detected at the inner layer of the fiber 1IND50 [59]. Hence, when the same mixture was used as internal and external coagulants, few and short finger-like structure was observed at both layers (see the symmetric cross-section morphology of the membrane 2IND50OUTD50 in Fig. 3.2.8). In the same way, when the maximum amount of DMAC in water (D60) was used only as an internal or external coagulant, sponge-like structure was observed at the inner or outer layer of the membrane (see the cross-sections of 1IND60 in [59] and 2OUTD60 in Fig. 3.2.1, respectively). Therefore, the hollow fiber membrane prepared with the mixture D60, as both inner and outer coagulants, exhibited a fully sponge-like structure, as a result of the combination of both effects (see 2IND60OUTD60 cross-section in Fig. 3.2.8). The resultant morphologies were the consequence of using weak nonsolvents (D50 or D60) as coagulants reducing the phase inversion rate. Therefore, each coagulant may act individually in its respective layer along the gap distance, being the outer layer structure independent to the inner behavior and vice versa. The hollow fiber membranes prepared by He et al. [64] and Bonyadi and Chung [8] with a mixture of NMP and water as the bore liquid and pure NMP as external coagulant were also symmetric and totally spongy.

Moreover, the inner surfaces of the membranes 2IND50OUTD50 and 2IND60OUTD60 had similar structure to that corresponding to the inner surfaces of the fibers 1IND50 and 1IND60 [59]. The outer surface of the fiber prepared with the mixture D60 as both internal and external coagulant (2IND60OUTD60) has more porous structure than the external surface of the fiber 2OUTD60 (see Figs. 3.2.1 and 3.2.8). It can be also observed that both the inner and outer surface pores of the membrane 2IND60OUTD60 were larger than those of the fiber 2IND50OUTD50, as it will be confirmed by AFM analysis. Finally, it is worth noting that the inner surfaces of the hollow fibers 2IND50OUTD50 and 2IND60OUTD60 were different to their outer surfaces, although the same coagulant mixture was used for membrane preparation. Figure 3.2.8 shows less porous outer surfaces than the inner surfaces. It might be the consequence of the shorter period of time during which these external coagulants were in contact with the nascent hollow fibers; and to the low affinity of water of the quench bath with these nonsolvent mixtures, which favored the aforementioned appearance of the external surface.

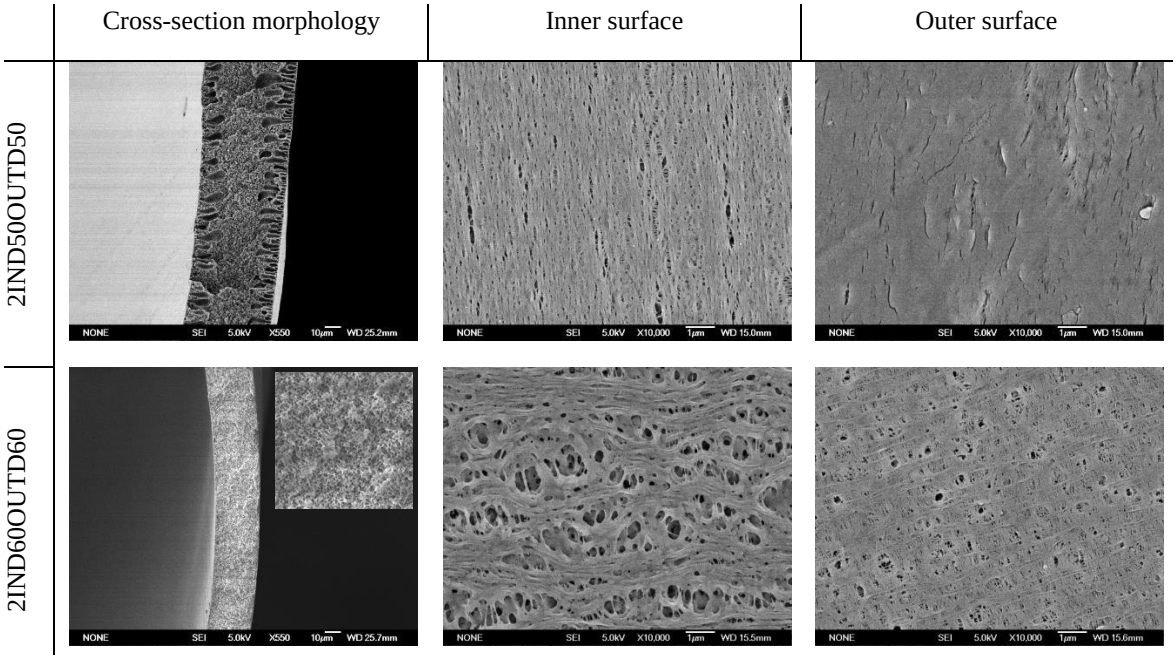

Fig. 3.2.8. SEM images of the cross-section morphology and inner and outer surfaces of the hollow fiber membranes prepared with simultaneous internal and external coagulant mixtures.

Structural properties and DCMD experiments of the hollow fiber membranes prepared with simultaneous internal and external coagulant mixtures

The thickness, inner and outer diameters of the membranes 2IND50OUTD50 and 2IND60OUTD60 were measured. From Table 3.2.3 it can be clearly seen that the thicknesses of these hollow fibers were much lower than those obtained for the other membranes prepared in this study. The membrane prepared with the mixture D60 as internal and external coagulant was the thinnest one. The weak nonsolvent mixtures (D50 and D60) employed as internal and external coagulants reduced the phase inversion rate at both sides of the fibers. Therefore, the nascent hollow fiber membranes were partially coagulated and the effect of the stretching force along the gap distance was more pronounced reducing their thicknesses, as observed in [59]. It is important to mention that the small thickness of the membranes made difficult the accurate measurement of their diameters, obtaining high experimental uncertainties. Furthermore, the complexity of preparing any sample module with 2IND60OUTD60 hollow fiber membrane due to its lowest thickness, did not allow its characterization by some techniques such as porosity, contact angle, gas permeation test, etc. DCMD experiments could not be carried out for the same reason. However, the properties of the membrane 2IND50OUTD50 could be determined because this membrane was thicker than the membrane 2IND60OUTD60. Table 3.2.3 shows that the hollow fiber

2IND50OUTD50 had the highest void volume fraction and great inner and outer contact angles confirming the hydrophobic character of this membrane. Its largest porosity was totally consistent with its structural morphology, especially with its thick and open sponge-like structure in the middle of the fiber´s section (see Fig. 3.2.8); and with the largest mean pore size (see Table 3.2.5).

The mechanical properties of the 2IND50OUTD50 and 2IND60OUTD60 hollow fiber membranes were studied based on stress-strain curves shown in Fig. 3.2.9. The results are summarized in Table 3.2.4. No significant changes were detected on the Young´s modulus of the membranes prepared with different nonsolvent mixtures as external coagulants. However, greater elasticity parameter and higher yield stress were observed when the concentration of DMAC in the aqueous internal coagulant was increased from 50 to 60 wt% [59]. Similar tendencies were observed between 2IND50OUTD50 and 2IND60OUTD60 for both mechanical parameters. Therefore, the stiffness of the hollow fiber membranes could be determined mainly by the inner layer structure. The completely sponge-like structure of the 2IND60OUTD60 fiber cross-section, and the more interconnected inner surface morphology could justify the slightly increase of both Young´s modulus [15] and yield stress, respectively. The most significant mechanical changes were observed for the membrane 2IND60OUTD60, which exhibited the highest tensile stress and strain at break (see Table 3.2.4). The resultant parameters were extremely larger than those obtained for the membrane 2IND50OUTD50. The plastic deformation region of the membrane 2IND60OUTD60 was larger (i.e. higher strain at break, Fig. 3.2.9), showing the pronounced ductile behavior of this membrane, which could be associated to its lower crystallinity.

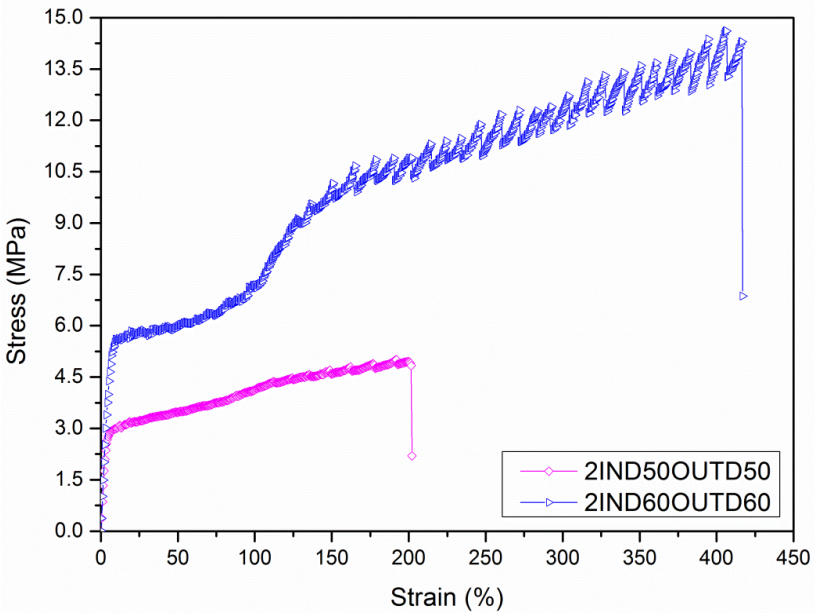

Fig. 3.2.9. Stress-strain curves of the hollow fiber membranes prepared with simultaneous internal and external coagulant mixtures.

Both the inner and outer surfaces of the hollow fibers 2IND50OUTD50 and 2IND60OUTD60 were analyzed by AFM. 3D images of their surfaces are shown in Fig. 3.2.10 and their roughness as well as their mean pore sizes are summarized in Tables 3.2.6 and 3.2.7, respectively. These membranes had low surface roughness and presented the largest surface pore sizes of both the inner and outer surfaces among all the prepared hollow fibers in this study and the previous one [59]. These effects on membranes surfaces can be the result of an extremely slow coagulation process at both sides of the nascent hollow fibers when very weak nonsolvents such as D50 and D60 were used simultaneously as both internal and external coagulants. Following the same tendency obtained separately by the internal and external coagulant effects, the surface pore sizes became larger with the increase of DMAC content in the nonsolvent mixture. The cumulative pore size distribution and the probability density functions of the surfaces of these hollow fibers are shown in Fig. 3.2.11. It can be seen that the membrane 2IND60OUTD60 had bigger mean pore sizes and wider pore size distributions than the fiber 2IND50OUTD50 for both the inner and outer surfaces. The widest pore size distribution corresponded to the internal surface of the membrane 2IND60OUTD60 (see Fig. 3.2.11(a2)). This result is in accordance with the SEM images (see Fig. 3.2.8).

The thermal parameters of the hollow fiber membranes 2IND50OUTD50 and 2IND60OUTD60 are shown in Table 3.2.8. No differences were detected in both melting and crystallization temperatures, but their corresponding enthalpies were lower than the values obtained for the membranes prepared only with DMAC/water mixture as internal [59] or external coagulant. The crystallinity of these membranes decreased, being smaller for the 2IND60OUTD60 membrane. Their lower crystallinity means fewer ordered polymer chains, which is totally in accordance with the ductile behavior observed by the mechanical test analysis.

Finally, DCMD experiments were carried out using the membrane 2IND50OUTD50. According to the resultant hollow fiber membrane characteristics: low thickness, spongy and porous morphology, skinless inner and outer surfaces with large pore size and narrow pore size distribution, greatest porosity, largest mean pore size and good hydrophobic character, compared to all the prepared hollow fiber membranes, the obtained permeate flux was the highest. The resultant fluxes were (23 ± 3) kg/m^{2}h and (19.5 ± 2.5) kg/m^{2}h, with distilled water and 3 wt% NaCl salt aqueous solution as feed, respectively; with a good salt rejection factor of 99.29%. Therefore, an incredibly improvement of the DCMD performance was obtained with this fiber, prepared with the nonsolvent mixture D50 as internal and external coagulants. The performance of this hollow fiber membrane was significantly better than that obtained for the optimal PVDF-HFP hollow fiber membrane (i.e. 13.5 kg/m^{2}h for 3 wt% NaCl feed solution at 75 °C and a permeate temperature of 20 °C) obtained by the statistical

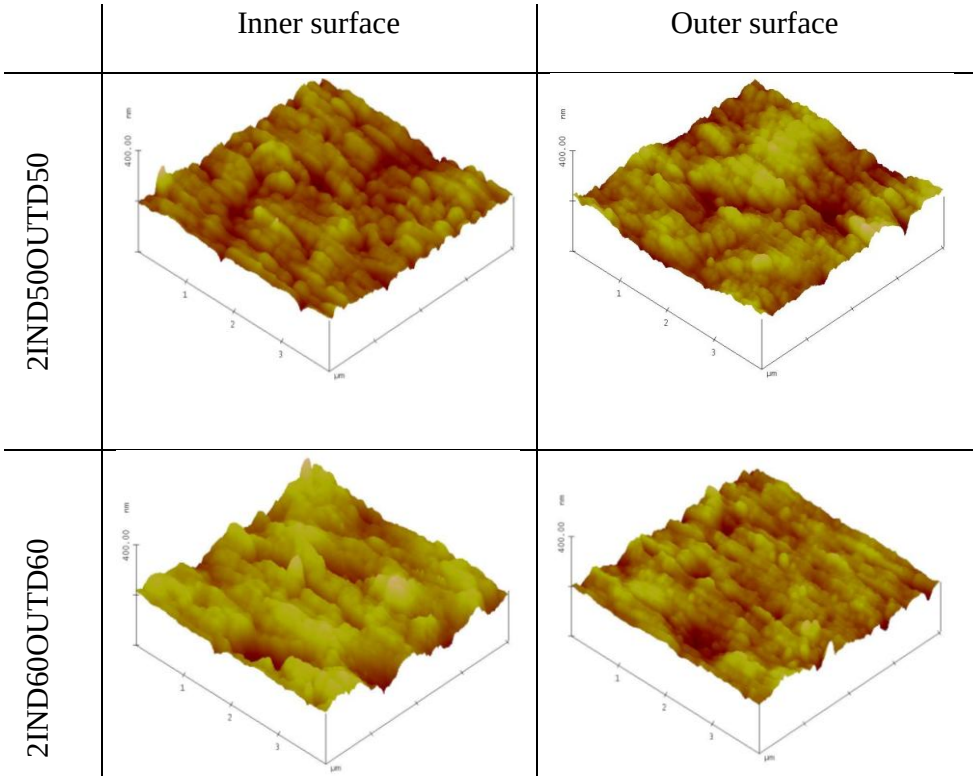

Fig. 3.2.10. 3D AFM images of the inner and outer surfaces of the hollow fiber membranes prepared with simultaneous internal and external coagulant mixtures.

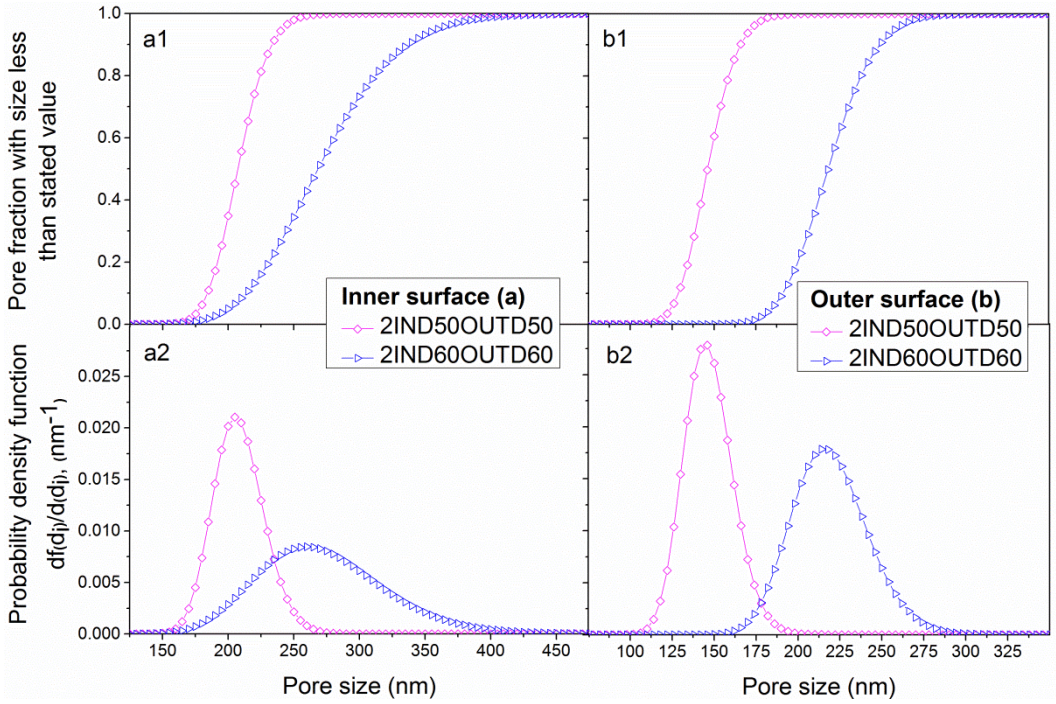

Fig. 3.2.11. Cumulative pore size (a1, b1) and probability density function (a2, b2) curves generated from the pore sizes obtained from AFM images of the inner (a) and outer (b) surfaces of the hollow fiber membranes prepared with simultaneous internal and external coagulant mixtures.

experimental design developed by Khayet et al. [21] tested at the same temperature gradient and with feed salt aqueous solution. DCMD water production of this fiber was compared to the highest permeate fluxes of the membranes prepared for the external and internal coagulant effect studies, when salt aqueous solution was used as feed. The permeate flux increased by 78% respect to the flux of the membrane 2OUTD60, prepared with 60 wt% DMAC/40 wt% water mixture only as external coagulant; and by 58% enhancement respect to the fiber prepared with 60 wt% DMAC/40 wt% water mixture used only as internal coagulant (i.e. membrane 1IND60 of [59]). It can be concluded that this hollow fiber resulted to be the best membrane among those prepared in the present study and in [59].

3.2.4 Conclusions

The skin-layer formation on the outer surface of the hollow fiber membranes was avoided when the gap distance of the spinning process was changed from dry to wet. The external structure evolution of the membranes was analyzed via Hansen solubility parameters in agreement with different interactions that took place at the outer layer of the nascent fiber during its fabrication process. Studying a priori these interactions is an easy way to find out the most advisable coagulant composition range to prepare the desired hollow fiber membrane structure (i.e. sponge morphologies and porous outer surfaces).

It can be confirmed that the gap distance suppression could not remove the dense skin on the outer surface of the membrane. However, by using a wet gap distance with DMAC/water nonsolvent mixtures as external coagulants not only were porous outer surfaces formed, but other membrane characteristics were improved such as smaller thickness, larger mean pore sizes and rougher inner surfaces. The highest DCMD performance was obtained for the membrane prepared with the nonsolvent mixture 60 wt% of DMAC/40 wt% of water as external coagulant. Its large pore size and slight compact outer surface could justify the obtained great permeate flux and the excellent salt rejection factor.

Despite the positive effects observed on the morphology and DCMD performance of the membranes prepared with mixed external coagulants, the effect of using 50 and 60 wt% DMAC/water mixtures as internal coagulants enhanced even more the fiber properties and permeability [59]. The same nonsolvent mixtures were used as internal and external coagulants, trying to benefit from the advantages of both effects simultaneously. The hollow fiber membrane prepared with 60 wt% of DMAC in water as the nonsolvent mixture was extremely thin and ductile, being impossible to pack it in a membrane module for testing by DCMD. Nevertheless, the membrane 2IND50OUTD50, prepared with 50 wt% of DMAC in water as both internal and external coagulants exhibited the best membrane characteristics for MD among all the fabricated membranes. Therefore, according to its excellent properties, the

hollow fiber membrane 2IND50OUTD50 had the highest DCMD performance, being the permeate flux more than two times greater than that of the membranes prepared with DMAC/water mixture as internal or external coagulant.

References

[1] M. Khayet, T. Matsuura, Membrane Distillation. Principles and Applications, Elsevier, The Netherlands (2011).

[2] M. Khayet, Membranes and theoretical modeling of membrane distillation: a review, Adv. Colloid Interface Sci. 164 (2011) 56-88.

[3] L. García-Fernández, M. Khayet, M.C. García-Payo, Membranes used in membrane distillation: preparation and characterization, Elsevier (Woodhead Publishing), Cambridge (2015) 317-359.

[4] M. Qtaishat, M. Khayet, T. Matsuura, Guidelines for preparation of higher flux hydrophobic/hydrophilic composite membranes for membrane distillation, J. Membr. Sci. 329 (2009) 193-200.

[5] M. Essalhi, M. Khayet, Self-sustained webs of polyvinylidene fluoride electrospun nanofibers at different electrospinning times: 1. Desalination by direct contact membrane distillation, J. Membr. Sci. 433 (2013) 167-179.

[6] P.S.T. Machado, A.C. Habert, C.P. Borges, Membrane formation mechanism based on precipitation kinetics and membrane morphology: flat and hollow fiber polysulfone membranes, J. Membr. Sci. 155 (1999) 171-183.

[7] Z. Cui, E. Drioli, Y.M. Lee, Recent progress in fluoropolymers for membranes, Prog. Polym. Sci. 39 (2014) 164-198.

[8] S. Bonyadi, T.S. Chung, Highly porous and macrovoid-free PVDF hollow fiber membranes for membrane distillation by a solvent-dope solution co-extrusion approach, J. Membr. Sci. 331 (2009) 66-74.

[9] K. Yu Wang, T.S. Chung, M. Gryta, Hydrophobic PVDF hollow fiber membranes with narrow pore size distribution and ultra-thin skin for the fresh water production through membrane distillation, Chem. Eng. Sci. 63 (2008) 2587-2594.

[10] S. Wongchitphimon, R. Wang, R. Jiraratananon, L. Shi, C.H. Loh, Effect of polyethylene glycol (PEG) as an additive on the fabrication of polyvinylidene fluoride-co-hexafluropropylene (PVDF-HFP) asymmetric microporous hollow fiber membranes, J. Membr. Sci. 369 (2011) 329-338.

[11] L. Shi, R. Wang, Y. Cao, C. Feng, D.T. Liang, J.H. Tay, Fabrication of poly(vinylidene fluoride-co-hexafluropropylene) (PVDF-HFP) asymmetric microporous hollow fiber membranes, J. Membr. Sci. 305 (2007) 215-225.

[12] C. Feng, R. Wang, B. Shi, G. Li, Y. Wu, Factors affecting pore structure and performance of poly(vinylidene fluoride-co-hexafluoro propylene) asymmetric porous membrane, J. Membr. Sci. 277 (2006) 55-64.

[13] M.C. García-Payo, M. Essalhi, M. Khayet, Effects of PVDF-HFP concentration on membrane distillation performance and structural morphology of hollow fiber membranes, J. Membr. Sci. 347 (2010) 209-219.

[14] B.S. Lalia, E. Guillen, H.A. Arafat, R. Hashaikeh, Nanocrystalline cellulose reinforced PVDF-HFP membranes for membrane distillation application, Desalination 332 (2014) 134-141.

[15] L. Shi, R. Wang, Y. Cao, D.T. Liang, J.H. Tay, Effect of additives on the fabrication of poly(vinylidene fluoride-co-hexafluropropylene) (PVDF-HFP) asymmetric microporous hollow fiber membranes, J. Membr. Sci. 315 (2008) 195-204.

[16] M.M. Teoh, T.S. Chung, Membrane distillation with hydrophobic macrovoid-free PVDF–PTFE hollow fiber membranes, Sep. Purif. Technol. 66 (2009) 229-236.

[17] L. García-Fernández, M.C. García-Payo, M. Khayet, Effects of mixed solvents on the structural morphology and membrane distillation performance of PVDF-HFP hollow fiber membranes, J. Membr. Sci. 468 (2014) 324-338.

[18] N. Peng, N. Widjojo, P. Sukitpaneenit, M.M. Teoh, G. Glenn Lipscomb, T.S. Chung, J.Y. Lai, Evolution of polymeric hollow fibers as sustainable technologies: Past, present, and future, Prog. Polym. Sci. 37 (2012) 1401– 1424.

[19] P. van de Witte, P.J. Dijkstra, J.W.A. van den Berg, J. Feijen, Phase separation processes in polymer solutions in relation to membrane formation, J. Membr. Sci. 117 (1996) 1-31.

[20] A.C. Sun, W. Kosar, Y. Zhang, X. Feng, A study of thermodynamics and kinetics pertinent to formation of PVDF membranes by phase inversion, Desalination 309 (2013) 156-164.

[21] M. Khayet, C. Cojocaru, M. Essalhi, M.C. García-Payo, P. Arribas, L. García-Fernández, Hollow fiber spinning experimental design and analysis of defects for fabrication of optimized membranes for membrane distillation, Desalination 287 (2012) 146-158.

[22] Y. Tang, N. Li, A. Liu, S. Ding, C. Yi, H. Liu, Effect of spinning conditions on the structure and performance of hydrophobic PVDF hollow fiber membranes for membrane distillation, Desalination 287 (2012) 326-339.

[23] C.Y. Feng, K.C. Khulbe, T. Matsuura, A.F. Ismail, Recent progresses in polymeric hollow fiber membrane preparation, characterization and applications, Sep. Purif. Technol. 111 (2013) 43–71.

[24] A. Xu, A. Yang, S. Young, D. deMontigny, P. Tontiwachwuthikul, Effect of internal coagulant on effectiveness of polyvinylidene fluoride membrane for carbon dioxide separation and absorption, J. Membr. Sci. 311 (2008) 153-158.

[25] M. Rahbari-sisakht, A.F. Ismail, T. Matsuura, Effect of bore fluid composition on structure and performance of asymmetric polysulfone hollow fiber membrane contactor for CO2 absorption, Sep. Purif. Technol. 88 (2012) 99-106.

[26] M. Khayet, The effects of air gap length on the internal and external morphology of hollow fiber membranes, Chem. Eng. Sci. 58 (2003) 3091-3104.

[27] M. Khayet, M.C. García-Payo, F.A. Qusay, M.A. Zubaidy, Structural and performance studies of poly(vinyl chloride) hollow fiber membranes prepared at different air gap lengths, J. Membr. Sci. 330 (2009) 30-39.

[28] C.M. Hansen, Hansen Solubility Parameters: A User´s Handbook, 2nd ed., CRC Press, Taylor & Francis Group, Boca Ratón, FL (2007).

[29] J.E. Mark (Ed.), Polymer Data Hanbook, Oxford University Press (1999).

[30] S. Abbott, C.M. Hansen, H. Yamamoto, Hansen Solubility Parameters in Practice-Complete with Software, Data, and Examples, 3rd ed., Ebook, available from www.hansen-solubility.com (2010).

[31] Q. Li, Z.L. Xu, L.Y. Yu, Effects of mixed solvents and PVDF types on performances of PVDF microporous membranes, J. Appl. Polym. Sci. 115 (2010) 2277-2287.

[32] L. Setiawan, R. Wang, L. Shi, K. Li, A.G. Fane, Novel dual-layer hollow fiber membranes applied for forward osmosis process, J. Membr. Sci. 421-422 (2012) 238-246.

[33] A.F. Ismail, L.P. Yean, Review on the development of defect-free and ultrathin-skinned asymmetric membranes for gas separation through manipulation of phase inversion and rheological factors, J. Appl. Polym. Sci. 88 (2003) 442–451.

[34] M.L. Yeow, Y.T. Liu, K. Li, Isothermal phase diagrams and phase-inversion behaviour of poly(vinylidene fluoride)/solvents/additives/water systems, J. Appl. Polym. Sci. 90 (2003) 2150-2155.

[35] M. Khayet, C.Y. Feng, K.C. Khulbe, T. Matsuura, Preparation and characterization of polyvinylidene fluoride hollow fiber membranes for ultrafiltration, Polymer 43 (2002) 3879-3890.

[36] M.C. García-Payo, M.A. Izquierdo-Gil, C. Fernández-Pineda, Wetting study of hydrophobic membranes via liquid entry pressure measurements with aqueous alcohol solutions, J. Colloid Interface Sci. 230 (2002) 420-431.

[37] K. Smolders, A.C.M. Franken, Terminology for Membrane Distillation, Desalination 72 (1989) 249-262.

[38] J. Zhang, J.D. Li, M. Duke, Z. Xie, S. Gray, Performance of asymmetric hollow fibre membranes in membrane distillation under various configurations and vacuum enhancement, J. Membr. Sci. 362 (2010) 517-528.

[39] M. Essalhi, M. Khayet, Self-sustained webs of polyvinylidene fluoride electrospun nano-fibers: Effects of polymer concentration and desalination by direct contact membrane distillation, J. Membr. Sci. 454 (2014) 133-143.

[40] M. Khayet, T. Matsuura, Determination of surface and bulk pore sizes of flat-sheet and hollow fiber membranes by atomic force microscopy, gas permetaion and solute transport methods, Desalination 158 (2003) 57-64.

[41] M. Khayet, M.C. García-Payo, F.A. Qusay, K.C. Khulbe, C.Y. Feng, T. Matsuura, Effects of gas gap type on structural morphology and performance of hollow fibers, J. Membr. Sci. 311 (2008) 259-269.

[42] M. Khayet, Membrane surface modification and characterization by X-ray photoelectron spectroscopy, atomic force microscopy and contact angle measurements, Appl. Surf. Sci. 238 (2004) 269-272.

[43] X. Tian, X. Jiang, Poly(vinylidene fluoride-co-hexafluoropropene) (PVDF-HFP) membranes for ethyl acetate removal from water, J. Hazard. Mater. 153 (2008) 128-135.

[44] M. Tazaki, R. Wada, M. Okabe, T. Homma, Crystallization and gelation of poly (vinylidene fluoride) in organic solvents, J. Appl. Polym. Sci. 65 (1997) 1517-1524.

[45] Z.K. Xu, L.Q. Shen, Q. Yang, F. Liu, S.Y. Wang, Y.Y. Xu, Ultrafiltration hollow fiber membranes from poly(ether imide): preparation, morphologies and properties, J. Membr. Sci. 223 (2003) 105-118.

[46] Q. Li, Z.L. Xu, M. Liu, Preparation and characterization of PVDF microporous membrane with highly hydrophobic surface, Polym. Adv. Technol. 22 (2011) 520-531.

[47] P. Zhang, Y. Wang, Z. Xu, H. Yang, Preparation of poly (vinyl butyral) hollow fiber ultrafiltration membrane via wet-spinning method using PVP as additive, Desalination 278 (2011) 186-193.

[48] D.T. Clausi, W.J. Koros, Formation of defect-free polyimide hollow fiber membranes for gas separations, J. Membr. Sci. 167 (2000) 79-89.

[49] H.A. Tsai, D.H. Huang, S.C. Fan, Y.C. Wang, C.L. Li, K.R. Lee, J.Y. Lai, Investigation of surfactant addition effect on the vapor permeation of aqueous ethanol mixtures through polysulfone hollow fiber membranes, J. Membr. Sci. 198 (2002) 245-258.

[50] C. Ma, C. Zhang, Y. Labreche, S. Fu, L. Liu, W.J. Koros, Thin-skinned intrinsically defect-free asymmetric mono-esterified hollow fiber precursors for crosslinkable polyimide gas separation membranes, J. Membr. Sci. 493 (2015) 252-262.

[51] Z. Wang, L. Sun, Q. Wang, B. Li, S. Wang, A novel approach to fabricate interconnected sponge-like and highly permeable polyvinylidene fluoride hollow fiber membranes for direct contact membrane distillation, Eur. Polym. J. 60 (2014) 262-272.

[52] S.H. Choi, F. Tasselli, J.C. Jansen, G. Barbieri, E. Drioli, Effect of the preparation conditions on the formation of asymmetric poly(vinylidene fluoride) hollow fibre membranes with a dense skin, Eur. Polym. J. 46 (2010) 1713-1725.

[53] J. Zhang, N. Dow, M. Duke, E. Ostarcevic, J.D. Li, S. Gray, Identification of material and physical features of membrane distillation membranes for high performance desalination, J. Membr. Sci. 349 (2010) 295-303.

[54] X. Zhang, J. Hu, Q. Chang, Y. Wang, J.e. Zhou, T. Zhao, Y. Jiang, X. Liu, Influences of internal coagulant composition on microstructure and properties of porous YSZ hollow fibre membranes for water treatment, Sep. Purif. Technol. 147 (2015) 337-345.

[55] M.C. García-Payo, M. Essalhi, M. Khayet, L. García-Fernández, K. Charfi, H. Arafat, Water desalination by membrane distillation using PVDF-HFP hollow fiber membranes, Membrane Water Treatment 1 (2010) 215-230.

[56] G. Wypych, Handbok of Polymers, ChemTec PUBLISHING, Toronto (2012).

[57] A. Moriya, T. Maruyama, Y. Ohmukai, T. Sotani, H. Matsuyama, Preparation of poly(lactic acid) hollow fiber membranes via phase separation methods, J. Membr. Sci. 342 (2009) 307-312.

[58] L. García-Fernández, M.C. García-Payo, M. Khayet, Mechanism of formation of hollow fiber membranes for membrane distillation: 2. Outer coagulation power effect on morphological characteristics, J. Membr. Sci. http://dx.doi.org/10.1016/j.memsci.2017.03.038 (2017).

[59] L. García-Fernández, M.C. García-Payo, M. Khayet, Mechanism of formation of hollow fiber membranes for membrane distillation: 1. Inner coagulation power effect on morphological characteristics, J. Membr. Sci. http://dx.doi.org/10.1016/j.memsci.2017.03.036 (2017).

[60] I. Pinnau, W.J. Koros, A qualitative skin layer formation mechanism for membranes made by dry/wet phase inversion, J. Polym. Sci., Part B: Polym. Phys. 31 (1993) 419-427.

[61] X. Wang, L. Zhang, D. Sun, Q. An, H. Chen, Effect of coagulation bath temperature on formation mechanism of poly(vinylidene fluoride) membrane, J. Appl. Polym. Sci. 110 (2008) 1656-1663.

[62] J.G. Wijmans, J.P.B. Baaij, C.A. Smolders, The mechanism of formation of microporous or skinned membranes produced by immersion precipitation, J. Membr. Sci. 14 (1983) 263-274.

[63] D.G. Yu, W.L. Chou, M.C. Yang, Effect of draw ratio and coagulant composition on polyacrylonitrile hollow fiber membranes, Sep. Purif. Technol. 52 (2006) 380-387.

[64] T. He, M.H.V. Mulder, M. Wessling, Preparation of porous hollow fiber membranes with a triple-orifice spinneret, J. Appl. Polym. Sci. 87 (2003) 2151–2157.

[65] M.H.V. Mulder, J.O. Hendrikman, J.G. Wijmans, C.A. Smolders, A rationale for the preparation of asymmetric pervaporation membranes, J. Appl. Polym. Sci. 30 (1985) 2805-2820.

[66] D.R. Lide, ed., CRC Handbook of Chemistry and Physics, Internet Version 2005, http://www.hbcpnetbase.com, CRC Press, Boca Raton, FL, 2005.

[67] C.C. Pereira, R. Nobrega, C.P. Borges, Spinning process variables and polymer solution effects in the die-swell phenomenon during hollow fiber membranes formation, Braz. J. Chem. Eng. 17 (2000) 599-606.

[68] L. Shi, R. Wang, Y. Cao, Effect of the rheology of poly(vinylidene fluoride-co-hexafluropropylene) (PVDF–HFP) dope solutions on the formation of microporous hollow fibers used as membrane contactors, J. Membr. Sci. 344 (2009) 112-122.

4

Polymeric hollow fiber membranes:

Spinneret and gap type effect on the structural properties and MD performance

Poly(vinylidene fluoride-co-hexafluoropropylene) (PVDF-HFP) hollow fiber membranes were prepared using the phase inversion spinning technique under a wet gap mode. Different corrugated outer surfaces were obtained by means of a micro-engineered spinneret, spraying the external coagulant on the nascent fiber along gap, and different spinning parameters, namely, the gap distance and the external coagulant flow rate. A quantitative evaluation of the corrugation size and shape was carried out by electron scanning microscopy and atomic force microscopy. The effect of the corrugation size and shape on the direct contact membrane distillation (DCMD) performance has been studied. The corrugated outer surface acted as micro-turbulence promoters mitigating the temperature polarization effect and enhanced the external effective surface area for condensation. Both factors improved the DCMD permeability of the hollow fiber membranes. However, corrugations with V-shaped valleys depths greater than about 30 μm did not always improve the DCMD permeate flux. It was found that the membrane prepared with the spray wetting mode exhibited the best desalination performance. The salt rejection factor of all prepared hollow fiber membranes was greater than 99.9% and the highest DCMD permeate flux of this study was greater than those reported so far for the PVDF-HFP hollow fiber membranes.

Hollow fiber membranes with different external corrugated surfaces for desalination by membrane distillation

4.1 Introduction

Membrane distillation (MD) is a water treatment technology that involves both heat and mass transfer through porous and hydrophobic membranes. It is a non-isothermal process whose driving force is the transmembrane vapor pressure. Desalination is the principal application of MD technology, permitting the production not only distilled water but also ultrapure water and the treatment of high saline aqueous solutions [1-3].

Nowadays, MD membrane engineering is gaining importance because there are not suitable commercial membranes designed specifically for this process. On the other hand, hollow fiber membrane is the most attractive configuration owing to its high packing density in tubular modules. Not only these membranes must meet the specific MD requirements in order to be competitive, but they should also exhibit high water production rate with excellent rejection factors. It is worth quoting that direct contact membrane distillation (DCMD) is the most used MD configuration due to its easy operating mode. However, in this configuration the heat loss by conduction through the membrane matrix is high compared to the other MD configurations (i.e. air gap membrane distillation, AGMD and vacuum membrane distillation, VMD). Therefore, the temperature polarization (TP) effect is more significant in DCMD than in these other MD configurations and becomes the main source of the permeate flux reduction [4-6].

In 1987, Schofield et al. [7] emphasized first the importance of the temperature polarization (TP) phenomenon in MD performance. Briefly, TP refers to the temperature difference between the bulk liquid and the membrane surface associated to the established thermal boundary layers at both sides of the membrane. This represents a decrease in the effective thermal driving force for the mass transfer. Its effect is influenced by different operating parameters such as the feed and permeate temperatures and their circulation flow rates. For instance, a high feed temperature negatively affects the TP, but it is necessary to keep a significant temperature gradient through the membrane to get high water production rates. On

the other hand, by increasing the flow rate of both the feed and permeate liquids, the TP effect is reduced [8, 9]. Different studies have been carried out to quantify the TP coefficient [6, 10]. Ali et al. [10] designed a specific DCMD cell with several temperature sensors, whereas Manawi et al. [6] developed a predictive model. Another alternative to reduce the TP phenomenon is to incorporate turbulence promoters in membrane modules. Flat-sheet membrane modules with channel spacers of different configurations and shapes were commonly used for this purpose [6, 11, 12]. The increase of the circulation flow rate as well as the use of spacers in the membrane module induce turbulent flows and better hydrodynamics inside the liquid channels, reducing the thermal boundary layer and enhancing the MD permeate flux as consequence. However, both strategies increase the overall cost of the MD process (i.e. operating cost and initial investment cost of the membrane module).

An interesting challenge for MD membrane engineers is to prepare membranes with corrugated surfaces that act as internal turbulence promoters. Kharraz et al. [13] succeeded to prepare a corrugated composite flat-sheet membrane by the phase inversion. Two layers of polyvinylidene fluoride (PVDF) were cast in two steps, the first one defined the pore size of the membrane while the second one set the corrugation on the surface by means of a net spacer, which imprinted in the surface the desirable pattern. It was found that the corrugated membrane exhibited higher DCMD permeate flux and lower scaling than the non-corrugated one. Based on the obtained promising results of corrugated membranes, further MD studies have been suggested. Yang et al. [14] designed novel hollow fiber membrane modules with improved DCMD performance. It was observed that the module prepared with curly fibers resulted to be most efficient in terms of TP mitigation. It is worth noting that the PVDF hollow fibers packed in this module were commercial membranes and the curly fiber geometry was obtained after a heat treatment of these fibers under a winding angle. Hollow fibers with other microstructured geometries (i.e. wavy and gear-shaped) were explored in DCMD by computational fluid dynamic (CFD) simulations [15]. This study was focused on the permeate flux improvement by reducing the thermal boundary layer using different fiber geometries with enhanced hydrodynamics of the liquid circulation channels. It was found that the gear shape at the outer side of the fiber was the most promising membrane geometry for DCMD. The CFD results showed that this kind of microstructure acted as turbulence promoter, decreasing the TP effect and the thickness of the thermal boundary layer without applying high flow rates or channel spacers.

In the present study, hollow fiber membranes with corrugated outer surfaces have been prepared for desalination by DCMD in order to confirm the conclusions drawn by Yang et al. [15] based on CFD simulations. In fact, hollow fibers with microstructured outer layers have been already prepared by the phase inversion method following diverse strategies, either using micro-engineered spinnerets with different patterns, modifying spinneret dimension (i.e.

annular gap), changing spinning parameters (i.e. polymer solution composition, air gap distance and take-up speed) or employing a double-coaxial microfluidic device under different preparation conditions [16-20]. These fibers were prepared, characterized and some of them were applied in gas permeation [16], ultrafiltration [17] or cross-flow filtrations [20]. In all these studies, hydrophilic polymers (polyethersulfone (PES), polyimide (PI) and polyvinyl pyrrolidone (PVP)) were used and the hollow fiber membranes were prepared under short or zero air gap lengths. However, this is the first research study in which hydrophobic corrugated hollow fiber membranes with microstructured cross-section geometries are prepared for MD application. A micro-engineered spinneret, a long wet gap distance and a novel fiber outer layer wetting mode have been considered to prepare the corrugated external surface of hollow fiber membranes. The effect of the corrugation size and shape of the membrane outer surface on the DCMD performance has been studied.

4.2 Experimental

4.2.1 Materials

The copolymer poly(vinylidene fluoride-co-hexafluoropropylene) (PVDF-HFP, M_w = 455,000 g/mol), the additive poly(ethyleneglycol) (PEG, M_w = 6000 g/mol) and the solvents *N,N*-dimethyl acetamide (DMAC) and trimethyl phosphate (TMP) used to prepare the spinning solution were purchased from Sigma Aldrich. The sodium chloride (NaCl) of the feed aqueous solution employed to perform the DCMD experiments was purchased from Panreac.

4.2.2 Hollow fiber membrane preparation

The hollow fiber membranes were prepared by the wet/wet spinning technique with an external coagulant along the gap distance, which is a modified version of the well-known dry/wet spinning technique described elsewhere [21, 22]. The fabrication parameters are summarized in Table 4.1. The spinning solution composition was selected according to the conclusions drawn in our previous study [23]. The surface tension was measured at room temperature by the pendant drop shape analysis with an optical contact angle meter (CAM 200). A stainless steel needle with an outer diameter of 1.832 mm was used keeping constant the drop volume at 12.4 μL for all samples. The viscosity of the spinning solution was obtained by a Digital Viscometer (Brookfield, Model DV-I+) using the SC4-31 spindle at 4 rpm and a cylindrical sample container. The temperature of the spinning solution was maintained constant at 42 ºC (i.e. the same temperature considered to prepare the hollow fiber membrane) by a thermostat (Techne, Model TU-16D).

Table 4.1. Spinning parameters of the prepared hollow fiber membranes.

Parameters	**Operating conditions**
Dope solution composition (wt%)	Polymer (19): PVDF-HFP Additive (5): PEG Solvents (76): DMAC (40)/TMP (60)
Dope solution viscosity (mPa s)	3690 ± 80
Dope solution surface tension (mN/m)	30.45 ± 0.20
Dope solution temperature (ºC)	42
Extrusion pressure (kPa)	60
Spinneret 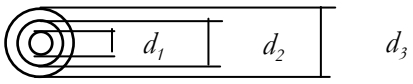	d_1= 1.0 mm / d_2= 2.4 mm / d_3= 4.75 mm
Internal and external coagulant	Distilled water
Internal and external coagulation temperature	Room temperature
Internal coagulant flow rate (10^{-6} m^3/s)	0.27
Liquid coagulation bath	Tap water
Liquid coagulation bath temperature (ºC)	42
Take-up speed (rpm)	12
Variable spinning parameters	
Spinneret mode	Single / double
Spinneret shape	Circular / star
Fiber outer layer wetting mode	Longitudinal / spray
Gap distance (m)	0.275 / 0.115 / 0
External coagulation flow rate (10^{-6} m^3/s)	3.3 / 0.12

To prepare hollow fiber membranes with a thin skin-layer and a corrugated outer surface but maintaining a long gap distance between the spinneret and the coagulation bath, a wet gap was considered. The method is termed hereafter wet/wet spinning and the two following strategies were adopted: i) use of a micro-engineered triple-orifice spinneret with a star-shaped orifice (i.e. copolymer solution orifice) and ii) spray the outer surface of the fiber by micro-jet nozzles along the gap distance. It is worth noting that the use of relatively high gap distances is advisable to prepare polymeric hollow fiber membranes with adequate mechanical properties [24].

The triple-orifice spinneret was designed as illustrated in Fig. 4.1. The interchangeable piece (P) of this spinneret enabled the preparation of hollow fiber membranes with the common circular cross-section as well as with a star-shaped contour, by using the pieces (P1) or (P2) shown in Fig. 4.1 respectively. As it is summarized in Fig. 4.2 the triple-orifice spinneret can be used in single or double mode if the external coagulant circulates or not through the outermost channel of the spinneret. Depending on the type of the piece P selected, the cross-section of the spinneret shows the circular or the star-shaped orifice. If the double mode of the spinneret is considered, with either circular or star-shaped P piece, the external coagulant (i.e. distilled water) goes through the outermost channel of the spinneret and circulates longitudinally to the outer layer of the fiber, as presented in Fig. 4.2 (i.e. fiber outer layer wetting mode: longitudinal external coagulant flow). This type of wet gap requires the use of the star-shaped spinneret in order to obtain corrugated hollow fiber membranes.

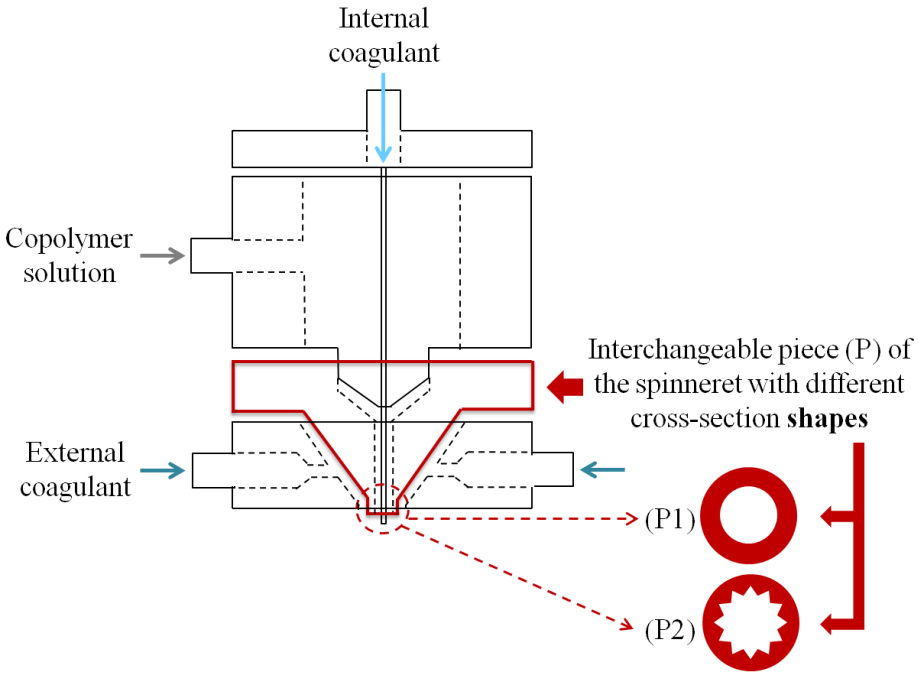

Fig. 4.1. Schematic diagram of the triple-orifice spinneret and the cross-section shapes (P1 and P2) of the interchangeable piece (P).

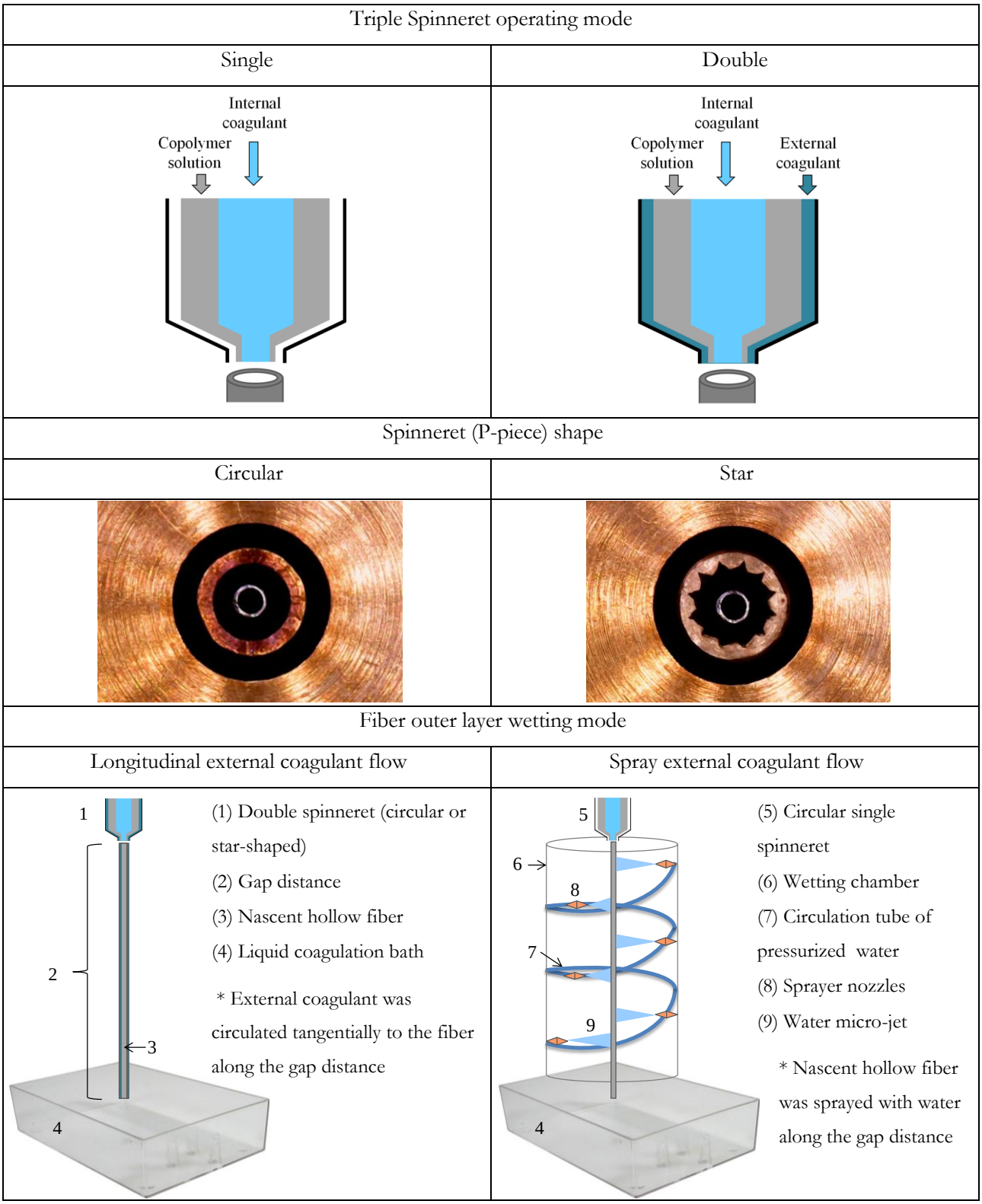

Fig. 4.2. Spinneret design and fiber outer layer wetting modes considered to prepare hollow fiber membranes.

The other wetting mode that permits to prepare corrugated outer surface is the spray mode also shown in Fig. 4.2. The water micro-jets from the nozzles placed along the gap distance pulverized the outer surface of the nascent hollow fiber, resulting in a membrane with an external irregular contour. In the present study, the circular-shaped spinneret in single mode is used only in combination with the spray external coagulant way. Besides the type of the spinneret and the wetting gap mode considered, other spinning parameters such as the gap distance and the external coagulant flow rate were also changed. The prepared hollow fiber membranes are identified in Table 4.2 according to the aforementioned parameters. The variable spinning parameters were modified in order to prepare hollow fiber membranes with different corrugated outer surfaces and structures, but a statistical experimental design about the operating conditions was not carried out. The effects of the mentioned spinning parameters on the structural characteristics of the prepared hollow fiber membranes as well as on their DCMD performance were studied.

Table 4.2. Hollow fiber membranes prepared in this study.

Membrane name	Spinneret		Fiber outer layer wetting mode	Gap distance (m)	External coagulant flow rate (10^{-6} m^3/s)
	Mode	Shape			
CL	Double	Circular	Longitudinal	0.275	3.3
SL-ref	Double	Star	Longitudinal	0.275	3.3
CSN	Single	Circular	Spray	0.275	N.A.
SL-1	Double	Star	Longitudinal	0.115	3.3
SL-2	Single	Star	N.A	0	N.A.
SL-3	Double	Star	Longitudinal	0.275	0.12

4.2.3 Characterization of the hollow fiber membranes

The digital microscope (Dino-Lite) and the optical microscope (OLYMPUS BX60M) were used to analyze the outer surface corrugations of the prepared hollow fiber membranes with a low magnification (20x and 50x, respectively). Moreover, the optical microscope with a precision of ± 1 μm was employed to measure the inner diameters of the membranes.

Both the external surface and the cross-section of the hollow fibers were examined by field emission scanning electron microscope (FESEM, JEOL Model JSM-6335F). The cross section of the membrane was prepared by fracturing the hollow fiber in liquid nitrogen. Subsequently, all the samples were gold coated by a rotary-pumped sputter coater (QUORUM Q150R S) during 60 s under 20 mA. The corrugation's height (H_c), the corrugated perimeter of the fiber

and the perimeter of a drawn circumference passing through the middle of the peaks and valleys of the corrugations (i.e. the equivalent perimeter of the external surface without corrugation) were obtained from the SEM cross-section images using ImageJ software. The H_c value was determined as the average height between the peaks and the valleys of the corrugated hollow fiber. For the same length of the fibers (20 cm considered in this study to prepare the hollow fiber membrane modules), the external surface area of the fibers was calculated from their perimeters. Then, the surface area enhancement (*SAE*) of the fiber associated to the corrugated surface area ($SA_{corrugated}$) was calculated taking as reference the middle surface area (SA_{middle}) as follows:

$$SAE = \frac{SA_{corrugated} - SA_{middle}}{SA_{middle}} \times 100 \quad (4.1)$$

The atomic force microscopy (AFM, Nanoscope III) equipped with 1553D scanner (Digital Instruments Inc., Santa Barbara, Ca) in a tapping mode was used to analyze an area of (75 x 18.75) μm^2 of the outer surface of the hollow fiber membranes. All samples were cut longitudinally and scanned transversely (i.e. perpendicular to the spinning direction). The software NanoScope Analysis© version 1.5 (Bruker Corporation) was employed to treat the provided images and determine some properties of membrane´s surface. Different types of analysis were performed from the obtained AFM images, but first these were treated under certain conditions described as follows. In order to show the 3D images and to study the corrugated outer surfaces, 1st order flattening was previously carried out to center the Z-data and remove the tilt. The following procedure is considered for the first time to quantify the shape at the top of the surface corrugations. Two parameters were determined from the cross-section profiles (i.e. section analysis) of the hollow fiber outer surface (see Fig. 4.3): i) the surface length difference (*SLD*), which represents the percentage of the external perimeter enhancement due to the corrugations induced on the surface, was calculated using the following equation (see Fig. 4.3(a)):

$$SLD = \frac{Surface\ distance\ (SD) - Horizontal\ distance\ (HD)}{Horizontal\ distance\ (HD)} \times 100 \quad (4.2)$$

and ii) the bow angle (α), which shows the curvature of the surface corrugations as indicated in Fig. 4.3(b). For each line profile, left and right angles were taken into consideration (α_1 and α_2 in Fig. 4.3(b), respectively). All reported parameters were the average of the values obtained from at least three different line profiles traced along the scanned area of each membrane sample.

In order to determine the roughness of the outer surfaces of the prepared hollow fibers, 2nd order flattening were applied on the AFM images in order to remove the intrinsic curvature of the hollow fiber and therefore obtain adequate roughness results of the

membrane. In this study, the mean roughness (R_a) and the maximum roughness (R_{max}) were determined [25, 26]. R_a is the arithmetic average of the surface height values relative to the mean plane. R_{max} represents the maximum distance in height between the highest and the lowest values.

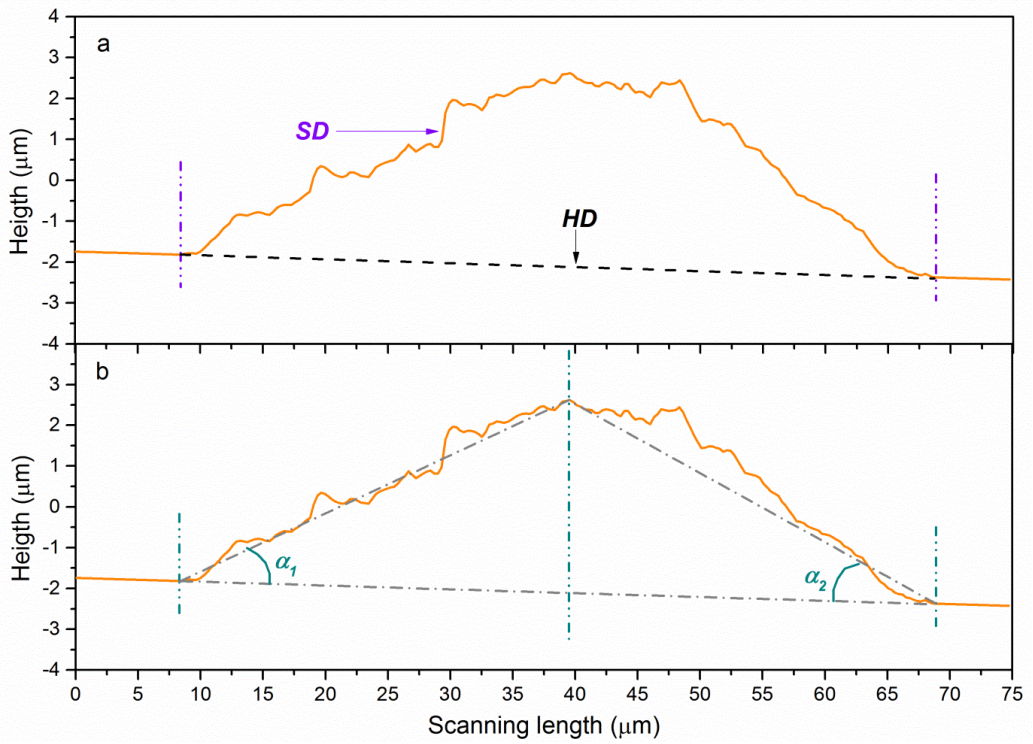

Fig. 4.3. Example of the cross-sectional profile of the external hollow fiber surface obtained from the AFM images showing the following parameters determined by NanoScope Analysis© version 1.5 (Bruker Corporation) software: (a) surface distance (*SD*) and horizontal distance (*HD*) of a corrugation sample; and (b) left angle (α_1) and right angle (α_2) of the curvature of the corrugation.

4.2.4 Direct contact membrane distillation experiments

DCMD experiments were carried out using a salt aqueous solution of 3 wt% NaCl. In this study, the effects of the external corrugation of the hollow fiber membranes on the DCMD performance were analyzed. The feed solution was circulated tangentially to the inner side of the membrane (i.e. non-corrugated side) while the permeate (i.e. distilled water) was circulated in a counter-current way through the outer side the membrane. The experimental set-up used to perform the DCMD experiments was described in [23]. Six hollow fibers were assembled in a stainless-steel tubular module with a length of 20 cm. After checking that the membrane modules had no leakage, DCMD experiments were performed first with distilled water as feed and then with the aforementioned salt aqueous solution. All experiments were carried out keeping constant both the feed and permeate temperatures at 80 °C and 25 °C, respectively, as well as their flow rates at 13.8 ± 1.2 kg/h and 20.7 ± 0.6 kg/h, respectively. The permeate flux

was calculated taking into consideration the internal surface of the membrane while the salt rejection factor was determined from the feed and permeate concentrations at the beginning and at the end of each experiment. The feed and permeate concentrations were calculated from their corresponding electrical conductivities as described elsewhere [23].

4.3 Results and discussions

All PVDF-HFP hollow fiber membranes were prepared using the same spinning solution (i.e. equal rheological parameters such as viscosity and surface tension) and the spinning conditions indicated in Tables 4.1 and 4.2. Therefore, the prepared hollow fiber membranes were analyzed in terms of the following effects (see Table 4.2): i) Spinning operating type by comparing the membranes CL, SL-ref and CSN; ii) gap distance by studying the differences between the fibers SL-ref, SL-1 and SL-2; and iii) external coagulant flow rate by analyzing the membranes SL-ref and SL-3. For sake of comparison, the hollow fiber membrane SL-ref is considered as membrane reference in this study, because it is common in the three groups.

4.3.1 Morphological characterization of the prepared hollow fiber membranes

4.3.1.1 Visual inspection of the outer surfaces

The external surfaces of the prepared hollow fiber membranes were examined by digital and optical microscopes in order to ensure the formation of the corrugations and to find out the main differences between them according to the employed preparation parameters. The optical microscope was also used to measure the inner diameters of the prepared hollow fiber membranes. The results are summarized in Table 4.3. The inner diameters of the membranes SL-ref and CSN were lower than those of the circular hollow fiber CL. Both the star-shaped orifice of the spinneret and the pressure exerted by the micro-jets on the outer surface of the nascent hollow fiber membrane (i.e. spray mode) could reduce their die-swell effect and consequently decreased their inner diameter. The reduction of the wet gap distance decreased the fiber elongation during its preparation and increased the inner diameter (compare the diameters of the membranes SL-ref, SL-1 and SL-2 in Table 4.3) [21]. Nevertheless, the external coagulant flow rate did not affect the inner diameter of the membrane as quite similar inner diameters values were obtained for the hollow fibers SL-3 and SL-ref if the corresponding standard deviations are taking into account. It is worth noting that the inner diameters listed in Table 4.3 will be used to calculate the DCMD permeate flux based on the internal surface of the membrane.

Figure 4.4 shows the digital and optical images of the outer surfaces of all prepared hollow fiber membranes. For an easier comparison, these images are placed longitudinally (i.e. parallel

Table 4.3. Inner diameters (d_i), corrugation´s height (H_c) and surface area enhancement (SAE) of the hollow fiber membranes.

Membrane	d_i (µm)	H_c (µm)	SAE (%)
CL	1330 ± 90	0	0
SL-ref	1070 ± 120	15 ± 3	10.17 ± 0.16
CSN	1020 ± 110	55.4 ± 1.4	15.0 ± 0.5
SL-1	1355 ± 150	33.5 ± 0.7	9.30 ± 0.01
SL-2	1600 ± 160	5.5 ± 1.9	4.10 ± 0.03
SL-3	1135 ± 110	61 ± 3	17.70 ± 0.20

to the spinning direction). The spinning operating type induced different types of outer microstructures. The hollow fibers CL, SL-ref and CSN exhibited smooth, striped and bumpy surfaces, respectively. The non-corrugated external surface of the hollow fiber CL had the common surface appearance of any polymeric membrane prepared with a circular spinneret under stable spinning conditions. The star-shaped pattern of the spinneret cross-section (i.e. see P2 in Fig. 4.1 and the corresponding photograph in Fig. 4.2) was transferred to the outer layer of the hollow fiber SL-ref. The images of its surface show these corrugations. The outer surface of the hollow fiber CSN was completely different. In this case, the applied water spray on the nascent hollow fiber membrane along the gap distance induced irregular structures on its surface (see bumpy structure in Fig. 4.4).

The SL hollow fiber membranes, prepared with the same star-shaped spinneret but with different wet gap distances and external coagulant flow rates, exhibited regular microstructured patterns on their outer surfaces (i.e. parallel longitudinal lines along the spinning direction). It is known that the preparation of hollow fiber membranes by the dry/wet spinning technique with microstructured outer surfaces requires short air gap distances. The size of the corrugation decreased becoming rounder or even disappeared when the air gap distance was increased. This is attributed to the surface tension, which tends to round the shape of the fiber during its residence time in the air gap in order to minimize the surface free energy [16, 17]. Nijdam et al. [16] observed that the corrugations induced on the gas permeation polyethersulfone-polyimide (PES/PI) hollow fiber membranes by a smart spinneret completely disappeared for air gap distances larger than 10 mm. However, in the present study it was possible to apply much larger gap distances retaining the transferred microstructure due to the external coagulation of the nascent fiber along the whole gap. The strong nonsolvent (i.e. water) for the PVDF-HFP copolymer, used as external coagulant, fixed

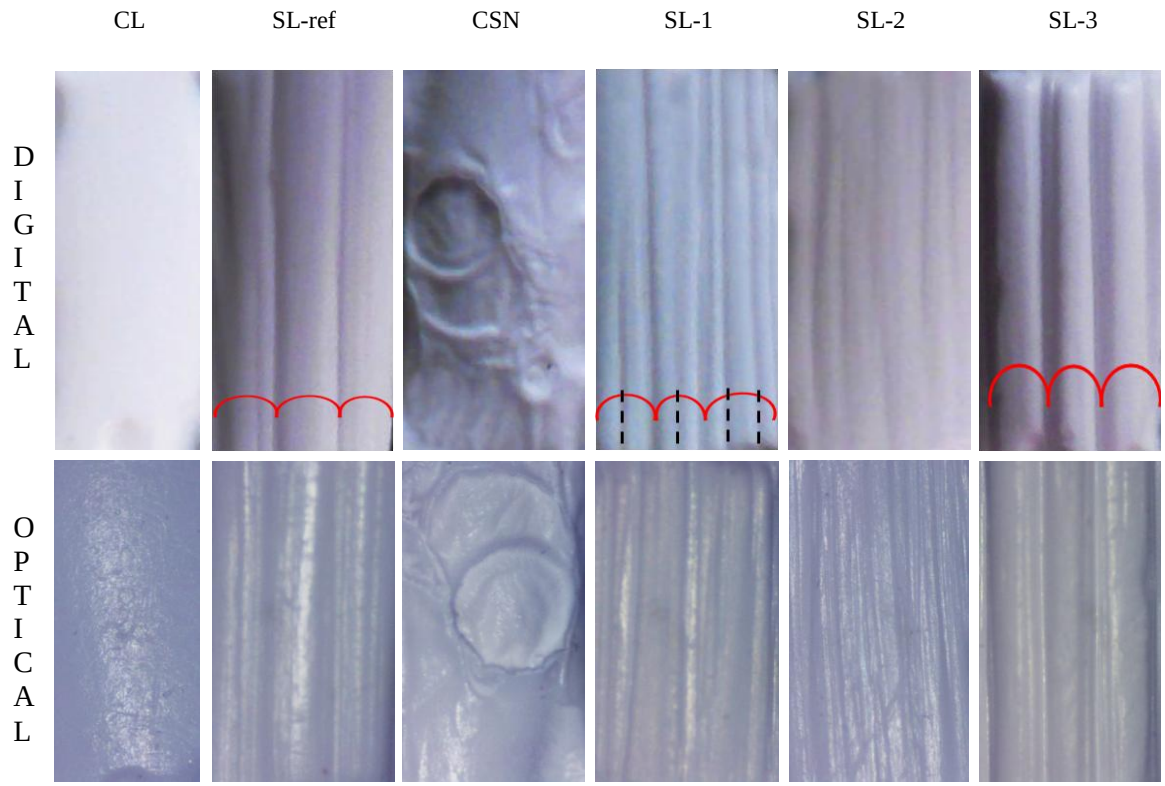

Fig. 4.4. Digital and optical images of the outer surface of the prepared hollow fiber membranes.

the formed microstructured shape (i.e. the primary corrugations) on the outer surface maintaining their size as much as possible along the gap distance.

Immediately after the extrusion at the exit of the spinneret, the original contour of the fiber with sharp peaks associated to the star-shaped orifice of the spinneret disappeared, resulting in rounded edges (i.e. flower-shaped contours instead of star-shaped). This was consequence of the die-swell effect on the nascent fiber at the exit of the spinneret, which change the size and shape of the edges of the extruded material [27]. Furthermore, when using an external coagulant, the visco-elastic expansion associated to the die-swell could be partially counteracted by the pressure exerted from the water circulation through the outermost channel of the spinneret (i.e. water pressure force inwards against the die-swell force outwards) [28]. This might reduce the size of the primary formed corrugations and induced the formation of secondary corrugations, as consequence of the instabilities generated by the water on the copolymeric spinning solution.

The images of the hollow fibers SL-ref and SL-1 showed the same three primary corrugations (see red lines in Fig. 4.4) transferred from the star-shaped orifice of the spinneret to their outer surfaces. However, these corrugations were better-defined for the membrane SL-1 prepared under a smaller wet gap compared to SL-ref, with clear secondary corrugations

(see black discontinuous lines in Fig. 4.4) formed between the primary ones. It can be concluded that the higher gap distance increased the stretching of the fibers due to the greater gravity force along the gap distance, making the primary corrugation shape on the outer surface less pronounced and the secondary corrugations poorly defined.

The hollow fiber prepared without any gap distance (SL-2 membrane) presents a slightly wavy surface without clear corrugations. In this case, the microstructured shape of the external layer almost disappeared due to the high die-swell effect of the fiber at the exit of the spinneret [29]. On the contrary, Nijdam et al. [16] found that the PES/PI hollow fiber membrane prepared without air gap was the membrane that best reproduced the corrugated microstructure of the spinneret´s insert. This was attributed to the high viscosity of PES/PI blend (20707 mPa·s), which is one order of magnitude higher than the viscosity of the PVDF-HFP spinning solution used in this study (see Table 4.1). The effect of the polymer solution viscosity on the final membrane microstructure was studied by Çulfaz et al. [17]. It was observed that the reduction of the viscosity from 150000 to 28000 mPa·s resulted in a rapid disappearance of the transferred microstructure along the air gap.

The biggest primary corrugations were observed on the external surface of the membrane SL-3. As shown in both the digital and optical images of the surface of this membrane, the same three primary corrugations observed for the hollow fibers SL-ref and SL-1 were seen again on the SL-3 membrane surface (see red line in Fig. 4.4). This membrane was also prepared with the star-shaped spinneret, under a longitudinal wet gap distance of 27.5 cm (i.e. the same conditions used for the SL-ref membrane preparation), but with a slower external coagulant flow rate ($0.12\ 10^{-6}$ against $3.3\ 10^{-6}$ m^3/s for SL-ref). These preparation conditions caused a better imprint of the star-shaped orifice of the spinneret on the fiber surface. The decrease of the external coagulant flow rate reduced its pressure exerted on the dope solution at the exit of the spinneret, resulting in better defined cross-section profiles. Furthermore, minor disturbances were caused with a slower external coagulant flow rate avoiding the formation of the secondary corrugations. A similar behavior was reported on the inner contour of the hollow fibers [30, 31]. The induced corrugations were reduced or even destroyed by using high internal coagulant flow rates.

4.3.1.2 SEM images of the cross-sections and the outer surfaces

Figure 4.5 shows the cross-sections and the outer surfaces of the prepared hollow fiber membranes. All membranes exhibit common overall symmetric cross-section morphology consisting of a finger-like structure at both the internal and external layers and a sponge-like structure at the middle of the section. The finger-like structure was the consequence of using water (i.e. a strong coagulant for the copolymer PVDF-HFP) as both internal and external coagulant, which induced a quick phase inversion at the inner and outer layers of the hollow

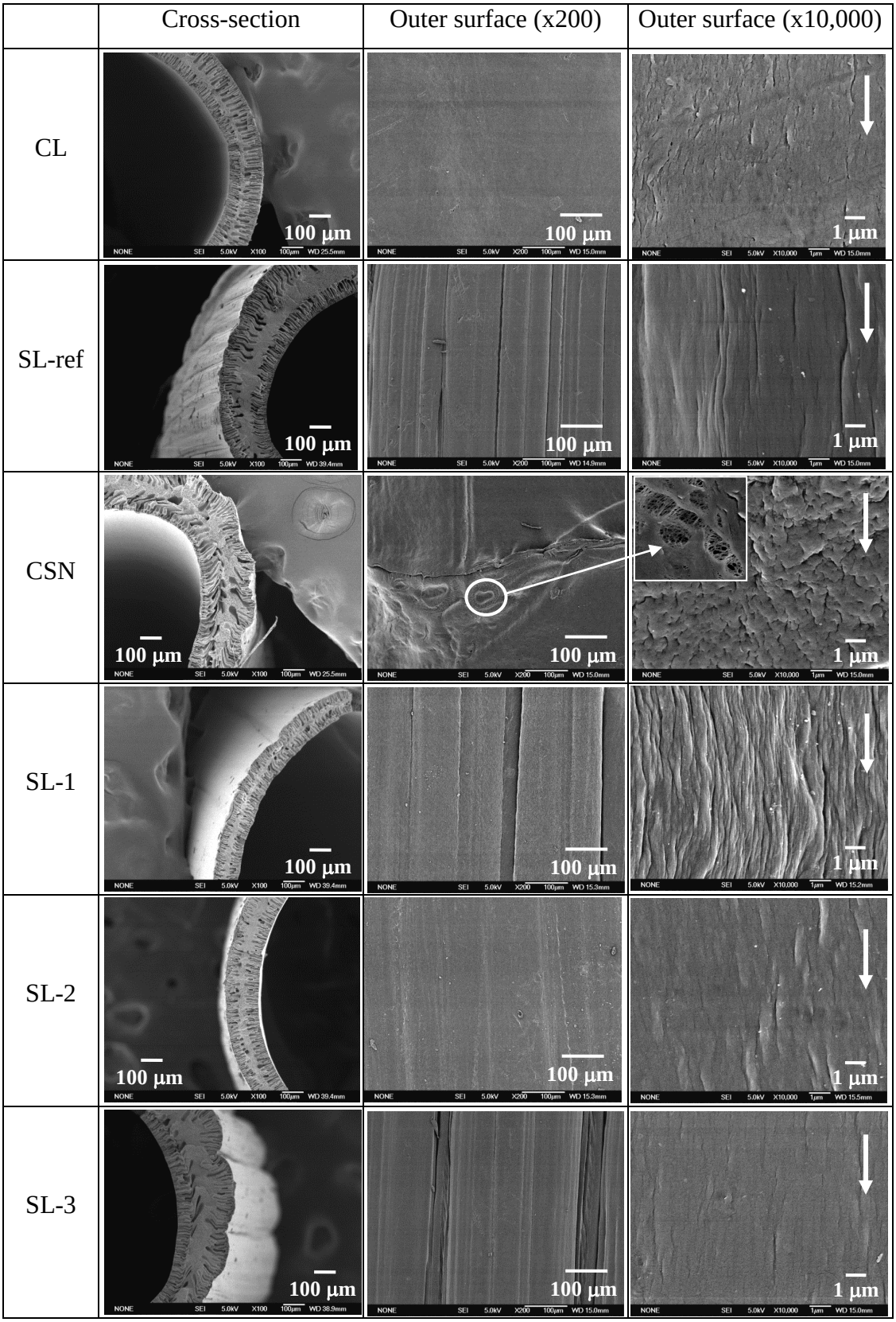

Fig. 4.5. SEM images of the cross-section and the outer surface of the hollow fiber membranes. Arrows represent the stretching direction during hollow fiber formation.

fiber, respectively [23, 32-34]. In general, the conclusions drawn from the digital and optical images about the microstructured shape of the prepared hollow fibers agree with those of the SEM cross-section and outer surfaces images at low magnification (x200). All SEM surface images at high magnification (x10,000), except the membrane CSN, show an axial stretched morphology in the spinning direction that is associated to the nascent fiber elongation when using gap distance and/or take-up speed. For the membrane CSN, the axial stretching due to the gap distance and take-up speed is counteracted by the normal pressure exerted by the micro-jets on the outer surface of the nascent hollow fiber membrane.

The cross-section of the hollow fiber membranes presented different shape outer structures according to the applied spinning operating type. Table 4.3 summarizes the determined values of the parameters H_c and SAE from the SEM cross-section images of the hollow fibers. As it can be seen in Fig. 4.5, the outer surface of the membrane CL is completely circular (i.e. zero H_c and SAE), whereas all other hollow fibers (SL and CSN) show corrugated external contours. Both H_c and SAE values of the membrane CSN are larger than those of the membrane SL-ref (see Table 4.3). A convex corrugation curvature is observed for the membrane SL-ref according to the star-shaped orifice of the spinneret, while that for the membrane CSN is concave. The corrugation of the hollow fiber CSN was induced by water that was sprayed on the outer layer of the nascent fiber pressing inwards the wall of the polymeric membrane. This explains the irregular shape of the observed corrugations and their concave curvature on the surface of the CSN hollow fiber membrane. By SEM analysis at x10,000 magnification of the outer surface of this membrane, a highly rough surface was observed. Some surface areas with more porous structures were also detected. These correspond to the border of the tracks of the water micro-jets left on the outer surface of the hollow fiber along the gap distance.

The outer surfaces (x200 images) of the hollow fiber membranes prepared with the star-shaped spinneret under the largest and medium gap length (i.e. SL-ref and SL-1) are similar with several wrinkles along the spinning direction. However, the wrinkles of the fiber SL-1 are more pronounced due to the lower fiber stretching associated to the smaller gap distance compared to the membrane SL-ref. From the cross-section images of these membranes, similar SAE but higher H_c values were obtained with the reduction of the gap distance (see Table 4.3). However, as it was expected after analyzing the digital and optical images, the gap distance suppression provided a rounded hollow fiber cross-section (see SL-2 membrane in Fig. 4.5 and the low H_c and SAE values of the SL-2 membrane in Table 4.3).

Compared to the SL-ref hollow fiber membrane, the lower external coagulant flow rate applied to prepare the SL-3 membrane induced the largest corrugations (i.e. a flower-shaped microstructure with deepest channels as it can be seen in Fig. 4.5 and the highest H_c and SAE values as shown in Table 4.3, 61 μm and 17.7%, respectively).

The H_c values obtained in this study (Table 4.3) can be compared with the parameter R_z (i.e. height between the peak and the valley of a corrugation) of the microfluidic-fabricated PES hollow fiber membranes by Deng et al. [19] also determined from the SEM images. The R_z value of the PES hollow fiber prepared at 25 °C (i.e. 6.28 μm) was similar to the H_c value obtained for the hollow fiber SL-2 but much lower than the H_c data of the other prepared PVDF-HFP hollow fiber membranes. However, the R_z value of the PES hollow fiber prepared at 40 °C (i.e. 84.52 μm) was significantly greater than the highest H_c value registered in this study (see membrane SL-3 in Table 4.3). Furthermore, Deng et al. [19] indicated that other authors [35, 36] defined the corrugated character of the outer surface of the hollow fiber membrane to have R_z value equal or higher than 3.2 μm. Based on this definition, the external surfaces of all the hollow fibers prepared in this study (except the membrane CL) can be classified as corrugated.

Çulfaz et al. [17] reported *SAE* values for the PES hollow fibers between 27 and 89% for air gap lengths ranging from 38 to 5 mm, respectively. However, these hollow fiber membranes exhibited dense outer skin-layers and compact cross-section structures (i.e. not highly porous). The observed greater *SAE* values and the morphological characteristics of these hollow fibers were due to the high viscosity of the used spinning solutions as it was previously mentioned. The morphological structures of the PVDF-HFP hollow fiber membranes prepared in the present study were significantly porous and the dense skin-layer formation at the outer layer was reduced due to the applied wet gap type [37].

4.3.1.3 AFM analysis of the outer surfaces

As it was stated previously, the outer surfaces of all prepared hollow fiber membranes were analyzed by AFM. Figure 4.6 shows the images obtained by means of the optical microscope incorporated to the AFM system. The white rectangle drawn on each image indicates the scanned region of the membrane surface the AFM tip. The double arrow inside the rectangle represents the AFM scanning direction (i.e. perpendicular to the spinning direction). The AFM tip could not reproduce completely the membrane surface corrugation when the differences in height were greater than 6 μm (i.e. Z limit). This means that only the top of the corrugation was scanned and consequently it was impossible to analyze two consecutive corrugations via this technique because the Z limit was exceeded. Therefore, the AFM scanning length could not be longer than the width of the primary corrugation and a scanning length of 75 μm was used to analyze all samples.

The 3D AFM images of the external surfaces of the hollow fiber membranes are also shown in Fig. 4.6. The type of curvature and the Z range of the membrane surfaces can be determined from these images. As it was expected and observed from SEM cross-section images (Fig. 4.5), all membrane surfaces show a convex curvature except that of the hollow

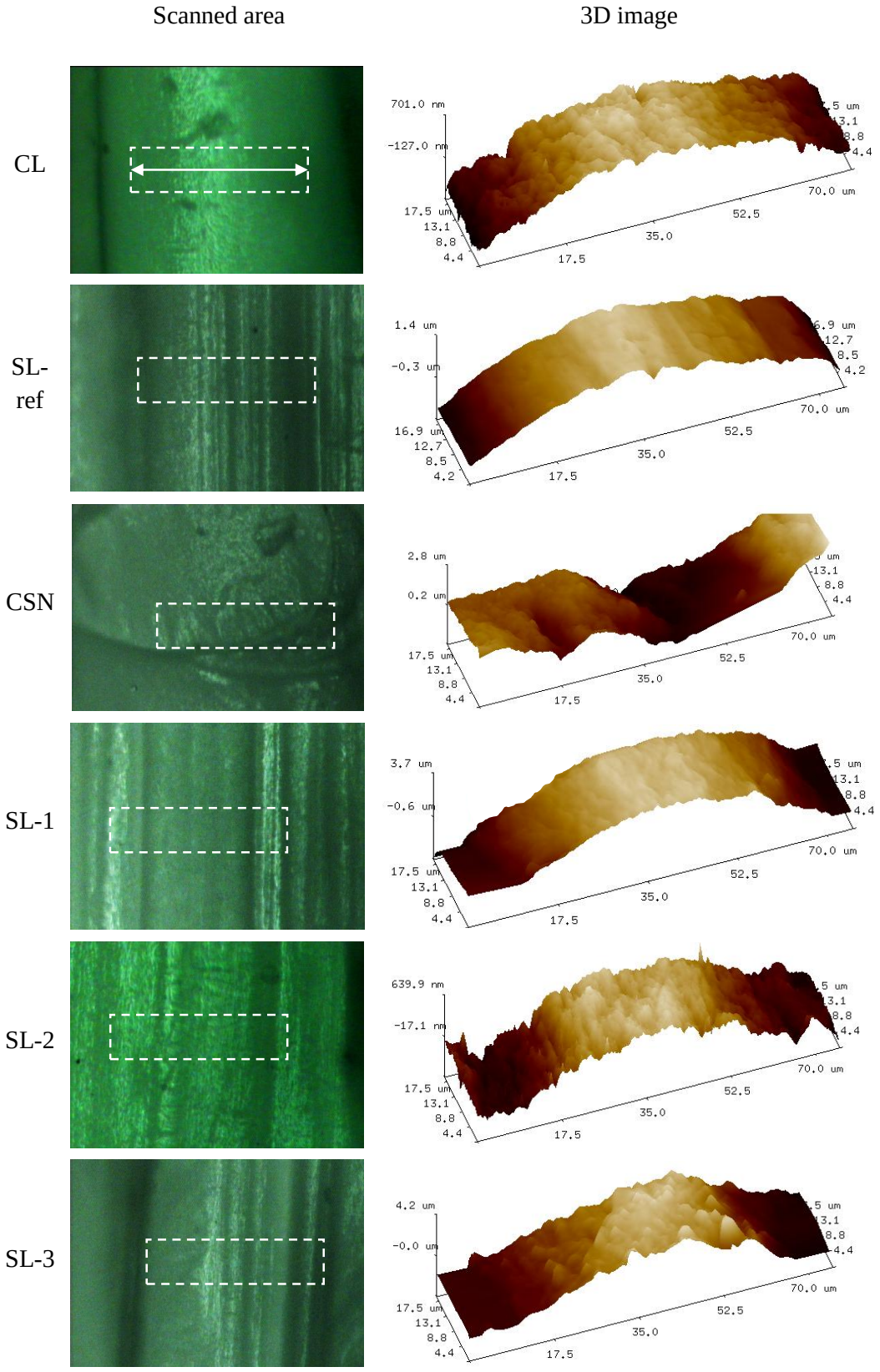

Fig. 4.6. Optical visualization of the AFM scanned areas and 3D AFM images of the outer surfaces of the hollow fiber membranes.

fiber CSN, which is concave. Table 4.4 summarizes the obtained parameters from AFM analysis. The data of the Z range indicate that the membranes CL and SL-2 are extremely flat (i.e. very low Z range) compared to the other corrugated hollow fiber membranes. Changing the circular spinneret by the star-shaped one and keeping the gap distance at 0.275 m together with the longitudinal wetting mode, the Z range increased about 2 times for the membrane SL-ref compared to the membrane CL. When the spray wetting mode was used to corrugate the outer layer of the hollow fiber, the resultant Z range was increased further for the membrane CSN. By reducing the gap distance (from 0.275 to 0.115 m) or the external coagulant flow rate, the Z ranges of the membranes SL-1 and SL-3 became 1.90 and 2.03 times greater than that of the membrane SL-ref (see Table 4.4 and Fig. 4.6). The highest Z range of all membranes prepared in this study was obtained for the hollow fiber membrane SL-3. As it was expected, the hollow fiber membrane SL-2, prepared under zero gap distance, was flatter than the rest of the fibers with a similar Z range to that of the membrane CL. All these results were in accordance with those drawn by the digital and optical microscopes as well as the SEM images and their corresponding H_t and *SAE* data. Therefore, the better-defined corrugated outer surfaces with deeper channels have higher Z range values.

Table 4.4. AFM analysis results (*Z* range, surface length difference, *SLD*; bow angle, α; mean roughness, R_a; and maximum roughness, R_{max}) of the outer surface of the hollow fiber membranes (scan range considered 75 μm × 18.75 μm).

Membrane	1st order flattering			2nd order flattering	
	Z range (nm)	***SLD* (%)**	**α (°)**	**R_a (nm)**	**R_{max} (nm)**
CL	1444	0.45 ± 0.02	1.74 ± 0.04	84	617
SL-ref	2623	0.49 ± 0.06	3.45 ± 0.16	93	683
CSN	4454	1.52 ± 0.15	- 4.33 ± 0.17	458	2623
SL-1	4981	3.82 ± 0.17	7.35 ± 0.22	198	1703
SL-2	1409	0.47 ± 0.04	1.49 ± 0.16	101	1103
SL-3	5318	5.50 ± 0.88	9.36 ± 0.53	478	3623

In order to quantify the degree of corrugation of the surfaces, the AFM section analysis was performed for all hollow fiber membranes as stated previously. The parameters *SLD* and α were calculated from the cross-sectional profiles of the outer surfaces shown in Fig 4.7 and the obtained values are summarized in Table 4.4. In accordance with the Z range values, the hollow fibers CSN, SL-1 and SL-3 exhibited a significant perimeter enhancement (i.e. higher *SLD* values). The highest *SLD* value corresponded to the hollow fiber membrane SL-3, which

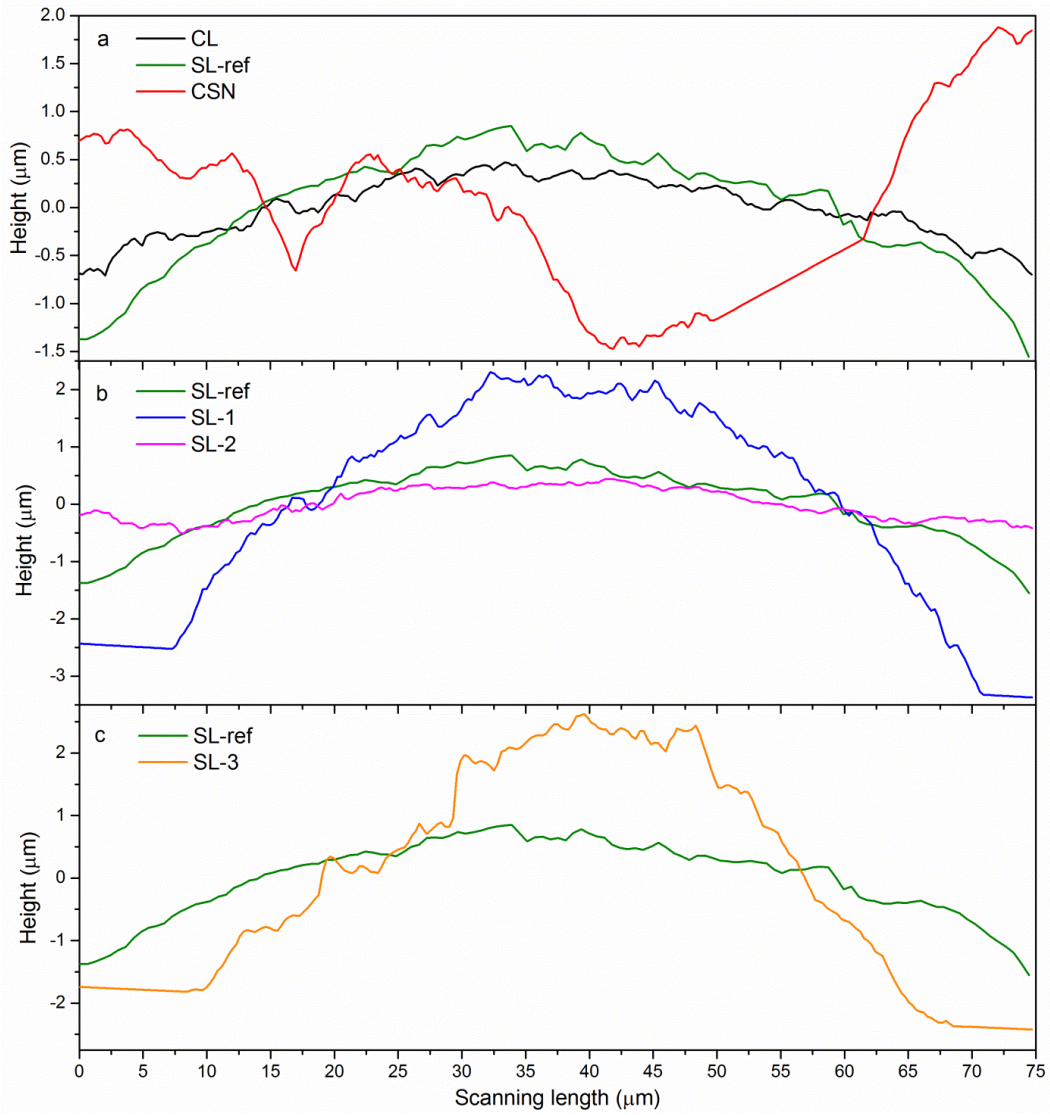

Fig. 4.7. Cross-sectional profile of the outer surface of the hollow fiber membranes: (a) spinning operating type effect, (b) gap distance effect and (c) external coagulant flow rate effect.

increased in more than 12 times respect to that obtained for the CL hollow fiber. It is worth noting that *SLD* is related to the external surface area enhancement (*SAE*) of the hollow fiber obtained from SEM images, but it is referred only to the top of the corrugation.

The bow angles of the corrugations formed on the outer surface of the hollow fiber membranes were all positive (i.e. convex curvature), except that of the membrane CSN, which was negative according to its concave curvature (see Fig. 4.7). By changing the spinning operating type of the hollow fiber from circular to corrugated shape, the absolute bow angle increased following the same tendency of the Z ranges: CL < SL-ref < CSN. The curvature of the corrugations increased significantly by reducing the gap distance (i.e. compare α of the membranes SL-ref and SL-1 in Table 4.4) whereas it decreased with the total suppression of

the gap (see α of the hollow fiber SL-2 in Table 4.4) obtaining a similar angle to the circular-shaped hollow fiber (membrane CL). This low angle means that the outer surface of the membrane SL-2 was almost flat with insignificantly corrugations (i.e. similar surface to that obtained for the hollow fiber CL). As it was expected, the hollow fiber membrane with the biggest corrugations (i.e. SL-3 membrane) exhibited the greatest bow angle. Corrugations with greater bow angles could act as micro-turbulence promoters for DCMD experiments.

The roughness of the external surface of the prepared hollow fiber membranes are also presented in Table 4.4. In general, rough surfaces were obtained as a result of wetting the external layer of the nascent hollow fiber along the gap distance or when the hollow fibers were prepared without gap (i.e. wet spinning technique). In this case, the swollen fiber at the exit of the spinneret due to the die-swell phenomenon was quickly coagulated by a strong coagulant forming wrinkled outer surface structure [22, 38]. The membrane SL-1 exhibited a higher mean roughness than that of the membrane SL-ref. This is due to the fact that the shorter gap distance reduced the elongation stress caused by the gravity force leading to a rougher outer surface [21, 39]. The outer surfaces with the greatest R_a values corresponded to the hollow fiber membranes CSN and SL-3. As it was explained earlier, the higher roughness of the membrane CSN was the result of the surface disturbances induced by the water spraying micro-jets on the outer surface of the nascent fiber, while the low external coagulant flow rate permitted to maintain the shape of the corrugation and its roughness. As it can be seen in Table 4.4, the maximum roughness parameter (R_{max}) of the prepared hollow fiber membranes follows the same trend as that observed for R_a, leading to a wider intrinsic roughness range for the CSN and SL-3 membranes.

4.3.2 DCMD performance

DCMD experiments were carried out using all prepared hollow fiber membranes in order to analyze the effect of the corrugations of the outer surface on the membrane performance. The obtained permeate fluxes (J) are shown in Fig. 4.8(a). As it was expected, for all membranes the permeate flux decreased when NaCl salt was added in the feed aqueous solution. This is due to the decrease of the water vapor pressure of the feed solution (i.e. reduction of the vapor pressure difference through the membrane). All membranes proved to be highly selective to the NaCl salt since the rejection factors were greater than 99.9%. It is worth quoting that the reported DCMD permeate fluxes of the PVDF-HFP hollow fiber membranes are lower than those obtained for the PVDF-HFP hollow fibers prepared in this study, even when using a wet gap instead of an air gap during membrane preparation [23, 37, 40-42].

Figure 4.8(a) shows that the corrugated shape of the outer surface of the hollow fibers enhanced significantly the DCMD permeate flux (except the membrane SL-2). For each

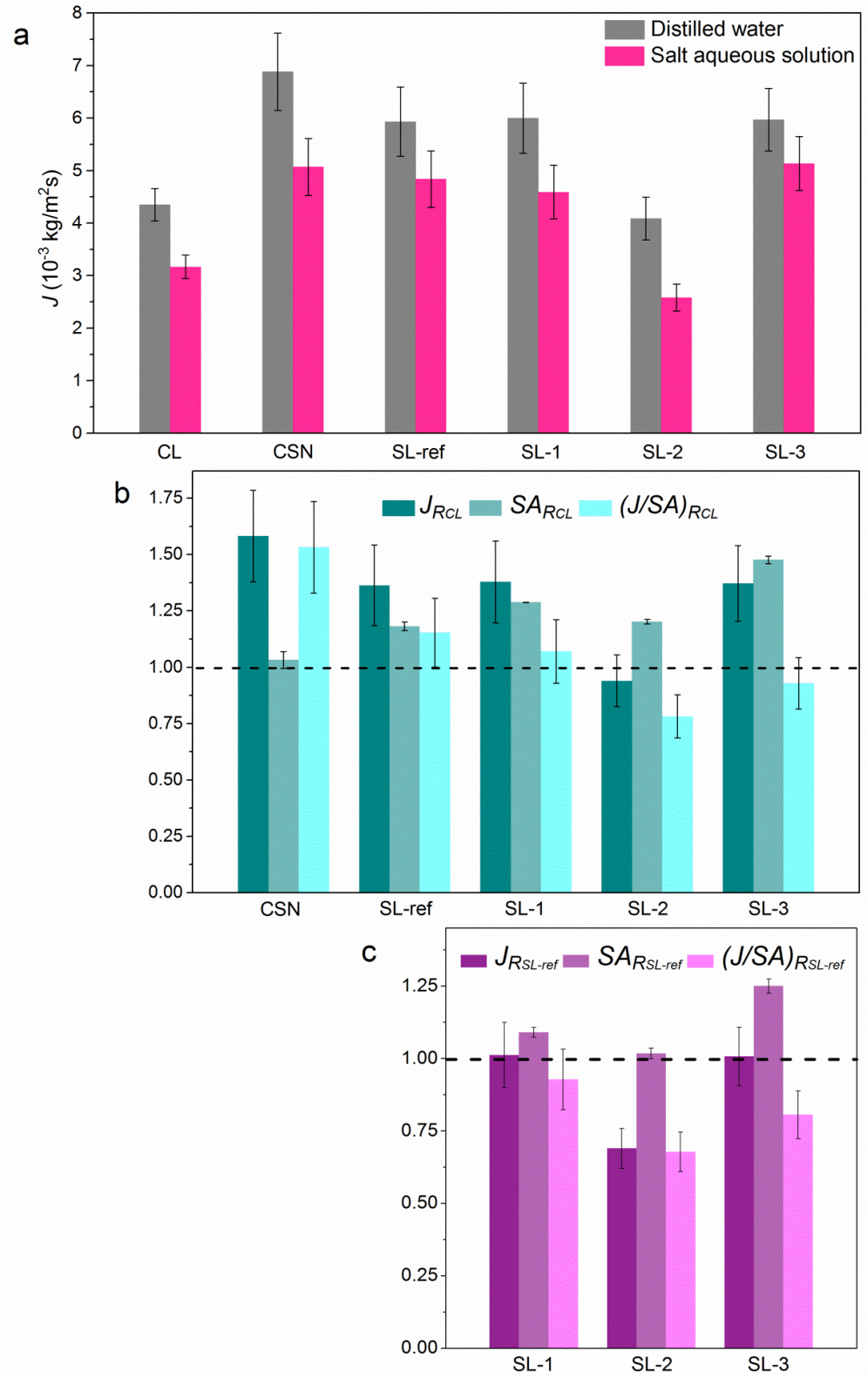

Fig. 4.8. (a) DCMD permeate flux (J) of the prepared hollow fiber membranes. Permeate flux ratio (J_R), external surface area ratio (SA_R) and $(J/SA)_R$ respect to the hollow fiber membrane CL (b) and SL-ref (c).

membrane, two modules were tested and the plotted resultant permeate flux was the corresponding average value together with its standard deviation. The permeate fluxes of the corrugated membranes SL-ref and CSN were, respectively, 36% and 58% higher than that of the original circular hollow fiber CL, when distilled water was used as feed. This DCMD improvement could be due to the enhancement of the cooling surface area, which resulted in a greater surface area available for vapor condensation (see *SAE* in Table 4.3) and to the reduction of the temperature polarization (TP) effect attributed to the micro-turbulences generated by the corrugations in the permeate side of the membrane (see H_c and α parameters in Tables 4.3 and 4.4). In addition, the roughness of the outer surface of the membrane might also contribute to the TP reduction effect, but to less extent compared to the corrugation size effect. It was observed that the increase of the permeate flux agreed well with the noticeable increase of the absolute value of the bow angle, α, and the H_c value as well as with the increase of the *SAE* value (i.e. CL < SL-ref < CSN). The other parameters (*SLD*, R_a and R_{max}) were significantly higher for the hollow fiber membrane CSN but were almost equal for the membranes CL and SL-ref.

Figure 4.8(a) also shows the gap distance and the external coagulant effects on the DCMD permeate flux when the star-shaped spinneret was used to induce corrugations on the outer surface of the membrane. The permeate flux decreased when the gap distance was suppressed due to the reduction of the corrugation size (i.e. the permeate flux of the membrane SL-2 was reduced by 31% compared to the membrane SL-ref, see Fig. 4.8(a) for distilled water as feed). The permeate flux of the hollow fiber membrane SL-2 was almost the same as that of the circular-shaped fiber CL if the standard deviations were considered. This was in accordance with the results obtained from the SEM images and AFM analysis as summarized in Tables 4.3 and 4.4 (i.e. compare H_c, *SAE*, Z range, *SLD*, α and R_a of the membranes SL-2 and CL).

The DCMD permeate flux of the hollow fiber membrane SL-ref was similar to that of the membranes SL-1 and SL-3, as it can be seen in Fig. 4.8(a). However, it was expected to obtain better permeate fluxes for the hollow fiber membranes SL-1 and SL-3 as a result of their larger corrugations observed at the outer surface of these membranes. All the parameters that defined the corrugation of the outer surface, both those obtained from the SEM images (i.e. H_c, *SAE*) and those obtained from the AFM analysis (i.e. Z range, *SLD*, α, R_a and R_{max}) were significantly higher for the hollow fiber membranes SL-1 and SL-3 than those of the membrane SL-ref (see Tables 4.3 and 4.4). Furthermore, for the hollow fiber membrane SL-3 these parameters were higher than those of the membrane CSN, which exhibited higher permeate flux (i.e. the greatest MD performance in this study and those reported so far for PVDF-HFP hollow fiber membranes).

As it was mentioned previously, the DCMD improvement could be due to the enhancement of the cooling surface area and to the reduction of the TP effect attributed to the micro-turbulences generated by the corrugations of the outer side of the membrane. It is worth quoting that the permeate flux, *J*, was calculated per unit of the internal membrane area brought into contact with the feed solution. In order to analyze whether the corrugation of the external surface of the hollow fiber or the simple increase of the external surface area improved or not the DCMD performance, the following factors were calculated to take into account the effect of the external surface enhancement on the permeate flux. The permeate flux ratio of distilled water used as feed, $J_R = J_{corrugated}/J_i$, the ratio of the external surface area, $SA_R = SA_{corrugated}/SA_i$ and the ratio $(J/SA)_{Ri}$ were calculated respect to the permeate flux and surface area of the membrane CL used as reference (i.e. subscript i = CL). The results were plotted in Fig. 4.8(b). The permeate flux ratio respect to the membrane CL (J_{RCL}) of the corrugated membranes, except the membrane SL-2, were higher than one. However, the ratio of the external surface area (SA_{RCL}) was greater than one for all hollow fibers prepared with star-shaped spinneret and almost unity for the membrane CSN prepared with circular-shaped spinneret. Therefore, it can be stated that the star-shaped spinneret induces an enhancement of the surface cooling area, which results in an increase of the condensation rate of the generated water vapor molecules at the feed/membrane interface, whereas the spray wetting mode does not improve the surface cooling area respect to the membrane CL. The $(J/SA)_{RCL}$ value represents the improvement of the DCMD permeate flux with respect to the membrane CL, when the external surface area is taken into account. Therefore, this parameter is related to the corrugation acting as micro-turbulence promoters that reduces the TP effect and not to the simple increase of the condensation surface area (i.e. *SAE*). As it can be seen in Fig. 4.8(b), the highest $(J/SA)_{RCL}$ value was obtained for the membrane CSN, indicating that the main factor improving the DCMD permeate flux of the membrane CSN was due to the micro-turbulences induced by the corrugation. For the hollow fiber membranes SL-ref and SL-1, both the micro-turbulence effect and the increase of the surface area (i.e. *SAE*) improved the DCMD permeate flux. However, for the hollow fiber membranes SL-2 and SL-3, the *SAE* was the main factor affecting J_{RCL} value while the corrugation exerted a negative effect on the DCMD permeate flux.

In order to study the effect of the corrugation depth of the SL membranes on the DCMD permeate flux, the same factors were calculated but in this case respect to the membrane SL-ref taken as reference (see Fig. 4.8(c)). The $J_{RSL\text{-}ref}$ values were almost unity, whereas the $SA_{RSL\text{-}ref}$ values were higher than one for the hollow fiber membranes SL-1 and SL-3 indicating that the deeper corrugation did not reduce the TP effect (i.e. $(J/SA)_{RSL\text{-}ref}$ lower

than one in Fig. 4.8(c)). The lowest $(J/SA)_{RSL\text{-}ref}$ value obtained for the hollow fiber membrane SL-2, might be due to the lowest H_c value and the highest dense skin layer of this membrane. In a previous study [37], it was observed that zero gap distance induced lower permeate flux than that of the PVDF-HFP hollow fiber membranes prepared under a wet gap and water as external coagulant.

Hence, it can be confirmed that the TP phenomenon greatly affect the DCMD membrane performance, as described elsewhere [6, 7, 10, 14], and it is the main responsible of the DCMD permeate flux enhancement due to the corrugated outer surfaces of the hollow fiber membranes prepared in this study.

Yang et al. [15] analyzed the effect of the gear-shaped microstructure at the outer side of the hollow fiber membrane on the DCMD membrane productivity (in terms of the TP phenomenon) via computational fluid dynamic (CFD) simulations. Based on their drawn conclusions the DCMD results of this study can be explained as follows. Corrugations on the outer surface (i.e. permeate side) of the fiber can act as micro-turbulence promoters [16], developing intense secondary flows along the circulation channel, which enhanced its hydrodynamics. This flow disturbance reduced the thickness of the thermal polarization boundary layer at the external side of the fiber, facilitating the heat transfer [6, 15]. The flow eddies also induced a constant renewal of the permeate liquid at the outermost layer of the hollow fiber, which decreased the buildup rate of the boundary layer along the permeate circulation direction, as it was observed by Yang et al. [15]. The thinner polarization boundary layer led to reach a lower temperature at the outer surface of the hollow fiber increasing the DCMD driving force [10].

The surfaces with a convex curvature as well as high H_c, α and Z range exhibited deep valleys (i.e. V-shaped valleys) between two consecutive big corrugations. These higher H_c values may induce a better-defined microscopic velocity profile of the permeate circulation on the corrugated outer surface of the fiber. As it can be seen in the qualitative diagram of Fig. 4.9, the maximum velocity corresponds to the peak of the corrugation while the minimum corresponds to the V-shaped valley, according to the hydrodynamics of the corrugated channel. It is well known that lower circulation flow rates reduce the flow micro-turbulences resulting in thicker thermal boundary layers [6, 10]. Consequently, the temperature at the membrane surface may differ from that of the bulk depending on the regions of the hollow fiber (i.e. depending on the boundary layer thickness). In the present case, in the V-shaped valley the TP effect should be greater than at the peak of the corrugation. Both effects can be globally counteracted obtaining similar permeate flux for the membranes SL-1, SL-3 and SL-ref, which might exhibit a more uniform thermal boundary layer at its outer surface due to its small corrugation size. In addition, the lower flow rate at the V-shaped valleys of the

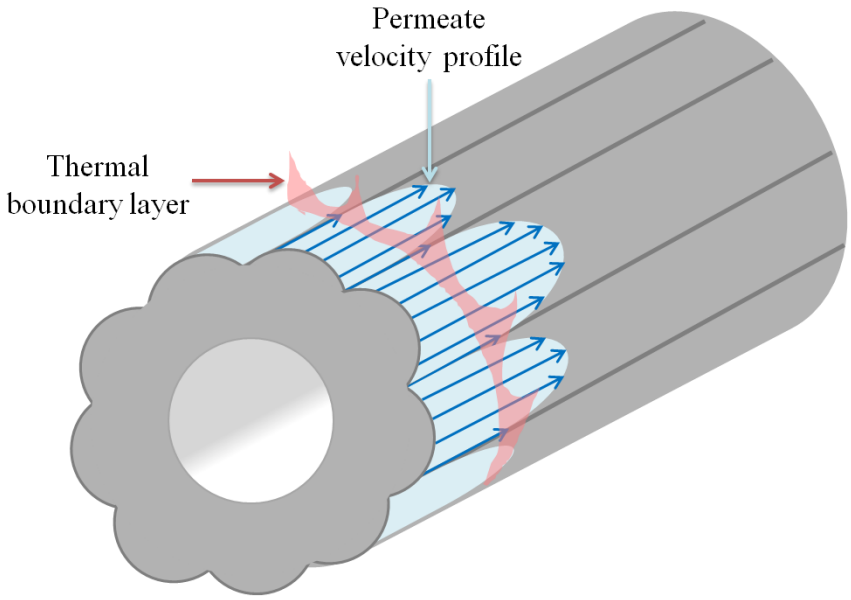

Fig. 4.9. Schema of TP phenomenon in hollow fiber membranes with highly corrugated outer surfaces with V-shaped valleys.

membranes SL-1 and SL-3 may slow down the condensed water vapor dragging at this region of the outer surface. Therefore, despite the significant difference in the corrugations size, the corresponding DCMD permeate fluxes of the prepared hollow fiber membranes SL-ref, SL-1 and SL-3 were similar.

It can be concluded that the corrugations on the outer surface of the hollow fibers acted as micro-turbulence promoters, reducing the TP effect and increasing the DCMD mass transport as consequence. However, corrugations with deeper V-shaped valleys (i.e. H_c values higher than about 30 μm, for the hollow fiber membrane SL-1, H_c = 33.5 ± 0.7 μm) did not always induce an improvement of the DCMD permeate flux.

4.4 Conclusions

PVDF-HFP hollow fiber membranes with corrugated outer surfaces were successfully prepared by wet/wet spinning technique using a micro-engineered spinneret or spraying the external coagulant by micro-jet nozzles on the nascent fiber along gap distance. It was observed considerable changes of the microstructured geometry of the prepared fibers according to different applied spinning parameters such as the spinneret shape, the wetting gap mode (i.e. longitudinal or spray mode), the gap distance and the external coagulant flow rate.

The biggest corrugations and the roughest surface were observed for the hollow fiber membrane SL-3, prepared using the star-shaped spinneret, the longitudinal fiber outer layer wetting mode and the lowest external coagulant flow rate.

Excellent salt rejection factors (i.e. 99.9%) were obtained for all hollow fiber membranes. A significant difference was observed in the DCMD permeate flux obtained for the hollow fibers prepared with different spinning operating types (i.e. CL < SL-ref < CSN). However, no improvement was obtained for the DCMD performance of the hollow fibers prepared under different gap distances or by changing the external coagulant flow rate (i.e. SL membranes).

The permeate flux was affected by the corrugation size and shape. The corrugations enhanced the external effective surface area of the fibers available for water vapor condensation and act as micro-turbulence promoters mitigating the TP effect and improving the DCMD mass transport as consequence. However, large corrugations with deep V-shaped valleys (i.e. H_t values higher than about 30 μm) did not always induce an improvement of the DCMD permeate flux.

The fiber CSN, prepared by spraying the external coagulant on the nascent fiber using micro-jet nozzles along gap distance, exhibited a highly corrugated outer surface with the most irregular microstructure and provided the highest DCMD permeate flux in this study, which is also higher than the permeate fluxes of the PVDF-HFP hollow fiber membranes prepared so far for MD.

References

[1] M. Khayet, T. Matsuura, Membrane Distillation. Principles and Applications, Elsevier, The Netherlands (2011).

[2] Y. Zhang, Y. Peng, S. Ji, Z. Li, P. Chen, Review of thermal efficiency and heat recycling in membrane distillation processes, Desalination 367 (2015) 223-239.

[3] P. Wang, T.S. Chung, Recent advances in membrane distillation processes: Membrane development, configuration design and application exploring, J. Membr. Sci. 474 (2015) 39-56.

[4] L. García-Fernández, M. Khayet, M.C. García-Payo, Membranes used in membrane distillation: preparation and characterization, Elsevier (Woodhead Publishing), Cambridge (2015) 317-359.

[5] M. Khayet, Membranes and theoretical modeling of membrane distillation: a review, Adv. Colloid Interface Sci. 164 (2011) 56-88.

[6] Y.M. Manawi, M.A.M.M. Khraisheh, A.K. Fard, F. Benyahia, S. Adham, A predictive model for the assessment of the temperature polarization effect in direct contact membrane distillation desalination of high salinity feed, Desalination 341 (2014) 38-49.

[7] R.W. Schofield, A.G. Fane, C.J.D. Fell, Heat and mass transfer in membrane distillation, J. Membr. Sci. 33 (1987) 299-313.

[8] L. Martínez-Díez, M.I. Vázquez-González, F.J. Florido-Díaz, Temperature Polarization Coefficients in Membrane Distillation, Sep. Sci. Technol. 33 (1998) 787-799.

[9] L. Martínez-Díez, M.I. Vázquez-González, Temperature and concentration polarization in membrane distillation of aqueous salt solutions, J. Membr. Sci. 156 (1999) 265-273.

[10] A. Ali, F. Macedonio, E. Drioli, S. Aljlil, O.A. Alharbi, Experimental and theoretical evaluation of temperature polarization phenomenon in direct contact membrane distillation, Chem. Eng. Res. Des. 91 (2013) 1966-1977.

[11] L. Martínez-Díez, M.I. Vázquez-González, F.J. Florido-Díaz, Study of membrane distillation using channel spacers, J. Membr. Sci. 144 (1998) 45-56.

[12] L. Martínez, J.M. Rodríguez-Maroto, On transport resistances in direct contact membrane distillation, J. Membr. Sci. 295 (2007) 28-39.

[13] J.A. Kharraz, M.R. Bilad, H.A. Arafat, Flux stabilization in membrane distillation desalination of seawater and brine using corrugated PVDF membranes, J. Membr. Sci. 495 (2015) 404-414.

[14] X. Yang, R. Wang, A.G. Fane, Novel designs for improving the performance of hollow fiber membrane distillation modules, J. Membr. Sci. 384 (2011) 52-62.

[15] X. Yang, H. Yu, R. Wang, A.G. Fane, Optimization of microstructured hollow fiber design for membrane distillation applications using CFD modeling, J. Membr. Sci. 421-422 (2012) 258-270.

[16] W. Nijdam, J. Dejong, C. Vanrijn, T. Visser, L. Versteeg, G. Kapantaidakis, G. Koops, M. Wessling, High performance micro-engineered hollow fiber membranes by smart spinneret design, J. Membr. Sci. 256 (2005) 209-215.

[17] P.Z. Çulfaz, E. Rolevink, C. van Rijn, R.G.H. Lammertink, M. Wessling, Microstructured hollow fibers for ultrafiltration, J. Membr. Sci. 347 (2010) 32-41.

[18] N. Widjojo, T.S. Chung, Thickness and air gap dependence of macrovoid evolution in phase-inversion asymmetric hollow fiber membranes, Ind. Eng. Chem. Res. 45 (2006) 7618-7626.

[19] K. Deng, Z. Liu, F. Luo, R. Xie, X.H. He, M.Y. Jiang, X.J. Ju, W. Wang, L.Y. Chu, Controllable fabrication of polyethersulfone hollow fiber membranes with a facile double co-axial microfluidic device, J. Membr. Sci. 526 (2017) 9-17.

[20] P.Z. Çulfaz, M. Haddad, M. Wessling, R.G.H. Lammertink, Fouling behavior of microstructured hollow fibers in cross-flow filtrations: Critical flux determination and direct visual observation of particle deposition, J. Membr. Sci. 372 (2011) 210-218.

[21] M. Khayet, The effects of air gap length on the internal and external morphology of hollow fiber membranes, Chem. Eng. Sci. 58 (2003) 3091-3104.

[22] M. Khayet, M.C. García-Payo, F.A. Qusay, M.A. Zubaidy, Structural and performance studies of poly(vinyl chloride) hollow fiber membranes prepared at different air gap lengths, J. Membr. Sci. 330 (2009) 30-39.

[23] L. García-Fernández, M.C. García-Payo, M. Khayet, Effects of mixed solvents on the structural morphology and membrane distillation performance of PVDF-HFP hollow fiber membranes, J. Membr. Sci. 468 (2014) 324-338.

[24] H.A. Tsai, D.H. Huang, S.C. Fan, Y.C.Wang, C.L. Li, K.R. Lee, J.Y. Lai, Investigation of surfactant addition effect on the vapor permeation of aqueous ethanol mixtures through polysulfone hollow fiber membranes, J. Membr. Sci. 198 (2002) 245-258.

[25] M. Khayet, M.V. Álvarez, K.C. Khulbe, T. Matsuura, Preferential surface segregation of homopolymer and copolymer blend film, Surf. Sci. 601 (2007) 885-895.

[26] M. Khayet, Membrane surface modification and characterization by X-ray photoelectron spectroscopy, atomic force microscopy and contact angle measurements, Appl. Surf. Sci. 238 (2004) 269-272.

[27] W.A. Gifford, The Effect of Surface Tension on Extrudate Swell From Square and Rectangular Channels, Polym. Eng. Sci. 38 (1998) 1167-1173.

[28] C.C. Pereira, R. Nobrega, C.P. Borges, Spinning process variables and polymer solution effects in the die-swell phenomenon during hollow fiber membranes formation, Braz. J. Chem. Eng. 17 (2000) 599-606.

[29] E. Mitsoulis, G.C. Georgiou, Z. Kountouriotis, A study of various factors affecting Newtonian extrudate swell, Comput. Fluids 57 (2012) 195-207.

[30] P.Z. Çulfaz, M. Wessling, R.G.H. Lammertink, Hollow fiber ultrafiltration membranes with microstructured inner skin, J. Membr. Sci. 369 (2011) 221-227.

[31] Y. Santoso, T. Chung, K. Wang, M. Weber, The investigation of irregular inner skin morphology of hollow fiber membranes at high-speed spinning and the solutions to overcome it, J. Membr. Sci. 282 (2006) 383-392.

[32] M. Khayet, C.Y. Feng, K.C. Khulbe, T. Matsuura, Preparation and characterization of polyvinylidene fluoride hollow fiber membranes for ultrafiltration, Polymer 43 (2002) 3879-3890.

[33] Q. Li, Z.L. Xu, M. Liu, Preparation and characterization of PVDF microporous membrane with highly hydrophobic surface, Polym. Adv. Technol. 22 (2011) 520-531.

[34] A. Xu, A. Yang, S. Young, D. deMontigny, P. Tontiwachwuthikul, Effect of internal coagulant on effectiveness of polyvinylidene fluoride membrane for carbon dioxide separation and absorption, J. Membr. Sci. 311 (2008) 153-158.

[35] D.J. Whitehouse, Surfaces and Their Measurement, Hermes Penton Science, London (2004).

[36] D.J. Whitehouse, Handbook of Surface Metrology, Institute of Physics Publishing, Bristol (1994).

[37] L. García-Fernández, M.C. García-Payo, M. Khayet, Mechanism of formation of hollow fiber membranes for membrane distillation: 2. Outer coagulation power effect on morphological characteristics, J. Membr. Sci. http://dx.doi.org/10.1016/j.memsci.2017.03.038 (2017).

[38] T.S. Chung, E.R. Kafchinski, The effects of spinning conditions on asymmetric 6FDA/6FDAM polyimide hollow fibers for air separation, J. Appl. Polym. Sci. 65 (1997) 1555-1569.

[39] K.C. Khulbe, C.Y. Feng, F. Hamad, T. Matsuura, M. Khayet, Structural and performance study of micro porous polyetherimide hollow fiber membranes prepared at different air-gap, J. Membr. Sci. 245 (2004) 191-198.

[40] M. Khayet, C. Cojocaru, M. Essalhi, M.C. García-Payo, P. Arribas, L. García-Fernández, Hollow fiber spinning experimental design and analysis of defects for fabrication of optimized membranes for membrane distillation, Desalination 287 (2012) 146-158.

[41] M.C. García-Payo, M. Essalhi, M. Khayet, L. García-Fernández, K. Charfi, H. Arafat, Water desalination by membrane distillation using PVDF-HFP hollow fiber membranes, Membr. Water Treat. 1 (2010) 215-230.

[42] L. García-Fernández, M.C. García-Payo, M. Khayet, Mechanism of formation of hollow fiber membranes for membrane distillation: 1. Inner coagulation power effect on morphological characteristics, J. Membr. Sci. http://dx.doi.org/10.1016/j.memsci.2017.03.036 (2017).

5

Ceramic hollow fiber membranes:

Various spinning parameters effects on the structural properties and MD performance

Alumina hollow fiber membranes were prepared by the phase inversion technique under different spinning conditions in order to induce various types of structural morphologies. In the membrane fabrication process, the studied parameters were the polymer concentration in the inorganic suspension and its flow rate, the gap distance, the bore liquid, the outer coagulant composition and their flow rates. After sintering, the hollow fibers were chemically modified by grafting (1H,1H,2H,2H-perfluorodecyltriethoxysilane) rendering them hydrophobic for their use in membrane distillation (MD) process. The effects of the membrane morphology on the obtained MD membrane characteristics and on air gap membrane distillation (AGMD) desalination performance were studied in order to figure out the most promising structure for MD. The suitability of alumina hollow fibers for AGMD was confirmed by various membrane characterization techniques. In general, the membranes prepared with lower polymer concentration in the inorganic suspension exhibited higher AGMD performance (i.e. higher permeate flux with a smaller flux reduction factor and a good salt rejection factor). Among all prepared hollow fiber membranes prepared in this study, the one with the largest micro-channel structure exhibited the best AGMD performance, even better than all hydrophobic ceramic membranes used so far in desalination by AGMD and DCMD.

Morphological design of alumina hollow fiber membranes for desalination by air gap membrane distillation

5.1 Introduction

Water desalination by membrane distillation (MD) is an environmentally-friendly alternative able to tackle the global water scarcity issue in combination with other water treatment techniques [1-3]. MD process can be used to produce not only distilled water but also ultrapure water, and stands out for its capability to treat concentrated salt aqueous solutions [3-5]. Porous hydrophobic membranes are used in this non-isothermal process in which the driving force for the mass transfer is the transmembrane vapor pressure.

The majority of MD studies were performed with membranes made from hydrophobic polymers such as polyvinylidenefluoride (PVDF), polypropylene (PP) and polytetrafluoroethylene (PTFE) [5]. Ceramic membranes can endure harsh environments, opening up the possibility of treating a broader variety of feed solutions and operating conditions [6-9]. It is well known that the superior structural, thermal and chemical characteristics of these membranes, facilitate membrane cleaning process after fouling without reducing the membrane properties and maintain its lifetime as consequence reducing therefore the membrane´s replacement cost [10]. In spite of the excellent thermochemical stability of ceramic membranes, these are seldom explored for MD applications, mainly due to their hydrophilic nature. In other words, ceramic membranes cannot be used directly in MD, but are rendered hydrophobic by surface modification using diverse agents and techniques as described elsewhere [11].

Different inorganic membranes of metal oxides (i.e. alumina, zirconia and titania) and non-oxides (i.e. silicon nitride) were used in desalination by MD. Research studies with commercial ceramic membranes have been carried out analyzing different properties such as the pore diameter of the zirconia layer on the microporous alumina tubular support [12], the grafting efficiency in terms of hydrophobic stability of the tubular titania membrane with time [13] and the effect of modifying agent type on alumina anodisc^{TM} membranes [14]. Other research studies have been devoted to the preparation of ceramic membranes with different inorganic

suspension compositions in order to perform the most promising one in MD [8, 15, 16]. Das et al. [15] studied the effect of the clay/alumina suspension proportions on the characteristics of the capillary membranes. By means of rheological properties, Zhang et al. [8] and Wang et al. [16] analyzed first the stability of silicon nitride and β-Sialon suspensions, respectively. Then, other parameters such as the powder/polymer binder ratio of the silicon nitride hollow fiber membranes and the β-Sialon hollow fiber composition and sintering temperature were investigated looking for the suitable properties of an MD membrane.

Other researches using ceramic membranes focused on the study of the effects of the MD operation parameters (i.e. sodium chloride concentration of the feed aqueous solution, feed and permeate temperatures and flow rates) [12, 17] and the different MD configurations (i.e. air gap membrane distillation (AGMD), direct contact membrane distillation (DCMD) and vacuum membrane distillation (VMD)) [8, 16, 18] on the desalination efficiency. In all cases, compared to the other MD configuration the VMD permeate flux was the highest. Zhang et al. [8] found a significant difference between VMD and DCMD permeate fluxes of the grafted silicon nitride hollow fiber membranes mainly due to the temperature polarization effect. Wang et al. [16] managed to reduce this difference by using β-Sialon ceramic membranes with a lower thermal conductivity, but VMD flux remained the highest. In VMD configuration, the mass transfer resistance is reduced due to the air removal from the membrane pores and the conductive heat loss through the membrane is the smallest compared to the other MD configurations. However, this configuration is not very attractive from an industrial point of view since external condensers are necessary to collect the distillate outside the membrane module, complicating in this way the system assembly and increasing the operational cost [4]. Cerneaux et al. [18] also compared the VMD and DCMD permeate fluxes of the zirconia tubular membranes with those of AGMD configuration. In AGMD configuration, as a consequence of the high thermal conductivity of ceramic materials, the temperature at the permeate side of the membrane is higher than that registered when using polymeric membranes with lower thermal conductivity. However, owing to the low thermal conductivity of the air gap, the temperature of the condensing surface is kept low, leading to a higher effective temperature gradient than that observed in DCMD when using ceramic membranes and comparatively better water production rates are obtained in AGMD. In addition to the lower heat transfer by conduction through the membrane in AGMD than in DCMD [4], other advantage of AGMD is the less risk of membrane pore wetting [12]. Nevertheless, the ceramic membranes used so far in MD showed very low AGMD permeate fluxes [12, 13, 15, 17, 18].

It is worth quoting that very few MD studies have been performed in desalination by ceramic hollow fiber membranes. However, it is important to emphasize the competitive interest of this membrane configuration against tubular, capillary or flat-sheet due to its higher packing density in modules (i.e. up to 9000 m^2/m^3) [19, 20]. Among the proposed ceramic

membrane materials, alumina is the most commonly used one because of its chemical and mechanical stability as well as its wide availability and low cost.

The morphological characteristics of the membranes play a key role in MD performance [21-23]. However, the effect of the membrane morphology on MD performance has not been thoroughly studied yet for ceramic membranes. As such, this work is focused on the preparation of alumina hollow fiber membranes with different morphological designs in order to figure out the suitable structure inducing better AGMD performance. It will be shown through proper structural morphologies that ceramic hollow fiber membranes have the potential to obtain high permeation flux competitive in desalination when using AGMD process.

5.2 Experimental

5.2.1 Materials

Aluminium oxide powders (Al_2O_3 Powder, Ultra-Pure Grade, 99.99%) with an average particle size of 0.5 – 1.0 μm were purchased from Inframat® Advanced Materials™. The polymeric binder was polyethersulfone (PESf, Radel A-300, Solvay Advanced Polymers GmbH, Dusseldorf, Germany). The additive was Arlacel P135 (polyethylene glycol 30-dipolyhydroxystearate, Uniqema, Wilton, UK). The solvent N-Methyl-2-pyrrolidone (NMP, GPR RECTAPUR, VWR Chemicals), ethanol (VWR Chemicals) and deionized (DI) water were used as coagulants. The grafting solution consists of 1H,1H,2H,2H-Perfluorodecyltriethoxysilane (97%, Sigma-Aldrich) and methanol (HiPerSolv CHROMANORM, VWR Chemicals). POREFIL® (Porometer) and isopropyl alcohol (IPA, Sigma-Aldrich Chemical) were the wetting liquids used for the gas-liquid displacement test and the void volume fraction measurement, respectively. The feed salt aqueous solutions of AGMD experiments were composed by sodium chloride (NaCl), which was purchased from Scharlab.

5.2.2 Preparation of alumina hollow fiber membranes

First, the spinning suspensions were prepared by dissolving 0.42 wt% of the dispersant (Arlacel P135) in 35.75 wt% of solvent (NMP) and then, the 63.83 wt% of aluminium oxide powder was added to the mixture. In order to obtain a good inorganic dispersion, the mixture was ball milled (SFM-1 Desk Top Planetary Ball Miller, MTI Corportation) with 40 zirconia milling balls of 8-mm for 7 days. Subsequently PESf was added in two different concentrations, 6 wt% (PESf/alumina ratio = 1/10, low polymer concentration, LP) and 10.6 wt% (PESf/alumina ratio = 1.9/10, high polymer concentration, HP). After the addition of

Table 5.1. Spinning parameters of alumina hollow fiber membranes.

Inorganic suspension (IS)	Membrane	IS flow rate (ml/min)	Bore liquid (BL)	BL flow rate (ml/min)	Outer coagulant (OC)	OC flow rate (ml/min)	Gap distance (cm)
LP	LP1	15	DI water	10	N.A.	N.A.	0
	LP2	8	DI water	10	Ethanol/NMP (50/50 wt%)	4	5
	LP3	8	DI water	15	Ethanol/NMP (50/50 wt%)	4	5
	LP4	8	DI water	30	NMP	5	25
HP	HP1	8	DI water	10	Ethanol/NMP (50/50 wt%)	4	5
	HP2	8	DI water	15	Ethanol/NMP (50/50 wt%)	4	5
	HP3	8	Ethanol/NMP (40/60 wt%)	12	N.A.	N.A.	0

PES, LP suspension was milled for a further 24 h and HP for 48 h. Once the homogeneous alumina suspensions were prepared, these were degassed under vacuum (Self-Cleaning Dry Vacuum System™, Model 2025, Welch®) with stirring (yellow^{line}, OST 20 digital, Veriserv) for approximately 3 h, and then transferred to a stainless steel syringe (200 mL). The bore liquid and the outer coagulant solutions were also introduced in stainless steel syringes of 200 mL and 100 mL, respectively. The flow rate of the fluids was controlled by infusion pumps (Harvard Apparatus, PHD 2000 Programmable and Chemyx Inc., Model Nexus 6000). The inorganic suspension, the bore liquid and the outer coagulant were simultaneously extruded vertically through a triple-orifice spinneret with diameters of 0.9, 2.6 and 3.5 mm, and fall into a DI water coagulation bath. The spinning parameters are summarized in Table 5.1. After spinning, the alumina hollow fiber membrane precursors were stored overnight in a DI water bath at room temperature to remove the residual solvent. Then, they were straightened and dried overnight at room temperature before calcination and sintering in air atmosphere (Carbolite RHF 1600 furnace) as follows. The temperature was raised from room temperature to 600 °C at 1 °C/min and kept for 3 h, and then it was increased from 600 °C to the target temperature (1450 °C) at 1 °C/min and hold for 5 h. Finally, it was reduced to room temperature at a rate of 2 °C/min. More details of inorganic suspension preparation and ceramic hollow fiber membrane fabrication can be found in previous studies [9, 24].

5.2.3 Modification of alumina hollow fiber membranes

The prepared ceramic hollow fiber membranes were hydrophilic in nature. For MD applications, these must be modified to become hydrophobic [6, 12]. The used grafting

solution was composed by 2 vol.% of 1H,1H,2H,2H-perfluorodecyltriethoxysilane in methanol [17, 25]. Two stages conformed the experimental procedure: i)- the hollow fibers were soaked in the grafting solution under vacuum (Self-Cleaning Dry Vacuum System™, Model 2025, Welch®) for 30 min, and then dried in air (1 h) and in oven (1 h) (Thermocenter, SalvisLAB, John Godrich); ii)- the hollow fibers were soaked again under vacuum for 15 min and dried in air (1 h) and in oven (1 h).

5.2.4 Characterization of alumina hollow fiber membranes

Both the inner and outer diameters as well as the thickness of the fibers were determined by a digital microscope (VHX, Keyence VH-Z100R) and the corresponding software (VHX-900F).The cross-section morphology together with the internal and the external surfaces structures of the prepared alumina hollow fiber membranes were analyzed by scanning electron microscopy (SEM, Gemini LEO 1525). All the samples were previously coated with gold.

Gas-liquid displacement porometer (Porolux™ 1000, Porometer) was used to determine the bubble pore size, the mean pore size and the smallest pore size of all the prepared hollow fiber membranes. The experimental porometry method was described elsewhere [26-28], Porefil® (Porometer) was used as the wetting liquid and pure nitrogen was the gas employed in this test. The mercury intrusion porosimetry (MIP) technique (Micromeritics AutoPore IV) was employed to obtain the pore size distribution of the membranes and the pore tortuosity factor. The applied pressure was between 3.45 10^4 and 2.28 10^8 Pa with an equilibration time of 10 s for the low pressure range and 20 s for the high pressure range. An angle of 130° was considered as the mercury advancing contact angle.

The overall void volume fraction (i.e. porosity) (ε) of the membranes was measured by the gravimetric method as described elsewhere [29] and calculated as follows:

$$\varepsilon = \frac{(m_w - m_d)/\varrho_{IPA}}{(m_w - m_d)/\varrho_{IPA} + m_d/\varrho_{Al}} 100 \qquad (5.1)$$

where m_w and m_d are the weighted mass of the membrane wetted by isopropyl alcohol (IPA) and the mass of the dry sample, respectively. ρ_{IPA} is the density of the wetting liquid IPA (0.785 g/cm^3, Sigma-Aldrich Chemical) and ρ_{Al} is the density of the alumina powder (3.97 g/cm^3, Inframat® Advanced Materials™).

The dynamic contact angles (θ) of the hollow fiber membranes were indirectly measured at room temperature by Wilhelmy balance method technique [30, 31]. The fiber was first hung on the microbalance of the tensiometer (Kruss K100), and then immersed in DI water at a rate of 3 mm/min. The side of the fiber, which was immersed into the testing liquid, was closed with epoxy resin.

Liquid entry pressure of water (LEP_w) on the membranes was determined using the experimental set-up and the procedure described elsewhere [32]. This parameter together with the dynamic contact angle are useful to confirm the hydrophobic character of the modified ceramic hollow fibers and to ensure their applicability in AGMD.

In general, the mechanical strength of the ceramic hollow fiber membranes is not altered with the grafting modification as it was previously confirmed elsewhere [31, 33]. Therefore, the mechanical strength was measured only for the original alumina hollow fibers by means of the three-point bending test, which was carried out using an Instron system (model 5543, Bluehill 3). Three samples of 30 mm long of each membrane were performed using a 1 kN load cell and a cross-head speed of 0.01 mm/s. The bending strength (σ_F) was calculated from the equation described elsewhere [34, 35] and the flexure test scheme and procedure was also shown in [36].

5.2.5 Air gap membrane distillation experiments

AGMD experiments were performed using the experimental device schematized in Fig. 5.1(a). The temperature of the feed solution (1) was controlled by a heating thermostat (2) (DT Heto) and a heat exchanger (4). The feed solution was circulated tangentially through the lumen side of the alumina hollow fiber membrane module (7) by means of a peristaltic pump (3) (Cole Parmer Masterflex easy-load model 7529-20). The shell side of the membrane module was cooled by a PolyScience chiller (8) in order to keep constant the temperature of the condensation surface. The mass of the produced water (9) and the inlet and outlet temperatures of the membrane module were determined by a balance (10) (AND GF-1200) and calibrated Pt-100 probes (6) connected to a multimeter (12) (Keithley 199 System DMM/SCANNER), respectively. Both the balance and the multimeter were connected to a computer (13), which registered the mass and temperatures measurements over time. All the experiments were carried out keeping both the inlet feed and cooling temperatures of the module at 80 ºC and 20 ºC, respectively. The feed flow rate was maintained at 35 L/h by means of a flow meter (11) (Tecfluid) and the hydrostatic pressure was controlled by a pressure gauge (5) (Wika), before the entrance of the liquid in the membrane module. The hollow fiber membrane module and all the elements of the set-up were thermally insulated. After ensuring that the membrane module had no leakage, the AGMD experiments were carried out using first distilled water as feed and then salt (NaCl) aqueous solutions of different concentrations (1.2, 3 and 6.5 wt%). The salt concentration of the feed and permeate solutions was measured during the experiments by an electrical conductivity meter (Metrohm model 712). The AGMD permeate flux (J) was obtained from the registered mass of the produced water (Δm) over time (Δt) and the internal surface area of the membrane (A_{in}). The permeate flux and the salt rejection factor (α) were calculated as follows:

$$J = \frac{\Delta m}{A_{in}\,\Delta t} \tag{5.2}$$

$$\alpha = \left(1 - \frac{C_p}{C_f}\right) 100 \tag{5.3}$$

where C_p and C_f are the concentration of the permeate and feed solutions, respectively.

The permeate flux reduction factor (*FRF*) represents the relative difference between the obtained permeate flux when distilled water (J_w) and NaCl aqueous solution ($J_{NaCl\ wt\%}$) are used as feed. This parameter can be used to compare the efficiency of the membranes for the same NaCl feed solution and AGMD operating conditions. *FRF* for a given NaCl feed solution ($FRF_{NaCl\ wt\%}$) was determined by the following equation:

$$FRF_{NaCl\ wt\%}(\%) = \left(\frac{J_w - J_{NaCl\ wt\%}}{J_w}\right) \times 100 \tag{5.4}$$

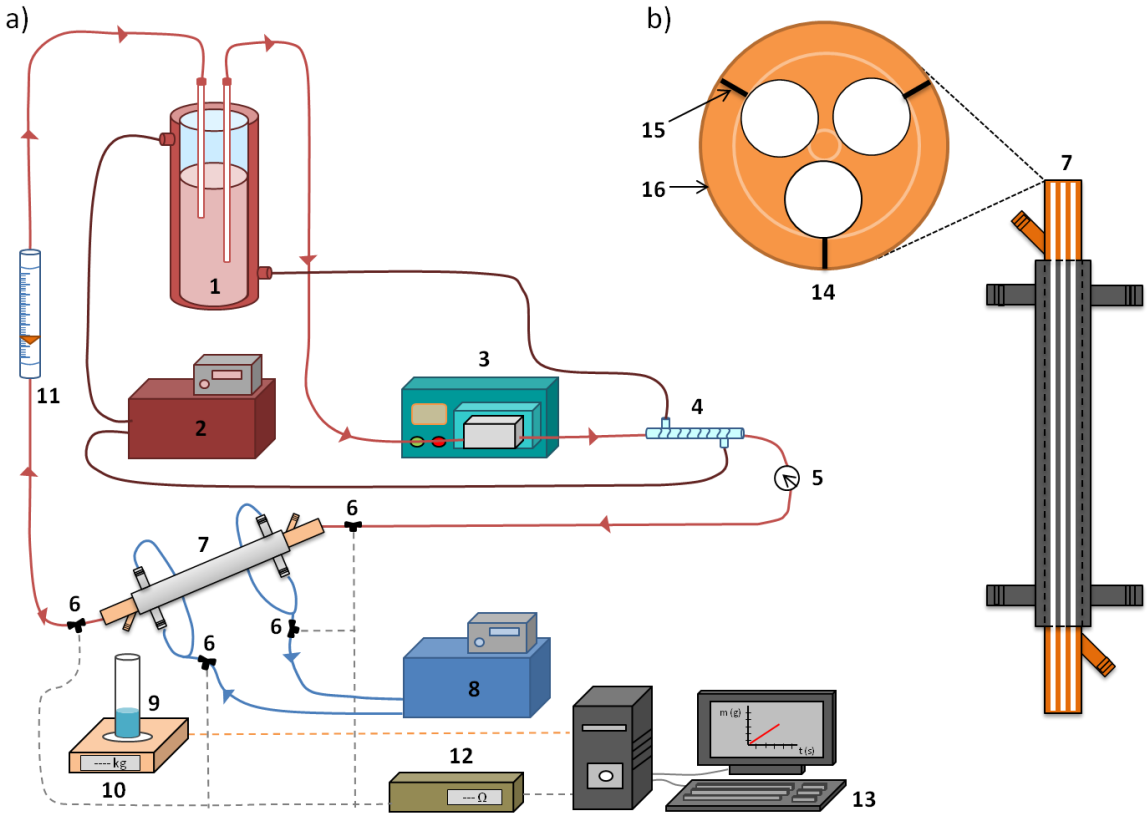

Fig. 5.1. a) AGMD experimental set-up: (1) Feed; (2) heating thermostat; (3) peristaltic pump; (4) glass heat exchanger; (5) pressure gauge; (6) Pt-100 probes; (7) hollow fiber membrane module; (8) cooling thermostat; (9) permeate; (10) balance; (11) flow meter; (12) multimeter; (13) computer; b) hollow fiber membrane module: (14) three-holed cover; (15) minimum air gap width = 1 mm; (16) condensation surface.

The AGMD hollow fiber membrane module was specifically designed and fabricated for these experiments (see Fig. 5.1(b)). It is worth noting that this membrane module can be used for all MD configurations (i.e. DCMD, AGMD, sweeping gas membrane distillation (SGMD) and VMD). Three hydrophobic alumina hollow fibers were packed in a copper tube, which was coaxially placed inside the stainless-steel shell used as the cooling chamber. A three-holed cover (14) was welded at each end of the copper tube. Each hollow fiber was introduced through the corresponding holes of each top and bottom covers and then it was fixed with epoxy resin at both ends. The three-holed covers were designed to maintain parallel the hollow fibers inside the tubular module, keeping constant the space between them and the distance between the fibers and the copper condensation surface (16) (i.e. the radial minimum air gap distance (15) was 1 mm). The effective length of the AGMD tubular module was 120 mm.

5.3 Results and discussions

5.3.1 Structural characteristics

The inner and outer diameters as well as the thickness of the sintered ceramic hollow fiber membranes are summarized in Table 5.2. These parameters are significantly affected by the viscosity of the ceramic suspension and the precipitation rate during spinning, which determine the resistance of the nascent fibers to gravity that induces elongation. In general, for the two used suspensions, the fibers made from the more viscous HP suspension, due to its higher polymer concentration, exhibited bigger diameters and thicker walls compared with the fibers made from the less viscous LP suspension when the same spinning parameters were considered. The minimum diameters (i.e. minimum MD membrane permeate surface) corresponded to the membrane LP2 and the maximum ones to the membrane HP3. This membrane exhibited the biggest external and internal diameters as it was prepared under a zero-gap distance using a weak non-solvent (40 wt% EtOH/60 wt% NMP) as a bore liquid. The highest and lowest thickness of these hollow fibers was determined for the membranes LP1 and LP4, respectively. The hollow fiber LP1 was prepared under a zero-gap distance and a strong non-solvent (i.e. water) in contact with both the inner and outer sides of fiber immediately after extrusion. The membrane LP4 was prepared under a wet-gap distance of 25 cm and the solvent NMP was circulated through the outer channel of the spinneret leading to a precipitation delay. It is well known that spinning with a longer gap distance increased the fiber elongation stress resulting in a thinner membrane [37]. This effect could be even intensified for a slowly coagulated hollow fiber membrane, which suffered more the stretching force during the long gap distance.

Table 5.2. Diameters and thickness of the alumina hollow fiber membranes.

Membrane	Inner diameter (μm)	Outer diameter (μm)	Thickness (μm)
LP1	1102 ± 11	1809 ± 17	354 ± 7
LP2	921 ± 6	1282 ± 18	180 ± 4
LP3	974 ± 6	1337 ± 13	181 ± 3
LP4	1003 ± 3	1293 ± 9	145 ± 1
HP1	1075 ± 10	1701 ± 10	313 ± 5
HP2	1417 ± 4	1953 ± 10	268 ± 2
HP3	1812 ± 3	2308 ± 12	248 ± 2

Other than the diameters and thickness, wall structure is crucial dictating the properties of the hollow fiber membrane. Tuning the structure of the hollow fiber membrane consists of manipulating the occurrence and arrangement of micro-channels in the wall, which largely determines the asymmetric structure and hence the transport resistance during MD process. The generation of micro-channels in ceramic hollow fibers is based on a spontaneous fingering process induced by the density difference between the inorganic suspension and the coagulant. In other words, the Rayleigh-Taylor instability, which amplifies the interfacial disturbing waves, lead to the periodical irregular invasion of the light fluid into the heavy one [38-41]. When the phase inversion starts, a strong non-solvent (e.g. water) comes into contact with the inorganic suspension and consequently, the solvent outflow from the inorganic suspension to the non-solvent promotes the contraction of the inorganic suspension. This induces a highly accelerated movement of the interface between the inorganic suspension and the non-solvent towards the suspension side (i.e. Rayleigh-Taylor instability initiation). The interfacial accelerates towards the heavier fluid (i.e. inorganic suspension is heavier than the non-solvent) and the secondary condition of the Rayleigh-Taylor instability is then met. Therefore, the fingering process starts and the micro-channels are formed due to the invasion of the periodical micro-streams of the non-solvent in the ceramic suspension [38]. According to the Rayleigh-Taylor instability theory, the initial momentum and the number of micro-channels are mainly affected by the interfacial acceleration, which is in turn determined by the exchange rate of the solvent and non-solvent. In general, when the solvent/non-solvent exchange rate is fast, the initial momentum and the number of micro-channels would be higher, and vice versa. After initiation, the growth of the micro-channels is driven by the momentum of the invading micro-streams. The interaction between different factors such as the initial momentum, densities, viscosities, precipitation rate, etc. determine the final length and width of the micro-channels [38]. Commonly, the micro-channels grow perpendicular to

the surface where its formation is initiated according to the physical nature of the Rayleigh-Taylor instability. During the micro-channel formation process, when the momentum of the non-solvent micro-streams is dissipated, the micro-channels stop growing and a sponge-like layer will be formed. Dissipation of the momentum can be accomplished by two means, one is the consumption of the initial momentum by the friction in the deforming suspension surrounding the micro-streams, which is determined by the viscosity and precipitation of the suspension; the other happens when two sets of micro-streams meet from opposite directions, in this case, a sponge-like layer will be sandwiched in between the micro-channels in the precursors. The sponge-like layer is a tight layer after sintering and it contributes to the most of transport resistance. This sponge-like layer is also important to the mechanical property of the membranes, as a large amount of material is distributed in it. Immediately after the initiation of the micro-streams, the entrance of the micro-channels on the suspension/non-solvent interface starts to contract because of the tension surrounding the entrance. At the same time, the polymer content at the interface and the entrance start to precipitate due to solvent/non-solvent exchange. Hence, the final size of the entrance of the micro-channels is largely determined by the competition between the contraction and the precipitation speeds. In general, a faster precipitation rate of the interface and the micro-channel entrance would be favored to obtain bigger entrance sizes, and the entrance could be completely closed if the precipitation rate is slow. Based on above theories, the morphology and pore structure of the hollow fibers will be reasonably interpreted in the following sub-sections.

5.3.1.1 Morphology control of the prepared alumina hollow fiber membranes

Figures 5.2 and 5.3 show the SEM images of the cross-sections of the ceramic hollow fiber membranes. It can be observed that different morphologies were designed and prepared according to the spinning parameters summarized in Table 5.1. Figure 5.2 corresponds to the morphologies of the alumina hollow fibers prepared with the LP suspension and Fig. 5.3 to those of the membranes prepared with HP suspension.

DI water was used as internal and external coagulants for LP1 membrane preparation. By using this strong coagulant, fast precipitation occurred simultaneously at the inner and outer layer of the hollow fiber and micro-channels grew from both sides of the membrane and met in the middle of the wall to form a sandwich structure.

The alumina hollow fiber membranes LP2 and LP3 were prepared employing a weak outer coagulant (i.e. 50 wt% ethanol/50 wt% NMP) along the short gap (i.e. 5 cm). Such combination of the spinning parameters led to slower overall precipitation of the nascent hollow fibers, and the elongation effect from gravity permitted the formation of a thinner membrane wall and smaller diameters of the hollow fibers compared with LP1. For the hollow

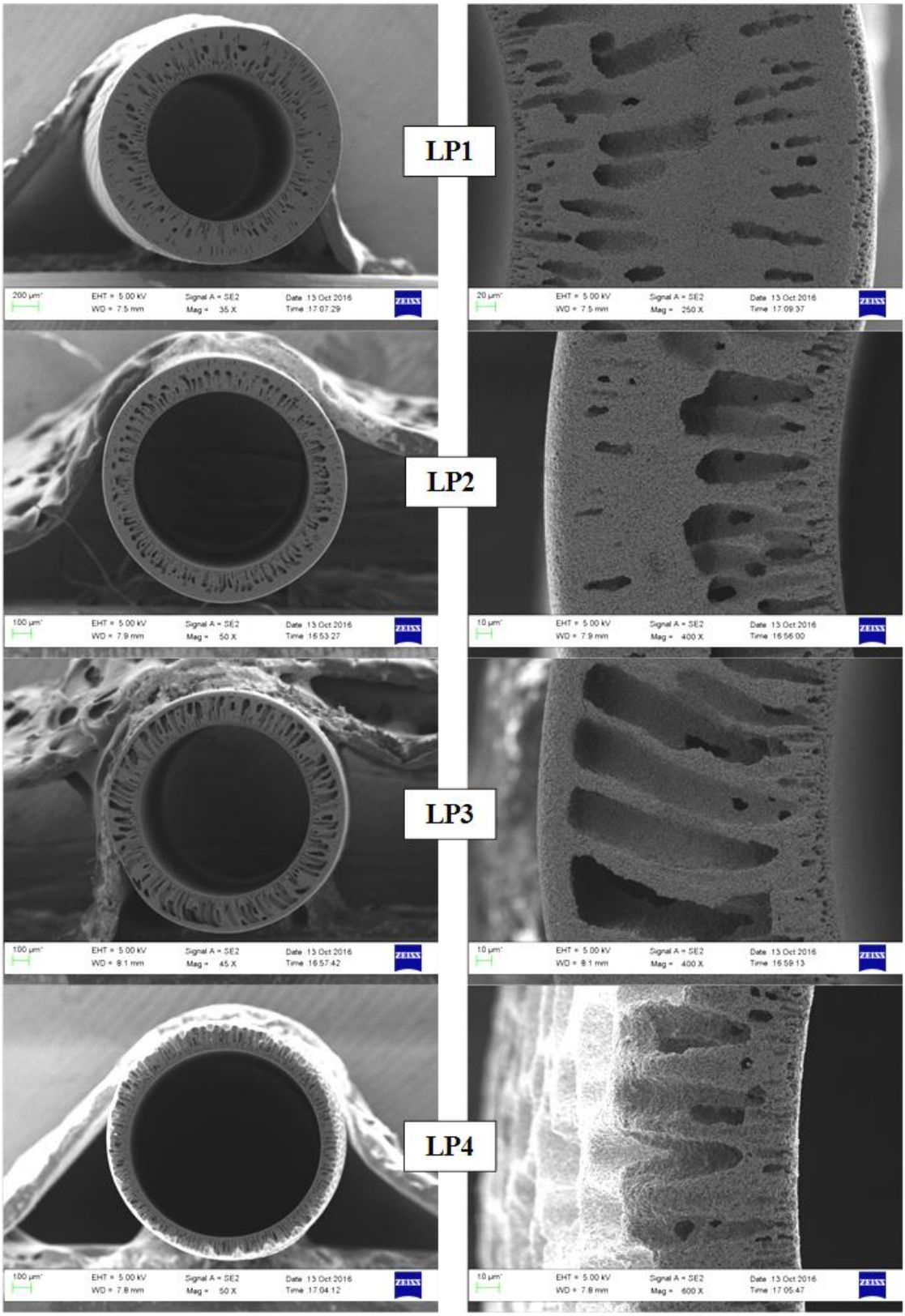

Fig. 5.2. SEM cross-section images of the alumina hollow fiber membranes prepared with the LP inorganic suspension.

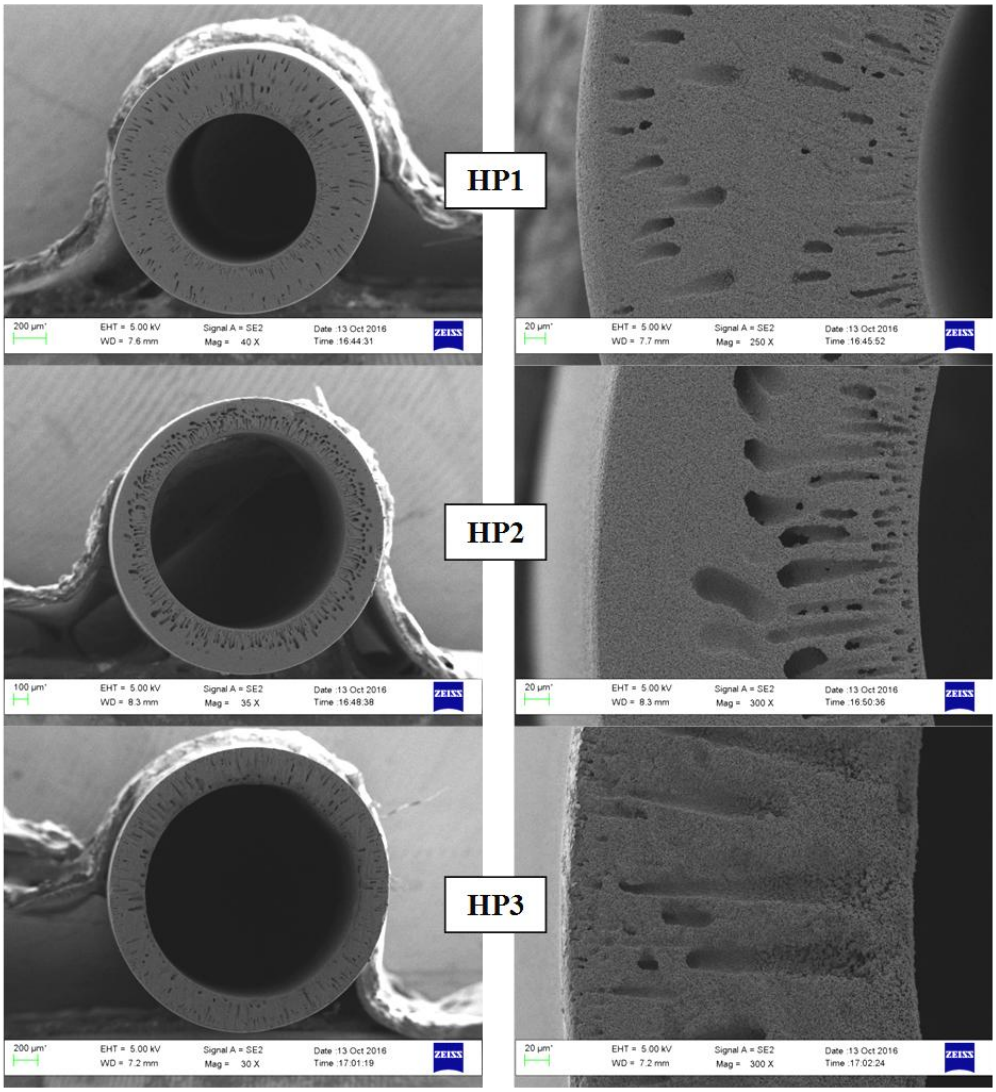

Fig. 5.3. SEM cross-section images of the alumina hollow fiber membranes prepared with HP inorganic suspension.

fiber LP2, the weak outer coagulant increased the viscosity of the outer surface suspension of the nascent fiber along the short gap. When the fiber entered into the water bath, the increased viscosity induced a slower solvent/non-solvent exchange at the outer surface, which resulted in less micro-channels from the shell side. For the hollow fiber LP3, the velocity of the bore liquid water was increased considerably (i.e. the flow rate was increased to 15 ml/min compared to 10 ml/min for LP2). This increase of the flow rate enhanced the solvent/non-solvent exchange rate at the inner surface, therefore the micro-channels from the lumen side got higher initial momentum to grow faster and longer than that corresponding to the hollow fiber LP2, reaching finally the position next to the outer surface. As a consequence, the viscosity of the outer surface was increased further (owing to solvent/non-solvent exchange with the water in the micro-channels) before entering the water bath compared to LP2, and micro-channels from the shell side were not formed. The most different morphology was

observed for the ceramic hollow fiber membrane LP4 (see Fig. 5.2). For this membrane a very high bore liquid (i.e. water) flow rate of 30 ml/min was used during spinning. This led to the fastest solvent/non-solvent exchange rate at the lumen side and thus the micro-channels had the highest initial momentum to break through the outer surface. By using a pure solvent (i.e. NMP) as the outer liquid along a large gap distance (i.e. 25 cm), coagulation was avoided during this gap, giving enough time for the micro-channels to reach the external layer before falling into the water bath, resulting in open micro-channels at the outer side of the membrane. It is worthy to mention that the combination of a high bore liquid (i.e. water) flow rate and a long gap distance was commonly considered [42]. Although the micro-channels could reach the outmost layer, such breaking through the outer surface was not observed in these studies. It is speculated that the surface tension on the outer surface of the nascent fiber provides a force against the direction of micro-channel growth and therefore hindered the breaking process of the micro-channels. In our case, by flowing NMP on the outer surface, the tension of the outer surface of the nascent fiber was eliminated and consequently the micro-channels could break the surface easily.

The hollow fibers HP1 and HP2 used the same spinning parameters (except the inorganic suspension) as those of LP2 and LP3, respectively. The greater viscosity of the HP suspension reduced the solvent/non-solvent exchange rate and therefore the micro-channels had lower initial momentum to grow from the lumen side. Furthermore, the higher viscosity of the HP suspension dissipated the momentum faster than the LP suspension, inhibiting therefore the growth of micro-channels more efficiently [38]. As a consequence, despite the fact that HP1 and HP2 showed similar structures as LP2 and LP3, respectively, the micro-channels at the lumen side are shorter and smaller than those of LP2 and LP3.

Completely different cross-section morphology was observed in Fig. 5.3 for the membrane HP3, when a weak non-solvent mixture was employed as a bore liquid (i.e. 40 wt% ethanol/60 wt% NMP) under a zero-gap distance. This coagulant induced a slow solvent/non-solvent exchange rate and precipitation at the lumen side, leading to a micro-channel free sponge-like structure at the inner layer of this fiber. On the one hand, micro-channel structure formation started at the shell side of the membrane HP3, owing to the fast solvent/non-solvent exchange induced by water in the coagulation bath. The micro-channels formed from the shell side stopped next to the inner surface due to momentum dissipation by the viscosity and the slow precipitation of the suspension at the lumen side.

5.3.1.2 Pore structure of the prepared alumina hollow fiber membranes

The bubble, mean and smallest pore sizes of the alumina hollow fiber membranes were determined by gas-liquid displacement test. These results are summarized in Table 5.3. All membranes exhibited similar pore sizes, except the hollow fiber LP4, which had significantly

larger pore sizes due to its unique structure. The average mean pore size of the other alumina hollow fiber membranes were (233 ± 8) nm. This is an adequate pore size for MD membranes [4, 43]. Another suitable characteristic of an MD membrane is a narrow pore size distribution [4, 22]. The hollow fibers prepared in this study met this requirement (except the membrane LP4). The maximum difference between the bubble pore sizes and the smallest pore sizes (i.e. the widest pore size distribution) was 205 nm for the hollow fiber HP3, which was prepared with a high concentration of solvent in the bore liquid mixture (40 wt% ethanol/60 wt% NMP). Comparatively, Zhang et al. [44] prepared yttria-stabilized zirconia (YSZ) hollow fiber membranes with a wider pore size distribution when higher NMP content was used in the bore liquid mixture (i.e. NMP/water). The bubble pore sizes and the smallest pore sizes of the original hollow fiber membranes LP2 and LP3 differed only by about 50 nm. This means that both membranes had the narrowest pore size distributions.

Gas-liquid displacement only detects the effective open pore size, which is the 2-D projection of the real pore structure. However, it does not provide the full information of the 3-D hierarchical pore structure. On the other hand, MIP gives full information of the pore structure, but it does not permit to get an effective open pore size. Therefore, it is important to combine these two techniques to obtain a clear view of the pore structure. Figure 5.4 shows the pore size distributions (PSD) of the prepared alumina hollow fiber membranes determined by MIP analysis. All the hollow fibers showed a hierarchical pore structure consisting of more than one pore size including the inter-granule pore size between alumina particles and the micro-channel entrance pore size at different pore structure levels. All fibers have a common pore size with a first peak around 247 nm, which corresponds to the primary inter-granule

Table 5.3. Bubble pore size, mean pore size, and smallest pore size of the alumina hollow fiber membranes before and after grafting determined by gas-liquid displacement test.

Membrane	Bubble pore size (nm)		Mean pore size (nm)		Smallest pore size (nm)	
	Original	Grafted	Original	Grafted	Original	Grafted
LP1	340 ± 14	344 ± 15	237 ± 6	250 ± 16	203.7 ± 0.7	220 ± 18
LP2	270.0 ± 0.6	288.7 ± 1.2	231.4 ± 0.8	232 ± 3	213 ± 17	195 ± 15
LP3	267.2 ± 1.2	280 ± 14	228.0 ± 0.7	227 ± 3	222.1 ± 0.5	185 ± 30
LP4	1085 ± 50	1181 ± 40	537 ± 29	556 ± 22	490 ± 50	434 ± 33
HP1	345.15 ± 0.21	370 ± 3	229 ± 8	223 ± 3	189 ± 15	193 ± 18
HP2	332.6 ± 0.9	360.4 ± 1.2	247.6 ± 1.7	255 ± 7	198 ± 15	205 ± 10
HP3	382.1 ± 27	369.8 ± 1.8	228 ± 16	251 ± 11	177 ± 3	175 ± 7

pores between alumina particles. This is the smallest pores at the lowest level in the ceramic matrix, and it is close to the mean pore size determined by the gas-liquid displacement technique, except that of the hollow fiber LP4. This means that the effective open pore size is determined by the primary inter-granule voids. As it can be seen in Fig. 5.4(a), LP1 showed an additional peak around 324 nm, which corresponds to the size of the entrance of the micro-channels. Similarly, LP2 presented an entrance size of the micro-channels at 480 nm, and LP3 at 735 nm. The change of the size of the micro-channel entrance is related to the precipitation rate of the surfaces, as it will be explained later on. For the hollow fibers LP1 and LP2, the flow rate of the bore liquid water was the same, 10 ml/min, but the inorganic suspension flow rate and the gap distance were different. The hollow fiber membrane LP1 was prepared using a higher inorganic suspension flow rate (15 ml/min compared to 8 ml/min employed for LP2) and zero gap distance, inducing a greater thickness after extrusion and reducing the solvent/non-solvent exchange rate as consequence. When using a higher extrusion rate, the non-solvent/solvent ratio exchanged during the spinning was lower, leading to a slower precipitation rate. Therefore, the micro-channel entrance had more time to contract before solidification resulting in a smaller size than that of LP2. The hollow fiber LP3 used a higher flow rate of the water bore liquid than LP2 leading to a higher precipitation rate of the inner surface and hence larger micro-channel entrance size than LP2. Compared with LP1, LP2 and LP3, the hollow fiber LP4 did not show any predominant secondary peak, but had a broaden pore size distribution ranging from tens of microns to sub-micron. This unique distribution corresponded to the open micro-channel structure of LP4. As the open micro-channels of LP4 have a conical shape, during MIP measurement, mercury was pushed into the big openings at low pressures, and the penetrated mercury volume increased smoothly when the pressure was increased. Then the incremental intrusion volume was kept small for each pressure increment, leading to a broaden pore size distribution. The size of the micro-channel entrances at the inner surface of LP4 could not be detected by the MIP technique, because it was the last part penetrated by mercury and the volume increase corresponding to this part is too small to produce a meaningful signal. The micro-channel entrance pore sizes can only be measured by the gas-liquid displacement technique, which determined a mean pore size of 537 nm. Although a higher bore liquid water flow rate was used for the LP4 fiber spinning its micro-channel entrance pore size was smaller than that of the hollow fiber LP3. The precipitation rate at the inner surface of the hollow fiber LP4 might be slowed down by the solvent used as outer coagulant. Figure 5.4(b) shows the PSD of the alumina hollow fiber membranes prepared with HP suspension. In addition to the primary inter-granule pore size, the HP fibers exhibited another peak around 306 nm. This indicated that part of inter-granule pores between alumina particles were expanded due to the higher polymer concentration used for the HP suspension preparation. Furthermore, these fibers presented an additional peak

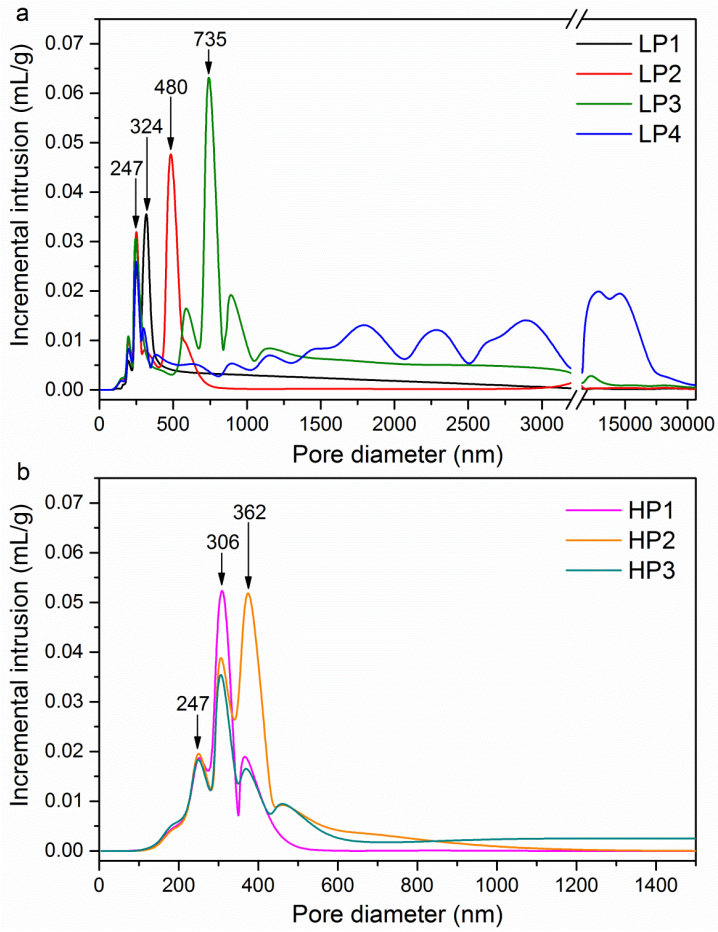

Fig. 5.4. Pore size distributions of the original alumina hollow fiber membranes prepared with the LP suspension (a) and the HP suspension (b) determined by MIP analysis.

around 362 nm, corresponding to the entrance size of the micro-channels. The incremental intrusion volume of this peak is greater for the membrane HP2 than for the other fibers, owing to the numerous and bigger micro-channels through its cross-section. This micro-channel entrance size was smaller than that of the membrane LP3 (prepared under the same spinning conditions) because of the higher viscosity (i.e. slower solvent/non-solvent exchange rate) of the HP suspension. It is worth noting that the inter-granule pore sizes of the prepared hollow fiber membranes were of the same order of magnitude as that reported by Lee et al. [45] for the alumina hollow fiber prepared with the same powder size, 1 μm, and sintered at the same temperature, 1450 °C.

The tortuosity of the membrane pores was also determined by MIP analysis. As it can be seen in Table 5.4, no significant changes were observed for the tortuosity factors of all prepared ceramic hollow fiber membranes. All obtained values were lower than 2, which is the value commonly considered for the tortuosity factor of MD membranes to carry out the permeate flux predictions [4]. The lowest value corresponded to the hollow fiber LP3 while the greatest one was obtained for HP3.

Table 5.4. Tortuosity factor of the original alumina hollow fiber membranes determined by MIP technique and void volume fraction (i.e. porosity) (ε) of the original and grafted fibers determined by gravimetric method.

Membrane	Tortuosity factor	ε (%)	
		Original	Grafted
LP1	1.801	50.5 ± 0.7	48.6 ± 0.5
LP2	1.814	54.4 ± 1.3	57.0 ± 1.1
LP3	1.706	55.5 ± 1.1	57.0 ± 1.9
LP4	1.782	70.4 ± 0.4	74.8 ± 2.2
HP1	1.794	48.1 ± 1.3	50.3 ± 2.7
HP2	1.738	51.7 ± 1.2	54.6 ± 1.2
HP3	1.817	51.0 ± 1.3	50.3 ± 1.4

The void volume fraction of the prepared alumina hollow fiber membranes was determined by means of the gravimetric method, and the results are shown in Table 5.4. The highest porosity was obtained for the hollow fiber membrane LP4, which exhibited the largest pore sizes (see Table 5.3) and open micro-channels at the outer side (see Fig. 5.2). The other membranes had similar void volume fraction values around 52%. The hollow fibers LP2 and LP3 showed slightly higher void volume fraction values. This is attributed partly to their larger micro-channel structures through their cross-sections (see Fig. 5.2).

5.3.1.3 Surface morphology and hydrophobicity of the membranes after grafting

Figures 5.5 and 5.6 show the SEM images of the inner and outer surfaces of the alumina hollow fiber membranes prepared with LP and HP suspension, respectively. The majority of the inner surfaces were similar and more porous than the outer ones. Similar results were described elsewhere [46, 47]. The outer surfaces of the membranes LP1 and HP3 prepared without a gap distance seem to be less dense than the others. The faster solvent/non-solvent exchange rate at the outer side of the fibers induced by water in the coagulation bath could lead to slightly porous external surfaces. The most different outer surface morphology corresponded to the membrane LP4 (see Fig. 5.5), which presented very large pores due to the open micro-channels at the outer side of the fiber. As it can be seen in Fig. 5.6, the membrane HP3 has a rougher inner surface induced by the slow precipitation at the inner side due to the weaker bore coagulant mixture [48].

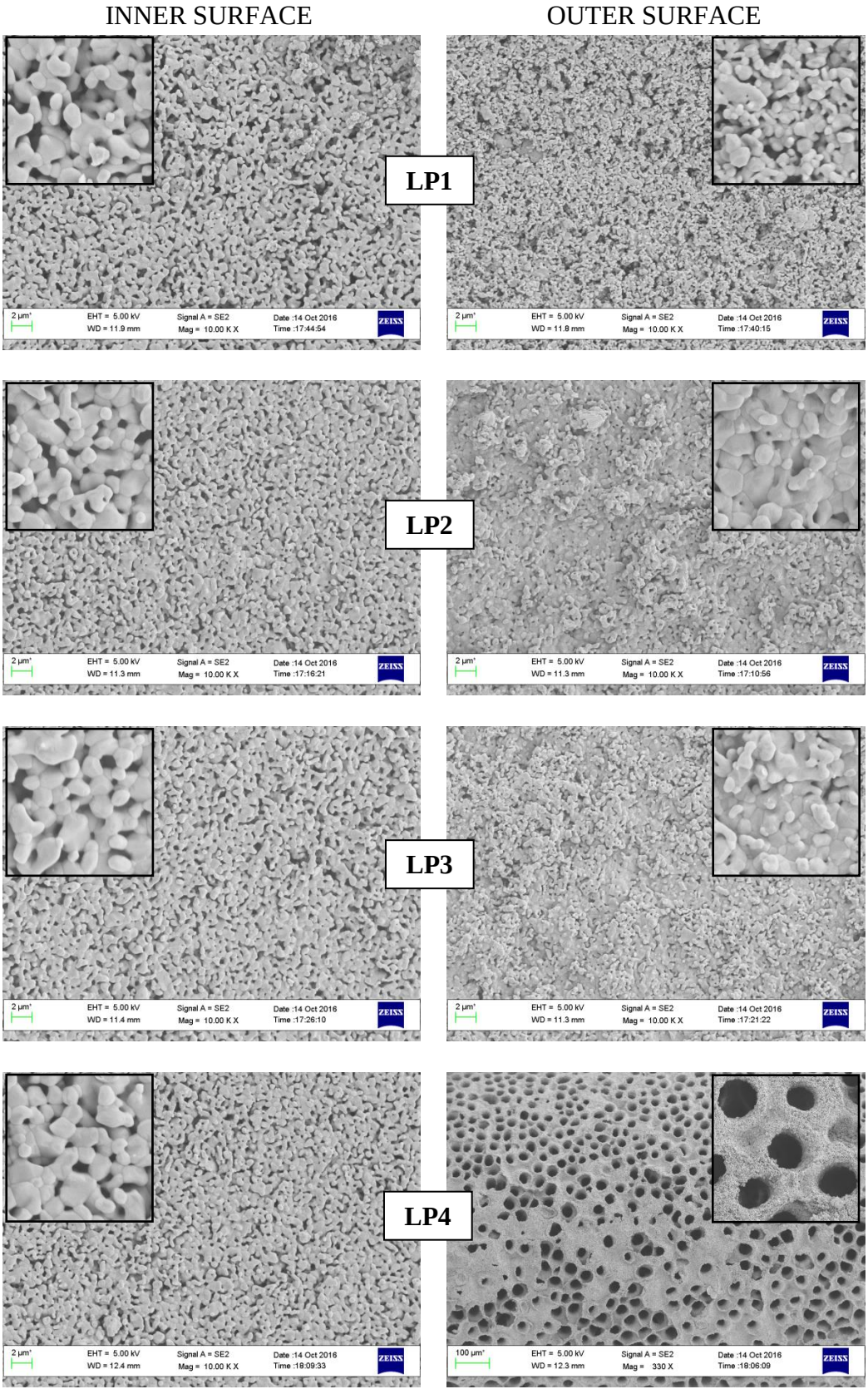

Fig. 5.5. SEM surface images of the alumina hollow fiber membranes prepared with the LP inorganic suspension.

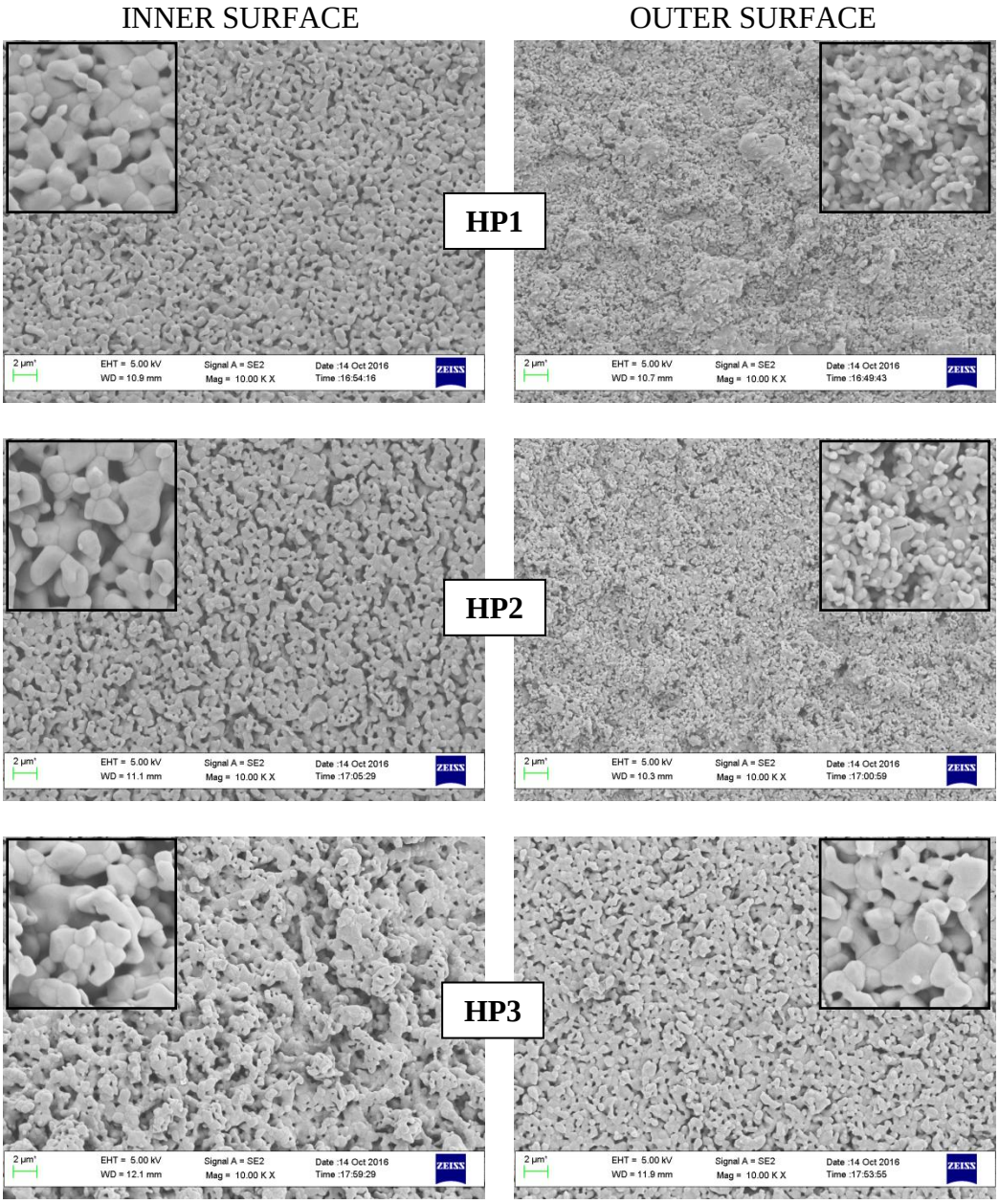

Fig. 5.6. SEM surface images of the alumina hollow fiber membranes prepared with the HP inorganic suspension.

Both the internal and external surfaces of the grafted alumina hollow fiber membranes were also analyzed by SEM. As it was expected, no significant changes were observed when comparing the surfaces of the grafted alumina membranes to those of the corresponding original ones. In fact, the followed grafting modification technique changed only the chemistry of the ceramic membrane as it was observed in previous studies [6, 31]. Hendren et al. [14] employed different chemicals to modify the hydrophobicity of alumina anodisc^{TM} membranes for their application in MD. For the same chemical used in the present study (i.e. 1H,1H,2H,2H-perfluorodecyltriethoxysilane), the pores of the membrane surface were not

blocked as shown by the SEM images. Consequently, other properties such as the pore size and porosity of the prepared hollow fiber membranes were not altered after grafting modification (see Tables 5.3 and 5.4).

The hydrophobicity of both the original and modified hollow fiber membranes was analyzed by means of the water contact angle measurements (Figure 5.7). The considered grafting modification technique proved to be very effective because it changed the intrinsic hydrophilic nature of the alumina membranes (i.e. $(57 \pm 8)^{o}$ is the average water contact angle of the original fibers) to be hydrophobic (i.e. $\theta > 90^{o}$, $(147 \pm 9)^{o}$ is the average water contact angle of the grafted fibers). Some hollow fibers were rendered superhydrophobic (i.e. $\theta > 150^{o}$ of the hollow fibers LP2, LP3 and HP3). The water contact angles of the grafted membranes in this study were higher than those determined for other grafted alumina hollow fibers (i.e. contact angles lower than 120^{o}) [31]. It is well known that the grafting method consists on a chemically bonding between the hydrolysable groups of the modified agent and the hydroxyl groups of the ceramic membranes. The number of the functional groups of the modified agent structure is one of the parameters that directly affects the grafting efficiency. Hendren et al. [14] demonstrated that the grafting success of the 1H,1H,2H,2H-perfluorodecyltriethoxysilane was due to the three available functional sites of each molecule. It is worth noting that the lowest contact angle measurement and the highest experimental uncertainty were registered for the membrane LP4. This was in agreement with the extremely large pores observed on its outer surface (see Fig. 5.5).

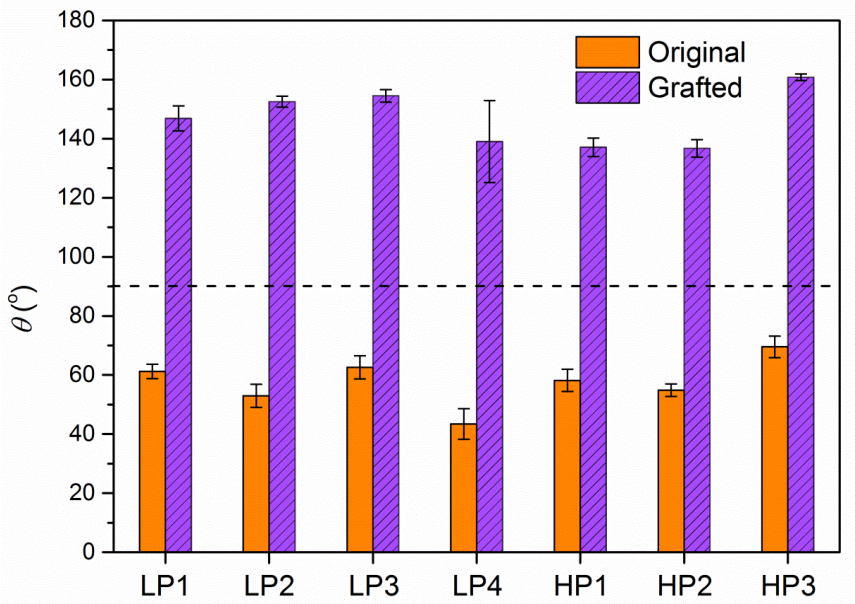

Fig. 5.7. Advancing contact angles of the prepared alumina hollow fiber membranes before and after grafting modification.

The hydrophobic character and consequently the MD applicability of the grafted hollow fiber membranes were confirmed by measuring LEP_w. All the measured LEP_w values of the prepared membranes were higher than 3.8 10^5 Pa, which is the maximum pressure limit of the experimental device, except that of the hollow fiber LP4. The LEP_w value of this membrane was 0.3 10^5 Pa. This lowest LEP_w value could be due to some defects found in the membrane structure corresponding to open micro-channels passing through the entire fiber cross-section. Therefore, all hollow fibers, except LP4, can be used in AGMD without any wetting problem as the applied transmembrane hydrostatic pressure was lower than the LEP_w values. It is worth quoting that the obtained LEP_w values were higher than those reported for other modified alumina hollow fiber membranes used in desalination by MD, which were around 1-1.5 10^5 Pa [6, 15]. However, the LEP_w values obtained for some grafted zirconia and titania membranes reached up to 9 10^5 Pa and 10^6 Pa [13, 18].

5.3.2 Mechanical property of the prepared alumina hollow fibers

It is important to guarantee a good mechanical strength of the hollow fiber membranes in order to ensure their good packing in tubular modules for MD applications. The bending strengths of the original alumina hollow fibers are summarized in Table 5.5. The bending strength of all prepared alumina membranes were within the range (50 – 250 MPa) reported previously by Koonaphapdeelert and Li [31] for alumina hollow fibers sintered under the target temperatures 1400 and 1500 °C. The hollow fiber HP3 exhibited the highest bending strength attributed partly to the lower number of micro-channels in its structure. Lee et al. [35] stated that the mechanical properties of the hollow fiber membranes were reduced with the formation of micro-channel structures. This is corroborated by the membrane LP4 having the lowest bending strength and large micro-channels through the fiber cross-section, which were opened at its outer surface (see Fig. 5.2 and 5.5).

Table 5.5. Bending strength (σ_F) of the original alumina hollow fiber membranes.

Membrane	σ_F (MPa)
LP1	142 ± 7
LP2	150 ± 14
LP3	110 ± 8
LP4	50 ± 5
HP1	156 ± 12
HP2	120 ± 8
HP3	183 ± 10

5.3.3 AGMD experiments of the grafted alumina hollow fiber membranes

The AGMD performance of all the grafted alumina hollow fiber membranes is shown in Fig. 5.8. The permeate fluxes (*J*, Fig. 5.8(a)) as well as both the salt rejection and flux reduction factors (α and $FRF_{NaCl\ 3wt\%}$, Fig. 5.8(b)) were related with the morphology and characteristics of the prepared hollow fiber membranes. The structural design of the hollow fiber LP4 provided the highest permeate flux in this study, which was significantly greater than those obtained from the other membranes (see Fig. 5.8(a)). This membrane exhibited the highest porosity, the largest pore size, and the lowest thickness as a consequence of the open micro-channel structures at the outer side of this fiber (i.e. big pores of the outer surface). However, not only was the water vapor transported through the membrane pores, but the feed solution also crossed the entire membrane wall through some defects (i.e. micro-channels opened at both inner and outer layers). Apart from increasing the permeate flux, these defects reduced both the resultant salt rejection factor (i.e. 97.97%) and the $FRF_{NaCl\ 3wt\%}$ of the hollow fiber LP4 to the minimum values of this study as shown in Fig. 5.8(b). This result was anticipated since the hydrostatic pressure of these AGMD experiments was 0.3 10^5 Pa, coinciding with the LEP_w of this hollow fiber. Therefore, it can be concluded that the hollow fiber membrane LP4 is not an adequate membrane for MD applications. Nevertheless, in spite of its low salt rejection factor, the average concentration of the permeate solution was 0.54 g/L, which is slightly higher than the concentration limit of drinking water (i.e. 0.5 g/L) [49].

In general, among the other hollow fiber membranes, the LP fibers exhibited greater permeate fluxes than those of the HP fibers. Particularly, it can be clearly seen that the permeate fluxes of the hollow fiber membranes prepared under the same spinning conditions but with the lower polymer concentration in the inorganic suspension were higher (compare the membranes LP2 with HP1 and LP3 with HP2 in Fig. 5.8(a)). This is related with the morphological difference between the LP and HP hollow fibers, where LP fibers have longer, bigger and more micro-channels than the HP hollow fibers, which have thicker and tighter sponge-like structure with less micro-channels. The large micro-channels provided better AGMD permeate flux because this kind of structure reduced more the heat transfer by conduction following Fourier´s law and consequently the mass transport resistance through the membrane than that of the tight sponge-like structure. The lowest AGMD performance was observed for the hollow fiber HP3, whereas the highest one was registered for the hollow fibers LP2 and LP3.

The hollow fiber HP3 had the minimum permeate flux mainly because this membrane had less number of micro-channels and a sponge-like structure at the inner layer, resulting in a

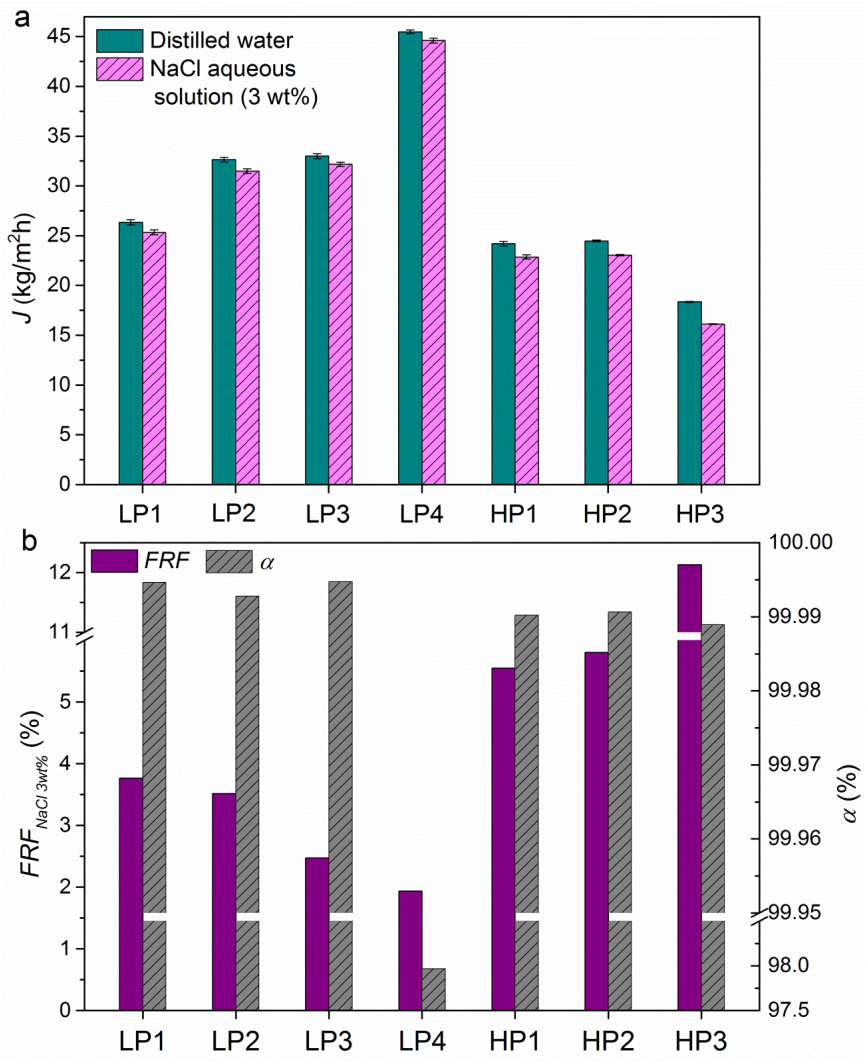

Fig. 5.8. AGMD (a) permeate flux (*J*) and (b) permeate flux reduction factor (*FRF*) and salt rejection factor (α) at 3 wt% NaCl feed aqueous solution, of the grafted alumina hollow fiber membranes.

membrane with a higher thermal conductivity coefficient. Furthermore, this membrane had the highest tortuosity factor (see Table 5.4), which contributed also to the reduction of the permeate flux.

The hollow fibers LP2 and LP3 exhibited similar characteristics, which resulted in an improved AGMD permeate fluxes compared with the other hollow fiber membranes. These hollow fibers had bigger micro-channels, thinner wall, larger entrance size of micro-channels at the lumen side and slightly greater void volume fractions. As it is well-known, the large micro-channels and the high porosities reduce the thermal conductivity of these membranes. Moreover, the hollow fiber membrane LP3 had larger micro-channels and lower tortuosity factor, leading to a slightly greater permeate flux than that obtained for the hollow fiber LP2. When comparing the AGMD permeate fluxes of the prepared grafted hollow fiber

membranes (Fig. 5.8(a)) with those reported for other hydrophobic ceramic membranes used in different MD configurations (see Table 5.6), it can be demonstrated the excellent water production rates of the hollow fiber membranes prepared in the present study. The resultant permeate fluxes obtained in this study were generally greater than the majority of those summarized in Table 5.6 and significantly higher than those used in AGMD configuration. Only the VMD permeate fluxes obtained for the grafted alumina hollow fiber membrane prepared by Fang et al. [6] were higher than the best AGMD permeate flux prepared in this study (i.e. LP3 in Fig. 5.8(a)). In fact, VMD configuration usually leads to higher permeate fluxes than those obtained in other MD configurations such as DCMD and AGMD (see Table 5.6 for some comparative studies [8, 16, 18]). Furthermore, VMD configuration requires a more complicated system design and a higher energy consumption [4].

As it can be seen in Fig. 5.8(a), by using distilled water as feed the permeate fluxes of all the hollow fiber membranes were slightly higher than those obtained with feed salt aqueous solution, resulting in low $FRF_{Nacl\ 3wt\%}$ as presented in Fig. 5.8(b). All the $FRF_{NaCl\ 3wt\%}$ values of the prepared hollow fibers were lower than 6%, except the membrane HP3, which had the highest $FRF_{NaCl\ 3wt\%}$ attributed partly to its lower water permeate flux compared to the other alumina hollow fibers.

In addition to the good AGMD permeate fluxes and $FRF_{NaCl\ 3wt\%}$, excellent salt rejection factors were obtained (i.e. higher than 99.988%). This means that the salt concentrations of the permeate solutions were lower than 3 10^{-3} g/L indicating the high purity of the produced water by AGMD with the prepared grafted alumina hollow fiber membranes. The hollow fiber membranes LP1 and LP3 had the greatest salt rejection factor (i.e. 99.995%). Their AGMD performance was further analyzed using feed aqueous solutions of different NaCl concentrations (i.e. 0, 1.2, 3 and 6.5 wt%). The resultant permeate fluxes are plotted in Fig. 5.9. As it was expected, the AGMD permeate flux decreased with the increase of the feed NaCl concentration. However, the obtained permeate flux reduction was very low for both LP1 and LP3 membranes, because even for the highest feed salt concentration (i.e. 6.5 wt%, NaCl), the corresponding $FRF_{NaCl\ 6.5wt\%}$ were only 5.6 and 7.2%, respectively. Furthermore, the salt rejection factors were higher than 99.985% for all the AGMD experiments being the permeate concentrations lower than 2.3 10^{-3} g/L. These experiments demonstrated the promising applicability of the grafted alumina hollow fiber membranes for the treatment of brines. The obtained $FRF_{NaCl\ 6.5\ wt\%}$ results were significantly better (i.e. lower) than the following $FRF_{NaCl\ 6wt\%}$ values calculated for other grafted ceramic membranes tested in desalination by MD: 13.3% in [12] for AGMD; 20.6% in [50] for DCMD; 32.8% and 35.4% in [8] for DCMD and VMD, respectively (see details in Table 5.6).

Appropriate membranes for desalination by MD must exhibit a high permeate flux and salt rejection as well as a low flux reduction factor. Therefore, the hollow fiber LP3 formed by

large micro-channel structures, provided the best AGMD performance in this study and it is well ranked between the MD ceramic membranes used in desalination (see Table 5.6).

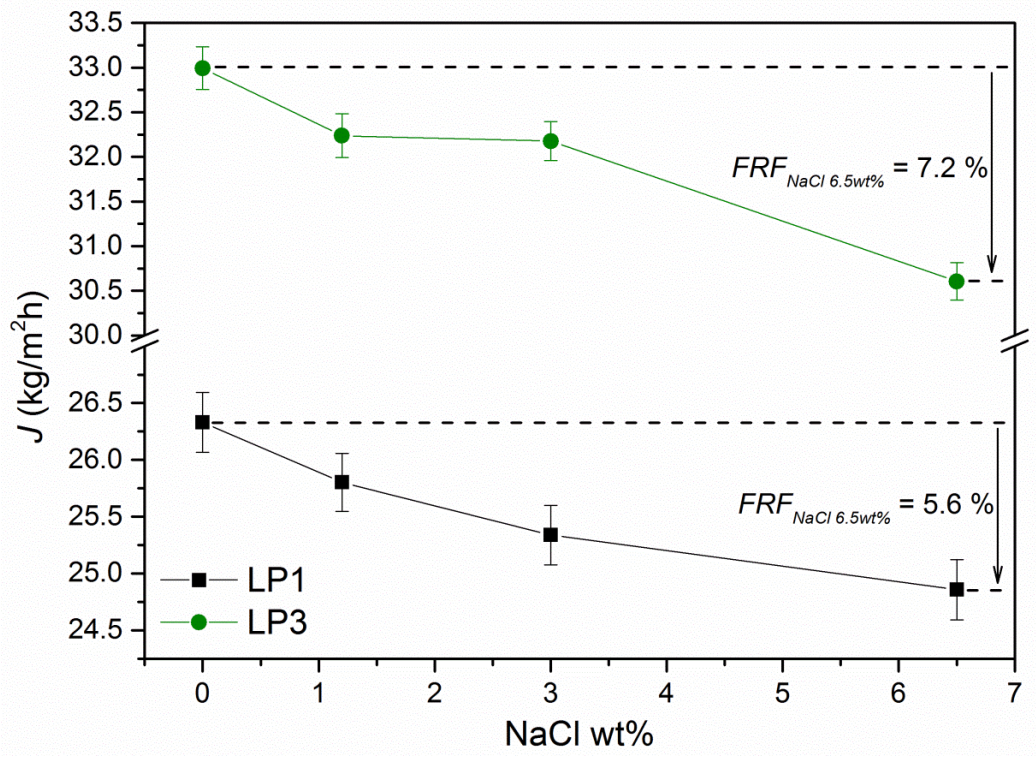

Fig. 5.9. Effect of the NaCl concentration of the feed solution on the AGMD permeate flux (*J*) of the grafted alumina hollow fiber membranes LP1 and LP3

Table 5.6. Reported MD performance of different types of grafted ceramic membranes.

MD configuration	Membrane material (grafting agent)	Membrane shape	Feed solution and temperatures (feed, T_f; permeate, T_p; cooling, T_c)	Permeate flux (L m^{-2} h^{-1})	Separation factor (%)	Ref
AGMD	Alumina, Al200 (1H, 1H, 2H, 2H-perfluorodecyltriethoxysilane, T-PFS) Zirconia, Zr50 (T-PFS)	Tubular	3 - 6 wt% NaCl T_f = 95 °C T_c = 25 °C	5.03 (3 wt%) 4.16 (6 wt%) 5.25 (3 wt%) 4.59 (6 wt%)	99.6 (3 wt%) 90.7 (6 wt%) 100	[17]
AGMD	Clay-alumina, C-55-M (T-PFS)	Capillary	3 wt% NaCl T_f = 70 °C T_c = 10 °C	4.1	99.96	[15]
AGMD	Zirconia layer/alumina support, M3 (T-PFS)	Tubular	Pure water (0 wt%) - 6 wt% NaCl T_f = 99 °C T_p = 5 °C	6.25 (0 wt%) 5.42 (6 wt%)	100	[12]
AGMD	Titania, Ti-300kD-tC6 (1H,1H,2H,2H-perfluorooctyltriethoxysilane, T-PFOS)	Tubular	3 wt% NaCl T_f = 90 °C T_p = 5 °C	3.7	N.A.	[13]
AGMD	Alumina, LP3 (T-PFS)	Hollow fiber	0 - 1.2 - 3 - 6.5 wt% NaCl T_f = 80 °C T_c = 20 °C	33.0 (0 wt%) 32.2 (1.2 wt%) 32.1 (3 wt%) 30.6 (6.5 wt%)	>99.99	This study
AGMD			3 wt% NaCl T_f = 95 °C T_c = 5 °C	4.7	99.8	
DCMD	Zirconia, Zr50 (T-PFS)	Tubular	3 wt% NaCl T_f = 95 °C T_c = 5 °C	4	99.8	[18]
VMD			3 wt% NaCl T_f = 40 °C Pressure = 3 mbar	7.5	96.1	

DCMD	Alumina (T-PFS)	Tubular	0.6 - 6 wt% NaCl T_f = 95 °C T_p = 5 °C	6.8 (0.6 wt%) 5.4 (6 wt%)	100	[50]
DCMD	Alumina (T-PFOS)	Planar	2 - 4 - 6 wt% NaCl T_f = 80 °C T_p =20 °C	19.1 (2 wt%) 17.0 (4 wt%) 15.5 (6 wt%)	> 99.5 (2 wt%)	[51]
DCMD	Alumina, Anodisc-200 (T-PFS)	Planar	0.6 wt% NaCl T_f = 53 °C T_p = 18 °C	17 - 8	93 - 99	[14]
DCMD VMD	Silicon Nitride (T-PFOS)	Hollow fiber	0.5 - 2 - 4 - 6 wt% NaCl T_f = 80 °C T_p = 20 °C) 0.5 – 2 – 4 - 6 wt% NaCl T_f = 80 °C Pressure = 0.02 bar	13.4 (0.5 wt%) 12.2 (2 wt%) 11.0 (4 wt%) 9.0 (6 wt%) 36.7 (0.5 wt%) 32.1 (2 wt%) 28.3 (4 wt%) 23.7 (6 wt%)	99 - 100	[8]
DCMD VMD	β-Sialon, $Si_{6-z}Al_zO_zN_{8-z}$, z = 2 (T-PFOS)	Hollow fiber	2 - 4 wt% NaCl T_f = 80 °C T_p = 20 °C 2 - 4 wt% NaCl T_f = 80 °C Pressure = 0.02 bar	7.9 (2 wt%) 6.8 (4 wt%) 12.2 (2 wt%) 10.75 (4 wt%)	99 - 100	[16]
VMD	Alumina (T-PFOS)	Hollow fiber	2 - 4 - 6 wt% NaCl T_f = 80 °C Pressure = 0.04 bar	45 (2 wt%) 42.9 (4 wt%) 41 (6 wt%)	> 99.5 (4 wt%)	[6]
VMD	Silicon Nitride (T-PFOS)	Hollow fiber	2 - 4 wt% NaCl T_f = 70 °C Pressure = 0.02 bar	25 (2 wt%) 22.25 (4 wt%)	99 - 100	[52]

5.4 Conclusions

Alumina hollow fiber membranes with different morphologies were prepared and modified for desalination by AGMD. The spinning parameters were manipulated in order to obtain the desired membrane structures, based on the well-recognized Rayleigh-Taylor instability theory. The effects of these morphological structures on the characteristics and performance of the membranes were analyzed.

The prepared hollow fiber membranes exhibited two types of pores: the primary inter-granule pores between alumina particles, which coincided with the effective open pores through the membrane; and the micro-channel entrance pores, related to each membrane morphology. The majority of the alumina hollow fiber membranes obtained similar mean pore sizes and porosities (about 233 nm and 52%, respectively), which were within the range of MD applicability. The tortuosity values of the membrane pores were lower than two, which is a good factor for MD membranes. Furthermore, all the prepared alumina membranes provided suitable mechanical properties for packing in tubular modules.

The alumina hollow fiber membranes were successfully modified by grafting, rendering them hydrophobic (i.e. water contact angles higher than 136°) without altering any other membrane characteristics. The membranes LP2, LP3 and HP3 were superhydrophobic (i.e. water contact angles higher than 150°). Except the hollow fiber LP4, none of the grafted membranes showed any wetting problems (i.e. LEP_w values greater than 3.8 10^5 Pa). Therefore, excellent salt rejection factors (i.e. higher than 99.985%) and *FRF* values were obtained for desalination by AGMD. It is worth noting that the LP fibers prepared with the low polymer concentration in the inorganic suspension exhibited greater desalination performance (i.e. higher permeate flux and salt rejection factor as well as lower $FRF_{NaCl\ 3wt\%}$) than the HP fibers prepared with the high polymer concentration in the inorganic suspension. The best AGMD performance was obtained for the hollow fiber LP3 with large micro-channel structure and good characteristics (i.e. lower thickness, slightly higher void volume fraction and the lowest pore tortuosity factor) that reduced the mass transport resistance.

In general, compared to the hydrophobic ceramic membranes used so far in desalination by MD, the grafted alumina hollow fiber membranes proposed in this study have excellent AGMD performance.

References

[1] F. Macedonio, E. Drioli, A.A. Gusev, A. Bardow, R. Semiat, M. Kurihara, Efficient technologies for worldwide clean water supply, Chem. Eng. Process.: Process Intensification 51 (2012) 2-17.

[2] A. Chafidz, E.D. Kerme, I. Wazeer, Y. Khalid, A. Ajbar, S.M. Al-Zahrani, Design and fabrication of a portable and hybrid solar-powered membrane distillation system, J. Cleaner Prod. 133 (2016) 631-647.

[3] P. Wang, T.S. Chung, Recent advances in membrane distillation processes: Membrane development, configuration design and application exploring, J. Membr. Sci. 474 (2015) 39-56.

[4] M. Khayet, T. Matsuura, Membrane distillation: Principles and applications, Elsevier, The Netherlands, 2011.

[5] Y. Zhang, Y. Peng, S. Ji, Z. Li, P. Chen, Review of thermal efficiency and heat recycling in membrane distillation processes, Desalination 367 (2015) 223-239.

[6] H. Fang, J.F. Gao, H.T. Wang, C.S. Chen, Hydrophobic porous alumina hollow fiber for water desalination via membrane distillation process, J. Membr. Sci. 403-404 (2012) 41-46.

[7] W. Kujawski, J. Kujawa, E. Wierzbowska, S. Cerneaux, M. Bryjak, J. Kujawski, Influence of hydrophobization conditions and ceramic membranes pore size on their properties in vacuum membrane distillation of water–organic solvent mixtures, J. Membr. Sci. 499 (2016) 442-451.

[8] J.W. Zhang, H. Fang, J.W. Wang, L.Y. Hao, X. Xu, C.S. Chen, Preparation and characterization of silicon nitride hollow fiber membranes for seawater desalination, J. Membr. Sci. 450 (2014) 197-206.

[9] A.F. Ismail, K. Li, From Polymeric Precursors to Hollow Fiber Carbon and Ceramic Membranes, Membr. Sci. Technol. 13 (2008) 81-119.

[10] M. Lee, Z. Wu, R. Wang, K. Li, Micro-structured alumina hollow fibre membranes – Potential applications in wastewater treatment, J. Membr. Sci. 461 (2014) 39-48.

[11] E. Drioli, A. Ali, F. Macedonio, Membrane distillation: Recent developments and perspectives, Desalination 356 (2015) 56-84.

[12] S. Krajewski, W. Kujawski, M. Bukowska, C. Picard, A. Larbot, Application of fluoroalkylsilanes (FAS) grafted ceramic membranes in membrane distillation process of NaCl solutions, J. Membr. Sci. 281 (2006) 253-259.

[13] J. Kujawa, S. Cerneaux, W. Kujawski, Investigation of the stability of metal oxide powders and ceramic membranes grafted by perfluoroalkylsilanes, Colloids Surf., A 443 (2014) 109-117.

[14] Z.D. Hendren, J. Brant, M.R. Wiesner, Surface modification of nanostructured ceramic membranes for direct contact membrane distillation, J. Membr. Sci. 331 (2009) 1-10.

[15] R. Das, K. Sondhi, S. Majumdar, S. Sarkar, Development of hydrophobic clay–alumina based capillary membrane for desalination of brine by membrane distillation, J. Asian Ceram. Soc. 4 (2016) 243-251.

[16] J.W. Wang, L. Li, J.W. Zhang, X. Xu, C.S. Chen, β-Sialon ceramic hollow fiber membranes with high strength and low thermal conductivity for membrane distillation, J. Eur. Ceram. Soc. 36 (2016) 59-65.

[17] L. Gazagnes, S. Cerneaux, M. Persin, E. Prouzet, A. Larbot, Desalination of sodium chloride solutions and seawater with hydrophobic ceramic membranes, Desalination 217 (2007) 260-266.

[18] S. Cerneaux, I. Strużyńska, W.M. Kujawski, M. Persin, A. Larbot, Comparison of various membrane distillation methods for desalination using hydrophobic ceramic membranes, J. Membr. Sci. 337 (2009) 55-60.

[19] L. García-Fernández, M. Khayet, M.C. García-Payo, Membranes used in membrane distillation: preparation and characterization, in: A. Basile, A. Figoli, M. Khayet (Eds.) Pervaporation, Vapour Permeation and Membrane Distillation: Principles and Applications, Elsevier (Woodhead Publishing), Cambridge, 2015, pp. 317-359.

[20] X. Zhang, B. Lin, Y. Ling, Y. Dong, D. Fang, G. Meng, X. Liu, Highly permeable porous YSZ hollow fiber membrane prepared using ethanol as external coagulant, J. Alloys Compd. 494 (2010) 366-371.

[21] M. Gryta, M. Barancewicz, Influence of morphology of PVDF capillary membranes on the performance of direct contact membrane distillation, J. Membr. Sci. 358 (2010) 158-167.

[22] M. Khayet, Membranes and theoretical modeling of membrane distillation: a review, Adv. Colloid Interface Sci. 164 (2011) 56-88.

[23] P. Wang, M.M. Teoh, T.S. Chung, Morphological architecture of dual-layer hollow fiber for membrane distillation with higher desalination performance, Water Res. 45 (2011) 5489-5500.

[24] B.F.K. Kingsbury, Z. Wu, K. Li, A morphological study of ceramic hollow fibre membranes: A perspective on multifunctional catalytic membrane reactors, Catal. Today 156 (2010) 306-315.

[25] H. Cao, H. Zheng, J. Yin, Y. Lu, S. Wu, X. Wu, B. Li, Mg(OH)2 Complex Nanostructures with Superhydrophobicity and Flame Retardant Effects, J. Phys. Chem. C 114 (2010) 17362-17368.

[26] X. Yang, R. Wang, L. Shi, A.G. Fane, M. Debowski, Performance improvement of PVDF hollow fiber-based membrane distillation process, J. Membr. Sci. 369 (2011) 437-447.

[27] L. García-Fernández, M.C. García-Payo, M. Khayet, Effects of mixed solvents on the structural morphology and membrane distillation performance of PVDF-HFP hollow fiber membranes, J. Membr. Sci. 468 (2014) 324-338.

[28] M. Essalhi, M. Khayet, Self-sustained webs of polyvinylidene fluoride electrospun nanofibers: Effects of polymer concentration and desalination by direct contact membrane distillation, J. Membr. Sci. 454 (2014) 133-143.

[29] X. Li, C. Wang, Y. Yang, X. Wang, M. Zhu, B.S. Hsiao, Dual-biomimetic superhydrophobic electrospun polystyrene nanofibrous membranes for membrane distillation, ACS Appl. Mater. Interfaces 6 (2014) 2423-2430.

[30] Y. Yuan, T.R. Lee, Contact Angle and Wetting Properties, in: G. Bracco, B. Holst (Eds.) Surface Science Techniques, Springer-Verlag Berlin Heidelberg 2013, pp. 3-34.

[31] S. Koonaphapdeelert, K. Li, Preparation and characterization of hydrophobic ceramic hollow fibre membrane, J. Membr. Sci. 291 (2007) 70-76.

[32] M.C. García-Payo, M. Essalhi, M. Khayet, Effects of PVDF-HFP concentration on membrane distillation performance and structural morphology of hollow fiber membranes, J. Membr. Sci. 347 (2010) 209-219.

[33] C.C. Wei, K. Li, Preparation and Characterization of a Robust and Hydrophobic Ceramic Membrane via an Improved Surface Grafting Technique, Ind. Eng. Chem. Res. 48 (2009) 3446-3452.

[34] S. Liu, K. Li, R. Hughes, Preparation of porous aluminium oxide (Al2O3) hollow fibre membranes by a combined phase-inversion and sintering method, Ceram. Int. 29 (2003) 875-881.

[35] M. Lee, B. Wang, K. Li, New designs of ceramic hollow fibres toward broadened applications, J. Membr. Sci. 503 (2016) 48-58.

[36] K. Wang, A.A. Abdalla, M.A. Khaleel, N. Hilal, M.K. Khraisheh, Mechanical properties of water desalination and wastewater treatment membranes, Desalination 401 (2017) 190-205.

[37] M. Khayet, The effects of air gap length on the internal and external morphology of hollow fiber membranes, Chem. Eng. Sci. 58 (2003) 3091-3104.

[38] M. Lee, B. Wang, Z. Wu, K. Li, Formation of micro-channels in ceramic membranes – Spatial structure, simulation, and potential use in water treatment, J. Membr. Sci. 483 (2015) 1-14.

[39] D.J. Lewis, The Instability of Liquid Surfaces when Accelerated in a Direction Perpendicular to their Planes. II, Proc. R. Soc. Lond. Ser. A Math. Phys. Sci. 202 (1950) 81-96.

[40] D.H. Sharp, An overview of Rayleigh-Taylor instability, Physica D 12 (1984) 3-18.

[41] G. Taylor, The Instability of Liquid Surfaces when Accelerated in a Direction Perpendicular to their Planes. I, Proc. R. Soc. Lond. Ser. A Math. Phys. Sci. 201 (1950) 192-196.

[42] B.F.K. Kingsbury, K. Li, A morphological study of ceramic hollow fibre membranes, J. Membr. Sci. 328 (2009) 134-140.

[43] M. Mulder, Basic Principle of Membrane Technology, Kluver Academic Publisher, Netherlands, 1996.

[44] X. Zhang, J. Hu, Q. Chang, Y. Wang, J.e. Zhou, T. Zhao, Y. Jiang, X. Liu, Influences of internal coagulant composition on microstructure and properties of porous YSZ hollow fibre membranes for water treatment, Sep. Purif. Technol. 147 (2015) 337-345.

[45] M. Lee, Z. Wu, B. Wang, K. Li, Micro-structured alumina multi-channel capillary tubes and monoliths, J. Membr. Sci. 489 (2015) 64-72.

[46] C.C. Wei, O.Y. Chen, Y. Liu, K. Li, Ceramic asymmetric hollow fibre membranes—One step fabrication process, J. Membr. Sci. 320 (2008) 191-197.

[47] E. Gbenedio, Z. Wu, I. Hatim, B.F.K. Kingsbury, K. Li, A multifunctional Pd/alumina hollow fibre membrane reactor for propane dehydrogenation, Catal. Today 156 (2010) 93-99.

[48] X. Tan, N. Liu, B. Meng, S. Liu, Morphology control of the perovskite hollow fibre membranes for oxygen separation using different bore fluids, J. Membr. Sci. 378 (2011) 308-318.

[49] J.A. Sanmartino, M. Khayet, M.C. García-Payo, H. El Bakouri, A. Riaza, Desalination and concentration of saline aqueous solutions up to supersaturation by air gap membrane distillation and crystallization fouling, Desalination 393 (2016) 39-51.

[50] A. Larbot, L. Gazagnes, S. Krajewski, M. Bukowska, K. Wojciech, Water desalination using ceramic membrane distillation, Desalination 168 (2004) 367-372.

[51] C. Ren, H. Fang, J. Gu, L. Winnubst, C. Chen, Preparation and characterization of hydrophobic alumina planar membranes for water desalination, J. Eur. Ceram. Soc. 35 (2015) 723-730.

[52] J.W. Zhang, H. Fang, L.Y. Hao, X. Xu, C.S. Chen, Preparation of silicon nitride hollow fibre membrane for desalination, Mater. Lett. 68 (2012) 457-459.

Conclusions

Advanced hollow fiber membranes for desalination by membrane distillation (MD) have been developed in this PhD Thesis. The design of MD membranes must meet certain specific requirements. Therefore, a comprehensive analysis about the membrane formation mechanism in relation to the membrane morphology, its structural characteristics and MD performance has been carried out.

Organic and inorganic hollow fiber membranes were prepared by the dry/wet or wet/wet spinning techniques and thorough studies on the effects of different spinning parameters on the membrane structural characteristics and MD performance have been performed. The organic hollow fiber membranes were prepared with the copolymer poly(vinylidene fluoride-co-hexafluoropropylene) (PVDF-HFP) because of its high hydrophobicity and tested by direct contact membrane distillation (DCMD) configuration.

The type of solvent(s) strongly affected the rheological properties of the spinning solution and modified the polymer-solvent-nonsolvent (P-S-NS) interactions (i.e. Hansen solubility parameter, HSP, distance). Different solvents namely, single *N,N*-dimethyl acetamide (DMAC) and different mixed solvents (DMAC and trimethyl phosphate (TMP) as well as *N,N*-dimethyl formamide (DMF) and TMP) were employed. The selection of the solvent(s) dictates the coagulation kinetic and the thermodynamic precipitation of the membrane formation. It was found that the mixed solvents that increased the viscosity of the PVDF-HFP dope solution also improved its thermodynamic stability and reduced the coagulation rate of the phase inversion of the membrane, leading to macro-void free hollow fiber membranes with thicker sponge-like structure in their cross-sections, rougher outer surfaces, larger mean pore sizes and narrower pore size distributions. It was found that the thicker the sponge-like structure of the hollow fiber membrane, the higher the DCMD permeate flux was. According to the obtained membrane characteristics and MD performance, it was figured out the most adequate solvent mixture (i.e. the best spinning solution: 19 wt% of the copolymer PVDF-HFP, 5 wt% of the additive poly(ethylene glycol), PEG, and the solvent mixture 40 wt% DMAC/60 wt% TMP) in this study (Chapter 2). This was used in the subsequent research studies (Chapters 3 and 4) carried out in this PhD Thesis.

Based on the conclusions drawn from the previous study (Chapter 2), hollow fiber membranes with more porous as well as skinless inner and outer surfaces were prepared using different solvent/water mixtures (i.e. DMAC/water) as internal and external coagulants (Chapter 3). First, it was studied the coagulation power effectiveness of the nonsolvent

mixtures, determining whether it was possible to prepare a membrane or not depending on the limit amount of solvent in the nonsolvent mixture. It was confirmed that the use of the mixed solvent is beneficial for a wide range of DMAC/water ratios (i.e. between 28 and 75 wt% of DMAC) as nonsolvent mixture. It was determined that the most promising conditions for an appropriate membrane design (i.e. porous and sponge-like structure morphologies) required a similar interaction power between the nonsolvent with each individual solvent (i.e. better NS-S exchange). This condition for this P-S-NS system was found for DMAC concentrations between 50 and 60 wt% in the nonsolvent mixture.

The prediction via HSP analysis was confirmed after hollow fiber membrane preparation under the above cited operating conditions and their subsequent characterization. The increase of the solvent (DMAC) concentration in the aqueous nonsolvent mixture improved the NS-S affinity (i.e. weaker NS-S interaction), delaying the precipitation initiation and reducing the phase inversion rate of the membrane formation. Therefore, more porous and rougher inner surfaces with larger pore sizes were formed, and the finger-like structure of the inner layer was reduced or even disappeared forming an open-spongy structure when the highest content of DMAC was used in the bore liquid. Other structural characteristics were also enhanced, leading to hollow fiber membranes with lower thickness, higher porosity and narrower inner surface pore size distribution. Consequently, the highest DCMD performance (i.e. permeate flux and salt rejection factor) was obtained for the hollow fiber membranes prepared with the highest concentrations of solvent in the internal coagulant mixture, 50 and 60 wt%, in accordance with the promising conditions predicted for a suitable MD membrane design.

The above cited results could be further improved by removing the undesirable skin-layer from the outer surface of these PVDF-HFP hollow fiber membranes. This was possible by changing the external coagulation type from dry to wet. First, it was found that the total suppression of the air gap distance was an unsuccessful strategy to obtain porous hollow fiber external layer and improve the DCMD performance. Subsequently, a wet gap was considered for the hollow fiber membrane preparation (i.e. wet/wet spinning technique) using different DMAC/water mixtures, but in this case as external coagulants and distilled water as internal coagulant. This wet/wet spinning not only induced the formation of porous outer surfaces, but other membrane characteristics were improved. The best DCMD performance was obtained for the hollow fiber membrane prepared with the highest concentration of DMAC (i.e. 60 wt%) in water as external coagulant.

It is worth noting that the effects of the internal and external coagulants on the mechanism of formation of hollow fiber membranes cannot be explained exactly the in same way. The slower coagulation (i.e. better NS-S affinity) of the inner layer of the hollow fiber membranes, prepared with higher concentration of DMAC in the internal coagulant mixture, could be

extrapolated only to the effect of the external coagulant mixture on the outer layer of the nascent fiber when it was applied along the gap distance. However, a global understanding of the external structure evolution of the outer surface of these membranes required to consider other factors such as the time of NS-S interaction (only along the gap distance) and the strong coagulation power of water when the fiber reached the water coagulation bath.

Finally, the best nonsolvent mixtures (i.e. 50 and 60 wt% of DMAC in water) were used as internal and external coagulants, trying to benefit from the advantages of both effects simultaneously. The hollow fiber membrane prepared with 60 wt% of DMAC in water used as nonsolvent mixture did not have the minimum mechanical requirements to be tested in MD. Nevertheless, among all membranes prepared with DMAC/water mixture as internal or external coagulant, the membrane prepared with 50 wt% of DMAC in water as simultaneous internal and external coagulants exhibited the best MD membrane characteristics and permeate flux maintaining a good salt rejection factor.

The main conclusion that can be drawn from these three studies (Chapters 2 and 3) is described as follows. A suitable P-S-NS system can be chosen previous any membrane preparation if the HSP distance is thoroughly analyzed. The morphological structure of the membrane can be designed and/or predicted via this analysis making possible the preparation of an MD membrane with a high performance. The usefulness and validity of the HSP distance analysis can be applied to any phase inversion membrane prepared with different spinning solutions and coagulants minimizing therefore the number of the experimental tests.

A micro-engineered triple-orifice spinneret (i.e. star-shaped orifice for the copolymer solution) and a novel fiber outer layer wetting mode (i.e. spraying the external coagulant by micro-jet nozzles on the nascent fiber along gap distance) were considered to prepare corrugated PVDF-HFP hollow fiber membranes via wet/wet spinning (Chapter 4). For the first time, MD hollow fibers, with different microstructured geometries, were obtained by changing the spinneret type, the wetting mode of wet/wet spinning and the two spinning parameters, the gap distance and the external coagulant flow rate. After evaluating the degree of corrugation of the outer surface, it was obtained that the largest corrugations and the roughest surface corresponded to the hollow fiber membrane prepared with the star-shaped spinneret, the longitudinal fiber outer layer wetting mode and the lowest external coagulant flow rate. However, the most efficient membrane in terms of MD water production rate was the highly but irregularly corrugated hollow fiber prepared using the spray fiber outer layer wetting mode. This hollow fiber exhibited not only the highest DCMD permeate flux in this study (Chapter 4), but also the highest permeate flux compared to all PVDF-HFP hollow fiber membranes prepared so far for MD. The effect of the corrugation size and shape of the hollow fiber membrane outer surface on the DCMD desalination performance has been experimentally studied. It was found that the surface corrugations enlarged the external

surface area and acted as micro-turbulence promoters mitigating the temperature polarization effect and enhancing the DCMD mass transfer as consequence. However, corrugations with V-shaped valleys depths greater than about 30 μm did not always improve the DCMD permeate flux.

Inorganic hollow fiber membranes with different morphological structures were designed based on the well-recognized Rayleigh-Taylor instability theory. These membranes were prepared by the phase inversion technique using alumina suspensions with two concentrations of the polymer polyethersulfone and different spinning parameters such as the inorganic suspension flow rate, the gap distance, the bore liquid, the outer coagulant composition and their flow rates (Chapter 5). After sintering the alumina hollow fibers, these were successfully modified by grafting (1H,1H,2H,2H-perfluorodecyltriethoxysilane) to render them hydrophobic with high liquid entry pressure values (i.e. some of them were even superhydrophobic with water contact angle values above 150º). Excellent salt rejection factors were obtained when these membranes were used in desalination by air gap membrane distillation (AGMD).

The prepared alumina hollow fiber membranes exhibited different morphologies and two types of pores (the primary inter-granule pores between alumina particles and the micro-channel entrance pores). The micro-channel entrance pore size was related to the membrane structural design, whereas the inter-granule pores represented the effective open pores of the membrane for MD mass transport. These pore sizes and the obtained porosities were all within the range of the membranes designed for MD application. The tortuosity factor of the membrane pores was determined and excellent values (i.e. lower than two) were obtained for all prepared alumina hollow fiber membranes. Furthermore, these membranes exhibited sufficiently good mechanical integrity for packing in modules and testing in MD.

For the first time, the effects of the alumina hollow fiber membrane morphology on the MD membrane characteristics and on the AGMD desalination performance were studied. In general, the membranes prepared with lower polymer concentration in the alumina suspension provided higher AGMD desalination performance owing to their longer, bigger and numerous micro-channels in their cross-sections. This kind of structure led to lower heat transfer by conduction and mass transport resistance through the membrane compared to a tight sponge-like structure. It was found that the alumina hollow fiber membrane with the largest micro-channel structure and other good MD characteristics (i.e. lower thickness, slightly higher void volume fraction and the lowest pore tortuosity factor compared to all prepared alumina hollow fiber membranes in this study (Chapter 5)) exhibited not only the highest AGMD performance in this study, but also the highest permeate flux compared to all hydrophobic ceramic membranes used so far in desalination by AGMD and DCMD.

Future research projects

Several promising research studies in the field of hollow fiber membrane science and technology in general, and membrane distillation applications in particular, can be derived from this PhD Thesis. The following topics are some research projects that can be developed in near future or are under development stage by our research group.

Regarding membrane engineering, bi-layered hollow fiber membrane is an attractive design that should be developed taking into account the membrane preparation guidelines drawn in this PhD Thesis. Some useful and valid tools such as the Hansen solubility parameter distance can be used to select the most adequate materials (i.e. polymer, additive and solvent(s)) for a suitable membrane preparation according mainly to the polymer-solvent-nonsolvent interactions. For each layer, it should be considered the hydrophobicity of the main polymer and the nanoparticles that can be incorporated into the spinning solutions as well as the interrelated thermodynamics and kinetics of both layers during the phase inversion process. One of the roles of the nanoparticles´addition is to increase the mechanical properties and fouling resistance of the hollow fiber membranes. These bi-layered hollow fibers can be hydrophobic/hydrophilic permitting to enhance both the DCMD permeate flux and the thermal efficiency. The hydrophobic thin layer is the responsible of mass vapor transport and selectivity while the hydrophilic thick layer with bigger pores compared to those of the hydrophobic layer decreases the distance between the liquid/vapor interfaces improving therefore the permeate flux and reduces the heat transport by conduction depending on its thickness. Hollow fiber membranes with corrugated inner surfaces can also be prepared for MD applications in order to generate a turbulent flow regime in the lumen channel of the hollow fiber membrane module and to study its effect on the temperature and concentration polarization phenomena and the MD performance.

Based on the excellent results observed when using the ceramic hollow fiber membranes in MD desalination, attempts can be made to design other hollow fiber membranes with other structures, using other ceramic materials and exploring other modifying agents to render the membrane hydrophobic.

A promising membrane characterization technique is currently under development, which studies the wetting kinetics of the membrane pores via the light transmittance test through the membrane. This technique could provide information about the pore structure of an MD membrane by combining experimental and theoretical analysis.

It will be interesting to develop an efficient theoretical model based on the kinetic theory of gases through porous media and the heat transfer in hollow fiber membrane modules in order to predict the MD permeate flux of the prepared hollow fiber membranes in the present PhD Thesis. Computational Fluid Dynamics (CFD) simulation will also be very useful to study the temperature and concentration profiles along the tubular membrane module allowing to determine the temperature and concentration polarization coefficients.

The prepared hollow fiber membranes in this PhD Thesis can be used not only in desalination field like the treatment of brines but also in other MD applications such as the concentration of valuable non-volatile solutes present in wastewaters with a great interest in pharmaceutical and food industries, for example, removal of volatile organic compounds (VOCs) from water such as alcohols, benzene, chloroform, etc. Long-term MD experiments must be carried out in order to study the membrane´s operating life. Fouling (organic, inorganic or scaling) and biofouling must also be investigated. All these studies are especially interesting for ceramic hollow fiber membranes, which can stand harder environmental conditions than polymeric hollow fiber membranes.

Appendix A: abbreviations and symbols

Abbreviations

AFM	Atomic force microscopy
AG	Air gap
AGMD	Air gap MD
Al_2O_3	Aluminium oxide
BL	Bore liquid
BP	Bucky-papers
BS	Bench-scale
C	Cooling
CD	Condenser
CF_4	Carbon tetrafluoride
CFD	Computational fluid dynamic
CNT	Carbon nanotube
CNT-BP	CNT bucky-paper
DBP	Dibutyl phthalate
DCMD	Direct contact MD
DI	Deionized
DMAC	N,N-dimethylacetamide
DMF	N,N-dimethyl formamide
DOP	Dioctyl phthalate
DSC	Differential scanning calorimetry
E	Evaporator
EC	External coagulant
ECTFE	Poly(ethylenechlorotrifluoroethylene)
EG	Ethylene glycol

EIPS	Evaporation induced phase separation
ENM	Electrospun nanofibrous membrane
F	Feed
FEP	Poly(tetrafluroethylene-co-hexafluoropropylene)
FESEM	Field emission scanning electron microscopy
FO	Forward osmosis
F-PT	Fluorinated polytriazoles
FR	Flow rate
FS	Flat sheet
FSi	Fluorinated silica
FTCS	1H, 1H, 2H, 2H-perfluorododecyltrichlorosilane
GE	GE Osmonics
H/h	Hydrophobic/hydrophilic
H/H	Hydrophobic/hydrophobic
H	Heating
HF	Hollow fiber
HFP	Hexafluoropropylene
IP	Immersion precipitation
IPA	Isopropyl alcohol
I-PVDF	PVDF integrally-modified
IS	Inorganic suspension
LDR	Light dependence resistance
LED	Light-emitting diode
LGMD	Liquid gap MD
LiCl	Lithium chloride
LLLW	Liquid low-level radioactive waste
LPS	low-pressure sodium
LTH	Low temperature hydrothermal

MD	Membrane distillation
MDC	MD-crystallizer integrated system
MED	Multi-effect distillation
MeOH	Methanol
MF	Microfiltration
MIP	Mercury intrusion porosimetry
MS	Membrane solutions
MWCNTs	Multiwall carbon nanotubes
NaCl	Sodium chloride
NF	Nanofiltration
NIPS	Nonsolvent induced phase separation
NMP	N-methyl-2-pyrrolidone
NPs	Nanoparticles
NS	Nonsolvent
OC	Outer coagulant
–OH	Hydroxyl group
P(VDF-co-CTFE)	Poly(vinylidene fluoride-co-chlorotrifluoroethylene)
P(VDF-co-TFE)	Poly(vinylidene fluoride-co-tetrafluoroethylene)
P	Permeate
P	Polymer
PAN	Polyacrylonitrile
PD	Packing density
PDA	Poly-dopamine
PE	Poly(ethylene)
PEG	Poly(ethylene glycol)
PEI	Polyetherimide
PES, PESf	Polyethersulfone
PET	Polyethylene terephthalate

PF	Packing factor
PI	Polyimide
PP	Polypropylene
PSD	Pore size distribution
PSf	Polysulfone
PTFE	Polytetrafluoroethylene
PVDF	Polyvinylidene fluoride
PVDF-HFP	Poly(vinylidene fluoride-co-hexafluoropropylene)
PVB	Polyvinyl butyral
PVP	Polyvinylpyrrolidone
R	Refrigeration
RO	Reverse osmosis
RT	Retentate
S	Solvent
SEM	Scanning electron microscopy
SGMD	Sweeping gas MD
Si_3N_4	Silicon nitride
SiO_2	Silica
S_m	Solvent mixture
SMM	Surface modifying macromolecule
SPMD	Solar-powered membrane distillation
S-PVDF	PVDF surface-modified
TEP	Triethyl phosphate
TFE	Tetrafluoroethylene
THF	Tetrahydrofuran
TiO_2	Titanium dioxide
TIPS	Thermally induced phase separation
TMP	Trimethyl phosphate

TP	Temperature polarization
T-PFOS	1H, 1H, 2H, 2H-perfluorooctyltriethoxysilane
T-PFS	1H, 1H, 2H, 2H-perfluorodecyltriethoxysilane
TSGMD	Thermostatic SGMD
UF	Ultrafiltration
V	Velocity
VDF	Vinylidene fluoride
VIPS	Vapor induced phase separation
VMD	Vacuum MD
V-MEMD	Vacuum-multi-effect-membrane-distillation
VOCs	Volatile organic compounds
VP	Vacuum pressure
W	Water
XPS	X-ray photoelectron spectroscopy
YSZ	Yttria-stabilized zirconia
γ-BL	γ-butyrolactone

Symbols

A_m	Membrane surface area
b	Empirical parameter of solvent evaporation kinetics
C_m	Mass transfer coefficient
$C_{b,f}$	Bulk feed concentration
$C_{m,f}$	Concentration of the feed at the membrane surface
CPC	Concentration polarization coefficient
d_i	Inner diameter
D_m	Diffusion coefficient
d_p	Membrane pore size
E	Young´s modulus
FRF	Flux reduction factor

H_c	Corrigation´s height
HSP	Hansen solubility parameter
J	Permeate flux
J_R	Permeate flux ratio
k_g	Thermal conductivity of the gas-filled pores
k_m	Thermal conductivity of the membrane
Kn	Knudsen number
k_s	Thermal conductivity of the solid matrix of the membrane
L	Length
LEP	Liquid entry pressure
L_p	Effective pore length
m	Empirical parameter of solvent evaporation kinetics
P_v	Vapor pressure
Q_C	Heat loss by conduction
Q_J	Latent heat associated to the vapor flux
Q_m	Heat transfer through the membrane
R_a	Mean roughness
R_{HSP}	Hansen solubility parameter distance
R_{max}	Maximum roughness
r_p	Mean pore radius
SAE	Surface area enhancement
SA_R	Surface area ratio
SLD	Surface length difference
T	Temperature
$T_{b,f}$	Feed bulk temperature
$T_{b,p}$	Permeate bulk temperature
T_c	Crystallization temperature
T_m	Melting temperature

$T_{m,f}$	Feed temperature at the membrane surface
$T_{m,p}$	Permeate temperature at the membrane surface
T_{norm}	Normalized transmittance
TPC	Temperature polarization coefficient
S_{pore}	Pore surface area
VPC	Vapor pressure polarization coefficient
ΔH_c	Enthalpy of crystallization
ΔH_m	Enthalpy of melting
ΔH_w	Enthalpy of water vaporization
Δm	Produced water mass
ΔP_v	Transmembrane vapor pressure
$\Delta P_{v,b}$	Bulk vapor pressure difference
$\Delta P_{v,m}$	Vapor pressure difference between the feed and permeate at the membrane surface
Δt	Period of time
ΔT	Temperature difference
α	Salt rejection factor
α	Bow angle
χ_c	Crystallinity
δ	Thickness
δ_d	Solubility dispersion force component
δ_h	Solubility hydrogen bonding component
δ_p	Solubility polar component
ε	Porosity
ε_b	Strain at break
ε_e	Effective porosity
ε_s	Surface porosity

ε/L_p	Effective porosity
λ	Mean free path
μ_p	Mean pore size
θ	Dynamic contact angle
σ_b	Tensile stress at break
σ_F	Bending strength
σ_p	Geometric standard deviation
σ_y	Yield stress
τ	Tortuosity

Appendix B: figure captions

Appendix C: table headings